



UNIVERSITY OF  
BIRMINGHAM

# THE EFFECT OF SPATIAL SETTLEMENT PATTERNS ON URBAN CLIMATOLOGY

By:

**Mukhtar Abdulrasheed**

A thesis submitted to the University of Birmingham for the degree of

DOCTOR OF PHILOSOPHY

School of Geography, Earth, and Environmental Science,

College of Life and Environmental Science

University of Birmingham

July 2020

UNIVERSITY OF  
BIRMINGHAM

**University of Birmingham Research Archive**

**e-theses repository**

This unpublished thesis/dissertation is copyright of the author and/or third parties. The intellectual property rights of the author or third parties in respect of this work are as defined by The Copyright Designs and Patents Act 1988 or as modified by any successor legislation.

Any use made of information contained in this thesis/dissertation must be in accordance with that legislation and must be properly acknowledged. Further distribution or reproduction in any format is prohibited without the permission of the copyright holder.

# Abstract

Increasing urbanization, in addition to driving climate change and pollution, can have a profound effect on the ecosystem properties within and even far from urban areas. As such, it is important to understand the energy balance of cities including the extent of its modification by urban form. This PhD thesis examines the effect of spatial settlement pattern on urban climatology. The initial study focussed on UK overpasses of the Moderate Resolution Imaging Spectro-radiometer (MODIS) satellite instrument, covering the period between 2000 and 2017, were sampled to examine the seasonal (winter and summer) night-time clear-sky upwelling long-wave energy for 35 UK cities. Total (area-summed) emitted energy was calculated per city. Well-defined ( $R^2 \geq 0.79$ ) and robust 'allometric' scaling against city population was found for all samples. Total night-time emitted energy is found to scale sub-linearly with population on both summer and winter nights, with slope of  $0.85 \pm 0.03$ . The scaling of night-time emitted energy with urban areas is close to linear ( $1.0 \pm 0.05$ ). This indicates that UK Cities, although often appearing superficially very different, are similar in their gross thermal properties, i.e., in terms of the components of urban form, which dictate thermal properties. A case study of Nigeria's cities on allometric scaling of emitted energy with population is also investigated, and it turned out to be very different from the UK study with slope of  $0.41 \pm 0.05$ . Nigerian cities show much more sub-linear allometric scaling of total emitted energy with population, indicating slightly economy of scale in terms of nocturnal heat production. Local climate zones are further used to interpret results from the study. The study went further to investigate how the sum measure of the spatial distribution of emitted energy inside the city's boundary is affected by the urban morphology, using the previous UK study. A fitted distribution of both extremes' percentiles of emitted energy and land use maps within city were used as basis for comparison across cities in order to delineate the hottest and coldest spots in the distribution of long-wave energy for a sample night.

## **Dedication**

All praise and thanks are only dedicated to Allah, the sustainer of the Universe.

I thank God for giving me the strength and courage to make this thesis a reality. Alhamdulillah. And to my lovely and supportive parents, Alhaji  
Abdulrasheed Ibrahim Saeed and Hajiya Zulaihat Y. Saeed



## **Acknowledgements**

I am highly indebted to my supervisors: Prof. Angus Rob MacKenzie and Prof. Lee Chapman for their assiduous support and guidance throughout this PhD studies. I am particularly grateful for all the generous and quick responses at every short notice of any query I come with. Thank you so much! I sincerely appreciate the contribution of Prof. J. D. Whyatt for putting me through the GIS at the beginning of my program, to Chantal Jackson (geography map room), thank you for your support in editing the maps. I am also grateful to Deanne Brettle (Dee) for her administrative support through the course of my entire program, and to Gretchel Coldicott, thank you for your support.

Thanks is due to Petroleum Technology Development Fund (PTDF) for providing funding for the PhD program under the flagship of the Overseas Scholarship Scheme (OSS). I am particularly grateful to the staff of the training department at PTDF, especially Mall. Aminu Galadima, Hajia Rabi and Mr. Bello Mustapha. I would like to acknowledge Ahmadu Bello University (A.B.U) Zaria for giving me study leave to pursue this program. And to my colleagues at the department of Urban and Regional Planning (A.B.U – Zaria), thank you for your support, particularly Prof. M.B. Yunusa and Prof. Adamu Ahmed for their mentorship and encouragement.

Thanks, must also go to my fellow PhD scholars in office-room 412 and academic PhD research group (Rob-Group) for many fun times and brainstorming over the course of my time in Birmingham, particularly Edward Bannister and Karn Vohra, thank you for your support. And to other caring friends Dr. Mohammad Alharbi, Hussain Ali Adamu, among others. Thank you for being there for me.

Special thanks goes to my lovely parents for their prayers and support, and to my gorgeous wife Asiya Ahmad and children for their patient and understanding during the course of this academic long journey. Jazakumullahu Khair.

## Declaration

I hereby declare that except where specific reference is made to the work of others, the contents of this thesis are original and have not been submitted in whole or in part for consideration for any other degree of qualification in this, or any other university. This thesis is my own work and contains nothing which is the outcome of work done in collaboration with others, except as specified in the credit authorship contribution statement (below) and Acknowledgements. This thesis contains fewer than 65,000 words including supplementary, appendices, bibliography, tables, and figures.

Most of the materials in chapter 3 have been published in (Abdulrasheed et al., 2020). The study discussed in chapter 4 has been submitted “August 2020” for publication in:

**Abdulrasheed, M., Mackenzie, A.R., Bockarie, A., Chapman, L., (2020).** *Allometric scaling of emitted thermal infrared across Nigeria’s cities and its relation to urban form. “City and Environment Interaction Journal ”*. The study discussed in chapter 5 is in the revision stage of publication in: **Abdulrasheed, M., Mackenzie, A.R., Chapman, L., (2020).** *The spatial distribution of emitted long-wave energy within UK cities.*

### **CRedit authorship contribution statement (chapter 3)**

This study was conceived by ARMK and LC, developed from earlier work by JDW and ARMK. The investigation was carried out by MA with technical help by JDW and supervised by ARMK and LC. The manuscript was drafted by MA and all authors contributed to its final form.

### **CRedit authorship contribution statement (chapter 4)**

This study was conceived by ARMK and LC, developed from earlier work by JDW and ARMK. AB defined the city boundary. The investigation was carried out by MA with technical help by JDW and supervised by ARMK and LC. The manuscript was drafted by MA. MA, ARMK and LC contributed to its final form.

**Mukhtar Abdulrasheed**

**July 2020**

## **Publications arising from thesis**

M. Abdulrasheed, A.R. MacKenzie, J.D. Whyatt, L. Chapman 'Allometric scaling of thermal infrared emitted from UK cities and its relation to urban form'. *City and Environment Interactions* (2020), <https://doi.org/10.1016/j.cacint.2020.100037>

M. Abdulrasheed, Mackenzie, A.R., Bockarie, A., Chapman, L., (2020). *Allometric scaling of emitted thermal infrared across Nigeria's cities and its relation to urban form. "City and Environment Interactions* (2020),". (submitted August 2020).

M. Abdulrasheed, Mackenzie, A.R., Chapman, L., (2020). *The spatial distribution of emitted long-wave energy within UK cities*. (in the revision stage for publication)

# Table of Contents

<b>Abstract .....</b>	<b>ii</b>
<b>Dedication.....</b>	<b>iii</b>
<b>Acknowledgements.....</b>	<b>iv</b>
<b>Declaration .....</b>	<b>v</b>
<b>Publications arising from thesis.....</b>	<b>vi</b>
<b>Table of Contents .....</b>	<b>vii</b>
<b>List of Figures.....</b>	<b>x</b>
<b>List of Figures in Appendices.....</b>	<b>xi</b>
<b>List of Figures in Supplementary.....</b>	<b>xii</b>
<b>List of Tables .....</b>	<b>xiii</b>
<b>List of Tables in Supplementary.....</b>	<b>xiv</b>
<b>List of Acronyms .....</b>	<b>xv</b>
<b>1.0 Chapter 1 .....</b>	<b>1</b>
<b>INTRODUCTION .....</b>	<b>1</b>
1.1 Urbanization.....	1
1.2 Planning Theory: The Evolution of Cities .....	4
1.3 Inadvertent Modifications of Urban Areas .....	4
1.4 Research Aims and Objectives .....	7
1.4.1 Aims.....	7
1.5 Thesis Structure .....	8
<b>2.0 Chapter 2 .....</b>	<b>10</b>
<b>Literature Review .....</b>	<b>10</b>
2.1 Urban Climate .....	10
2.2 Urban Heat.....	11
2.3 Measuring the Urban Climate.....	13
2.4 Landuse and Urban Morphology: How it relates to the Causes of UHI effects .....	21
2.5 Allometry Scaling .....	24
2.6 Summary .....	27
<b>3.0 Chapter 3 .....</b>	<b>29</b>
<b>Allometric scaling of thermal infrared emitted from UK cities and its relation to urban form ....</b>	<b>29</b>
3.1 Introduction .....	30
3.2 Methodology.....	38

3.3 Results .....	42
3.4. Discussion.....	46
3.5 Conclusion .....	49
<b>4.0 Chapter 4 .....</b>	<b>51</b>
<b>Allometric scaling of emitted thermal infrared across Nigeria’s cities and its relation to urban form .....</b>	<b>51</b>
4.1 Introduction .....	52
4.2 <i>Methodology</i> .....	57
4.3 Results .....	63
4.4 Discussion.....	67
4.5 Conclusion .....	72
<b>5.0 Chapter 5 .....</b>	<b>74</b>
<b>The spatial distributions of emitted long-wave energy within UK cities .....</b>	<b>74</b>
5.1 Introduction .....	74
5.2 Methods.....	77
5.3 Results .....	81
5.4 Discussion.....	96
5.5 Conclusion .....	100
<b>6.0 Chapter 6 .....</b>	<b>102</b>
<b>Overall Synthesis and Conclusions .....</b>	<b>102</b>
6.1 Fulfilment of aims of the thesis .....	102
6.2 Critique of thesis .....	105
6.3 Future work.....	108
<b>References .....</b>	<b>110</b>
<b>Data Sources .....</b>	<b>128</b>
<b>Supplementary Materials .....</b>	<b>130</b>
<b>Supplementary 3SI .....</b>	<b>131</b>
(Materials for chapter 3).....	131
<b>Supplementary 4SI .....</b>	<b>141</b>
(Materials for chapter 4).....	141
<b>Appendices .....</b>	<b>157</b>
<b>Appendix A .....</b>	<b>158</b>
LONDON.....	158
<b>Appendix B.....</b>	<b>162</b>

SHEFFIELD .....	162
<b>Appendix C</b> .....	168
MILTON KEYNES .....	168
<b>Appendix D</b> .....	174
Published paper .....	174
CRedit authorship contribution statement .....	12
Acknowledgements.....	12

# List of Figures

Figure 1.1 Graph showing estimated and projected urban populations of the world, the more developed regions and the less developed regions, 1950 - 2050 (adopted from - United Nations et al., (2019)-----	2
Figure 1.2 Conceptual Framework and Study Structure-----	9
Figure 2.1 A Typical Urban Heat Island (UHI) Profile Sketch (uploaded from (Frumkin, 2002)) - originally from (Oke, 2002) -----	Error! Bookmark not defined.
Figure 2.2 An illustration of a remote sensing process, showing a passive, satellite-borne sensor receiving reflected solar radiation and emitted terrestrial radiation. The sensor signal is passed to a ground receiving station, sometimes via a data relay satellite, and converted into a data product in post-processing (sourced from Qihao, 2012) .....	17
Figure 2.3 Local Climate Zone (LCZ) Classes defined by (Stewart and Oke, 2012) -----	23
Figure 3.1 Relation between maximum air temperature heat island intensity ( $\Delta T_{u-r}$ (max), degrees Celsius) and population (P) for European Settlements (redrawn from Oke, 1982). Sources of $\Delta T_{u-r}$ (max) are literature and private communications dating from 1927 – 1972. It is not clear in Oke (1973; 1982) if the population data used is matched in time to the date for $\Delta T_{u-r}$ (max). Reported on the graph (top right) are the Coefficient of Determination ( $R^2$ ) for the best-fit regression, the slope of the regression, and the error on the slope ( $\epsilon$ ). -----	38
Figure 3.2 (a) 35 most populous urban areas in Great Britain (urban boundaries are contiguous Developed Land Use Areas from Meridian2 data); (b) Topographic map of central Great Britain with cities and major roads; (c) Average Sunshine of central Great Britain; (d) Mean 2m Temperature map of central Great Britain. The data were sourced from the Centre for Environmental Data Analysis (CEDA, 2011), (SolarGIS, 2019), Ordnance Survey - Meridian2 data(DLUA) and ArcGIS tools were used to plot the maps. -----	Error! Bookmark not defined.
Figure 3.3 (A) An example of allometric scaling of night-time emitted energy $\text{Log}_{10}(\langle E_j \rangle$ , in MW) against urban population for the 35 largest cities in Great Britain. Reported on the graph (top right) are the Coefficient of Determination ( $R^2$ ) for the best-fit regression, the slope of the regression, and the error on the slope ( $\epsilon$ ). (B) The ensemble of allometric relationships derived for the nights studied (Table 3.1). (C) Residual emitted energy (mean and standard deviation of $\text{Log}_{10}(\langle E_j \rangle$ in MW) for urban areas with respect to the allometric scalings shown in (B). -----	44
Figure 4.1 Local Climate Zone (LCZ) Classification and its 17 Standard Classes (after Stewart and Oke 2012)	54
Figure 4.2 The mean climate map of Nigeria: (a) 33 largest urban areas of Nigeria and climatic zones; (b) Topographic map of Nigeria with cities and major roads overlaid; (c) Average Sunshine of Nigeria; (d) Temperature map of Nigeria. Data source: Digimap (Relief) <a href="https://digimap.edina.ac.uk">https://digimap.edina.ac.uk</a> , Global Solar Atlas - (SolarGIS, 2019) and ArcGIS tools were used to plot the maps. -----	59
Figure 4.3 Regional classification of city's field sites by local climate zones- zones - Pixels above were adapted from the following papers: (Usman et al., 2016); (MyGuide, 2017)-----	60
Figure 4.4 (A) An example of allometric scaling of night-time emitted energy $\text{Log}_{10}(\langle E_j \rangle$ , in MW) against urban population for the 33 largest cities in Nigeria. Reported on the graph (top right) are the Coefficient of Determination ( $R^2$ ) for the best-fit regression, the slope of the regression, and the error on the slope. (B) The ensemble of allometric relationships derived for the nights studied (Table 4.1). (C) Residual emitted energy (mean and standard deviation of $\text{Log}_{10}(\langle E_j \rangle$ in MW) for urban areas with respect to the allometric scalings shown in (B). Colour-coding are used to classify cities (Ancient cities [red], New cities [green], Coastal cities [blue], the Federal capital [brown], and Other cities [black])--	65
Figure 5.1 Histograms and fitted distributions (left column), and percentiles graphs (right column) showing distributions of emitted energy ( $\text{W m}^{-2}$ , see Methods below) for three UK cities: London (top); Sheffield (middle); and Milton Keynes (bottom). Note that we use contiguous urban areas rather than administrative boundaries. Data for 02 <sup>nd</sup> Jan. 2017 from MODIS satellite Land Surface Temperature (see chapter 3 and Methods, below). The red curve (left column) is the best fit probability distribution	

function (PDF), calculated using the 'density' function in R, and is identical to the outline on the graphs in the right column, plotted using the ggplot function in R. ....	76
Figure 5.2 Landuse map showing city geography (plate A - top) and gridded code (interpolation- kriging) long-wave energy translated to city schematic map with magnitude indicating pattern of urban emission (plate B) for an average of all night's sample for London city. Data where sourced from MODIS (Earthdata, 2017), Ordnance survey (meridian2 data – DLUA) and Digimap ( <a href="https://digimap.edina.ac.uk/">https://digimap.edina.ac.uk/</a> ). ArcGIS 10.6 tool were used to plot the maps .....	84
Figure 5.3 Landuse map showing city geography (left panel) and gridded code (interpolation- kriging) long-wave energy translated to city schematic map with magnitude indicating pattern of urban emission (lower panel D) for an average of all night's sample for Sheffield city. Data where sourced from MODIS (Earthdata, 2017), Ordnance survey (meridian2 data – DLUA) and Digimap ( <a href="https://digimap.edina.ac.uk/">https://digimap.edina.ac.uk/</a> ). ArcGIS 10.6 tool were used to plot the maps .....	86
Figure 5.4 Landuse map showing city geography (left panel) and gridded code (interpolation- kriging) long-wave energy translated to city schematic map with magnitude indicating pattern of urban emission (lower panel F) for an average of all night's sample for Milton Keynes city. Data where sourced from MODIS (Earthdata, 2017), Ordnance survey (meridian2 data – DLUA) and Digimap ( <a href="https://digimap.edina.ac.uk/">https://digimap.edina.ac.uk/</a> ). ArcGIS 10.6 tool were used to plot the maps .....	88
Figure 5.5 Total emitted energy Versus total population (red), sum below 10 <sup>th</sup> (green) and sum above 90 <sup>th</sup> (blue) percentiles for all cities on a selected sample night (2 <sup>nd</sup> January 2017(B) Total emitted energy Versus Log <sub>10</sub> (total Area) (red), sum below 10 <sup>th</sup> (green) and sum above 90 <sup>th</sup> (blue) percentiles for all cities on a selected sample night (2 <sup>nd</sup> January 2017). Slope, error on slope ( $\epsilon$ ) and R <sup>2</sup> are reported on the panels. ....	89
Figure 5.6 Skewness versus population for all cities on a clear sample night (2 <sup>nd</sup> January 2017). (B) Skewness versus area for all cities on a clear sample night (2 <sup>nd</sup> January 2017). Slope, error on slope ( $\epsilon$ ) and R <sup>2</sup> are reported on the panels.....	91
Figure 5.7 Kurtosis versus population for all cities on a clear sample night (2 <sup>nd</sup> January 2017). (B) Kurtosis versus area for all cities on a clear sample night (2 <sup>nd</sup> January 2017). Slope, error on slope ( $\epsilon$ ) and R <sup>2</sup> are reported on the panels.....	91
Figure 5.8 Landuse map showing city geography (left plate) and gridded code (interpolation- kriging) long-wave energy translated to city schematic map with magnitude indicating pattern of urban emission (lower plate) for Aberdeen on a selected sample night (2 <sup>nd</sup> January 2017). Data where sourced from MODIS (Earthdata, 2017), Ordnance survey (meridian2 data – DLUA) and Digimap ( <a href="https://digimap.edina.ac.uk/">https://digimap.edina.ac.uk/</a> ). ArcGIS 10.6 tools were used to plot the maps .....	99

## List of Figures in Appendices

Fig. 5.9 The sum below 10 <sup>th</sup> (red) and the sum above 90 <sup>th</sup> (blue) percentiles for all sample nights in London city.....	160
Fig. 5.10 Skewness for all sample nights in London city.....	160
Fig. 5.11 Kurtosis for all sample nights in London city.....	160
Fig. 5.12 The sum below 10 <sup>th</sup> (red) and the sum above 90 <sup>th</sup> (blue) percentiles for all sample nights in Sheffield city.....	166
Fig. 5.13 Skewness for all sample nights in Sheffield city.....	166



<b>Fig. 5.14</b> Kurtosis for all sample nights in Sheffield city.....	166
<b>Fig. 5.15</b> The sum below 10 <sup>th</sup> (red) and the sum above 90 <sup>th</sup> (blue) percentiles for all sample nights in Milton Keynes city.....	172
<b>Fig. 5.16</b> Skewness for all sample nights in Milton Keynes city.....	172
<b>Fig. 5.17</b> Kurtosis for all sample nights in Milton Keynes city.....	172

## List of Figures in Supplementary

<b>Fig. 3S1</b> As for Figure 1 of the main text but re-drawn on log-log axes to show the power-law scaling. Reported on the graph (top right) are the Coefficient of Determination ( $R^2$ ) for the best-fit regression, the slope of the regression, and the error on the slope ( $\epsilon$ ).....	131
<b>Fig. 3S2</b> (A) Relationship between total city area and total population for 35 cities in Great Britain. The allometric regression relationship shown has a coefficient of determination ( $R^2 = 0.961$ ) and slope = $0.86 \pm 0.03$ . (B) Residuals (equation 2, main text) of city area plotted against city population. The best-fit regression values are reported but are not significant.....	131
<b>Fig. 3S3</b> Relationship between emitted energy and urban area for 35 cities in Great Britain. Reported on the graph (top right) are the Coefficient of Determination ( $R^2$ ) for the best-fit regression, the slope of the regression, and the error on the slope ( $\epsilon$ ).....	132
<b>Fig. 3S4</b> Hierarchical Area distribution for the 35 biggest cities in Great Britain.....	136
<b>Fig. 3S5</b> Hierarchical population distribution for the 35 biggest cities in Great Britain.....	136
<b>Fig. 3S6</b> Relationship between total emitted energy and total population across Cities in Great Britain for selected nights, listed in Table 3. Each colour represents a different night. Allometric regressions are plotted for each night, the equations for which are reported in Table 3. The overall best straight line through the data is $0.86 \pm 0.05$ .....	137
<b>Fig. 3S7</b> Residual Summary plot for all dates sample at 75% cloud free pixel.....	137
<b>Fig. 3S8</b> Residual Summary plot for all dates sample at 50% cloud free pixel.....	137
<b>Fig. 3S9</b> Mean Residuals plots Vs Mean Annual Temperature.....	138
<b>Fig. 3S10</b> Mean Residuals plots Vs Hours of Sunshine.....	138
<b>Fig. 3S11</b> Mean Residuals plots Vs Altitude.....	139
<b>Fig. 3S12</b> Mean Residuals plots Vs Latitude. The regression is not significantly different from zero and explain 0.3% of the variance.....	139

<b>Fig. 4S1</b> Relationship between total areas and total population across Cities in Nigeria. The allometric regression relationship shown has a coefficient of determination ( $R^2 = 0.749$ ) and slope = $0.41 \pm 0.04$ . (B) Residuals of urban area plotted against urban population. The best-fit regression values are reported but are not significant.....	141
<b>Fig. 4S2</b> Relationship between total emitted energy and total area across 33 cities in Nigeria. Reported on the graph (top right) are the Coefficient of Determination ( $R^2$ ) for the best-fit regression, the slope of the regression, and the error on the slope ( $\epsilon$ ).....	141
<b>Fig. 4S3</b> Hierarchical Area distribution for the 33 biggest cities in Nigeria.....	146
<b>Fig. 4S4</b> Hierarchical population distribution for the 33 biggest cities in Nigeria.....	146
<b>Fig. 4S5</b> Relationship between total emitted energy and total population across Cities in Nigeria for selected nights, listed in Table 1. Each colour represents a different night. Allometric regressions are plotted for each night, the equations for which are reported in Table 1. The overall best straight line through the data is $0.40 \pm 0.05$ .....	147
<b>Fig. 4S6</b> Residual Summary plot for all dates sample at 75% cloud free pixel.....	147
<b>Fig. 4S7</b> Residual Summary plot for all dates sample at 50% cloud free pixel.....	147
<b>Fig. 4S8</b> Classification of field sites by local climate zone (LCZ) according to some selected cities in Nigeria.....	155

## List of Tables

<b>Table 2.1</b> Suggested Causes of Urban Heat Island Effect.....	13
<b>Table 3.1.</b> Night-time emitted energy for thirty-five (35) UK large Cities on selected summer and winter nights. Results are ranked by the strength ( $R^2$ ) of the log-log correlation between emitted energy and population, for which the slope, and error on slope ( $\epsilon$ ) are reported at 50% cloud free pixels.....	45
<b>Table 4.1.</b> Night-time emitted energy for thirty-five (33) large Cities across Nigeria on selected nights. Results are ranked by the strength ( $R^2$ ) of the log-log correlation between emitted energy and population, for which the slope, error on slope ( $\epsilon$ ), and intercept are reported at 50% cloud free pixels.....	66
<b>Table 5.1.</b> A statistical description of the long-wave energy distribution for the three case-study cities for 2 <sup>nd</sup> January 2017.....	81
<b>Table 5.2.</b> All cities ranked by skewness for selected sample night 2 <sup>nd</sup> January 2017.....	92
<b>Table 5.3</b> Emission Distribution in London for all sample nights (dates) discussed in chapter 3.....	93

**Table 5.4** Emission Distribution in Sheffield for all sample nights (dates) discussed in chapter 3..... 95

**Table 5.5** Emission Distribution in Milton Keynes for all sample nights (dates) discussed in chapter 3

.....95

## List of Tables in Supplementary

**Table 3S1.** Hierarchical population distribution and area for 35 biggest cities in Great Britain (50km<sup>2</sup> and above; source: Meridian data 2017)..... 130

**Table 3S2.** Residuals for Emitted Energy and surface area for 35 biggest cities in Great Britain (cities are ranked by emitted energy residuals)..... 133

**Table 3S3.** Summary of night-time emitted energy scalings for thirty-five (35) UK large Cities on 28 selected summer and winter nights between 2000 and 2017. Results are ranked by the strength ( $R^2$ ) of the log-log correlation between emitted energy and population, for a threshold for inclusion of a city in the scatter plot of 75% cloud-free pixels. The table reports the allometry slope, error on slope ( $\epsilon$ ), intercept, and sample size at 50% and 75% cloud free pixels..... 134

**Table 3S4.** Summary of night-time emitted energy for UK large Cities with populations **>250,000 and >500,000** on selected summer and winter nights. Results are ranked by the strength ( $R^2$  [50%]) of the log-log correlation between emitted energy and population, for which the slope, error on slope ( $\epsilon$ ), and intercept are reported..... 135

**Table 4S1.** Hierarchical population distribution and area for 33 biggest cities across Nigeria (cities within the limit of 50km<sup>2</sup> and above. (Source: (SEDAC, 2017))..... 140

**Table 4S2.** Distribution of Emitted energy and area for 33 biggest cities across Nigeria..... 142

**Table 4S3.** Summary of night-time emitted energy for thirty-three (33) large Cities across Nigeria on 23 selected nights between 2000 and 2017. Results are ranked by the strength ( $R^2$  [50%]) of the log-log correlation between emitted energy and population, for a threshold for inclusion of a city in the scatter plot of 75% cloud-free pixels. The table reports the allometry slope, error on slope ( $\epsilon$ ), intercept, and sample size at 50% and 75% cloud free pixels..... 143

**Table 4S4.** Summary of night-time emitted energy for Nigeria's large Cities with populations **>250,000 and >500,000** on selected nights. Results are ranked by the strength ( $R^2$ ) of the log-log correlation between emitted energy and population, for which the slope, error on slope ( $\epsilon$ ), and intercept are reported..... 144

**Table 4S5.** Residuals for Emitted Energy and surface area for 33 biggest cities in Nigeria (cities are ranked by emitted energy residuals)..... 145

## **List of Acronyms**

AVHRR: Advanced Very High-Resolution Radiometer

ASTER: Advanced Spaceborne Thermal Emission and Reflection Radiometer

CBD: Central Business District

CEDA: Centre for Environmental Data Analysis

CPRE: Campaign to Protect Rural England

DJF: December, January, February

DLUA: Developed Land Use Areas

EMR: Electromagnetic Radiation

EOS: Earth Observation Satellite

GHG: Greenhouse Gas

GIS: Geographic Information System

GOV: Government

IDW: Inverse Distance Weighted

IPCC: Intergovernmental Panel on Climate Change

JJA: June, July, August

LCZ: Local Climate Zone

LPDAAC: Land Processes Distributed Active Archive Center

LST: Land Surface Temperature

LWIR: Long-wave Infrared

MODIS: MODerate resolution Imaging Spectroradiometer

MW: Megawatts

NPCN: National Population Commission of Nigeria

OECD: Organisation for Economic Co-operation and Development

ONS: Office of National Statistics

Org: Organisation

SEDAC: Socio-Economic Data and Applications Centre

SUHI: Surface Urban Heat Island Intensity

SVF: Sky View Factor

TIR: Thermal Infrared

TM/ETM+: Thematic Mapper/Enhanced Thematic mapping Plus

UHI: Urban Heat Island

UK: United Kingdom

UN: United Nations

UNDP: United Nations Development Programme

US: United State

USGS: United State Geological Survey

VIS: Visible

WUDAPT: World Urban Database and Access Portal Tool

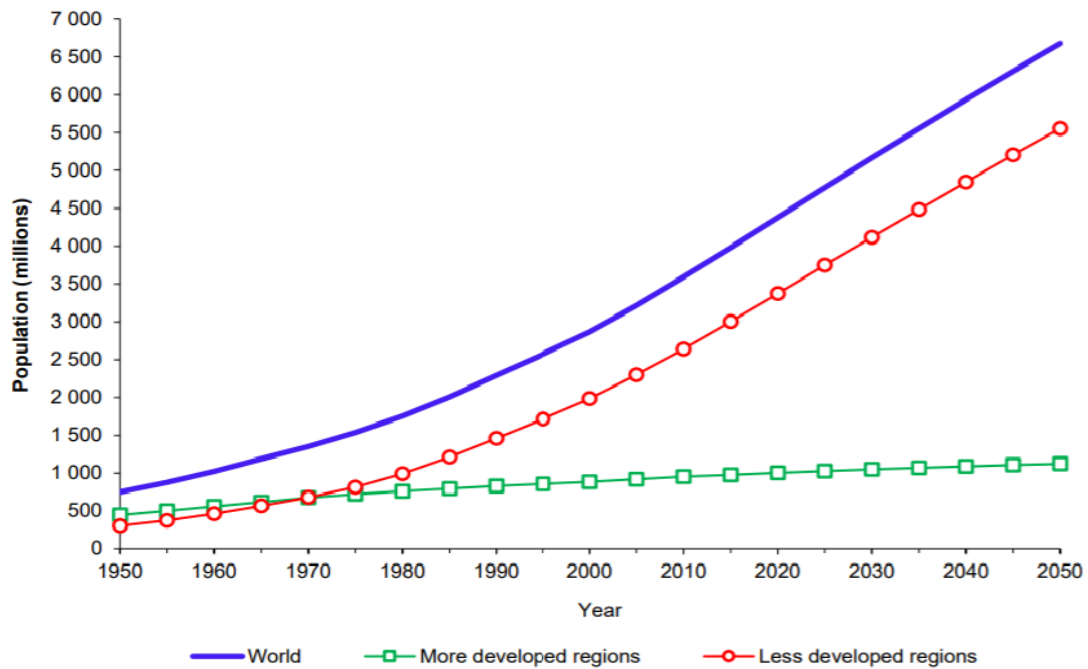
# **1.0 Chapter 1**

## **INTRODUCTION**

This opening chapter gives a broad overview of urbanization and its unintended consequence to urban areas. These impacts will not only affect the urban population but can also modify the earth's climate. The growth of urban areas causes urban heat Island (UHI) at city scale, where urban landscape experiences higher air temperature than its surrounding suburbs (Oke, 2002; Wang et al., 2016; Sheng et al., 2017; Li et al., 2019). Recently, the impact of vertical urban morphological components as a cause of UHI intensity is being investigated (Equere et al., 2020). This rise in global temperature due to urbanization and increase in Greenhouse effect trigger the need to understand the energy balance of the cities and the extent to which it is modified by urban form. This thesis investigates the spatial patterns of urban form on urban climate. This chapter presents a general overview of how city at neighbourhood scale impacts on urban climate. The chapter closes with the objectives of the study and the overall structure of the thesis.

## **1.1 Urbanization**

Half of the world's population (3.42 billion) as of 2009 lived in urban areas and this is projected to increase to 6.3 billion (68.7%) by 2050 (UN 2010; United Nations et al., 2019), with most of this growth to take place in Africa and Asia (Cohen, 2003; McGranahan and Satterthwaite, 2003 Bongaarts, 2009; Bremner et al., 2010; Puseerit et al., 2019). The extent and rate of global environmental changes, i.e. greenhouse effect, deforestation, flooding, UHI, etc. are largely driven by the rapid growth of the world's population. Figure 1.1 adopted from United Nations et al., (2019) showing estimated and projected urban populations of the world, the more developed regions and the less developed regions, 1950 – 2050



**Figure 1.1 Graph showing estimated and projected urban populations of the world, the more developed regions and the less developed regions, 1950 - 2050 (adopted from - United Nations et al., (2019)**

This growth, especially in cities, put significant demands on public services such as housing, transport infrastructure, health facilities, education, and employment, among others. Lack of these result in emergence and widespread slum and squatter settlements which pose a threat to the urban environment (Santamouris, 2013).

Settlements are far more informal than cities. The term 'settlement' is used here to refer to any place where people establish a community, whether temporary or permanent (Chang, 1962). A place of social and cultural interactions among people for the purpose of business or a densely populated area comprising mostly man-made activities involving all the administrative, cultural, residential, social, and religious functions among others in a society can be regarded as urban settlement. In some countries like Russia (former Soviet Union) and India, official urban municipalities may be regarded as an urban settlement if they meet the population and density criteria set by the Country's government. An urban settlement could have a population of a few thousand. In more developed Countries, an area is not considered urban unless it has a much larger population. In terms of density, the U.S Census

Bureau defines an urban area as having more than 50,000 people and at least 1,000 people per square mile (Massion, 2017)

The UK definition of settlement depends on an underlying Rural-Urban (RU) definition, in its original (RUC2001) and the updated (RUC2011) forms, both of which rely on physical characteristics. The 2001 census recommend that any physical settlement with a population of 10,000 or more should be treated as 'urban settlement' and all smaller settlements were to be treated as 'rural settlement' (Bibby and Brindley, 2013). The identification of urban settlement in Nigeria is based on population and legal or administrative criteria. A settlement comprising of 20,000 people or more is regarded as 'urban settlement', a relatively high minimum threshold compared to other Countries (Ofem, 2012).

These differences are important. Formal urban areas are more likely to be subject to planning control whereas settlements simply occur and evolve naturally (unplanned). This has implications for the delivery of services and ultimately, quality of life. Significant studies of urban settlements have been carried out by researchers from a variety of disciplines (Turner, 1968; Xu et al., 2014). According to Hillier et al., (1987), the plan of settlements may be perceived as singularly uninformative at a glance. He is also of the view that most settlements originated from the same kinds of basic spatial elements; "closed impermeable" elements such as dwelling, shops, public buildings, etc., which by their aggregation define a "permeable open" system of more or less open public space, street, alleys, squares, etc., which join the whole settlements together into a continuous system. It is the relationship between these "impermeable closed" and "permeable open" elements to form a global spatial thermal pattern, which both gives a settlement its spatial thermal individuality (i.e., the urban form) and permits its identification as a member of a generic class of similar settlements.



## **1.2 Planning Theory: The Evolution of Cities**

Planning theory provides a useful account of how cities evolve. Patrick Geddes, a scientist by profession became involved in the development of town planning in the early twentieth century and devoted half a century advocating how communities can be planned to meet up the needs and aspiration of the inhabitants (Goist, 1974; Payton, 1995). Cities exist to support the socio-economic functions of the society. Jacobs, (1962), in her study of New York, was of the view that cities are complex objects just like most geographical phenomena. The complex mix of urban activities clearly functions with a logic of its own, but logic however, as cities are one of the most successful creations of human society. As most cities exhibit this complexity, it is rational to presume that complexity is in a way an essential quality of them. Jacob's evidence was subjective, but research on the theory of dynamical and evolutionary systems provides fundamental evidence that complexity is an essential characteristics feature of cities (White and Engelen, 1993; Newman and Kenworthy, 1999).

## **1.3 Inadvertent Modifications of Urban Areas**

To appreciate the sustainability of a city, there must be a clear and common-held concept of what urban form will look like, how it will function, and how it will change over time. Anderson et al., (1996) sees urban form as a spatial pattern of human activities at a certain point in time. Urban form can be perceived differently according to geographical scales and categorical levels as metropolitan area, city and neighbourhood (Tsai, 2005). Interestingly, the study of form is difficult such that urban form is often characterized by simple geometries that postulate idealised structures (Winsborough, 1962). The urban spatial structure is a broader concept, according to Anderson et al., (1996) cited in Bourne, (1982), it consists of three elements; the urban form, urban interactions, and a set of organising principles that define the relationship between the two. The important aspect here is that urban form has an intense influence on the flows within the city but does not determine them completely.

According to Ellis, (2014), the fundamental requirement for a city can be categorised into three components: namely networks, buildings and open spaces. Ancient cities relied on streets, mostly narrow to transport food and animals. These cities subsequently grew and evolved with an increasing dependency on complex hierarchical mode of transportation, ranging from ten-lane freeways to pedestrian walkways (Neuman and Smith, 2010). Cities in America, the majority of trips are carried by the private automobile and mass transit for distant trips. This is in contrast to many European cities in which rail transit (account for a large proportion of passenger journeys/some other criterion) (Bauman and Muller, 2006). During the nineteenth century, developed countries began to install adequate sewer and water systems due to rapid growth and industrialization, which resulted in pollution, overcrowding and diseases in the urban areas (Rose, 2001). More facilities such as electricity, gas, and communication signals followed in the late nineteenth century. The cities experienced an organic (unplanned) trend of buildings during the industrial revolution, mostly residentials occupying about 50% of all urban land, with building types ranging from high density to low scattered single-family homes (Chadwick, 1842). Commercial buildings are clustered at the city centre (downtown) and at various sub-centres, with skyscrapers concentrated in the central business districts (C.B.D) and low-rise predominantly elsewhere (Whitehand, 2001).

The concentration of an increasing part of population as well as the economic activities into urban areas is characterized by changes in human settlement pattern and urban climate (Wiedenhofer et al., 2013). This pattern reflects the shift from agricultural economy to urban economy in which most people are employed in activities that are more spatially clustered. The pattern is more prominent in developing nations but shows a decline in the developed countries where 75% of the population are now inhabiting urban areas (Beale, 1975; Vining and Kontuly, 1978). Urban sprawl is another pattern of urban form, characterized by a general decline in intensity of all forms of land uses and an outward expansion of conurbation boundaries that separate urban from rural land uses. As cities grow larger in this way, previously green space is replaced by concrete and tarmac surfaces dramatically altering the energy balance of the location. This inadvertent modification significantly elevates urban

temperatures in a phenomenon called UHI (Oke, 1981; 1995). This has implications not only on temperature, but can also lead to urban precipitation anomalies (Changnon, 1992; Han et al., 2013), urban thermal plumes (T. R. Oke, 1995). It is important therefore to understand the effects of urbanization and the impact of an altered environment on human settlement.

The science of understanding urban climate has matured significantly during the past few decades (Grimmond et al., 2010). Recent studies on UHI have stressed the importance of land-use / land-cover within cities (Stewart and Oke, 2012; Tomlinson et al., 2012), emphasizing the systematic understanding of the climate-based response to urban planning and design strategies (Davoudi et al., 2009; Wamsler et al., 2013). The effect of urban form (sky view factor, street geometry and orientation, density and other morphology parameters) on microclimate differ according to climate conditions and spatial scale (Oke, 1981; Ng et al., 2011). This work is typically conducted at the micro- or meso scale, but cities are more than just a sum of their parts and hence there is scope to investigate the role of the city as a whole. If this can be achieved, a better understanding of how city scale planning and urban morphology impacts more broadly to inadvertent climate modification.

In terms of allometry, the term 'scaling' refers to the study of how the structure and behaviour of a system varies with its size, and results in the derivation of a power-law relationship (Wu et al., 2006). A phenomenon is assumed to be scaling if it lacks any characteristic length scale, i.e., its behaviour is independent of scale and defined by a power-law relationship (Wood, 1998) cited in Wu et al., (2006). This definition has long been adopted by biologist in terms of allometry that primarily relates to the relation between shape and size of organisms (Schmidt-Nielsen, 1984). In this context, it refers " the study of the influence of body size on form and function" (LaBarbera, 1989).

For urban studies, the 'organism' under study is the urban settlement and the 'length scale' is usually taken to be population (although other measures of size have been employed). Many urban allometry studies employ data aggregated at the scale of the urban settlement (e.g., Gross Domestic Product, crime statistics, and new business start-ups). These data will generally be available for all urban

settlements with sufficient administrative infrastructure to generate the data themselves, or for urban settlements to which national statistics are disaggregated by national agencies (e.g., census data).

Data on the physical form of cities (e.g., road length) are typically deduced from maps and geographic information systems. 'Space-filling' observations of urban characteristics (e.g., air pollution, radiative temperature) nearly always derive from Earth observation (EO) from aircraft or satellite. The spatial resolution of the EO data defines the minimum size of urban settlement that can be studied and 'pixelates' the irregular edge of urban settlements (see, for example, the appendices to chapter 5 of this thesis)

Therefore, although the urban form leads to local changes to urban climate, it is postulated that this will scale depending on how the city has developed over the years. Hence, by studying the bulk properties of cities, and how they impact on the climate of the city more generally, it is hypothesised that insights can be derived into the role of urban form more generally. This thesis seeks to contribute to this knowledge gap through assessment of the role of urban form in modifying the energy budget of the city and the extent of this modification using an allometric scaling model - a concept of studying the relationship between shape and size of a city. Earlier the evolution of the city and its organic modification as well as its effects on climate change in a general context is discussed, as this is a key rationale for undertaking this work. The chapter finally outlined the primary research aims and objectives.

## **1.4 Research Aims and Objectives**

### ***1.4.1 Aims***

The primary aim of this study is to investigate whether city-scale settlement patterns produce predictable effects on urban climatology. Drawing on the arguments outlined above, this aim requires

a measure of city-scale – population – and a measure of city-wide urban thermal properties for a range of cities with varying urban morphologies.

### **1.4.2 Objectives**

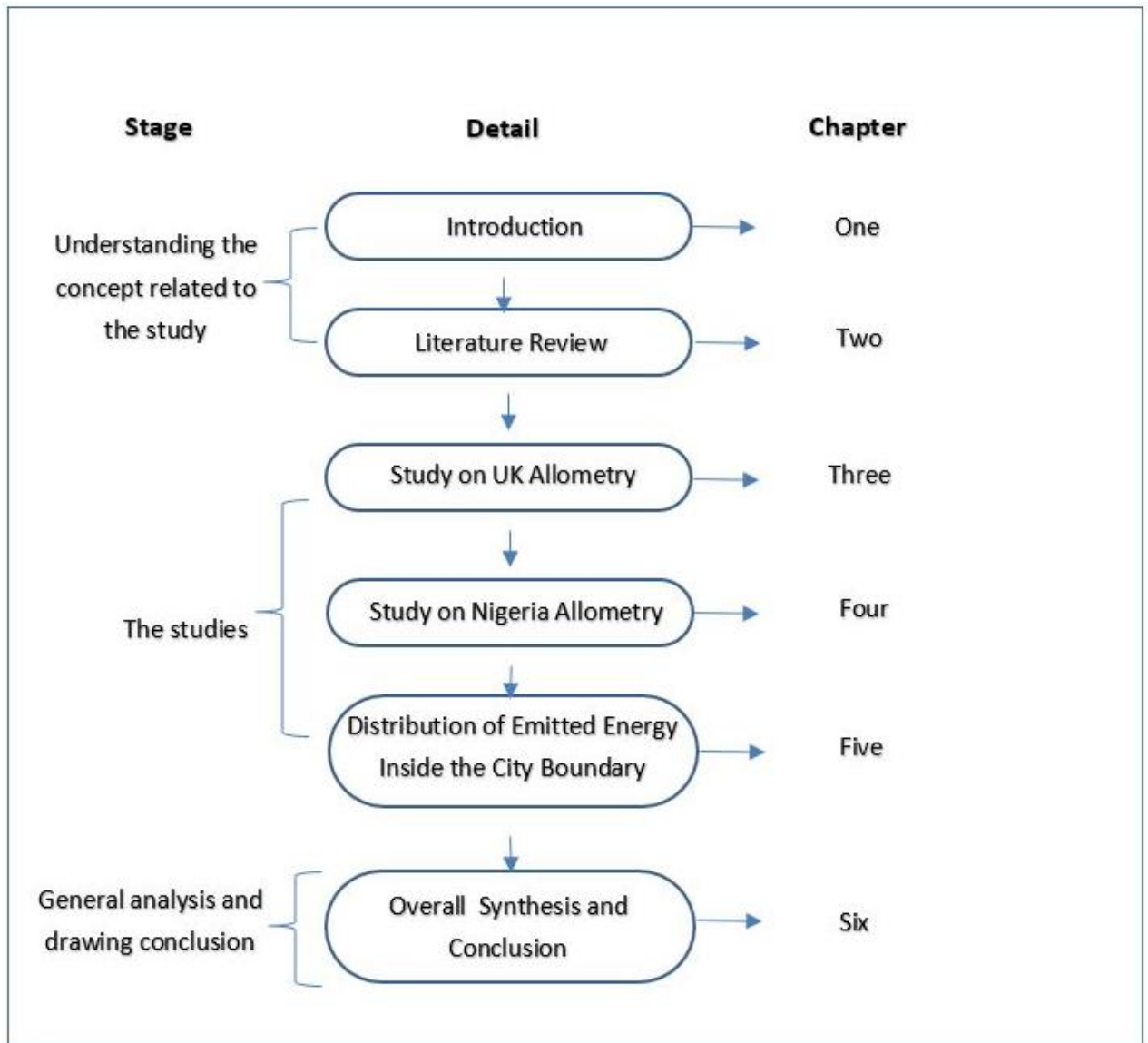
This aim will be realised by the following objectives:

1. Explore the relationship between urban morphology and the bulk thermal properties (emitted energy) of cities in the UK through appropriate scaling techniques i.e., by sampling MODIS data overpasses 2000 and 2017 to examine the seasonal variability in the night-time surface thermal climate for sample cities. Area-summed emitted thermal infrared for each city and each night shall be explored and interpreted by looking at the allometric scaling against the total population of the urban area.
2. Translate the methodology into the developing world within a different context of settlement, urban morphology, and planning constraints.
3. Explore how the spatial distribution of emitted energy within UK cities provides additional information regarding the unique urban form beyond that of a city-scale analysis.

## **1.5 Thesis Structure**

The study is structured into six (6) chapters, which comprise of the followings (Figure 1.2):

- Chapter One: Introduction, research gap, aims and objectives.
- Chapter Two: Theoretical framework of the study including literature review.
- Chapter Three (Paper 1): Allometric scaling of thermal infrared emitted from UK cities and its relation to urban form
- Chapter Four (Paper 2): Allometric scaling of emitted thermal infrared across Nigeria's cities and its relation to urban form
- Chapter Five (Paper 3): The spatial distribution of emitted energy within UK cities
- Chapter Six: Synthesis and conclusion



**Figure 1.2 Conceptual Framework and Study Structure**

## **2.0 Chapter 2**

### **Literature Review**

Following on from the research gaps and associated aims and objectives highlighted in Chapter 1, this literature review is separated into two parts. Part 1 will primarily focus on the contributing impact of urban form on urban heat (at the micro and meso scale). Part 2 will focus more on the role of bulk properties of cities followed by a discussion on the potential role of allometric scaling.

### **2.1 Urban Climate**

Urbanization is estimated to result in about 6 billion urban dwellers by 2050 (UN 2010; United Nations et al., 2019) with the world experiencing its most unprecedented urban growth, especially in developing countries in the mid twentieth century (Chadchan and Shankar, 2009). The expansion of cities to accommodate the continued growth of population has both local and global implications on weather and climate due to the significance of land cover changes (Pielke, 2013). Studies have demonstrated that these changes have greatly impacted on the surface temperature of the Earth (Balling and Cerverny, 2003; Bounoua et al., 2004).

The recent trend in urbanization has led to a proliferation of studies on urban climate and how effects can extend beyond the city, affecting the climate at regional scale, e.g., (Karl et al., 1988; Cui and Shi, 2012; Miller and Hutchins, 2017) and global scale, e.g., (Goldstein, 1990; Cohen, 2006; Grimmond, 2007). Urban areas have well documented effects on environmental climate modification, e.g., changes in cloud cover (Changnon, 1992; Rabin and Martin, 1996; McCoy et al., 2017; Toomey, 2017; Mao et al., 2019), reduced wind speeds (Lee, 1977; Guo et al., 2011; Ouahabi et al., 2017), changes in precipitation (Palumbo and Mazzearella, 1980; Han et al., 2013). Mishra,(2019) investigated changes in cloud cover using the relationship between precipitation extremes and clouds. Another area is increasing atmospheric turbulence (Oke, 1970; Arnfield, 2003) and, most relevant for this thesis, the

well documented Urban Heat Island (UHI) effect, e.g. (Oke, 1973; Landsberg, 1981; Wang et al., 2016; Li et al., 2019), and the surface UHI intensity (SUHI), e.g., (Peng et al., 2012; Zhou et al., 2017).

The UHI is a phenomenon whereby urban areas experience elevated temperature compared to their rural surroundings (Oke, 1973; 1982; Sheng et al., 2017; Li et al., 2019). This is due to the modification of the energy balance primarily through the replacement of pervious vegetated surfaces with impervious built surfaces. The SUHI is derived from the LST (from satellite) which is present at all times of the day and night . There are also other important factors to consider such as anthropogenic heat emissions, that result in higher temperatures in the built urban environment (Landsberg, 1981; Ichinose et al., 1999; Bohnenstengel et al., 2014; Lu et al., 2017; Wang et al., 2018). Indeed, cities are mediators of significant environmental impacts at local, regional and global scales, as such represent an important geographical scale to curtail the present global environmental challenges (IPCC, 2014). For example, increases in Greenhouse Gas (GHG) emissions, air pollution and other major consequences of urbanization exposes human health at risk (Basu and Samet, 2002; Patz et al., 2005; Smith et al., 2011) and also alter the urban climate by intensifying extreme weather conditions and heat waves (Patz et al., 2005; McCarthy et al., 2010). For example, about 15,000 death were recorded in the 2003 hot summer in Europe, due to heat related illness in Paris (Wright et al., 2016). About 50% excess mortality was recorded in the West Midlands region, UK during the August 2003 heat wave (Heaviside et al., 2015; 2016). Over 70,000 excess deaths was recorded throughout Europe during the summer of 2003 heat wave (Robine et al., 2008), more than 800 death toll in Chicago during the 1995 heat wave (Changnon et al., 1996).

## **2.2 Urban Heat**

The UHI effect was first discovered in the early 19<sup>th</sup> Century (Howard, 1833). It is a phenomenon that affects the lives of people around the world. The unprecedented urban population and infrastructure growth along with enhanced manmade activities, increased surface roughness, buildings, roads, and



other infrastructure replace open land and vegetation often result in the formation of UHI, especially at night as the urban areas experience elevated temperature compared to their rural surrounding (Oke, 1973; 1982; Sheng et al., 2017). Several factors contribute to the formation of UHI. Urbanization involves concentration of population, loss of natural surface and expansion of dwelling space. All these factors alter the energy balance, and generates a climate typical of urban areas (Yamamoto, 2006). This may be regarded as one of the major causes of UHI, i.e. the density and population of an urban area with its associated anthropogenic activities (Oke, 2002; Arnfield, 2003). Other factors contributing to UHI include; reduced sky view factors, i.e., canyon geometry in the central part of a city contribute in producing nocturnal UHI by trapping the outgoing long-wave radiation due to blockage of the sky by tall buildings (Oke, 1981; Oke, 2002), removal of vegetation alters the surface properties, as such modify the energy and mass balance (Oke, 2002; Alavipanah et al., 2015), anthropogenic heat from vehicles, air conditioners which stores and re-radiate heat from urban structures- (Memon et al., 2008). These factors are summarised in Table 2.1.

#### **a. Urban canopy layer heat island**

	Altered energy balance terms leading to positive thermal anomaly	Features of urbanization underlying energy balance changes
1	Increased absorption of short-wave radiation	Canyon geometry – increased surface area and multiple reflection
2	Increased long-wave radiation from the sky	Air pollution – greater absorption and re-emission
3	Decreased long-wave radiation loss	Canyon geometry – reduction of sky view factor
4	Anthropogenic heat source	Building and traffic heat losses
5	Increased sensible heat storage	Construction materials – increased thermal admittance
6	Decreased evapotranspiration	Construction materials – ‘water-proofing’
7	Decreased total turbulent heat transport	Canyon geometry – reduction of wind speed

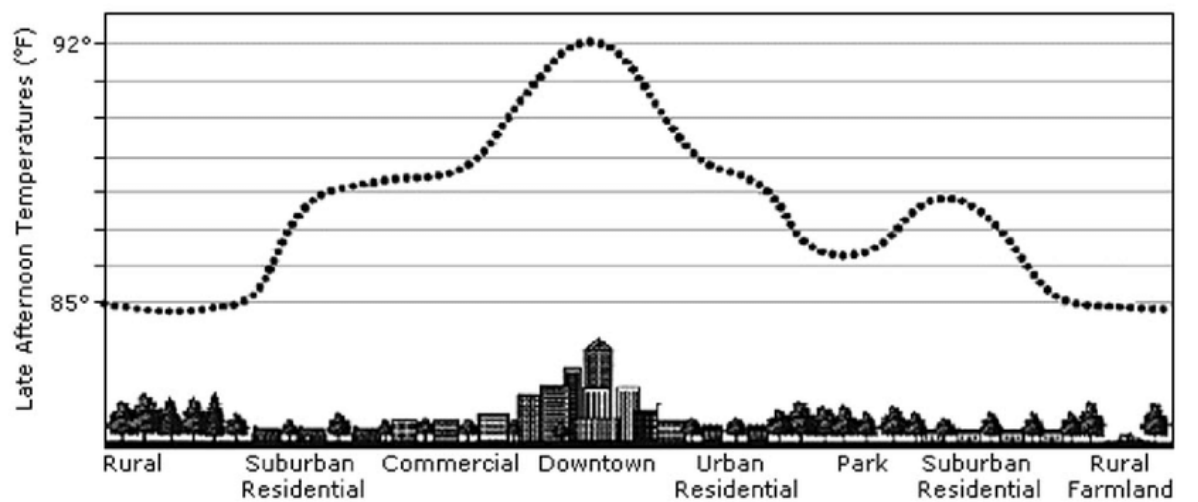
#### **b. Urban boundary layer heat island**

	Altered energy terms leading to a positive thermal anomaly	Features of urbanization underlying energy changes
1	Anthropogenic heat source	Chimney and stack releases
2	Increased sensible heat input – entrainment from below	Canopy heat island – increased heat flux from canopy layer and roofs
3	Increased sensible heat input – entrainment from above	Heat island, roughness – increased turbulent entrainment

4	Increased absorption of short-wave radiation	Air pollution – increased aerosol absorption

**Table 2.1 Suggested causes of urban heat island effect - after Oke, (1982)**

Figure 2.1 from Frumkin, (2002), demonstrates the typical cross profile of the UHI showing the relative variations in temperature experienced in different landuse types during late afternoon. Temperature is at its peak in the downtown where the city centre (CBD) is located with most of the landscape being replaced with impervious surface (buildings, road infrastructures, etc.) and temperature is at its minimum in the rural areas where there is an abundance of vegetation and farmland.



**Figure 2.1 A Typical Urban Heat Island (UHI) Profile Sketch (uploaded from (Frumkin, 2002)) - originally from (Oke, 2002)**

UHI intensity is measured by the difference between the urban and the rural temperature. Although present to some degree under all weather conditions, the effect is most noticeable at night under clear skies and calm winds (Oke, 1973; Landsberg, 1981; Arifwidodo and Tanaka, 2015).

## 2.3 Measuring the Urban Climate

Given the magnitude of the UHI, there is a growing need for meteorological observations as the urban population expands. Meteorological services are increasingly required to supply meteorological data for climate measurement of the urban environment. There are several ways to measure urban climate,

the surface UHI can be measured using fixed ground-based sensors, mobile vehicle mounted sensors (station pair), or through satellite data (remote sensing) (Oke, 1995; Oke, 2006). Previous studies have assessed the UHI at regional scale through the analysis of land surface temperature (LST) from satellite data (Yuan and Bauer, 2007; Mackey et al., 2012; Zhao et al., 2014; Bokaie et al., 2016; Mushore et al., 2019) and meteorological data from weather stations across developed areas (Peterson, 2003; Huang et al., 2008; Mohan et al., 2013).

### ***2.3.1 Station Pair***

This is the most traditional way of measuring the UHI effect – e.g., Voogt and Oke, (1997). A conventional arrangement of sensors consists of urban sites (although most cities are lucky to have even a single station) paired with nearby rural sites for comparison. The sensors are typically found at airports or meteorological stations, or even strategically placed across a city and its rural sites (Oke, 2006). Important criteria attached to this method is that the sensors must be adequately shaded and ventilated to provide reasonable measurements. Its major limitation is securing a suitable (i.e. representative) site to locate the stations (Oke, 2006). A number of studies have used this method for measuring urban climate – e.g., Karl et al., (1988) used a network of 1219 stations across US to analyse the effect of urbanisation on urban climate in small towns; Eliasson (1996) used two climatic stations sets in the central city of Sweden to analyse the influence of wind effect and cloud cover to urban air temperature and found out that UHI intensity decreases with increasing wind speed and cloud cover. The main limitation of this technique is the lack of sites available for analysis.

### ***2.3.2 Ground/Air Transect***

Often used as a method to infer temperature changes between fixed sites, logging devices are usually mounted on cars or aircrafts to perform measurement around the city and its countryside. This method is prominent for assessing and quantifying canopy layer UHI, e.g., (Unger, 2006; Unger et al., 2011). The ground transects (by car) is cost effective, although a number of people are required at the same time to carry out the transect measurement. Mobile transects are effective for sampling the

microscale features of an UHI, e.g., park or factory sites, weather condition and times of the day. Chandler, (1962) used a mobile traverse route to measure temperature difference between the warmest and coolest points of London; Sundborg, (1951), cited in (T.R. Oke, 1995), measured temperature difference between urban and rural areas of Uppsala, Sweden with stationary and/or mobile sensors. Despite their high resolution, mobile transects are temporally limited with the sampling period rarely exceeding several hours. The aircraft transect is impractical in the urban environment due to its limited resolution and that it provides only a snapshot of current conditions. Indeed, the main limitation of transect approaches is the practicalities of providing continuous data.

### ***2.3.3 Remote Sensing***

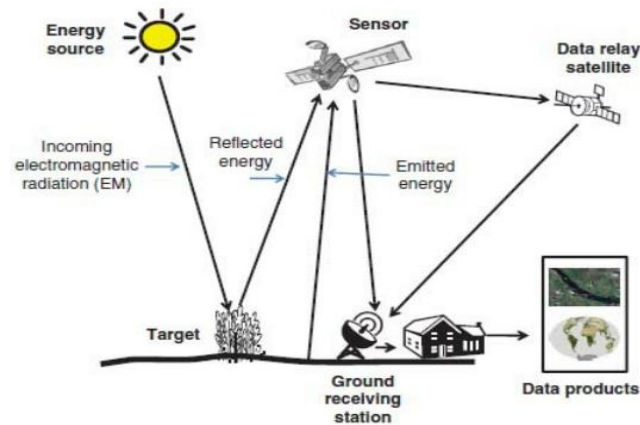
Remote sensing refers to the act of ‘recording, observing, and perceiving (sensing) objects or events through the analysis of data acquired by a device that is not in contact with the objects or phenomenon under investigation’ (Lillesand et al., 2015). Remote sensing techniques are usually built on reflectance, emittance or modification of electromagnetic radiation, and the output displayed as an image representing the scene being observed. Remote sensing may be the science of acquiring information about the earth’s surface (land and sea), and atmosphere using sensors onboard airborne (e.g. aircraft or balloons) or spaceborne (e.g. satellites and space shuttles) platforms (Weng, 2010).

The technology of remote sensing gradually grew into scientific subject after World war II. Remote techniques were initially used by the military, and later became widely applied for civil application. Since then remote sensing has been used across a variety of different fields e.g. meteorology and climatology couple with the use of Geographic Information Systems (GIS) for spatial analysis (Chapman and Thornes, 2003; Shalaby and Tateishi, 2007; Weng, 2010), land use land cover, e.g., (Anderson, 1976; Fichera et al., 2012; Chen et al., 2019), coastal studies e.g., (Fan et al., 2009; Zhang et al., 2014), natural forest, e.g., (Griend and Owe, 1993; Mundia and Aniya, 2005; Alonzo et al., 2015) among others.

Depending on the scope, remote sensing may be categorised by platform (i.e., tower, aircraft, drone, satellite), by spectral wavelength (i.e., ultraviolet, visible, infrared, radio-wave), by light source (particularly active versus passive techniques), and by whether the returned signal can be processed as an image. Examples include:

- a. Satellite remote sensing – when satellite platforms are used to carry the remote sensing instrument
- b. Photography and photogrammetry – when photographs are captured using reflected visible light and physical characteristics of objects estimated from analysis of overlapping images.
- c. Thermal remote sensing - when the thermal infrared portion of the spectrum is used to capture emitted radiation
- d. Radar remote sensing – active sensing using detection of microwave and radiowave wavelengths sent out from the instrument
- e. Lidar remote sensing – active sensing when laser pulses are transmitted toward the ground and the distance between the sensor and the ground is measured based on the return time of each pulse (Qihao, 2012).

There exists a number of platforms that have been used in the field of urban studies. The fundamental requirement for remote sensing is the detection of electromagnetic radiation (EMR) by sensors on a remote sensing platform. The sensors (for instance, digital scanners and special types of cameras) can be installed in aircraft, satellites, or space shuttles to take pictures of the objects or events on the Earth's surface. These sensors are not in direct contact with the objects or events being observed. Information about the object is transmitted to the sensor as electromagnetic radiation through an intervening medium (the atmosphere). The outcome of a remote sensing is often an image depicting the objects or events being observed (Qihao, 2012). Figure 2.2 shows an example of remote sensing.



**Figure 2.2** An illustration of a remote sensing process, showing a passive, satellite-borne sensor receiving reflected solar radiation and emitted terrestrial radiation. The sensor signal is passed to a ground receiving station, sometimes via a data relay satellite, and converted into a data product in post-processing (sourced from Qihao, 2012).

For example, the relationship between remotely sensed images at spatial resolution and spatial area at geographic scale has been explored (Quattrochi and Goodchild, 1997). For example, IKONOS and QuickBird provide high spatial resolution images, e.g., (Herold et al., 2003), and have been used to investigate the spatiotemporal form of urban growth in Santa Barbara, (Nichol and Wong, 2005). Studies such as this demonstrate the ability of satellite-based systems to depict parameters of urban environment over large areas at detailed level, (Tomlinson et al., 2012). At the city/regional scale, coarser imagery such as Landsat Thematic Mapper/Enhanced Thematic mapping Plus (TM/ETM+) and Terra Advanced Spaceborne Thermal Emission and Reflection Radiometer (ASTER) data are mostly utilized e.g., (Yuan and Bauer, 2007; Weng and Lu, 2008; Zhang and Seto, 2011; Yang et al., 2015; Bahi et al., 2016). The Advanced Very High-Resolution Radiometer (AVHRR) and Moderate Resolution Imaging Spectrometer (MODIS) data employed by coarse-spatial-resolution imagery, are mostly based at global scale, e.g., (Friedl et al., 2002; Schneider et al., 2009). The MODIS is a remote-sensing instrument on both NASA's Terra and Aqua missions, and is designed to provide simultaneous data about land, ocean, and atmospheric processes (see subsection 2.3.5 for more detail).

### ***2.3.4 Satellite Imaging of urban land***

Satellite imagery in the thermal infrared can provide repeated, quality-controlled, observations of the surface ('skin') temperature distribution over a city. When the sensor signal has been properly processed, the spatial distribution of temperature is observed directly from the resulting image. The image may be viewed as an extension of aerial photography because satellite remote sensing relies on the same processes of acquiring, interpreting, and extracting information without physical contact. The satellite images are acquired by electronic scanners and linear/area arrays and are taken at a higher altitude to allow large area coverage of the Earth surface at a time (Weng, 2011; Qihao, 2012). The individual picture elements, called pixels, are arranged in a 2D array in columns and rows with each pixel having an intensity value and location address in the 2D array, representing the electromagnetic energy received at the particular location on the Earth's surface (Qihao, 2012). In general, satellite pictures are built-up as a raster image across a swath width. The sensor records an electronic signal related to the electromagnetic radiation coming from the ground, pixel by pixel, producing a digital image that is a matrix of numbers, with each number representing (in this case) the degree of emission of thermal energy (numbers between 0 and 255 for an eight-bit data channel) (Lillesand et al., 2015).

With respect to thermal infrared (TIR) remote sensing, there are a number of different satellite remote sensing platforms with multiple sensors in the TIR spectrum which gives the meteorologist a number of potentially useful datasets to measure Land Surface Temperature (LST) of urban areas. Important factors that influence surface temperature must be comprehensively considered before using satellite image-base for heat island studies in urban areas with complex spatial characteristics (Chudnovsky et al., 2004; Weng, 2009). The choice of image timing in satellite remote sensing is also important, for example Hartz et al., (2006) utilizes day and night remotely sensed and ground data at neighbourhood scale, and found that night-time (10:40 pm LST) ASTER images were relatively consistent; Rigo et al., (2006) observed that MODIS LST was more accurate at night compared to daytime. However, a major

limitation of TIR satellite remote sensing techniques is the requirement for clear skies for accurate readings to be achieved, therefore cloud cover can be a serious setback. However, mitigating techniques have been investigated, according to Neteler, (2010), composite images from multiple passes can be created in order to construct an image without cloud cover limitations, also modelling or passive microwave remote sensing could be used if increased coverage is required (Wan, 2008). In this thesis, no composite or modelled gap-filling is used; cities are excluded from the analysis when the fraction of urban surface obscured by cloud exceeds a threshold, as described in subsequent chapter.

### ***2.3.5 Moderate Resolution Imaging Spectro-radiometer (MODIS)***

The Moderate Resolution Imaging Spectro-radiometer (MODIS) is an Earth-viewing sensor driven by the scientific community's desire to view the entire globe every 1 – 2 days at a moderate spatial resolution (250m, 500m and 1km at nadir, for different spectral channels), with spectral bands in the visible (VIS) through the long-wave infrared (LWIR) region to enable the measurement of numerous (40 – 50) geographical parameters (Qu et al., 2007). MODIS is specifically configured for Earth system science studies to include interaction of land and ocean surface with the atmosphere (Salomonson et al., 1989). The MODIS sensor is a key instrument on-board the Terra satellite successfully launched in December 1999 and complemented by another MODIS on the EOS Aqua satellite launched in May 2002. Both Aqua and Terra are on circular sun-synchronous polar orbits (<https://modis.gsfc.nasa.gov/about/>, last accessed 6<sup>th</sup> April 2021). The Terra overpass time is around 10:30am (local solar time) in its descending mode and 10:30pm in ascending mode. The Aqua overpass time is around 1:30pm in ascending mode and 1:30am in descending mode (Morisette et al., 2002; Justice et al., 2002; Wan et al., 2004). The MODIS instruments execute a  $\pm 55^\circ$  scanning pattern which, from the satellite orbital height of 705 km, results in a 2,330-km swath and global coverage every 1-2 days (<https://modis.gsfc.nasa.gov/about/design.php>, last accessed 6<sup>th</sup> April 2021). The effect of view angle on sensing of land surface temperature by MODIS is discussed further in chapter 3.



Data are available from the USGS Land Processes Distributed Active Archive Center (<https://lpdaac.usgs.gov/>) and useful LST products include MYD11A1 (Aqua) and MOD11A1 (Terra) which are daily LST and emissivity at 1 km spatial resolution. MODIS data are processed in several steps, each producing a data output at a different 'level' (e.g., L1B, L2, L3... [https://lpdaac.usgs.gov/documents/715/MOD11\\_User\\_Guide\\_V61.pdf](https://lpdaac.usgs.gov/documents/715/MOD11_User_Guide_V61.pdf), last accessed 6<sup>th</sup> April 2021). Level 1 and 2 data are swath scenes tied to longitude and latitude; level 3 data are gridded onto a map projection. Each product consists of land surface temperatures, quality flags, emissivity's at two wavelengths, and viewing angles and times. This study uses MODIS/Terra V006 composite products (MOD11A1) – MODIS/Terra Land Surface Temperature and Emissivity Daily L3 Global 1km Grid SIN V006 (Wan et al., 2015). No corrections for emissivity or viewing angle were attempted.

The Terra overpass time is around 10:30am (local solar time) in its descending mode and 10:30pm in ascending mode. The Aqua overpass time is around 1:30pm in ascending mode and 1:30am in descending mode (Morisette et al., 2002; Justice et al., 2002; Wan et al., 2004). Data are available from the USGS Land Processes Distributed Active Archive Center (<https://lpdaac.usgs.gov/>) and useful LST products include MYD11A1 (Aqua) and MOD11A1 (Terra) which are daily LST and emissivity at 1 km.

There is now a large body of literature that recognises the use of MODIS in the field of urban climatology, including (Tomlinson et al., 2012), analysing summer UHI of Birmingham; (Lehoczký et al., 2017), investigating the UHI effects in the city of Valencia; (Vancutsem et al., 2010), Estimating air temperature in different ecosystems over Africa. At global scale, (Imhoff et al., 2010) used MODIS data to calculate UHIs across continental U.S.A.; (Tran et al., 2006) Analyses of UHI effects in eight Asian mega-cities using MODIS data. Other studies that use MODIS outside of the climatology field, e.g., (Friedl et al., 2002), study on global land cover mapping using algorithms; (Schneider et al., 2009), mapping global urban extent from MODIS satellite data.

In summary, MODIS has fast become the platform of choice for urban studies that require datasets at a large spatial scale. In addition to the high temporal resolution, the MODIS sensor has high spectral, spatial, and radiometric resolution compared to previous sensor systems. The MODIS sensor was developed using lessons learnt from several earlier sensors, for example, the Advanced Very-High-Resolution Radiometer (AVHRR). This sensor detects radiation in the visible, near-, mid-, and thermal-IR region with spatial resolution of 1.1km. AVHRR main applications is in the areas of ice and snow mapping, sea surface temperature, vegetation, and crop monitoring, including studying urban heat islands.

## **2.4 Landuse and Urban Morphology: How it relates to the Causes of UHI effects**

Landuse and land cover change (LUCC) has become a key subject that needs to be addressed in the study of urban climate change. It contributes significantly to Earth environmental interactions, land degradation and loss of biodiversity (Haregeweyn et al., 2014). Land cover describes the spatial surface an area occupies on Earth. For instance, impervious built land, wetland, cotton fields, and other agricultural and natural land surfaces. Land use, on the other hand, describes how land surfaces are used by human activities: for example, residential, commercial, industrial, civic land uses among others (Lillesand et al., 2015). Researchers have recognized that land cover changes were mainly due to anthropogenic activities since the industrialization era, and that they are consequential to current global environmental problems (Turner et al., 1993; Verburg et al., 2013; Donnay et al., 2014; Chen et al., 2019).

The spatial configuration of cities contributes to how the urban environment alters the local energy budget of the cities (Arnfield, 2003). As shown in Figure 2.1 and Table 2.1, the underlying landuse is a major control on the factors that contribute to elevated urban temperatures and thus the UHI. Indeed, numerous UHI studies have looked at the role of landuse (Smith et al., 2011; Zhang et al., 2013; Os and Aa, 2016; Pal and Ziaul, 2017), but there has recently been a significant amount of

research activity to provide a universal means in which to classify urban areas. Given the large continuum between urban and rural landscape. Stewart and Oke, (2012) developed the Local Climate Zone (LCZ) concept to help redefine and quantify the UHI effect. The definition is based on quantitative and qualitative properties with each LCZ aiming to have homogenous air temperature. The fundamental advantage of the LCZ is the new perspective of UHI, looking into the temperature changes among LCZ classes rather than the traditional “urban and rural” classes. The importance of LCZ is not their ability to describe the site but to classify areas of a settlement into zones that are similar in their capacity to modify the local climate, and to sense potential transformations to different urban climate zones. It now serves as a standardized and quantitative method of describing the physical properties of urban morphology in relation to its urban climate (Stewart and Oke, 2009; 2010), with a range variables for different type of model parameters, e.g., sky view factor (SVF), building surface fraction, pervious and impervious surface fractions, height of roughness elements (Stewart and Oke, 2012). The LCZ classification (fig. 2.3) consists of 10 urban classes (built types) defining urban structure (morphology - streets and building, urban fabric – materials, urban cover – vegetation/built fraction and permeability, anthropogenic activity – man-made activity) and 7 land cover series (A-G) describing the natural land cover types (see Stewart and Oke, 2012 for more details). Cities around the globe are classified using the local climate zone (LCZ) to better understand the relationship between urban form and its surrounding climate.

The mapping of LCZ across an entire city with the aim to investigate potential source areas for temperature measurements has since been established (Emmanuel and Krüger, 2012). The urban areas is broken down into smaller spatial units with relatively homogenous built and vegetative forms. The approach is best as a sample strategy in urban setting where very little geographic data is available, hence efficient in deriving data – for example, identifying urban classification across city gave users a design target on ways to employ high resolution remote sensing to derive land cover parameters for LCZ within their domain (Bechtel et al., 2015). Instead of sampling the urban areas randomly, researchers can focus on identifying representative areas and so stratify their sampling. The

approach allows users to investigate the inconsistency of parameter values which means classification of LCZ parameters can be readily arbitrated.


















Built types	Definition	Land cover types	Definition
1. Compact high-rise 	Dense mix of tall buildings to tens of stories. Few or no trees. Land cover mostly paved. Concrete, steel, stone, and glass construction materials.	A. Dense trees 	Heavily wooded landscape of deciduous and/or evergreen trees. Land cover mostly pervious (low plants). Zone function is natural forest, tree cultivation, or urban park.
2. Compact midrise 	Dense mix of midrise buildings (3–9 stories). Few or no trees. Land cover mostly paved. Stone, brick, tile, and concrete construction materials.	B. Scattered trees 	Lightly wooded landscape of deciduous and/or evergreen trees. Land cover mostly pervious (low plants). Zone function is natural forest, tree cultivation, or urban park.
3. Compact low-rise 	Dense mix of low-rise buildings (1–3 stories). Few or no trees. Land cover mostly paved. Stone, brick, tile, and concrete construction materials.	C. Bush, scrub 	Open arrangement of bushes, shrubs, and short, woody trees. Land cover mostly pervious (bare soil or sand). Zone function is natural scrubland or agriculture.
4. Open high-rise 	Open arrangement of tall buildings to tens of stories. Abundance of pervious land cover (low plants, scattered trees). Concrete, steel, stone, and glass construction materials.	D. Low plants 	Featureless landscape of grass or herbaceous plants/crops. Few or no trees. Zone function is natural grassland, agriculture, or urban park.
5. Open midrise 	Open arrangement of midrise buildings (3–9 stories). Abundance of pervious land cover (low plants, scattered trees). Concrete, steel, stone, and glass construction materials.	E. Bare rock or paved 	Featureless landscape of rock or paved cover. Few or no trees or plants. Zone function is natural desert (rock) or urban transportation.
6. Open low-rise 	Open arrangement of low-rise buildings (1–3 stories). Abundance of pervious land cover (low plants, scattered trees). Wood, brick, stone, tile, and concrete construction materials.	F. Bare soil or sand 	Featureless landscape of soil or sand cover. Few or no trees or plants. Zone function is natural desert or agriculture.
7. Lightweight low-rise 	Dense mix of single-story buildings. Few or no trees. Land cover mostly hard-packed. Lightweight construction materials (e.g., wood, thatch, corrugated metal).	G. Water 	Large, open water bodies such as seas and lakes, or small bodies such as rivers, reservoirs, and lagoons.
8. Large low-rise 	Open arrangement of large low-rise buildings (1–3 stories). Few or no trees. Land cover mostly paved. Steel, concrete, metal, and stone construction materials.	<b>VARIABLE LAND COVER PROPERTIES</b>	
9. Sparsely built 	Sparse arrangement of small or medium-sized buildings in a natural setting. Abundance of pervious land cover (low plants, scattered trees).	b. bare trees	Leafless deciduous trees (e.g., winter). Increased sky view factor. Reduced albedo.
10. Heavy industry 	Low-rise and midrise industrial structures (towers, tanks, stacks). Few or no trees. Land cover mostly paved or hard-packed. Metal, steel, and concrete construction materials.	s. snow cover	Snow cover > 10 cm in depth. Low admittance. High albedo.
		d. dry ground	Parched soil. Low admittance. Large Bowen ratio. Increased albedo.
		w. wet ground	Waterlogged soil. High admittance. Small Bowen ratio. Reduced albedo.

Figure 2.3 Local Climate Zone (LCZ) Classes defined by (Stewart and Oke, 2012)

The local climate zone (LCZ) approach has fast become the standard means to classify urban landuse and has already been applied in numerous cities globally, which demonstrates its efficacy in understanding the urban climate and its effect through observation and transferring those results across multiple cities. For example Arnfield, (2003); Stewart and Oke, (2012), focuses on the effect of the urban surface at neighbourhood scale, using landuse classification of various kinds to generalize results. The use of LCZ approach as a sample strategy in urban settings where geographic and as well demographic data are insufficient is particularly important, because it aid users to design and employ high-resolution remote sensing to delineate land cover parameters for LCZ in and around their domain (Mushore et al., 2019; Wang et al., 2019). The standard nature of the approach has been further enhanced by the World Urban Database and Access Portal Tools (WUDAPT; <http://www.wudapt.org>) initiative that has also been developed to generate LCZ maps and collect data on urban morphology worldwide (Bechtel et al., 2015; Brousse et al., 2016; Wang et al., 2017).

Overall, the use of LCZ provides a step-change in universally classifying urban areas with respect to urban morphology. Effective urban planning and strategic placement of urban meteorological networks can be enhanced through mapping LCZ, e.g. The case of Hong Kong, a GIS-based and WUDAPT approach was used for mapping LCZ (Wang et al., 2017), another approach was used for urban morphology classification based on remote sensing data (Carlos et al., 2017). Recently, Kotharkar and Bagade, (2018) evaluated the approach to identify UHI intensity of Nagpur city through mapping LCZ.

## **2.5 Allometry Scaling**

### ***2.5.1 ‘Scaling Approach’ – What is Allometry?***

Allometric scaling is a method for examining the structural and functional consequences of changes in size or scale among otherwise similar organisms (Schmidt-Nielsen, 1984). The study of allometry is broad in the field of biological sciences, where it demonstrates that the various parts of an organism

is in constant ratio to the growth rate of the organism itself (Gould, 1966). More commonly, allometry is used to describe scaling relations between two ‘size’ measures of an organism or system under study (Mark and Peucker, 1978) cited in (Longley et al., 1991).

The law of allometric growth was first used by biologists to describe differences in proportions relating to changes in total magnitude of the total organism (Gould, 1966; Schmidt-Nielsen, 1984; Lee, 1989) and the law was introduced to social science by Naroll and Bertalanffy, (1956). According to Jones, (1975) the law can be established by growth study of individual organisms through time, or by observing groups of the same shaped organisms at a single time. If  $Y$  is the size of an organ, or a measure of a characteristic of the organism,  $X$  is the size of the organism, and  $a$  and  $b$  are constant, then

$$Y = aX^b \quad (2.1)$$

where here the exponent  $b$  is the most important constant (the rate of relative growth) (Lee, 1989).

Allometry has been frequently used by biologists e.g. in plant studies (Enquist et al., 1998; Urban et al., 2013; Alonzo et al., 2015), and fractal spatial patterning (Chen, 2010), but it is easily extended to other types of complex phenomena such as the distribution of income within an economic systems (Bettencourt et al., 2010; Sarkar et al., 2018), income inequality (Sarkar et al., 2018), population-size distribution and urbanization (Bettencourt and Lobo, 2016; Fluschnik et al., 2016) and the ratio of rural – urban population growth is consistent in a number of countries, e.g. U.S.A. (Naroll and Bertalanffy, 1956)

### ***2.5.2 Allometry applied to urban areas***

Cities exist in a recognizable but changing form, over a range of scale, from small towns with small populations to mega-cities with population of tens of millions of people (Batty, 2008; Bettencourt, 2013). In general, for urban studies, allometric scaling can be used to find simple emergent patterns that relates aspects of urban material, energy, or economic flows to the size of cities as determined

by their population (Lee, 1989; Longley et al., 1991), including growth and innovation driven by economies of scale (Batty, 2008), and urban form as a hierarchy of clusters, (Bettencourt, 2013). Allometric scaling relates properties of a system (i.e., in this case, urban settlements) to a measure of size such as population (Cottineau et al., 2017). In this context, allometry will be perceived by a few morphological and physiological variables, which are scaled, in relation to city size as determined by their population

The relationship between urban area and population size have been established to follow the scaling law of allometric growth. This allometric scaling follows the exponential growth of city size, thus can be called 'exponential allometry', which is associated with the concept of settlement patterning. Several studies in the urban climate literature offer an allometric perspective in terms of city size (e.g. Chandler, 1966; Oke, 1973; Oke, 1982; Rybski et al., 2017; MacKenzie et al., 2019). Notably, Oke (1982) presented the relationship between a measure of maximum UHI and population for European settlements (this is discussed further in the next chapter).

Overall, it is clear that although allometric techniques were common in early work to understand urban climates (e.g. (Naroll and Bertalanffy, 1956), there has been a clear resurgence in the use of the technique in recent years to investigate other urban phenomena (e.g. air quality: MacKenzie et al., 2019) or to infer a larger spatial perspective, such as comparing results at an international scale, (e.g., Fluschnik et al., 2016). Easy access to quality-controlled data, including remote-sensing data with high spatial resolution, and a series of studies that have postulated general allometric patterns for many aspects of city form and function (Batty 2008; Bettencourt 2013) have contributed to the renewed interest in urban allometry.

The present study seeks a quantitative scaling relationship between urban population and total emitted long-wave energy using allometry to determine whether simplicity emerges from complexity with respect to urban heat. A number of studies in the urban climate literature have been published with a 'scaling' or allometric perspective – e.g., Torok et al., (2001) investigated the magnitude of the

urban heat island (UHI) effect in four small towns, with populations of less than 10,000, and one large city with population of 3.02 million; Manoli et al., (2019) used the magnitudes of urban heat islands to describe climate and population studies by analysing summertime differences between urban and rural surface temperatures worldwide and found a nonlinear increase in temperature changes with precipitation. Studies over the years also recognise that UHI or SUHI increases with a measure of city size (e.g., Peng et al., 2012; Zhou et al., 2013; 2017). Also Batty, (2008) highlights that scaling allows synthesis on cities by searching for simple emergent patterns. Recently, there has been growing recognition of the vital links between urban climate studies and allometry scaling technique (e.g., Cottineau et al., 2017), allometric scaling recognises that complex interactions lead to simple patterns.

## **2.6 Summary**

In line with the research gap identified in Chapter 1, there now exists an opportunity to bring together a range of approaches to investigate the impact of urban form on the bulk thermal properties of a city. This literature review has demonstrated the state of the art in a number of areas and has highlighted the potential to revisit the approach of allometric scaling to study this element. This approach coupled with the use of LCZ and coarse resolution satellite imagery (i.e., MODIS) will provide a new (internationally standardised) lens in which to infer the role of urban form on urban heat.

The chapter provides a comprehensive overview of important remote sensing applications, by reviewing key concepts and methods illustrating practical uses of particular sensor/sensing systems (e.g., satellite imagery). It also provides insights into current development trends in remote sensing and further identifies its major limitations. Techniques to mitigate these limitations were described (Neteler, 2010): composite images from multiple passes can be created in order to construct a cloud-free image; also the remote sensing systems can utilize visible, reflected infrared, thermal infrared, and microwave (passive or active) to increase coverage or develop models for gap-filling. The chapter



gave a comprehensive review of selected data product, algorithms, and applications of MODIS and highlighting its origins in earlier sensors such as the Advanced Very High Resolution Radiometer (AVHRR).

The use of remotely sensed surface temperature and as well the ability of the proposed LCZ approach for modelling to produce spatial realistic surface temperature across cities was reviewed. The LCZ approach was a proposal to overcome many of the challenges relating to urban climate models applications across the globe especially areas with scarcity of data accessibility. The proposed LCZ approach seeks to reduce the data requirements of applying on urban climate studies across an entire city rather than the normal traditional approach researchers use for modelling in urban climate studies. The standard nature of the approach has been further enhanced by the World Urban Database and Access Portal Tools (WUDAPT; <http://www.wudapt.org>) initiative.

The concept of allometric scaling technique was reviewed on the chapter as used by biologist in the early stage and later manifested into other research fields including urban studies e.g., (Batty, 2008; Bettencourt, 2013). The chapter highlights the rebirth of the technique application to include study on air quality – e.g., (MacKenzie et al., 2019).

## 3.0 Chapter 3

### **Allometric scaling of thermal infrared emitted from UK cities and its relation to urban form**

This chapter contains verbatim material taken from a recent publication in (Abdulrasheed et al., 2020) (see appendix D). The chapter provides further rationale for the allometric approach and addresses objective 1 in the thesis: “[To] explore the relationship between urban morphology and the bulk thermal properties (emitted energy) of cities in the UK through appropriate scaling techniques”.

#### **Abstract**

As a result of differences in heat absorption and release between urban and rural landscapes, cities develop a climate different from their surroundings. The rise in global average surface temperature and high rates of urbanization, make it important to understand the energy balance of cities, including whether any energy-balance-related patterns emerge as a function of city size. In this study, images from the Moderate Resolution Imaging Spectro-radiometer (MODIS) satellite instrument, covering the period between 2000 and 2017, were sampled to examine the seasonal (winter and summer) night-time clear-sky upwelling long-wave energy for 35 UK cities. Total (area-summed) emitted energy per overpass per city is shown to correlate closely ( $R^2 \geq 0.79$ ) with population on a log-log ‘allometry’ plot. The production of emitted energy from the larger cities is smaller than would be produced from a constellation of smaller cities housing the same population. The mean allometry slope over all overpasses sampled is  $0.84 \pm 0.06$ , implying an ‘economy (or parsimony) of scale’ (i.e., a less-than-proportional increase) of about 21% (i.e.,  $100(2 - 10^{0.84 \log(2)})$ ) for each doubling of city population. City area shows a very similar economy of scale, so that the scaling of night-time emitted energy with urban area is close to linear ( $1.0 \pm 0.05$ ). This linearity with area indicates that the urban forms used in UK cities to accommodate people more efficiently per unit

area as the urban population grows, do not have a large effect on the thermal output per unit area in each city. Although often appearing superficially very different, UK cities appear to be similar in terms of the components of urban form that dictate thermal properties. The difference between the scaling of the heat source and literature reports of the scaling of urban-rural air (or surface) temperature difference is very marked, suggesting that the other factors affecting the temperature difference act to strongly decrease its scaling with population.

### **3.1 Introduction**

Urbanization is accelerating across the world, especially in developing countries across Africa and Asia (Martins, 2000; Cohen, 2006). Current projections indicate that by 2050, the global urban population will increase by 2.4 billion, i.e., about half the current population of 4.22 billion (United Nation, 2019) (Seto et al., 2012; Buhaug and Urdal, 2013; Bremner et al., 2010; Bongaarts, 2009). The change of land surface characteristics caused by urbanisation leads, amongst other things, to changes in the local energy balance that must be taken into account when determining long-term temperature trends (Chrysanthou et al., 2014). This change in thermal climate in urban areas, leads to the urban heat island (UHI), which is the tendency of an urban area to have warmer near-surface air temperatures than its rural surroundings (Bornstein, 1968; Landsberg, 1981; Oke, 1995; Sheng et al., 2017). Related phenomena include: urban thermal plumes (Oke, 1995; Heaviside et al., 2015) and urban precipitation anomalies (Han et al., 2013).

Recent conceptual UHI models have emphasised the importance of different land uses within cities (Stewart and Oke, 2012; Tomlinson et al., 2012), highlighting the prospect that urban planning choices can be used to mitigate adverse urban climate trends (Davoudi, 2012; Davoudi, 2014). Implicit in most studies of UHI, from Howard, (1818) on, is that local, one-dimensional (i.e., vertical), energy budgets for urban land uses, combine through the action of fluid stirring and mixing, to produce a three-dimensional dome of urban heating over a city — see, for example, the

very widely reproduced cross-sections of UHI through an idealised city (e.g., Lemmen and Warren, 2004).

We hypothesise that gross changes in urban form as the size of cities increase affect the storage of solar heating. We focus on night-time, clear-sky, emitted long-wave as a primary measure of heat storage, and we use population as our yardstick of city size. We use an extensive property — total emitted energy (in Megawatts) per city per night — rather than intensive property such as temperature or emission per unit area, to permit direct comparisons with other extensive properties such as urban area, and to explore the extent to which the behaviour of intensive properties, particularly UHI, differ from the behaviour of the extensive properties. We return to the question of appropriate variables for allometric investigation in the Discussion, below.

### ***3.1.1 Urban Form and urban heat***

The urban form of a city is the result of its social, economic, and environmental context. We focus on UK cities in this study; further work will focus on a different setting in order to try and distinguish the general from that dependent on UK context (Abdulrasheed, 2020). A recognised system of UK urban planning mostly originates from the industrial revolution, prior to which most people lived and worked in the countryside (Inikori, 2002; CPRE, 2018). As industries grew, people migrated to towns and cities in search of better wages, opportunities, and livelihood (Karp, 2013) leading to rapid growth in towns and cities. Many decrees and ordinances were issued to manage this growth, including, at the beginning of the 20<sup>th</sup> century, the Town Planning Act 1909, which was introduced to ensure that local authorities prepared schemes of town planning. This was followed by the Housing Act 1919, which required the design of houses to be approved by the Ministry of Health, and the Housing Act 1930, which required clearance of high-density ‘slums’, which were considered unsanitary (Carmon, 1999). The post-war 1940s was a period of uncertainty for the architects and town planners tasked with rebuilding Britain’s bomb-damaged cities (Tsubaki, 2000; Ball and Maginn, 2005; Hollow, 2012). Residential rebuilding in this period

often involved the replacement of low-rise private dwellings with fewer, but larger, high-rise public buildings (Carmon, 1999), sometimes with an intermediate period of low-rise prefabricated structures (Short, 1982). Cities across the UK such as Bristol, Coventry, Hull, Portsmouth, Southampton and Plymouth were very severely damaged during World War II (Hasegawa, 2013), and so were subject to significant post-war changes. For those neighbourhoods, which, by the 1960s and 1970s, had escaped slum clearance or destruction in wartime, the tendency was for renewal rather than replacement of low-rise and mid-rise residential buildings (Carmon, 1999). In the subsequent decades, and until the present day, a more laissez-faire approach has dominated, with renewal and replacement of housing and commercial buildings through private-public cost sharing of various kinds (Carmon, 1999; Hasegawa, 2013; Webb, 2018) .

Emerging in parallel, from the latter part of the nineteenth century and through the first part of the 20<sup>th</sup> century, was the Garden Cities movement, which advocated public health improvement by planning to build cities with more, and more accessible, green spaces, see e.g., (Burnett, 1986). This advocacy eventually led to the New Towns movement and New Towns Act 1946 (Goist, 1974; Rubin, 2009; Alexander, 2009; Tizot, 2018) which resulted in towns such as Telford, Letchworth and Milton Keynes. All the 20<sup>th</sup>-century housing and town planning policies in the UK led to notable changes in the urban form from the scale of individual dwellings, through neighbourhood scale land-use, to the patterns of use across whole urban areas.

The nature and patterns of urban form (i.e. building geometry, pervious surface fraction, building and tree densities, soil permeability etc.) determine the thermal characteristics of a place. Such characteristics can be used to define local climate zones (LCZ) (Stewart et al., 2014), which may vary over time as a result of planned or unplanned changes. For example, slum clearance often re-shaped low-rise, close-packed, terraced housing into a sparse array of high-rise towers e.g., (Carmon, 1999). Suburban extension of cities replaced farm fields (or, often, filled in parkland estates around large houses) with semi-detached two storey housing in wide boulevards (shifting

from linear form to cul-de-sac mid-century). Infilling (building in what had previously been back gardens) became prominent towards the end of the 20<sup>th</sup> century (Whitehand and Whitehand, 1983).

As cities grow, green space — trees and vegetation — are replaced with grey space, i.e., buildings and transport and utility infrastructure. The magnitude and nature of the change is often sporadic and patchy, and results in a wide variety of urban forms (Morris, 1974; Hopkins, 2012). In terms of the surface energy balance, changing from rural to urban land results, in general, in the absorption of a higher fraction of incoming solar radiation and a decrease in the Bowen ratio (i.e., the ratio of sensible to latent heat emission) (Arnfield, 2003; Aguado and Burt, 2015). Energy absorption and emission at the ground surface is therefore a key driver of urban climate, strongly influencing the near surface air temperature and the radiant fluxes relevant for health effects e.g., (Basu and Samet, 2002; Middel and Krayenhoff, 2019). Satellite based studies report thermal emission as land-surface temperature (or ‘skin’ temperature), from which surface UHI intensity (SUHI) can be derived (e.g., Peng et al., 2012; Zhou et al., 2014; Zhou et al., 2017). In-situ sensing reports air temperature directly. Near-surface air temperature UHI and SUHI do not always correspond for a variety of physical reasons (Voogt and Oke, 1997; 2003; Arnfield, 2003; Schwarz et al., 2011; Sheng et al., 2017) but both are driven by absorption and emission of energy at the ground surface. The fundamental role of surface energy exchange motivates us to investigate how surface energy parameters vary for a set of cities of very different size and urban form, in order to understand this foundational driver of both the UHI and SUHI.

Buildings also slow the wind near the surface, retaining the heat released from vehicles and buildings (Golden, 2004; Arifwidodo and Tanaka, 2015). Energy removed from the mean wind is lost to the surfaces or transformed into turbulent kinetic energy, affecting the dissipation of scalars such as temperature and trace-gas pollutants e.g., (Belcher et al., 2003). Dense building arrangements decrease the sky-view factor (Chapman and Thornes, 2004; Grimmond, 2007; Yang

et al., 2015). The net result of all these changes is the increased storage of heat, which is the root cause of the UHI effect. Increased heat storage can lead to a number of issues such as human health risk (Basu and Samet, 2002; Rosenzweig et al., 2011; Murray and Ebi, 2012; Smith et al., 2011; Patz et al., 2005; Hondula et al., 2015; Wouters et al., 2017; Krayenhoff et al., 2018; Middel and Krayenhoff, 2019), environmental hazard (e.g., Chapman and Thornes, 2006), and infrastructure failure (Chapman and Bell, 2018; Dawson et al., 2018), which themselves often require further energy consumption to offset (Li et al., 2015).

Researchers have long studied the effects of urban form on climate change, and the impacts of climate change on urban environment, as reviewed in (Mills, 2007) and (Seto et al., 2010). Urban planning responses to urban heat and climate change, including both mitigation and adaptation strategies, continue to evolve, especially with respect to sustainable urban development in cities (Jabareen, 2006 ; Rybski et al., 2017; Davoudi et al., 2009; Hendrickson et al., 2016; Castán Broto, 2017; Fujii et al., 2017). Urban climate adaptation focuses on reducing vulnerability and promoting resilience of people and properties (Amundsen et al., 2010; Carmin et al., 2012; Anguelovski et al., 2014). Microclimate planning and design modification to outdoor environments can also enhance thermal comfort, e.g., neighbourhood streets trees, green spaces and parks, (Brown, 2011; OECD, 2014). We expect that planning responses to urban heat will manifest in the relationship of urban form to city size.

### ***3.1.2 Allometry and urban heat***

Allometry is originally a concept from biology, relating morphological and physiological aspects of organism biology to some more easily measured parameters such as body mass (Schmidt-Nielsen, 1984; Gould, 1966; Lee, 1989; Small, 2012). Allometric approaches were introduced to urban studies (e.g. West and Brown, 2005; Naroll and Bertalanffy, 1956; Nordbeck, 1971) and used to model the relationship between a set of cities and the largest city within a geographical region (Small, 2012). Urban allometry studies have sought to elucidate decadal evolution of urbanized

area (Lee, 1989; Longley et al., 1991), fractal spatial patterning (Chen, 2010), income inequality (Sarkar et al., 2018), and between urban form and growth (Bettencourt et al., 2007). Interpretations drawn from urban allometry include growth by innovation driven by economies of scale (Batty, 2008), and urban form as a hierarchy of clusters, (Bettencourt, 2013).

In general, for urban studies, allometric scaling relates aspects of urban material, energy, or economic flows to the size of cities as determined by their population (Bettencourt, 2013; Batty, 2008; Lee, 1989; Longley et al., 1992). Because it focuses on the relative rate of change of properties with size, referred to as ‘scaling’ below, allometry lends itself to comparative studies of properties of very different character (Bettencourt and West, 2010). In our previous study of air pollutant emissions and concentrations, we found it informative to compare the scaling of an intensive property (urban air concentrations) with the scaling of extensive properties (area-summed pollutant emissions and urban area) (MacKenzie et al., 2019).

Allometric scaling recognises that the many microscopic interactions within a complex system often collapse to a simple pattern (Cottineau et al., 2017). Scaling, therefore, allows us a synthesising perspective on cities (Batty, 2008), by searching for simple patterns without becoming overwhelmed by details of local context.

Allometric patterns, where they exist, conform closely to an equation of the form:

$$Y = \beta X^{\alpha} \quad (3.1a)$$

The power law, equation (3.1a), describes a straight-line relationship between the X and Y variables when the function is plotted on a double logarithmic coordinate system, i.e.

$$\log(Y) = \log(\beta) + \alpha \cdot \log(X) \quad (3.1b)$$

where  $\log(\beta)$  is a constant offset and  $\alpha$  is the rate of relative growth (the allometric scaling factor or, simply, slope). Below, we will refer to  $\alpha$  as defining the ‘scaling’ of Y with respect to X.



Using allometry, this study seeks a quantitative scaling relationship between population and clear-sky upwelling emitted energy, in order to determine whether and how the many detailed processes affecting this part of the urban energy budget combine at the city-scale. The study evaluates whether simplicity emerges from urban complexity with respect to emitted long-wave. We compare our findings on clear-sky upwelling long-wave to a classical result in the literature of urban heat islands.

The empirical relationship between the UHI and structure of a city arises from the fact that tall, close-packed, concrete and brick buildings store solar energy in day time and emit it at night more slowly than a flat surface (Duckworth and Sandberg, 1954). The thermal infrared energy emitted from a surface is acted on by wind and radiation transfer processes; structural elements of a city affecting wind and radiative transfer will therefore influence UHI (Oke, 1973). Since structural elements of cities are often laid out block by block, one approach to analysing a city is to determine its energy budget and surface temperature explicitly on a block-by-block basis (Terjung and Louie, 1974; Chandler, 1966). Land-use categories and urban morphology types offer useful approaches to determining modifications to the surface energy budget that will produce a nocturnal urban heat Island (Oke, 1981; Landsberg, 1981; Eliasson, 1996). Other urban climate studies focus on the effect of the urban surface at the neighbourhood scale, using land-use classifications to generalise results (e.g. Arnfield, 2003; Stewart and Oke, 2012). At city scale the number of studies are fewer: (Landsberg, 1981) for North American settlements; (Lee, 1993) for Korea; (Eagleman, 1974) for Kansas city; and (Oke and Maxwell, 1975) for Montreal and Vancouver.

Several studies in the urban climate literature offer an allometric perspective (Oke, 1982; Torok et al., 2001; Manoli et al., 2019) and many other comparative studies show that UHI or SUHI increases with some measure of the size of the city (e.g., Zhou et al., 2013; 2017; Schwarz and Manceur, 2015) or focus on the largest cities because the UHI is assumed to be largest there (e.g., Peng et al., 2012; Zhou D., et al., 2014). Oke (1973; 1982) presented the relationship between a

measure of maximum UHI ( $\Delta T_{u-r}(\text{max})$ ) and population for European settlements (fig.3.1) and supports the hypothesis that the canopy air temperature,  $\Delta T_{u-r}$ , is a function of city size, with the absolute UHI increasing by about 0.6 °C (i.e.  $1.975 \cdot \log_{10}(2)$ ) for every doubling in population. Zhou et al. (2013) fitted a sigmoidal curve to the log-linear relationship of SUHI to urban areas. The sigmoidal function is approximately linear for urban clusters with areas between 2 and 200 km<sup>2</sup> with SUHI increasing by  $\sim 0.3^\circ\text{C}$  for an area doubling (Zhou et al., their Figure 2). Zhou et al. (2017) plot SUHI against  $\log_e(\text{urban area})$  similarly to find a log-linear regression in which SUHI increases by about 0.4 °C (i.e.,  $0.55 \cdot \log_e(2)$ ) for an area doubling.

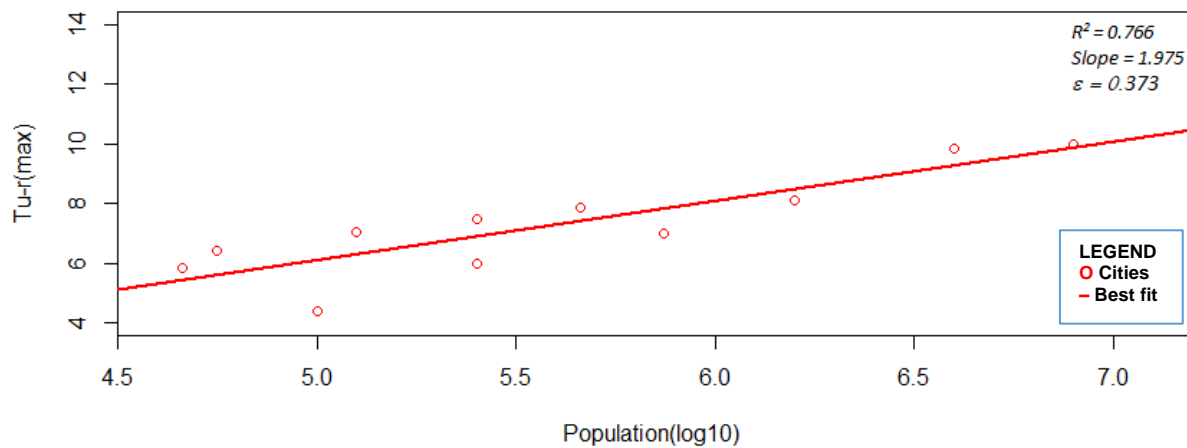
Figure 3S1 in the Supplementary Information presents the Oke (1973) data in a power-law log-log graph. Regressing on  $\log_{10}(\Delta T_{u-r}(\text{max}))$  gives more weight to the smaller cities, but a strong relationship is still found. The scaling of  $\Delta T_{u-r}$  in Fig S1 is small,  $0.11 \pm 0.03$ , but significantly different from zero — and equivalent to an increase of just 8% (i.e.  $100(10^{0.11 \cdot \log(2)} - 1)$ ) in UHI for a population doubling. Such a modest scaling with population has implications, such as that ‘densification’ of population into large urban centres presents a rather modest increased contribution of air temperature to thermal discomfort and associated health risk, at least to the extent that this can be gauged by the UHI of the 20<sup>th</sup> century city forms in Oke’s (1973; 1982) sample.

Having identified the best-fit scaling relationship, the residual offset from this best-fit for any individual city is also informative (Bettencourt et al., 2010). The residual for any city on any night,  $r_{j,k}$ , is calculated as the vertical distance of the datum for that city to the best-fit line:

$$r_{j,k} = \log(Y_{j,k}) - \{\log(\beta_k) + \alpha_k \cdot \log(X_j)\} \quad (3.2)$$

where  $Y_{j,k}$  is the measured value of dependent variable (in our case, the summed emitted energy of city,  $j$ , on a given night,  $k$ ),  $X_j$  is the population, of city  $j$ , and the parameters  $\alpha_k$  and  $\beta_k$  define the allometric scaling relationship. In Oke’s scaling data (Figs 3.1 and 3S1), the largest-magnitude

residual is a large negative deviation (i.e. less heat island than expected) for the UK town of Reading (Oke, 1973).



**Figure 3.1** Relation between maximum air temperature heat island intensity ( $\Delta T_{u-r}(max)$ , degrees Celsius) and population ( $P$ ) for European Settlements (redrawn from Oke, 1982). Sources of  $\Delta T_{u-r}(max)$  are literature and private communications dating from 1927 – 1972. It is not clear in Oke (1973; 1982) if the population data used is matched in time to the date for  $\Delta T_{u-r}(max)$ . Reported on the graph (top right) are the Coefficient of Determination ( $R^2$ ) for the best-fit regression, the slope of the regression, and the error on the slope ( $\epsilon$ ).

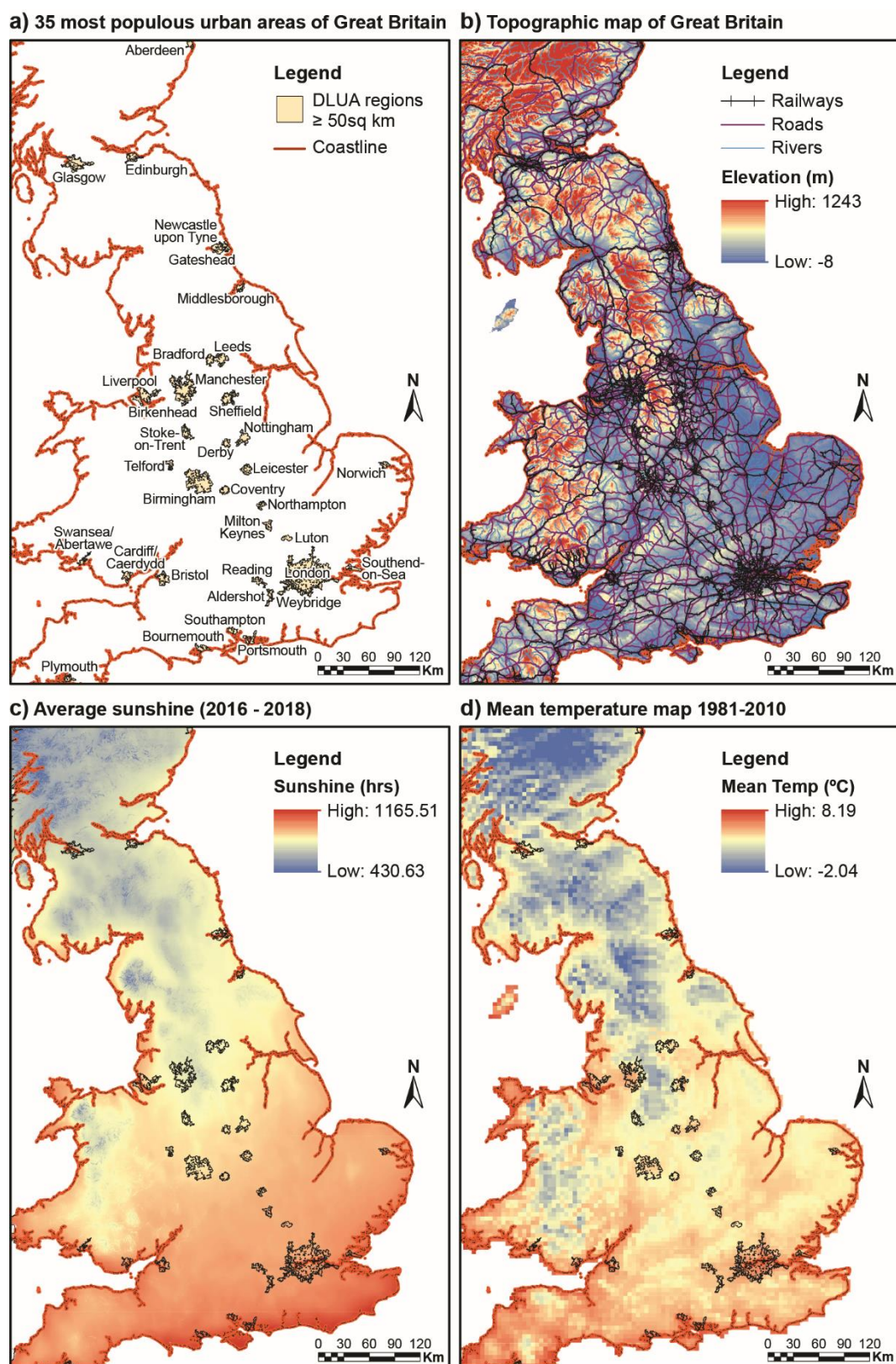
Since both, the canopy air temperature UHI, and the surface temperature SUHII result from heat storage, the scaling of emitted energy (with population or urban area) will be an important contributor to the scaling of UHI and SUHII. When the observed scaling of emitted energy is larger than that for UHI or SUHII, other factors must be acting to dampen the overall scaling.

## 3.2 Methodology

### 3.2.1 The study area

According to the Office for National Statistics (ONS), the population of UK as at 30<sup>th</sup> June 2016 is estimated to be 65,648,000, concentrated in urban areas in the southern half of the country (Fig. 3.2a), and with a rate of increase of 0.8% (538,000) per annum (Office for National Statistics, 2017). The climate of the UK is temperate, but variable, particularly because of altitude and distance from the

coast (Fig. 3.2b). Average temperature is 4°C January (winter) and 15°C in July (summer) (Kennedy et al., 2017; Briney, 2019). Mean climate data are shown in figure 3.2. This study focuses on the thirty-five (35) most populous settlements in the Great British mainland of the UK (see Fig. 3.2a below and Table 3S1 and Fig 3S5 in supplementary 3SI). Boundaries for the cities were extracted from medium scale Ordnance Survey digital map data (Meridian2; see Data Sources, below) and represent contiguous Developed Land Use Areas (DLUA) rather than administrative demarcations. UHI, SUHII, and urban allometry studies are sensitive to the choice of urban boundary and this should be borne in mind in the comparisons discussed below. The urban boundary used to define population in Oke (1973) is likely administrative; the urban cluster areas used in Zhou et al. (2013, 2017) are similar to our contiguous DLUA. Population counts were retrieved from the Office of National Statistics (2017) at the lowest level of geographical aggregation (output area) and attributed to the contiguous DLUAs.



**Figure 3.2 (a) 35 most populous urban areas in Great Britain (urban boundaries are contiguous Developed Land Use Areas from Meridian2 data); (b) Topographic map of central Great Britain with cities and major roads; (c) Average Sunshine of central Great Britain; (d) Mean 2m Temperature map of central Great Britain. The data were sourced from the Centre for Environmental Data Analysis (CEDA, 2011), (SolarGIS, 2019), Ordnance Survey - Meridian2 data(DLUA) and ArcGIS tools were used to plot the maps.**

### 3.2.2 Data collection and analysis

This study uses MODIS/Terra V006 composite products (MOD11A1) – MODIS/Terra Land Surface Temperature and Emissivity Daily L3 Global 1km Grid SIN V006 (Wan, 2015). This product is useful because it is gridded, has high resolution, is cloud-cleared, is quality-controlled and quality-assured, and has accurate calibration in multiple thermal infrared bands designed for retrievals of Land Surface Temperature (LST) and atmospheric properties (Wan and Dozier, 1996). LST from MODIS are retrieved from clear sky observations at daytime and night-time with the aid of a generalized split-window algorithm (Wan and Dozier, 1996; Wan, 2008). Satellite sensors looking in the nadir oversample horizontal urban surfaces and undersample vertical surfaces (Voogt and Oke, 1998; Arnfield, 2003). This sampling will tend to overemphasise both day-time heating and night-time cooling. The extent to which horizontal and vertical surface contribute to any given radiance varies with the angle of view. Angle of view also affects the native spatial resolution of the satellite radiances; interpolation in the MOD11A1 processing pipeline brings the dataset to a uniform 1-km grid. The MOD11A1 dataset contains information on view angle but we have not implemented any correction for off-nadir view geometries. For simplicity, only night-time overpasses (0130h local time) are considered for the present study.

Area-summed clear-sky night-time long-wave upwelling emitted energy (hereafter ‘emitted energy’) for mainland Great Britain was derived for selected days from 2000-2017. We interpret emitted energy in preference to LST because it gives proper weighting to radiance from the highest temperatures and provides a sum in physically meaningful units. The LST data used was selected to have as much clear sky over the region as possible. LST data for each pixel,  $i$ , within the city,  $j$ , on night,  $k$ , was converted to emitted energy,  $\epsilon_{i,j,k}$  in  $\text{W m}^{-2}$ , using the Boltzmann law:

$$\epsilon_{i,j,k} = \sigma T_{i,j,k}^4 \quad (3.3)$$

where,  $\sigma$  is the Stefan-Boltzmann constant =  $5.67 \times 10^{-8} \text{ W m}^{-2} \text{ K}^{-4}$ , and  $T_{i,j,k}$  is the LST in Kelvin. The effect of varying surface emissivity is not taken into account. Area-summed emitted energy,  $\langle E_j \rangle$  in

MW, for each city on each night, was then calculated by summing the  $p$  unobscured land-surface pixels inside the city boundary:

$$\langle E_{j,k} \rangle = \sum_{i=0}^p \epsilon_{i,j,k} \Delta a \quad (3.4)$$

where  $\Delta a = 1 \text{ km}^2$  and the factor of  $10^6$  converting  $\text{km}^2$  into  $\text{m}^2$  is accommodated in the units of  $\langle E_j \rangle$ .

For example, at  $LST \sim 278 \text{ K}$  ( $5^\circ \text{C}$ ), the Boltzmann Law with unit emissivity yields a value of ca.

$340 \text{ W m}^{-2}$ , or 340 MW per  $1 \text{ km}^2$  pixel, and the emitted energy for the whole area of London on the order of  $5 \times 10^5 \text{ MW}$  or 0.5 GW (see city areas below).

A default 50% threshold of clear sky was set for each city on each image based on the assumption that adequate coverage of the study region can be achieved by sampling a large enough set of imagery. The threshold was implemented in ArcGIS simply by comparing the maximum area of each city as given by the Meridian dataset (Table 3S1) with the area inside the city containing valid LST (i.e.  $p \cdot \Delta a$ ) from the satellite dataset. The effect of using a 75% clear-sky threshold is discussed below.

### ***3.2.3 Scaling Study Methodology***

35 cities were selected for study using an arbitrary threshold of city area greater than  $50 \text{ km}^2$ , from which population and emitted energy were derived (Table 3S3 in SI). Clear-sky nights were selected based on the prevalent synoptic meteorology (i.e., fog-free anticyclone conditions in the absence of fronts). A total of 28 nights was selected: 15 in winter (30 November – 28 February) and 13 in summer (1 June – 31 August) in the period 2000 – 2017.

## **3.3 Results**

Area-summed emitted energy varies over 1.5 orders of magnitude for cities with populations ranging over 2 orders of magnitude (Fig. 3.3a). Although the exact slope varies from night to night (Fig. 3.3b), the tight log-log correlation is always present. Strong correlations are present on both summer and

winter nights (Table 3.1) with no obvious pattern. The correlations suggest that population is a good predictor variable for total emitted energy, despite substantial differences in urban form of British cities. Figure 3.3b shows the plots for all dates sampled in this study. Slopes are similar, varying between  $0.73 \pm 0.06$  (13 December 2010; Table 3.1) and  $0.92 \pm 0.09$  (17 December 2011) and are ranked in Table 3.1 by their  $R^2$  value when using a 50% cloud-free threshold. Standard error on the slope increases as  $R^2$  decreases but there is no obvious trend in the value of the slope.

The derived regression equation for the averaged allometry over 28 nights is:

$$\log(\bar{Y}) = \log(\bar{\beta}) + \bar{\alpha} \cdot \log(\langle \bar{E}_j \rangle), \quad (3.5)$$

Where

$$\langle \bar{E}_j \rangle = \frac{\sum_{k=0}^n E_{j,k}}{n}. \quad (3.6)$$

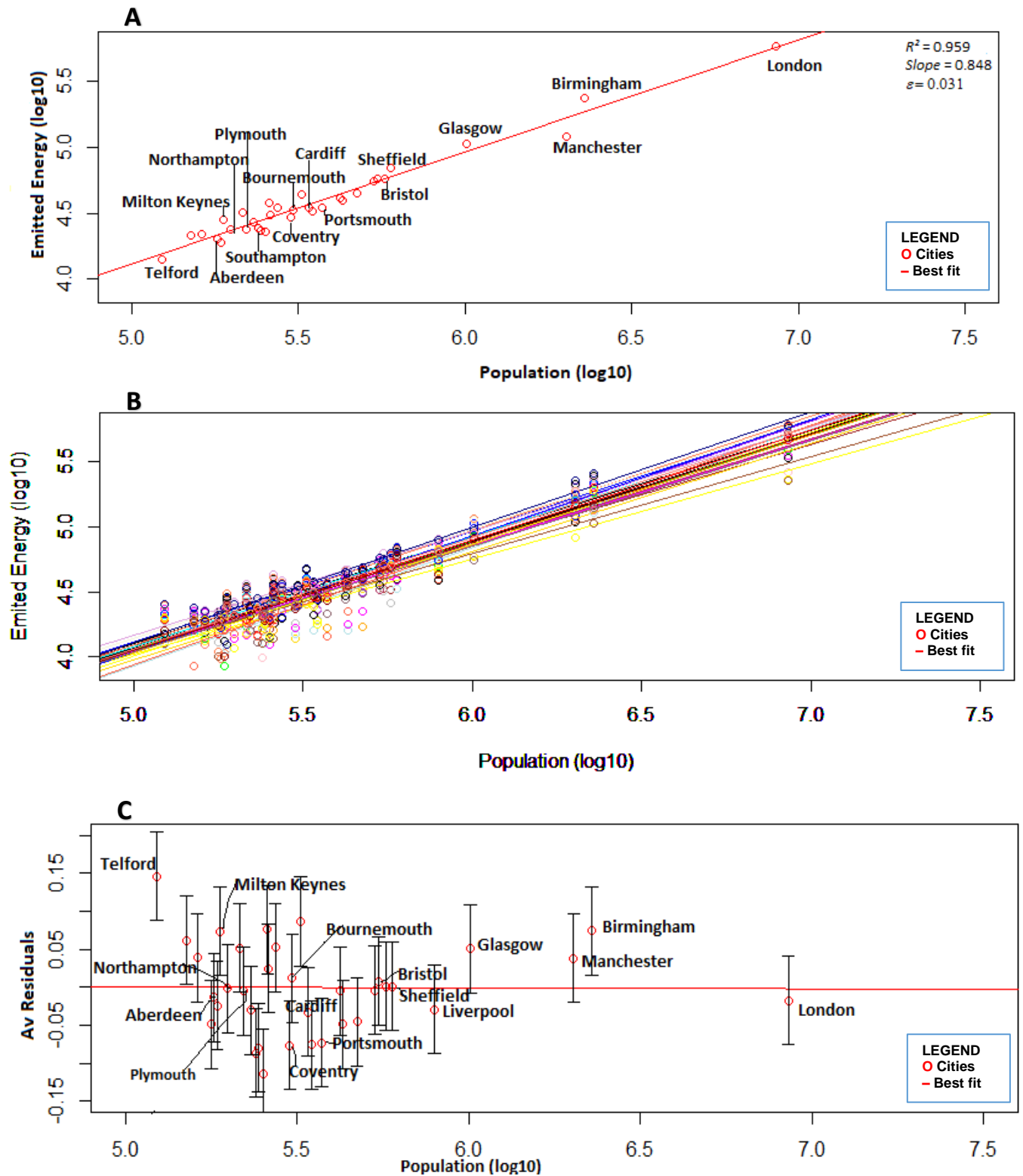
That is,  $\langle \bar{E}_j \rangle$  is the average emitted energy (in MW) over all nights for city,  $j$ , and  $n$  is the number of nights = 28.

Although the two extreme values of the allometric slope are statistically different (i.e., the means are further apart than the sum of the standard errors, Table 3S3, Supplementary 3SI), Figure 3.3a does not show any clustering of the regression slopes in the sample. It is assumed, therefore, that, to a first approximation at least, the results indicate that a single overall allometric scaling of total emitted energy with a population of  $0.84 \pm 0.06$  is plausible (Fig. 3.3b). If this assumption is justified, the variation observed in the regression slope must derive from difficult-to-quantify errors in the retrieval of the emitted energies, including the effect of partially obscured urban areas on the slope.

To test the impact of partial cloud obscuring, the analysis was repeated increasing the threshold for inclusion of an urban area in the analysis to 75% cloud-free (see Table 3S3 and Fig. 3S6 in supplementary 3SI). The scaling of emitted energy with population under this more stringent condition



has a slope of  $0.86 \pm 0.05$  (Table 3S3 in Supplementary 3SI), which is, within error, indistinguishable from the mean slope from Table 3.1.



**Figure 3.3** (A) An example of allometric scaling of night-time emitted energy  $\log_{10}(\langle E_j \rangle$ , in MW) against urban population for the 35 largest cities in Great Britain. Reported on the graph (top right) are the Coefficient of Determination ( $R^2$ ) for the best-fit regression, the slope of the regression, and the error on the slope ( $\varepsilon$ ). (B) The ensemble of allometric relationships derived for the nights studied (Table 3.1). (C) Residual emitted energy (mean and standard deviation of  $\log_{10}(\langle E_j \rangle$  in MW) for urban areas with respect to the allometric scalings shown in (B).

**Table 3.1 Night-time emitted energy for thirty-five (35) UK large Cities on selected summer and winter nights. Results are ranked by the strength ( $R^2$ ) of the log-log correlation between emitted energy and population, for which the slope, and error on slope ( $\sigma$ ) are reported at 50% cloud free pixels**

Rank	Date	Number of Cities	$R^2$	Slope ( $\alpha$ )	Error on Slope
1	13 <sup>th</sup> Feb. 2017	26	0.97	0.86	0.03
2	15 <sup>th</sup> Feb. 2016	25	0.96	0.85	0.03
3	06 <sup>th</sup> Jun. 2000	33	0.96	0.85	0.03
4	22 <sup>nd</sup> Feb. 2003	28	0.96	0.88	0.04
5	07 <sup>th</sup> Jul. 2007	34	0.96	0.84	0.03
6	01 <sup>st</sup> Jan. 2007	32	0.96	0.85	0.03
7	02 <sup>nd</sup> Jan. 2017	35	0.94	0.84	0.04
8	26 <sup>th</sup> Dec. 2009	24	0.93	0.81	0.05
9	27 <sup>th</sup> Jun. 2010	32	0.93	0.80	0.04
10	16 <sup>th</sup> Aug. 2016	35	0.92	0.89	0.04
11	29 <sup>th</sup> Feb. 2000	21	0.92	0.83	0.05
12	01 <sup>st</sup> Jan. 2012	24	0.92	0.89	0.06
13	30 <sup>th</sup> Nov. 2016	20	0.92	0.86	0.06
14	13 <sup>th</sup> Dec. 2010	17	0.92	0.73	0.06
15	28 <sup>th</sup> Aug. 2001	25	0.91	0.88	0.06
16	30 <sup>th</sup> Aug. 2005	22	0.90	0.82	0.06
17	20 <sup>th</sup> Jan. 2009	18	0.88	0.83	0.08
18	09 <sup>th</sup> Jul. 2006	34	0.88	0.88	0.06
19	20 <sup>th</sup> Jan. 2011	22	0.88	0.74	0.06
20	08 <sup>th</sup> Aug. 2012	25	0.88	0.83	0.06
21	05 <sup>th</sup> Jan. 2005	34	0.88	0.80	0.05
22	10 <sup>th</sup> Jun. 2003	27	0.87	0.81	0.06
23	13 <sup>th</sup> Jul. 2002	28	0.87	0.77	0.06
24	03 <sup>rd</sup> Aug. 2017	22	0.86	0.82	0.07
25	25 <sup>th</sup> Feb. 2009	26	0.85	0.91	0.08
26	28 <sup>th</sup> Aug. 2009	30	0.84	0.81	0.07
27	17 <sup>th</sup> Dec. 2011	26	0.83	0.92	0.09
28	18 <sup>th</sup> Feb. 2006	25	0.79	0.84	0.09
	<b>Mean</b>			<b>0.84</b>	<b>0.06</b>
	<b>Median</b>			<b>0.83</b>	

Table 3S4 (supplementary 3SI) tests the effect of a population threshold by comparing the correlations for cities with populations greater than 250,000 and greater than 500,000. The mean slope of the regression is not significantly different for both subsets of cities.

### 3.4. Discussion

The findings from this study indicate that population is a good predictor variable for total emitted energy despite the differences in the urban form of UK cities. This study finds a much more significant scaling (i.e., larger values of  $R^2$ ) for upwelling clear-sky long-wave with population than was found for  $\Delta T_{u-r}(max)$  by Oke (1973; 1982) (cf., the  $R^2$  in Fig. 3S1 in 3SI and those in table 3.1).

Alternative variables for this allometric study could include the maximum value of  $\epsilon_{i,j,k}$ , or the mean of  $\epsilon_{i,j,k}$  for the  $j$ -th city, the maximum of  $T_{i,j,k}$  within a city, or  $\text{mean}(T_{i,j,k})$  within the city boundary. All these variables would make interesting subjects for further investigation, but time has prevented them being more fully investigated in the present thesis. The scaling of maximum values of variables within the city limits are discussed for air pollution and temperature in MacKenzie et al. (2019). They put forward an argument based on the likelihood of the occurrence of pollution hotspots,  $H$ , to be

$$H \propto \frac{Y_E}{Y_L} F \quad (3.7)$$

where  $F$  is the fraction of roads liable to poor ventilation (fumigation), and  $Y_E/Y_L$  is the average emission per unit road length in the urban area. Since high night-time temperatures also require poor ventilation, a similar equation could hold for the likelihood of  $\max(T_{i,j,k})$  being above some threshold, but with  $Y_E/Y_L$  replaced by the city-average emitted energy. Following the arguments in MacKenzie et al. (2019), the scaling of equation 3.7 is expected to be super-linear. Testing this hypothesis is outside the scope of the present thesis.

That said, we note that energy emitted from the surface is acted on by turbulent and radiative transfer processes, the net result of which is  $\Delta T_{u-r}(max)$  (Oke, 1982). Total emitted energy is, therefore, a more fundamental property of urban form than the temperature variables.

For properties like temperature, which depend on the combined effects of emitted energy and turbulent and radiative processes, scaling will be the sum of scalings for each process. Although it is

plausible that turbulent transfer processes scale with city size (as discussed in (MacKenzie et al., 2019)), it appears that the overall effect on the energy budget is to dampen very significantly the scaling of  $\Delta T_{u-r} (max)$  compared to the scaling of emitted energy. The difference in the scalings of the heat source and the final temperature difference is very marked: 0.84 (table 3.1) compared to 0.11 (Fig 3S1). Investigating this further will require a detailed investigation of the scaling of each aspect of the urban energy budget, which is outside the scope of the present study.

The scaling of emitted energy with population is very similar to that of total urban area with population (Fig. 3S2A in the SI). Hence, emitted energy varies linearly with urban areas for the 35 cities in our study (Fig. 3S3), even though that area becomes increasingly densely populated as city population increases. The implication is that, on average, there is no structural change of relevance to the total emitted energy between a single city the size of London or ten cities each a tenth of the area (i.e., roughly the size of Bristol). This quantitative scaling without qualitative structural change may be consistent with Oke's 1973 study on city size and the urban heat Island, and with his study in 1981 on canyon geometry and the nocturnal urban heat Island, in which he cited Chandler's 1967 observation on the similarities of London and Leicester temperature on the same night, despite their difference in size and population (Oke, 1973; 1981). Non-linearities may become more important when smaller urban centres are included, as in the study of Zhou et al. (2013).

Further information about the urban form can be derived by inspection of the residuals, i.e., the distances of each urban area from the line of best fit (Fig. 3.3c). We postulate that differences in urban form across Great British cities will be evident in both the magnitude and sign of the residuals. Firstly, however, we discount geographical and climate factors. Comparisons between mean emitted-energy residuals and each of altitude, latitude, mean hours of sunshine, and mean annual temperature for each city showed no significant correlations (see Figs. 3S9, 3S10, 3S11 and 3S12 in supplementary 3SI).

The magnitude of residual can be interpreted as the degree to which an individual city deviates positively or negatively from the value expected for a city of its size (Bettencourt et al., 2010). For the

case of emitted thermal energy, positive anomalies correspond to cities with warmer surfaces than expected and negative anomalies correspond to surfaces cooler than expected based on the best-fit population-based allometry. There is a tendency for the magnitude of residuals to be larger for the smaller urban areas (Fig. 3.3c). For example, the residual for Telford is positive and about 4% of its mean area-summed emission, whereas, for London, the residual is about 0.2% of the mean area-summed emission.

The cities of Coventry and Plymouth, which were reconstructed post-war (Hasegawa et al., 2013) have large negative residuals (-0.075 and -0.004 y-axis units ( $\log_{10}(\langle E_j \rangle$  in MW)), Fig. 3.3c), whereas the New Town 'Garden Cities' of Milton Keynes and Telford both have large positive residuals (0.08 and 0.15 units). These unexpected results do not seem to arise from sampling issues affecting the overall allometry because the residuals are robust for the various nights studied (variation bars in Fig. 3.3c). Instead, the results may arise from a greater area of impervious, low albedo, surface per person in the lower density Garden Cities. Residuals for the area allometry for each city are reported in (Table 3S2 supplementary 3SI). Milton Keynes and Telford have large positive residuals compared to their expected area (0.087 and 0.155 units, respectively), whilst Coventry and Plymouth have large negative residuals (-0.056 and -0.050 units). So, the Garden cities emit more than expected for their populations but spread that emission over a wider surface area than expected, whereas Coventry and Plymouth emit much less than expected from their population but spread that emission over a smaller-than-expected area.

Northampton, situated about 60 miles (97km) north-west of London and 45 miles (72km) south-east of Birmingham, had a population of 212,100 at the 2011 census. Northampton is predominantly a post-war settlement in which growth was limited until it was nominated as a New Town in 1968 (Whitehand and Whitehand, 1984). Its mean energy emission residual is close to zero, similar to Bristol (Fig. 3.3c), despite being radically different in terms of population and their histories of urban development. The residuals for urban areas are also similar for Northampton and Bristol. However,

Milton Keynes, the city closest to Northampton in population (Table 3S1, supplementary 3SI), similarly situated (about 50 miles (80km) north-west of London), and also a classic post-war New Town, has a large positive mean emitted energy residual (Fig. 3.3c) and large positive area residual.

City configuration, street patterns and orientation, structure of buildings and density, and ultimately the intensity of human activities are key factors that determine thermal behaviour in the city. In summary, the residuals (Fig. 3.3c) allow an assessment of the similarities and differences in emitted energy, relative to that expected by the best-fit line, for settlements of very different size.

### **3.5 Conclusion**

This study aimed at evaluating the extent and rate of clear-sky emitted long-wave energy with population in the cities for MODIS/Terra V006 composite products (MOD11 A1). This was achieved by assessing the night-time emitted energy across cities in Great Britain for 28 night-time samples across summer (JJA) and winter (DJF) between 2000 and 2017. British cities show a strong and consistent sub-linear allometric scaling of total emitted energy with population. That is, there is a substantial ‘economy (or parsimony) of scale’ in terms of nocturnal heat production in British cities: the production from the larger cities is smaller than would be produced from a constellation of smaller cities housing the same population. This uniformity of scaling occurs despite of the obvious differences in architecture and urban form in settlements with Medieval centres (e.g. Aberdeen), predominantly commercial/military (e.g. Southampton) or residential (Bournemouth) coastal settlements, and post-second world-war planned settlements (e.g., Milton Keynes).

The scaling of emitted energy with population is much larger than reported in the previous literature of the scaling of air temperature urban heat island (UHI) with population (Oke, 1973; Oke, 1982). It is possible to compare these scalings even though emitted energy and UHI have different units because the logarithmic scaling produces a dimensionless slope quantifying relative changes. Since long-wave emissions from the relatively warm urban surface are the source of the nocturnal UHI and SUHI,

turbulent and radiative transfer in the atmosphere must act to dampen significantly the scaling signal for heat island metrics. The concentration of population into larger urban areas, rather than spread out over more, smaller, cities, has only a marginal worsening effect on the risk to health arising from air temperature UHI but a much larger effect arising from radiant flux (cf., e.g., Middel and Krayenhoff, 2019).

The scaling of total emitted energy with population has a similar slope, within statistical error, as the scaling of urban areas with population. This equality of scaling suggests that energy emitted per unit area averages out to be approximately the same everywhere in cities at the granularity of the current analysis. This ‘emergent simplicity’ in the scaling of emitted energy for urban areas of different sizes seems counter intuitive given our understanding of the role of urban form in heat storage and emission in the built environment (Arnfield and Grimmond, 1998; Nunez and Oke, 1977). Instead, the particularities of British urban form seem to manifest in the residuals for each city, i.e., the magnitude of the difference in emitted energy measured from that predicted by the best-fit line. As yet, we have not been able to find any simple rules that would allow us to predict the size of the residual from its geographical context (including climate) or from its development history, but we believe this merit further study.

## **4.0 Chapter 4**

### **Allometric scaling of emitted thermal infrared across Nigeria's cities and its relation to urban form**

This chapter built on the previous study (Abdulrasheed et al., 2020) i.e., objective 1 and also addresses objective 2 in the thesis. The chapter aim to investigate the extent and rate of clear-sky long-wave energy with population across Nigeria's cities using MODIS/Terra V006 composite product (MOD11A1). This will be achieved by assessing the night-time long-wave energy across 33 Nigerian cities.

#### **Abstract**

High rates of urbanisation coupled with a rise in global average surface temperature, due to climate change, makes it increasingly important to understand the energy balance of cities. By understanding the impacts of population growth on urban heat, planners can better incorporate passive means to reduce the heat load of cities. In this study, images from the Moderate Resolution Imaging Spectroradiometer (MODIS) satellite, covering the period between 2000 and 2017, were sampled to examine the seasonal variability of night-time clear-sky upwelling long-wave energy for 33 cities across Nigeria. Total (area-summed) emitted energy was calculated per city and shown to correlate closely ( $R^2 \geq 0.71$ ) with population on a log-log 'allometry' plot. The total night-time emitted energy is found to scale sub-linearly with population on all the sample nights. The total night-time emitted energy is found to scale linearly with the area of cities, a result that has been shown for UK cities in the previous chapter. The common linear scaling of emitted energy with area in UK and Nigerian cities suggests that the changed energy budget of cities, compared to the rural land cover they replace, is driven by the thermal properties of built impervious surfaces rather than the distribution of urban morphological settings, as described by, say, the local climate zones concept.



## 4.1 Introduction

### *4.1.1 Urban Heat & Local Climate Zones*

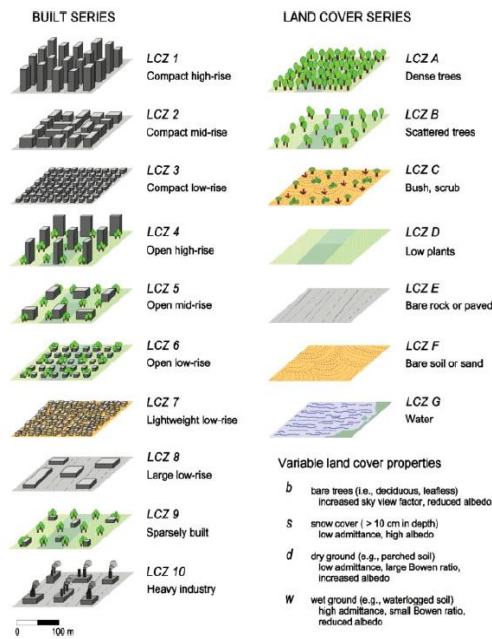
Climate change affects both developed and developing countries, though the impact is more on developing countries who contribute least to the changes (Ludwig et al., 2007). Developed countries who contribute more to the changes have effective mitigation and adaptation techniques (e.g. technologies, effective policies, and wealth) to curtail the adverse impact. The vulnerability of developing countries, especially in Africa, is aggravated by existing developmental challenges like poverty, low levels of infrastructure and technology, limited access to capital, and ecosystem degradation, among others. Adaptation capacity is generally weak, and mitigation strategies are few in Africa and African cities (Solomon et al., 2007; Rohat et al., 2019). One of the biggest concerns with climate change is understanding how it will impact in an urban context.

Urbanisation is accelerating, especially in Africa and Asia (Endsjö, 1973; Martins, 2000; Cohen, 2006 ; Aliyu and Amadu, 2017). By 2050, it is estimated that the global urban population will increase by 2.4 billion (United Nations et al., 2019), predominately in developing countries (Seto et al., 2012; Buhaug and Urdal, 2013; Bremner et al., 2010; UNDP, 2010; Bongaarts, 2009). Resource use in urban areas has global impact, accounting for approximately three-quarters of energy-derived greenhouse gas emissions (Hoornweg et al., 2011), with significant consequences for global climate (IPCC 2013).

Urbanisation changes land surface characteristics such that the local energy balance is altered, which must be accounted for in the estimation of long-term temperature trends (Chrysanthou et al., 2014). Well-documented phenomena arising from this change in thermal climate in urban areas, include the urban heat island (UHI) (Bornstein, 1968; Oke, 1995; Sheng et al., 2017; Landsberg, 1981), associated urban thermal plumes (Oke, 1995; Heaviside et al., 2015), and urban precipitation anomalies (Han et al., 2013). Conceptual models of these phenomena emphasise the role of different urban land uses (Stewart and Oke, 2012; Tomlinson et al., 2012), and highlight the role that planning choices at the neighbourhood scale can have in mitigating urban climate trends (Davoudi, 2012; Davoudi, 2014).

Following the seminal work of Landsberg and Oke on the surface energy modification which produces nocturnal UHI (Oke, 1981; Landsberg, 1981), land use classifications and urban morphology offer useful approaches to determine the city's local climate. Urban morphology parameters such as the sky view factor, surface roughness and aspect ratio (among others) all have influence on the urban climate. However, the direct link between these parameters and urban planning and design strategies is still weak.

As the study of urban climate grows, standards are necessary for meaningful and consistent exchange of data between regions across the globe. The Local Climate Zone (LCZ) concept developed by Stewart and Oke (2012) provides a means to standardise the methods used to describe urban form and its associated influence on thermal performance in UHI studies (Stewart and Oke, 2012). In the LCZ system, the nature, and patterns of urban form (i.e., building geometry, pervious surface fraction, building and tree densities, soil permeability etc.) determine its thermal classification. The methodology consists of 17 classes at a neighbourhood scale, of which 10 portray urban form identifiable in most cities and the remaining seven (7) describes land cover series, (Fig. 4.1, which refer back to the larger version in chapter 2) (Stewart and Oke, 2012). Hence, variations in LCZ results in the classification of the urban landscape into sub-divisions on the bases of characteristics such as surface structure (building/tree height and spacing), cover (pervious fraction), fabric (albedo, thermal admittance), and metabolism (anthropogenic heat flux) (Stewart and Oke, 2009; 2012).



**Figure 4.1 Local Climate Zone (LCZ) Classification and its 17 Standard Classes (after Stewart and Oke 2012)**

As cities grow, (green) trees and vegetation are replaced with (grey) buildings and infrastructure. The

magnitude and nature of the change depends on the morphology of the urban form controlled by the geographic setting (topography, building fabrics, surface roughness, closeness to water bodies etc.). In general, urban land absorbs a higher fraction of incoming solar radiation than rural land, and so has a smaller Bowen ratio (i.e., the ratio of sensible to latent heat emission) (Arnfield, 2003; Aguado and Burt, 2015). Buildings also slow the wind path within the street canyons, retaining the heat released from vehicles and buildings (Golden, 2004; Arifwidodo and Tanaka, 2015). Anthropogenic activities also result in cooling and heating demand in the city (Ahmed, 2003; Ho et al., 2015), this can generate distinct local scale climate within the neighbourhoods in the same city of similar land use and land cover (C. Wang et al., 2018). Overall, urban land stores more heat, giving rise to conditions that may place human health at risk (Basu and Samet, 2002; Rosenzweig et al., 2011; Murray and Ebi, 2012; Smith et al., 2011; Patz et al., 2005; Hondula et al., 2015; Wouters et al., 2017; Krayenhoff et al., 2018) and may require even more energy consumption to mitigate (Li et al., 2015).

Numerous studies have investigated the impacts of urban form on local climate modification in Africa (Adefolalu, 1984; Akpodiogaga-a and Odjugo, 2010; Eludoyin et al., 2014; Ayanlade, 2015; Ayanlade, 2016a; Adole et al., 2018). Urban planning responses to climate change, including both mitigation and adaptation strategies, continue to evolve, especially with respect to sustainable urban development

in cities (Davoudi et al., 2009; Daramola and Ibem, 2010; Anukwonke, 2015; Hendrickson et al., 2016; Rybski et al., 2017; Castán Broto, 2017 ;Fujii et al., 2017). Indeed, there exists a large body of work promoting urban climate adaptation towards reducing vulnerability and promoting resilience of people and properties as well as metropolitan activities has been assessed (Satterthwaite, 2007; Amundsen et al., 2010; Carmin et al., 2012; Anguelovski et al., 2014; Stefanovic et al., 2019; Pasquini, 2019). For example, microclimate planning and design modification to the outdoor environment can enhance thermal comfort, (i.e. neighbourhood streets, green spaces and parks among other) (Daramola and Ibem, 2010; Brown, 2011), and so provide adaptation to climate change through smart urban design and planning (OECD, 2014). Based on these studies, it is clear that Africa can provide a unique means to investigate urban climate in hot countries. There exists a tremendous variation in urban morphology across the African biomes (at a scale not seen in other continents). Furthermore, the unprecedented growth of people living in urban centres in African countries, in particular Nigeria, result in significant and widespread changes in the morphology of place and hence, the normal climatic condition of the place (Mabogunje, 1990; Rohat et al., 2019). With the aim of demonstrating this uniqueness of place, this paper will focus on Nigeria's urban form and its climate modification due to urbanisation at the whole-city or settlement scale.

#### ***4.1.2 Nigerian Cities***

Nigeria as a political entity is a pre-colonial product of nineteenth century wars. The era of colonial rule in Nigeria came together with significant changes in socio-economic well-being, especially in the pattern of demographic development of the country (Qşoba, 1969). The movement of people from rural to urban centres is a normal demographic phenomenon in any developing economy, although it has many implications (Goldstein, 1990; Cohen, 2006). Over the last two decades, Nigeria has experienced an unprecedented increase in urban growth. The country's urban population in 1975 was estimated at 21% of the total population, by 1993, 36.2% of the total populace lived in the urban centres and today about (37%) of the Nigerian population are urban dwellers. The long-term average

growth rate of the country's urbanization is  $5.8\% \text{ yr}^{-1}$  (Anukwonke, 2015; Aliyu and Amadu, 2017), with major cities such as Lagos, Kano, Ibadan, Aba and Onitsha growing at faster rates.

The movement of people from rural to urban communities has negatively affected the urban environment (Piault, 1963; Daramola and Ibem, 2010; Omole and Akinbamijo, 2012). Ancient cities — like Kano, Lagos, and Ibadan — and newer metropolises — like Port Harcourt, Kaduna, Enugu, and Jos — have overgrown beyond their capacity to absorb the influx of migrants. The consequences of this overflow during the colonial era included unemployment and underemployment (Qşqba, 1969), shortage of housing, the proliferation of slum and squatter settlements, overcrowding, sub-standard building construction, breakdown of waste disposal arrangements, air and water pollution, and inadequate utilities and infrastructure (Goldstein, 1990; Arimah and Adeagbo, 2000).

Following colonial rule, two key planning policies have been enacted in Nigeria (e.g. In 1992 the new Urban and Regional Planning Law replaced the 1946 Town and Country planning Law (Mabogunje, 1992; Arimah and Adeagbo, 2000; Oloyede and Akinbode, 2010; Omole and Akinbamijo, 2012). These policies led to notable changes in the urban form, for instance slum clearance re-shaped previously low rise close-packed housing into a sparsely distributed ones, the building of housing estates in most of the cities replaces farm field (or, often, large houses in parkland estates) and the re-organisation of the country into three regional levels for urban renewal, (Mabogunje, 1992).

#### ***4.1.3 Allometry***

Allometry, according to (Gould, 1966), is the study of size and its (predictable) consequences. It is the study of how many different properties of a system relate to a single easy-to-measure property, such as body mass for animals, or population for cities. Naroll and Bertalanffy (1956) were the first to apply allometry to urban studies. Since then, a considerable amount of literature has been published on urban allometric scaling, for aspects of material, energy, or economic flows, usually related to the size of cities as determined by their population (e.g. Bettencourt, 2013; Batty, 2008; Lee, 1989; Longley et al., 1992; MacKenzie et al., 2019). Allometric scaling recognises that the many microscopic interactions

within a complex system (i.e. in this case, an urban settlement), when measured against a simple parameter of size such as population, often collapse to a simple pattern such as a power law (Cottineau et al., 2017). Scaling, therefore, allows us to organise our knowledge about cities (Batty, 2008), by searching for simple, emergent, patterns. The price for this simplicity, however, is a loss of bottom-up detail that might evidence causal relations, although it is sometimes possible to compare allometric patterns (e.g., for road length and pollution emissions) to deduce more about factors driving the patterns (MacKenzie et al., 2019).

In the present study, techniques for allometry, developed for a previous study on allometric scaling of emitted energy for 35 UK cities (Abdulrasheed et al., 2020), are applied to the very different Nigerian context in order: (i) to compare allometric patterns for European and African settings; and (ii) to ascertain the role of urban morphology in the scaling pattern utilising the diverse range of urban forms evident across Nigeria.

## ***4.2 Methodology***

### ***4.2.1 The study area***

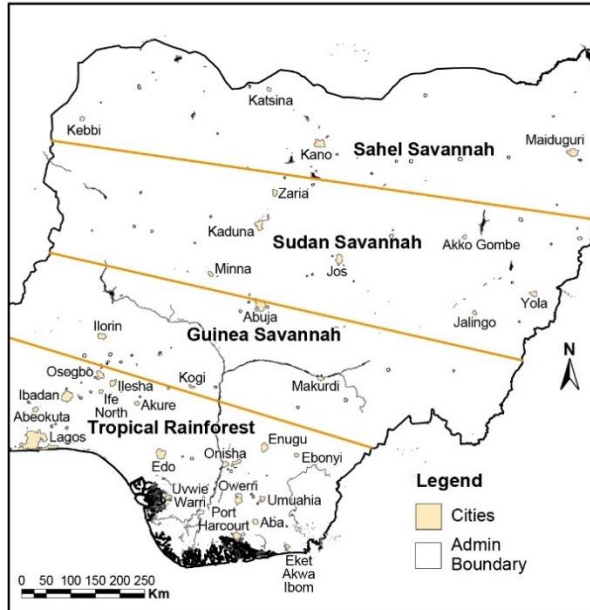
Nigeria lies between 4° and 14° N latitude and shares a land border with the Republic of Niger in the north. It is bounded to the east by Cameroon, to northeast by Chad, and to the west by the Republic of Benin. The country's southern boundary is the Gulf of Guinea (an arm of the Atlantic Ocean). Nigeria has a total land area of 983,213km<sup>2</sup> (Omofonmwan and Osa-Edoh, 2008). According to the National population Commission of Nigeria, the population of Nigeria, as at census 2016 is estimated to be 193,392,517 people, and the rate of annual growth is 3.2% of which over 41% of the population are under the age of 15 (NPCN, 2018). The climate of Nigeria is humid tropical, and classified into four climate zones (Ogunjobi et al., 2012; Balogun and Balogun, 2014)

1. The tropical rainforest zone has distinct dry and rainy seasons, average annual rainfall of 1489mm, and average temperature of 26.5°C. This zone experiences a dry season between November and March.
2. The guinea savannah zone around the middle-belt, has a rainfall distribution of 1051mm and an annual average temperature of 27.3°C. The zone is characterized by long dry periods.
3. The Sudan savannah zone covers more than one-quarter of Nigeria's total land area. It spans almost all the northern states bordering the Niger Republic and has low annual average rainfall (657mm) and a prolonged dry season of 6-9 months.
4. The Sahel savannah in the far north of the Country has the driest season in Nigeria, which sets in around September/October yearly and persists until April/May the following year.

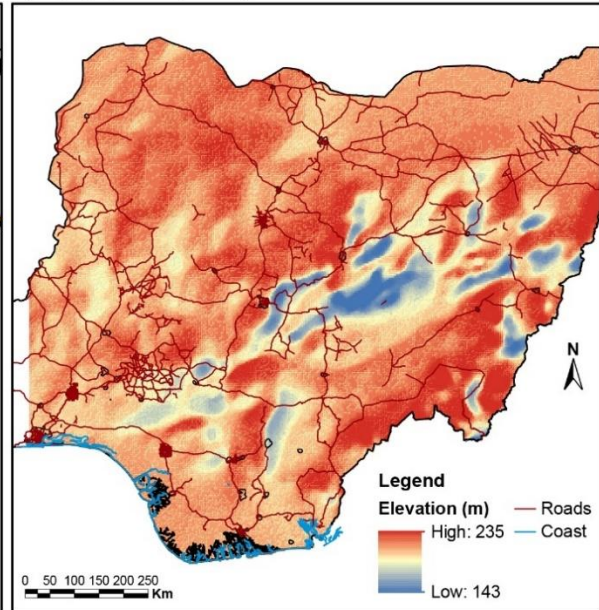
However, the regions are divided into 3 (northern region, middle belt, and southern region). The northern region has two distinct climates; the Sahel savannah at the upper north and the Sudan savannah – a transition towards the middle belt region (see Fig. 4.2a).

The mean climate map of Nigeria is shown in figure 4.2. The present study will focus on the thirty-three (33) largest urban areas across Nigeria (see Fig. 4.2a), and table 4S1 and figure 4S3 of the supplementary information.

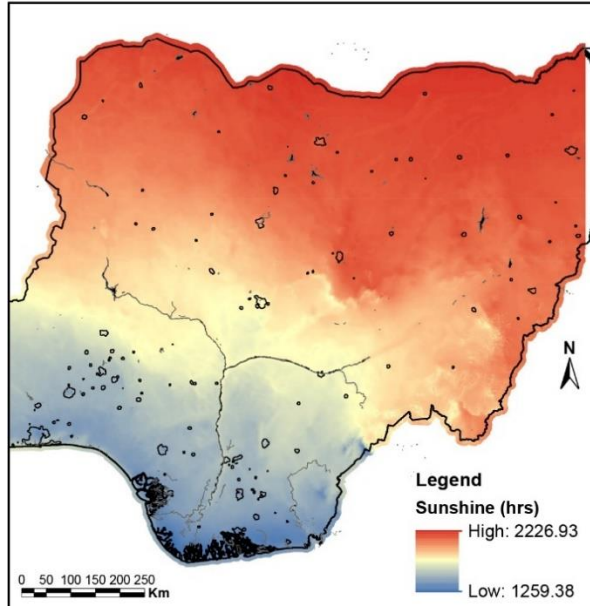
a) 33 largest urban areas of Nigeria and climatic zones



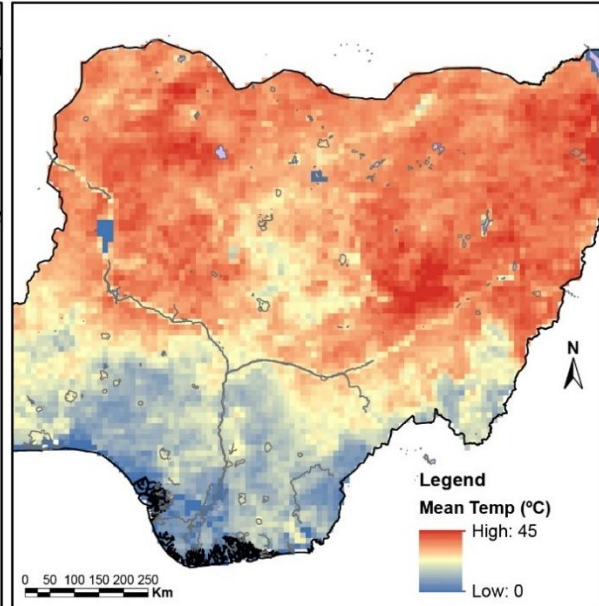
b) Topographic map of Nigeria



c) Average sunshine (2016 - 2018)



d) Mean temperature


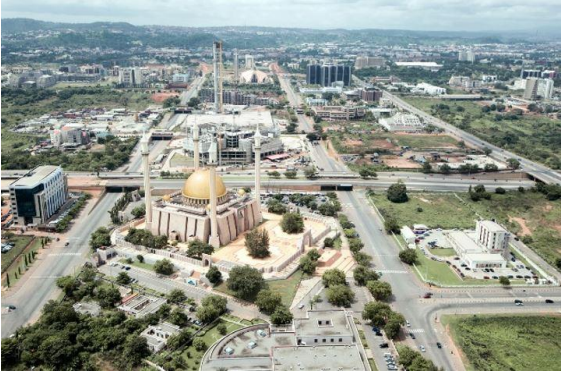



**Figure 4.2 The mean climate map of Nigeria: (a) 33 largest urban areas of Nigeria and climatic zones; (b) Topographic map of Nigeria with cities and major roads overlaid; (c) Average Sunshine of Nigeria; (d) Temperature map of Nigeria. Data source: Digimap (Relief) <https://digimap.edina.ac.uk>, Global Solar Atlas - (SolarGIS, 2019) and ArcGIS tools were used to plot the maps.**

In this study, Nigeria is divided into 3 main climate regions: the Northern region; Middle belt; and Southern region. Each of the study cities relates to these regions in-terms of cultural and climate contexts (Fig. 4.3). The land cover and built series are predominantly LCZ D — LCZ G in the northern and middle belt region, and LCZ B — LCZ G in the southern region. Cities in the north (Kaduna, Kano,



Kebbi, Zaria, Maiduguri and Akko) are mainly characterised by high, medium and low density urban sites with flat terrain (Ibrahim et al., 2011; Nduka and Abdulhamed, 2011). Around the middle belt (Bauchi, Abuja, Minna), the nature of urban sites demonstrates a transition from the northern region to the southern region with rocky and flat terrain (Kafi et al., 2014). The southern part region (Lagos, Port Harcourt, Akure, Onitsha, Ibadan etc.) is characterized by mainly medium and high density urban sites and wetland with trees / forest (Nduka and Abdulhamed, 2011; Ragatoa et al., 2019).

Northern Region Kaduna city		Central business district axis with tall dense mix buildings. Scattered trees and abundance of paved and unpaved land cover with moderate traffic density	LCZ2
Middle belt Region - Abuja		Spatially arranged mix of midrise buildings with abundance of impervious land cover and lots of trees scattered all around.	LCZ2 – LCZ9
Southern Region Lagos mainland		<ul style="list-style-type: none"> <li>-Busy coastal area along the commercial axis of Lagos with scattered evergreen trees and mid-rise buildings. Large open water body</li> <li>-Dense mix low-rise and single-story buildings with few or no trees</li> <li>-Sparsely tall buildings/industries with scattered trees around mainland of Lagos</li> </ul>	LCZ2 – LCZ10

**Figure 4.3 Regional classification of city's field sites by local climate zones- zones - Pixels above were adapted from the following papers: (Usman et al., 2016); (MyGuide, 2017)**

Cities are also categorised into three major types: Ancient Cities; New cities; and Coastal cities. We also identify the Federal capital specifically and have a final category 'other', for cities that do not fall into these categories. The development of coastal areas results in a dramatic changes of land use and land cover. Climate change is an additional problem for coastal communities. Despite all the problems, people continue to be strongly attracted to coastal areas. Population in these areas is growing faster than the capacity of the infrastructure in place if, indeed, any infrastructure is present at all. This overwhelming of infrastructure by growing population leads to the emergence of slum and squatter settlements, which would be expected to have a substantial influence on the temperature alteration (UHI or SUHI) of the city. For example, Wu et al., (2019) analysis of the seasonal effect of urban heat island in a coastal city concludes that seasonality contribute to the temperature modification (UHI effect) and distance to the coastline does not play a role in the UHI effect. In Nigeria for example, Lagos is regarded as Africa's most urbanized coastal megacity. It has been demonstrated that the UHI effect is higher in the morning on the islands adjacent to the Atlantic Ocean, due to marine influence, but the rest of the city is conditioned by the characteristics of the land-use type (Ojeh et al., 2016). The influence of nearby water on the satellite data used in this study is discussed below.

#### ***4.2.2 Data collection and analysis***

In this study, the urban heat budget was investigated by considering the total (area-summed) emitted energy from urban areas, measured from the MODIS (Moderate Resolution Imaging Spectroradiometer). About 6000 images from LST at different periods (summer and winter) were selected and sampled for the study. The primary quality control criteria for an image to be included in the analysis was the stipulation that at least half of a city was required to be cloud-free.

##### **4.2.2.1 MODIS (Moderate Resolution Imaging Spectroradiometer) data**

The methodology used for data collection is based on Abdurashheed et al. (2020) and uses MODIS/Terra V006 composite products (MOD11A1) – MODIS/Terra Land Surface Temperature and Emissivity Daily L3 Global 1km Grid SIN V006). MODIS data is extensively used in the scientific

literature for its enhanced spectral, spatial, radiometric, and geometric quality and also known for its global mapping and monitoring land cover (Salomonson et al., 1989; Friedl et al., 2002). In this study, area summed clear-sky night-time emitted energy was derived from MODIS data for the 33 largest cities in Nigeria. Land Surface Temperature (LST) between 2000 and 2017, at 1km spatial resolution was obtained for the study. Satellite measurements of land-surface temperature are affected by nearby water due to the resolution of the land-water mask (Carroll et al., 2017). Early versions of the MODIS data used 1-km resolution land-water mask derived from the earlier AVHRR satellite. The MOD11 LST dataset used in this thesis uses a 250-m land-water mask (Carroll et al., 2009), which greatly reduces the mis-categorisation of land and water.

LST data for each pixel,  $i$ , within the city,  $j$ , on night,  $k$ , was converted to emitted energy,  $\varepsilon_{i,j}$  in  $\text{W m}^{-2}$ , using the Stefan Boltzmann law:

$$\varepsilon_{i,j,k} = \sigma T_{i,j,k}^4 \quad (4.1)$$

where,  $\sigma$  is the Stefan-Boltzmann constant =  $5.67 \times 10^{-8} \text{ W m}^{-2} \text{ K}^{-4}$ , and  $T_{i,j,k}$  is the LST in Kelvin of pixel,  $i$ , in city  $j$ . Area-summed emitted energy,  $\langle E_j \rangle$  in MW, for each city on each night, was then calculated by summing the  $p$  unobscured land-surface pixels inside the city boundary:

$$\langle E_{j,k} \rangle = 10^6 \sum_{i=0}^p \varepsilon_{i,j,k} \Delta a \quad (4.2)$$

Where  $\Delta a = 1 \text{ km}^2$  and  $10^6$  is the factor converting  $\text{km}^2$  into  $\text{m}^2$ .

### 4.2.3 Allometry

Allometric patterns conform closely to an equation of the form:

$$Y = \beta X^\alpha \quad (4.3)$$

Equation (4.1) describes a straight-line relationship between the X and Y variables when the function is plotted on a double logarithmic coordinate system, or

$$\log(Y) = \log(\beta) + \alpha \log(X) \quad (4.4)$$

Where  $\beta$  is a constant offset and the more important constant,  $\alpha$ , is the rate of relative growth (referred to below as the slope, or scaling, of the allometric relationship).

Total (area- summed) emitted energy was calculated and interpreted by looking for ‘allometric’ scaling against the total population of the urban area. A goodness of fit criterion and standard measures in form of threshold were put in place to ensure accuracy.

The derived regression equation for the averaged allometry over 23 nights is:

$$\overline{\langle E_j \rangle} = \frac{1}{n} \sum_{k=0}^n \langle E_j \rangle_k \quad (4.5)$$

Where  $\overline{\langle E_j \rangle}$  is the average emitted energy in Watts for city  $j$ , and  $n$  is the number of nights = 23.

Having established the allometric relationship, the residual for any city,  $j$ , is calculated as the vertical distance of the datum for that city to the best-fit line:

$$r_j = \log(\overline{\langle E_j \rangle}) - \{ \log(\beta) + \alpha \cdot \log(X_j) \} \quad (4.6)$$

Where  $X_j$  is the population of city  $j$ .

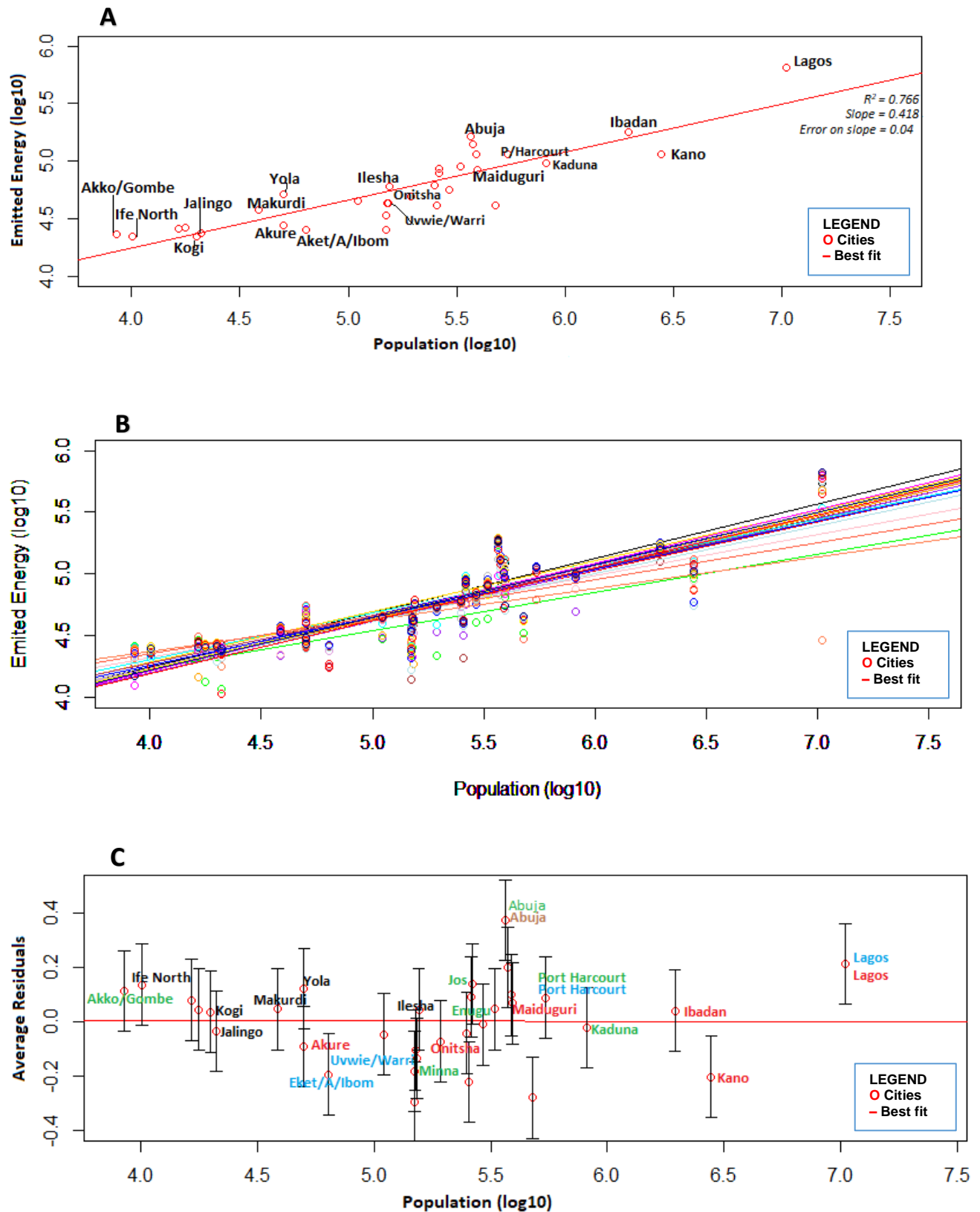
### 4.3 Results

Figure 4.4a & b and Table 4.1 indicate that allometric scaling appears present on the sample nights: 15 out of the 23 nights have  $R^2 > 0.70$  and only two nights have correlations less than 0.5. Such correlations suggest that population is a reasonably good predictor variable for total emitted energy, regardless of the previously discussed substantial differences in the urban form of Nigeria’s cities. However, it is the unexplained variation which is the key focus of this study as it is hypothesised that this will be a consequence of variations in urban form. As such, we now discuss departures from the scaling correlation (Fig. 4.4c) below, after considering factors that may affect the scaling pattern itself.

The days are ranked in Table 4.1 by their  $R^2$  value, whereas Figure 4.4b shows the correlations for all dates sampled in this study. Slopes are all sub-linear, varying between  $0.25 \pm 0.06$  (10 January 2005; Table 4.1) and  $0.44 \pm 0.06$  (16 November 2004). Taking only those samples with  $R^2 \geq 0.7$ , the mean slope is  $0.41 \pm 0.06$ , which corresponds closely to the median slope of the whole sample. Importantly, the clustering of slopes suggests that, to a first approximation at least, the results indicate a single overall allometric scaling of total emitted energy with a population of  $0.41 \pm 0.06$  (Fig. 4.4b).

However, care must be taken when interpreting these results as the 50% threshold for clouds may mean that some of the areas are partially obscured on some nights, which has the potential to impact the analysis. To test the impact of partial cloud obscuring, the analysis was repeated increasing the requirement for inclusion of an urban area in the analysis to 75% cloud-free (see Table 4S3 and Fig. 4S6 in supplementary 4SI). The scaling of emitted energy with population under this more stringent condition has a slope of  $0.40 \pm 0.05$  (Table 4S3), which is, within error, indistinguishable from the mean slope from Table 4.1 (50% cloud-free). This is an important finding as in many climates across the world, it can be challenging to produce an archive of clear sky satellite imagery of sufficient size for analysis.

An added consideration is city size. This was tested by taking a stratified approach to the analysis, A summary of findings from table 4S4 (supplementary 4SI), indicates that the slope of the regression is slightly different varying between  $0.44 \pm 0.16$  (10 January 2005) and  $0.48 \pm 0.11$  (15 February 2008) when we restrict our analysis to cities with populations  $>500,000$ . Slope varies between  $0.08 \pm 0.12$  (10 January 2005) and  $0.57 \pm 0.09$  (15 February 2008) when we restrict our analysis to cities with populations  $>250,000$ . Table 4.1 shows a summary of analyses for 50% cloud free thresholds, ranked by the  $R^2$  of the correlation. Standard error on the slope decreases as  $R^2$  increases, as one would expect, but there is no pattern in the value of the slope as  $R^2$  increases.



**Figure 4.4** (A) An example of allometric scaling of night-time emitted energy  $\text{Log}_{10}(\langle E_j \rangle$ , in MW) against urban population for the 33 largest cities in Nigeria. Reported on the graph (top right) are the Coefficient of Determination ( $R^2$ ) for the best-fit regression, the slope of the regression, and the error on the slope. (B) The ensemble of allometric relationships derived for the nights studied (Table 4.1). (C) Residual emitted energy (mean and standard deviation of  $\text{Log}_{10}(\langle E_j \rangle$  in MW) for urban areas with respect to the allometric scalings shown in (B). Colour-coding are used to classify cities (Ancient cities [red], New cities [green], Coastal cities [blue], the Federal capital [brown], and Other cities [black])

**Table 4.1 Night-time emitted energy for thirty-five (33) large Cities across Nigeria on selected nights. Results are ranked by the strength ( $R^2$ ) of the log-log correlation between emitted energy and population, for which the slope, error on slope, and intercept are reported at 50% cloud free pixels**

Rank	Date	Number of Cities	$R^2$	Slope ( $\alpha$ )	Error on Slope
1	15th Feb. 2008	29	0.81	0.43	0.04
2	12th Dec. 2003	23	0.80	0.39	0.04
3	07th Feb. 2006	31	0.79	0.41	0.04
4	16th Nov. 2004	19	0.79	0.44	0.06
5	02nd Jan. 2017	32	0.78	0.43	0.04
6	11th Apr. 2005	28	0.78	0.38	0.04
7	17th Nov. 2005	33	0.77	0.42	0.04
8	25th Dec. 2000	33	0.77	0.42	0.04
9	20th Dec. 2013	31	0.76	0.43	0.04
10	06th Feb. 2009	17	0.76	0.38	0.06
11	03rd Jan. 2012	32	0.76	0.41	0.04
12	29th Nov. 2016	30	0.75	0.43	0.05
13	26th Jan. 2001	31	0.73	0.40	0.05
14	05th Jan. 2013	29	0.72	0.42	0.05
15	25th Nov. 2003	22	0.71	0.42	0.06
16	20th Jan. 2016	28	0.69	0.39	0.05
17	02nd Jan. 2007	30	0.68	0.39	0.05
18	05th Jan. 2005	33	0.67	0.41	0.05
19	05th Feb. 2002	27	0.67	0.41	0.06
20	05th Jan. 2004	16	0.61	0.33	0.07
21	11th Apr. 2014	23	0.59	0.30	0.05
22	28th Feb. 2000	20	0.48	0.31	0.08
23	10th Jan. 2005	32	0.41	0.25	0.06
	Mean (all days)		0.71	0.39	0.05
	Mean ( $R^2 \geq 0.7$ )		0.71	0.41	0.05
	Median (all days)			0.41	

Overall, the analysis shows a general and robust scaling of urban heat with a population of 0.4, with the possible exception of the small sample of cities with populations > 500,000. The scaling of the area of cities with population yields a slope of  $0.41 \pm 0.04$  (Fig. 4S1(A) in supplementary 4SI), with a strong correlation ( $R^2 = 0.75$ ). From this, as was the case in the UK (Abdulrasheed et al., 2020) it can be confirmed that total urban emitted energy scales linearly (i.e., slope = 1) with the area of cities. For UK cities, urban built-form development with increasing population tends to ‘sprawl’ (or to spread horizontally) more compared to Nigerian cities, so that the scaling of area with population is more

sublinear for Nigerian cities than UK cities. The population density for UK cities is more nearly constant, but for Nigerian cities, population density is much higher for larger cities.

Abdulrasheed et al (2020) highlight how a close inspection of the residuals can yield Information pertaining to the urban form of the settlement. This analysis is employed here by investigating the residuals of the mean emitted energy with respect to the allometric relationship in Figure 4.4c, colour-coding cities as Ancient cities [red], New cities [green], Coastal cities [blue], the Federal capital [brown], and Other cities [black]. Each of these city types have their own distinct urban morphologies, which might be expected to define their thermal performance. For instance, the amount of built-up area and pavement would influence microclimate. The materials (asphalt and concrete) used for building and paving, absorbs, stores and transmits a higher amount of radiation during the day and releases the stored energy at night (Azevedo et al., 2016). However, no pattern is evident; each colour occurs about as often above the zero line as below. Abuja has the largest positive residual (i.e., emits more than expected from the best-fit line); Katsina has the most negative residual (i.e., emits less than expected) see table 4S5 in supplementary information.

## 4.4 Discussion

The results indicate that population is a good predictor variable for total emitted energy for Nigeria's cities, at least until the sample size becomes very small for cities with populations > 500,000. This efficacy of population as a predictor of total emitted energy is in line with our previous study on UK cities (Abdulrasheed et al., 2020), even though UK cities and Nigerian cities have considerably different urban morphologies. Moreover, the results obtained from Oke (1982) (described and discussed in Abdulrasheed et al (2020) are also consistent with the data (scaling of  $\Delta T_{u-r}$ ) from this study although, again, Oke's analysis focuses on a set of cities from across the global North. However, the actual values of the scaling slope for emitted energy versus population ( $\alpha = 0.4 \pm 0.05$ ) is quite different in this study compared to that from Abdulrasheed et al., (2020) ( $\alpha = 0.85 \pm 0.03$ ).



Although appearing very different, the UK and Nigerian cities are very similar in terms of the component of urban form which dictates thermal properties: i.e., both sets of cities show a linear increase in total emitted energy with urban area. The urban morphology for UK cities is somewhat proportionate to its population i.e., population density is approximately constant, and this corresponds to the scaling of its energy emitted. This is contrary to Nigerian situation where the population density is not constant. This attribute to the smaller slope of the scaling of emitted energy with population for Nigerian cities. There is a greater 'economy (or parsimony) of scale' in Nigeria than in the UK with respect to the heat 'cost' of increasing urban populations. Therefore, the scaling of emitted energy against the city area is linear. This is also true for both Nigerian cities and UK cities (Abdulrasheed et al., 2020), even though the scaling factor with population is very different in the two studies. We interpret this to mean that differences in built environment between Nigeria and the UK manifest in the scalings of urban heat (and urban area) with population, but not in the scalings of urban heat with urban areas. That is, the increase in emitted energy per unit increase in urban areas depends much more on the binary urban/rural distinction than on land-use classes within the urban category. By contrast, the increase in emitted energy per unit increase in urban population is much greater in UK cities than in Nigerian cities, presumably because, as argued above, UK and Nigerian urban morphologies affect population densities much more strongly than emitted energies.

A more subtle signal of how urban morphology changes the urban allometry of emitted energy may reside in the residuals for each city with respect to the best-fit allometric line (equation 4.6 and Figure 4.4c). Although the overall allometric scaling is a tight correlation, each city may perform better or worse for their size than the best-fit line would predict. No trend in residual size is apparent in Figure 4.4c, either in terms of city size or city type (Ancient city, Coastal city, etc., see above). Below, we compare selected cities with similar and contrasting built environments and local climate zone (LCZ) characteristics.

Historically, the development of urban centres, including the development of regular street patterns, has been well documented (Mabogunje, 1992; Oliveira, 2016), as has the growth of individual cities (Adams, 1970) and impacts on urban climate (Lee, 1984; Akpodiogaga-a and Odjugo, 2010; Sachindra et al., 2016; Emilsson and Ode Sang, 2017). Studies have shown most of these urban centres have undergone significant physical transformation since the first World war (Oşoba, 1969; Endsjö, 1973; Whitehand and Whitehand, 1983; Mabogunje, 1992; Omole and Akinbamijo, 2012). Cities in this study are not excluded from this circumstance especially during the colonial era of Nigeria's transformation.

Stewart and Oke emphasize the need for a classification, based on urban form and landscape, which determines a city's LCZ (Stewart and Oke, 2012). Akko (New town), for instance, is situated about 40km south of Gombe, with a population of 330,000 as at the 2006 census. A settlement in the northern part of the country with annual rainfall distribution of 657.3mm (Ogunjobi et al., 2012), Akko's is positive and comparable to the very much larger Lagos (Coastal/Ancient city) (Fig. 4.4c). Oke's seminal study on city size, canyon geometry, and the nocturnal urban heat Island, cited Chandler's 1967 observation that London and Leicester had similar UHI on the same night, despite having a very different size and population (Oke, 1973; Oke, 1981). By contrast, Abuja (New town/Nigeria's capital city), intermediate in size between Akko and Lagos, has a much larger positive residual (Fig. 4.4c). City configuration, street patterns and orientation, structure of buildings and density, and ultimately the intensity of human activities, are key factors that determine very different thermal behaviour in the city when compared with other Nigerian cities (refer to Fig. 4S8 - supplementary 4SI for photographic illustrations with LCZ).

From figure 4S8 (supplementary 4SI), the identified zone begins with Lagos, (a – f images) with classifications LCZ2 – LCZ10 (in built series) and LCZ B, LCZ E & LCZ G (land cover series) – see figure 4.1 for Stewart and Oke's standard illustration of LCZ classification adopted. The general landscape of Lagos sites (images a – f) appears to be well represented by the LCZ approach. The zones clearly portray the nature of urban landscape of Lagos conurbation as differences in built form (mid-rise,

dense mix and low-rise buildings and busy coastal areas) are captured by the zones. Judging by the positive residual result of Lagos (Fig. 4.4c), the pictorial figure validates the LCZ classification. This approach also applies to Abuja (plate a) in fig. 4S8, the portrait represents LCZ4 - sparsely tall buildings with abundance of impervious land cover which is attributed to its positive position in the residuals fig. 4.4c. If we take Akko (images a & b) fig. 4S8, high and medium density mixed buildings are spatially arranged with pervious and impervious land cover, and few trees, representing LCZ3 and LCZ5. This is evident in the residual – positively above the best fit line.

Kaduna (New town) on the other hand is slightly beneath the best fit line from the residual (Fig. 4.4c), and from the figure 4S8, the zone classification is adequately captured in the pixels (a & b) – LCZ2, LCZ3 and LCZ7 representing commercial areas along the C.B.D with dense solid buildings and narrow streets with heavy traffic and few trees. Kano, Onitsha, and Akure (all ancient cities) except Ibadan, all appeared to be below the best fit line, even though they are from different climatic regions but have some similarities in terms of zone classification. Kano built form demonstrates sparsely mid-rise, dense mix low-rise and pervious/impervious land cover with few scattered trees (LCZ4 – LCZ7). Meanwhile Onitsha (LCZ3 – LCZ5), Akure (LCZ4 – LCZ6) and Ibadan (LCZ3 – LCZ7) lie on the same climate region (Fig. 4.2a). There is an abundance of bare paved surface with few trees and dense mixed low-rise built form in Ibadan which might contribute to its positive position on the residual.

Another contrast is the coastal cities, Port Harcourt and Lagos have some similarities in terms of zone classification (LCZ2 – LCZ10) – built form series and similar land cover series, but this is different from other coastal cities of the same region - Uvwie/Warri and Eket/A/Ibom, both appearing well below the best fit lines and the zone classification seems similar (LCZ6) i.e., wetland and uncultivated field on the outskirts of the city, low plant cover with no traffic. Residential and commercial areas having sparsely mid-rise buildings and abundance of open land with plenty of trees (LCZ3 and LCZ7), contributes to their negative position in the residuals (Fig. 4.4c).

General observation indicates that some of the categories/landscape did not exactly march with the original Steward and Oke's (2012) standards. This can be attributed to the level of development within the study area or the physical planning patterns which are rarely similar by any other method. In this circumstance, the process of selecting 'best fit' zones are subject to skills judgement, knowledge of the field site is often applied.

There is no general pattern for coastal cities in the study as pointed out above. Some cities (e.g. Lagos and Port Harcourt) have large positive residuals, while others (e.g. Uvwie/Warri and Eket/A/Ibom) have negative residuals (Fig. 4.4c). Coastal cities are by far the most developed of Africa's urban areas (Douglas et al., 2008 ; Adelekan, 2010; Ayanlade, 2016). The implication of this is that these cities have a high concentration of residential, industrial, commercial, educational facilities (Adelekan, 2010) which might lead to thermal discomfort due to built forms and anthropogenic heat production. For example, Lagos is a low lying area beside the Atlantic ocean and is the hub of business and economic development in Nigeria (Ojeh et al., 2016; Ayanlade, 2016). It has experienced tremendous growth over the last five decades (from 305,000 in 1950 to 9.1 million in 2006) making it one of the fastest growing megacities in West Africa with about 70% of its population living in slums areas (Adelekan, 2010; Ojeh et al., 2016). All these factors are product of urbanization which come with spatiotemporal patterns of emitted energy and consequential to extreme contribution of thermal discomfort of the urban area (Daramola and Ibem, 2010; Ayanlade, 2017; Dissanayake et al., 2019).

On the other hand, Uvwie/Warri, and Eket/A/Ibom (coastal cities) have populations of <160,000 and < 65,000, respectively. Both areas are not developed, compared to Lagos and Port Harcourt (Table 4S1 and Fig. 4S4 – supplementary 4SI), the nature of urban form (building structure, street pattern, landscape, and fabric permeability etc.) in those areas are completely different. They are areas where oil extraction and processing takes place but have less energy emitted than expected for their population.

Abuja (new town/planned settlement) has a significantly positive mean residual, as does Lagos (coastal/commercial settlement), yet the cities differ greatly in-terms of population and built environment. This may be due to the former city's planning nature in-terms of lower heat capacity of the urban fabric or inadequate evapotranspiration. The increase in population coupled with the urban formation of Lagos particularly its coastal location and low-lying landmass with unprecedented urbanization increase influences the intensity of the city's energy budget. The urban morphology in Abuja is different from Lagos (see Fig. 4.3). Moreover, unprecedented population growth and anthropogenic activity in Abuja, being the federal capital, lead to vegetation removal as the built-up area increases, increasing the intensity of surface UHI in the city.

Kano and Onitsha (Ancient/commercial cities) have negative residuals, as does Akure (Ancient settlement) (Figs. 4.4a and 4.4c). The city's morphology can be influenced by the design and heterogeneity of the urban fabric, which to some extent differ from one another; however, the general deduction is that Nigeria's LCZ classifications appear to demonstrate similarities in-terms of characteristics features used to classify urban climate site irrespective of the size of the city.

## **4.5 Conclusion**

This study has established that, for Nigerian cities, an allometric relationship exists between city size, expressed as urban population, and night-time emitted thermal infrared energy. This finding is in agreement with previous work using data on 35 most populous cities in the UK (Abdulrasheed et al, 2020). Nigerian cities show much more sub-linear allometric scaling (slope,  $\alpha = 0.4 \pm 0.05$ ) of total emitted energy with population. That is, there is slightly presence of 'economy (or parsimony) of scale' in terms of nocturnal heat production in Nigerian cities: the production from the more populous cities is much smaller than would be produced from a constellation of less populous cities housing the same total population. This uniformity of scaling occurs despite of the obvious differences in architecture and urban form in settlements across Nigeria: Medieval centres (e.g., Ibadan); predominantly

commercial/military settlements (e.g., Enugu); residential areas (Lagos); coastal settlements; and planned settlements (e.g., Abuja).

The scaling of total emitted energy with population has the same slope, within statistical error, as the scaling of urban areas with population. This equality of scaling suggests that energy emitted per unit area is approximately the same everywhere at the 1-km<sup>2</sup> granularity of the current analysis. This 'emergent simplicity' in the scaling of emitted energy for urban areas of different sizes is counter intuitive given our understanding of heat storage and emission in the built environment (Arnfield and Grimmond, 1998; Nunez and Oke, 1977). The results also indicate that a relationship between urban form and local climate zone is weak but discernible at this scale. The local climate zone (LCZ) categories developed by (Stewart and Oke, 2012), covering general characteristics of built form and land cover, offer a useful simplification of urban complexity and uniqueness of place, and thereby help to facilitate the interpretation of results such as those presented above.

## 5.0 Chapter 5

### **The spatial distributions of emitted long-wave energy within UK cities**

Having established robust allometric scaling — with population or area — of total emitted infrared from cities in the UK (chapter 3; Abdulrasheed et al., 2020) and Nigeria (chapter 4), this chapter aims to investigate whether the spatial distribution of emitted energy within UK cities provides information complementary to the sum measure discussed to this point. The distribution of emitted energy inside cities is expected to tell us about hot spots and cold spots and allow us to ask whether their magnitude vary as a function of city size. This leads to the hypothesis that the allometry of extreme percentiles of the distribution will not scale in the same way as the sum measure. In contradiction to the hypothesis, we find that an allometric scaling of the high and low tails of the emitted energy distributions per city for a particular night is similar to that using the sum measure for the whole of each city but there is tentative evidence for a slower increase in the cooler areas than hotter areas as city size increases.

### **5.1 Introduction**

Urbanization generally leads to an expansion of city boundaries as well as densification of the urban form. The change of land surface characteristics due to urbanization leads in general to an alteration of the urban energy balance. The altered energy balance produces the urban heat Island (UHI), i.e. the difference between urban and background rural air temperature (Bornstein, 1968; Landsberg, 1981) and the surface UHI intensity (SUHII), which is derived from satellite data of thermal emission reported as land-surface temperature (or ‘skin’ temperature) (e.g., Peng et al., 2012; Zhou et al., 2014; Zhou et al., 2017). Intense UHI and SUHII lead to increased thermal discomfort and health related problems (Smith et al., 2011; Rosenzweig et al., 2011; Wouters et al., 2017; Krayenhoff et al., 2018) resulting, in turn, in higher energy demand for cooling. In addition, anthropogenic heat emissions are higher in cities (Christen and Vogt, 2004; Rizwan et al., 2008), adding to overall upwelling thermal emissions.

Having investigated the sum measure of the distribution of thermal emissions from UK and Nigerian cities (chapters 3 and 4), we note that, at least for cities with areas much greater than the pixel size of the satellite thermal emission data, there is information inside that totalized energy. The distribution of emitted energy within a city offers data that is amenable to statistical interpretation. Indeed, the conventional schematic diagram of the UHI (or SUHI) suggests just such an investigation (e.g., Lemmen and Warren, 2004); see fig. 2.1 in chapter 2.

Figures 5.1a, b & c, below, illustrate some real probability density functions of thermal emitted energy (see Methods, below) for London, Sheffield, and Milton Keynes on a sample night of 2<sup>nd</sup> January 2017. We will discuss the details of this figure in the Results section, below, but introduce it here to provide a rationale for the investigation to follow. The histograms show that the distributions from different cities are highly variable and far from Gaussian. A number of implications arise from the fact that the histograms are not Gaussian/Normal:

1. The mean and standard deviation will not be robust descriptions of the distributions;
2. Higher moments of the distribution (skewness, kurtosis) will help characterise the distributions;
3. The distributions will be better described as multi-modal to a greater or lesser degree; and
4. Long tails of the distribution are likely, representing the hottest and coldest areas within the cities.

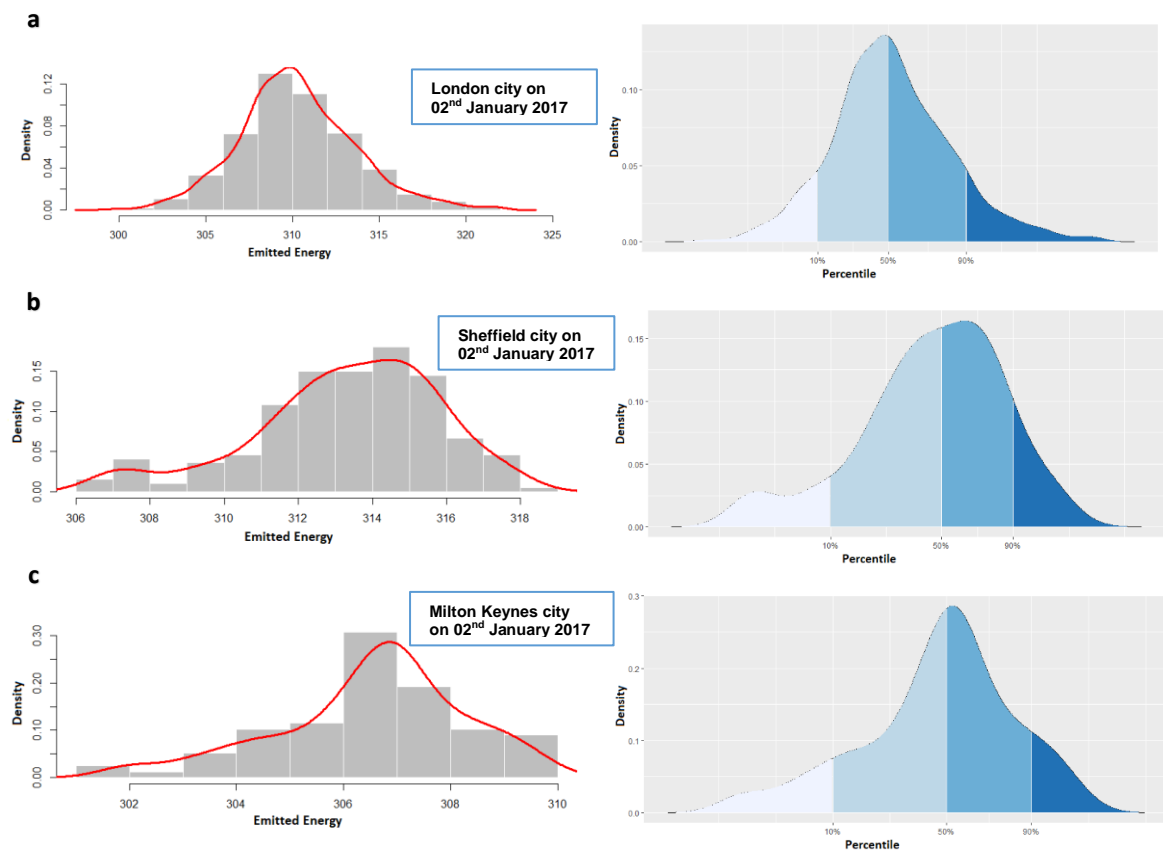
From these initial observations and similar inspections of other example distributions (not shown), we hypothesise that:

- a) The number of modes in a city's emitted energy distribution will not vary and can be identified with distinct urban forms;
- b) The allometry of the tails of the distribution will not be the same as that of the summed energy; and



- c) The residual emitted energy (i.e., the actual emitted energy minus that predicted from best-fit allometry) relates to the presence of long tails in the city's emitted energy distribution

It is not possible to carry out an exhaustive study in the present analysis. Rather, we focus on a single night, 2nd January 2017 for all the UK cities discussed in chapter 3. The rationale for choosing this particular night was that it had the best city coverage (lowest cloud contamination) among the samples used for the UK study in chapter 3. We then focus on how behaviour varies on different nights for three UK cities of very different size and character: London, Sheffield, and Milton Keynes (see methodology, below). These sample studies will indicate the merit of further investigation in future studies.



**Figure 5.1** Histograms and fitted distributions (left column), and percentiles graphs (right column) showing distributions of emitted energy ( $W m^{-2}$ , see Methods below) for three UK cities: London (top); Sheffield (middle); and Milton Keynes (bottom). Note that we use contiguous urban areas rather than administrative boundaries. Data for 02<sup>nd</sup> Jan. 2017 from MODIS satellite Land Surface Temperature (see chapter 3 and Methods, below). The red curve (left column) is the best fit probability distribution function (PDF), calculated using the 'density' function in R, and is identical to the outline on the graphs in the right column, plotted using the ggplot function in R.

## 5.2 Methods

This study aims to appraise the value of the information contained in the distribution of emitted energy inside city boundaries, using UK cities as a case study. Note that the cities are represented by contiguous Developed Land Use Areas (DLUA) rather than administrative demarcations (Meridian2 data produced by the Ordnance Survey (GB National Mapping Agency)).

The satellite data used for this study is that used in Abdulrasheed et al. 2020; (see also chapter 3), which uses daily MOD11A1 version 6 (V006) land surface temperature (LST) from the MODIS instrument on board the Terra satellite. Data is at a spatial resolution of approximately 1 km<sup>2</sup>. For allometry, the LST (in Kelvin) is converted to emitted energy (in W m<sup>-2</sup>) using the Boltzmann Law with unit emissivity, and area-summed:

$$\langle E_{j,k} \rangle_{\chi_1}^{\chi_2} = \sum_{i=0}^p \epsilon_{i,j,k} [\chi_1, \chi_2] \cdot \Delta a \quad (5.1)$$

where  $\langle E_{j,k} \rangle_{\chi_1}^{\chi_2}$  is the emitted energy (in MW) for city,  $j$ , on night,  $k$ , summed over  $p$  cloud-clear pixels within the city boundary and within some percentile range  $[\chi_1, \chi_2]$ .  $\Delta a = 1 \text{ km}^2$  and the factor of  $10^6$  converting km<sup>2</sup> into m<sup>2</sup> is accommodated in the units of  $\langle E_{j,k} \rangle_{\chi_1}^{\chi_2}$ . The percentile ranges used below are: minimum to 10<sup>th</sup> percentile  $[\chi_{min}, \chi_{10}]$ ; 90<sup>th</sup> percentile to maximum  $[\chi_{90}, \chi_{max}]$ ; and minimum to maximum  $[\chi_{min}, \chi_{max}]$ , which is, of course, equivalent to the total emitted energy analysis in chapter 3. In this chapter, by focusing on the extremes of the distributions, we investigate whether the scaling that appears for the total emitted energy also applies to the tails of the distribution. Since the hottest and coldest parts of a city will tend to have very different urban morphologies (see section 5.3, below), there is no reason to believe, a priori, that the tails of the urban emitted energy distributions will scale in the same way as the total emitted energy. To provide an example of the use of equation 5.1, at LST = 278 K (5 °C), the Boltzmann Law with unit emissivity yields a value of ca.

340 W m<sup>-2</sup>, or 340 MW per 1 km<sup>2</sup> pixel, and  $\langle E_{j,k} \rangle \Big|_{\chi_{min}}^{\chi_{max}}$  is on the order of 5 x 10<sup>5</sup> MW or 0.5 GW (see city areas below).

For allometry, we seek relationships that conform closely to an equation of the form:

$$\log(Y) = \log(\beta) + \alpha \cdot \log(X) \quad (5.2)$$

where  $X$  is some ‘yardstick’ measure of the size of the city,  $\log(\beta)$  is a constant offset and  $\alpha$  is the rate of relative growth (the allometric scaling factor or, simply slope). Below, as has been the case throughout the thesis, we will refer to  $\alpha$  as defining the ‘scaling’ of (in this case)  $\langle E_{j,k} \rangle \Big|_{\chi_1}^{\chi_2}$  with respect to population. We retain total population as our yardstick measure of city size even when the scaling we seek is for some fraction of the emitted energy (i.e., minimum to 10<sup>th</sup> percentile  $[\chi_{min}, \chi_{10}]$  or 90<sup>th</sup> percentile to maximum  $[\chi_{90}, \chi_{max}]$ ). One could choose to measure against the population only in those pixels contributing the fractional total of emitted energy. Time prevented a study along these lines to see what effect using such a yardstick would have on the analysis.

### 5.2.1 The case studies

Three cities (London, Sheffield, and Milton Keynes) of very different sizes and populations were chosen as a focus for the exploratory analysis in this study. Our previous study (chapter 3; Abdulrasheed et al., 2020) shows that, although UK cities appear very different to the eye or camera, they behave similarly in terms of the components of urban form that dictate their thermal properties. We therefore chose three representative cities with very different populations, and with different development histories, but all of which lie close to the mean emitted-energy allometry of UK cities (i.e., the line of best-fit in Figure 3.3). We speculate that these three sample cities with varying characteristics and population may perhaps be used to interpret and classify UK cities as a whole. The sample dates used for this study were from the previous study (Abdulrasheed et al., 2020). The dates (nights) were selected based on the default 50% cloud clear threshold set out for each city based on the assumption that the selected nights together provided sufficient coverage of the study cities to

provide a minimal test of hypotheses (a)-(c). The impact of sample size on the results of the study are discussed further in section 5.4.

**London** is in the southeast of Great Britain. The largest urban area and the capital city of the United Kingdom (Meridian2; see Data Sources, below). Using the previously applied method for defining urban areas (chapter 3), London region covers an area of 1,365 km<sup>2</sup> (Meridian data2, 2017; please note that, at 1-km<sup>2</sup> resolution, the maximum contiguous urban area designated 'London' in our analysis is 1,589 km<sup>2</sup>) and has a population of 8,519,128 (Office for National Statistics, 2017). The climate of London is moderate with an average January low temperature of 2.4°C and a July average temperature of 23°C (Met Office, 2020). **Sheffield** on the other hand has a population of 596,456, and area coverage of 164 km<sup>2</sup> (Meridian data2, 2017). It is situated in the north of England, on the eastern edge of the Peak District National Park, which is a 1,440 km<sup>2</sup> area of upland moor and farmland. The climate in Sheffield is generally temperate; July average maximum temperature is 20.8°C and average minimum temperature in January and February of 1.6°C (Met Office, 2020). **Milton Keynes** is a large town in Buckinghamshire, central England, about 80 km north-west of London. A third generation New Town (Alexander, 2009) with a population of 188,643 and area coverage of 50.27 square kilometres (Meridian data2, 2017). A post war settlement with limited growth until it was formally nominated as a New Town in 1967. Milton Keynes experiences a temperate climate as is typical of almost all the UK. Recorded maximum temperature range from 34.6°C during July, and to as low as -20.6°C in December 2010 (Met Office, 2020).

### **5.2.2 Statistical analysis**

To analyse the behaviour of the long tails of the distributions, we determine the sum of the emitted energy for the lowest 10 percent (i.e.,  $[\chi_{min}, \chi_{10}]$  in equation 1, above) and highest 10 percent ( $[\chi_{90}, \chi_{max}]$ ) of the distribution for a city. This will capture the colder and hotter 'spots' inside the city boundary, respectively. The percentile approach has a number of attractive features and was selected for its reliability and validity in terms of its universal interpretation. Percentiles do not assume a shape

to the probability density function of the data (cf., standard deviations, which assume a normal distribution) and are robust and resistant statistics in the sense of Wilks, (1995) (cf. the absolute maximum and minimum); the sum within percentile limits is robust but not resistant to the influence of outliers. For datasets larger than 100 entries, the percentiles are well-sampled to unit percentile resolution — i.e., 1<sup>st</sup> percentile, 10<sup>th</sup> percentile..... 99<sup>th</sup> percentile, 100<sup>th</sup> percentile. Therefore, for city areas much less than 100 km<sup>2</sup> (Figure 5.5,  $\log_{10}(\text{area}) < 2$ ), our estimates of the percentiles will be less accurate. To analyse further the effect of the non-Gaussian distribution, we compare mean to median, compare the differences between the median and the 10<sup>th</sup> percentile (i.e.,  $\chi_{50} - \chi_{10}$ ) and 90<sup>th</sup> percentile ( $\chi_{90} - \chi_{50}$ ) values, count (by eye) the modes in the distribution, and compute skewness and kurtosis of the distributions. A brief guide to these higher-moment statistics is provided below for ease of reference.

**Skewness ( $S$ )** is the tendency of a distribution to depart from a symmetrical form. In a normal distribution the curve is symmetrical, the skewness is zero, and the mean, median, and mode coincide. The absolute value of skewness,  $|S| < 0.5$  indicates a symmetric distribution, and  $0.5 \leq |S| < 1$  indicates a slightly skewed distribution. If  $|S| > 0.5$ , the distribution is highly skewed. Skewness is the third moment about the mean and is defined statistically as the average of the cubed deviations from the mean divided by the cube of the standard deviation (Friedman, 1962; Bao, 2013). The sign of the skewness indicates whether the distribution is skewed towards values smaller than the mean (a negative skew) or towards values greater than the mean (a positive skew). **Kurtosis ( $X$ )** measures the peakedness of a given curve. A curve of a frequency distribution may be symmetrical yet may differ from a normal curve by its degree of peakedness. Equivalently, the kurtosis is a measure of how concave-upwards ('pointy') or convex-upwards ('flat') the distribution curve is, a positive value indicating 'pointy', a negative value indicating 'flat'. The kurtosis of a normal curve is equal to 3 (Friedman, 1962; Bao, 2013). Practically, a frequency distribution may be considered to be normal if it has a skewness close to zero and a kurtosis close to three (Friedman, 1962). Note that skewness and

kurtosis, because they sum higher-order deviations, are not resistant to outliers in the sense of Wilks (1995) and will be affected by outliers more severely than the percentile-sums,  $\langle E_{j,k} \rangle \Big|_{\chi_1}^{\chi_2}$ .

To assess whether a sample (in our case, of emitted energy values) is drawn from a single or from multiple populations, we simply count the modes that are apparent by eye in the distributions. Samples drawn from distinct populations will tend to have more than one more if the means of the populations are sufficiently far apart. Modes were counted when they appeared as a distinct local maximum in the probability distribution function, or as a distinct ‘shoulder’ on a larger maximum. So, in Figure 5.1, for example, we count 2, 2, and 3 modes for figures 5.1a-c.

The statistical programming tool “R” (Gandrud, 2013; Horton and Kleinman, 2015) was used to plot the histograms and percentile plots with the aid of the “moments”, “MASS”, “dplyr”, and “ggplot2” packages, respectively (code stubs are provided in the digital appendix). ArcGIS 10.4 was also used to map London, Sheffield, and Milton Keynes in order to illustrate the different patterns of morphological features (appendices a, b, and c).

## 5.3 Results

### 5.3.1 A case study: London, Sheffield, and Milton Keynes on 2nd January 2017

A statistical description of the emitted energy distribution is shown in table 5.1 for the three case-study cities for 2<sup>nd</sup> January 2017 (cf. Figure 5.1).

**Table 5.1 A statistical description of the long-wave energy distribution for the three case-study cities for 2<sup>nd</sup> January 2017**

Cities	$\chi_{50} - \chi_{10}$ , W m <sup>-2</sup>	Median ( $\chi_{50}$ ), W m <sup>-2</sup>	$\chi_{90} - \chi_{50}$ , W m <sup>-2</sup>	Skewness $S$	Kurtosis $X$	Cloud-free area (km <sup>2</sup> )	Mean, W m <sup>-2</sup>	Mode Count	Integrative measures: $\log_{10}(\langle E_{j,k} \rangle [\chi_1, \chi_2])$		
									$[\chi_{min}, \chi_{max}]$	$[\chi_{min}, \chi_{10}]$	$[\chi_{90}, \chi_{max}]$
London	4.0	310.1	4.4	0.3	3.6	1560	310.3	2	5.765	4.754	4.803
Sheffield	4.0	314	2.0	-0.7	3.2	194	313.3	2	4.720	3.809	3.785
Milton Keynes	3.0	307	2.0	-0.6	3.1	78	306.5	3	4.235	3.335	3.268

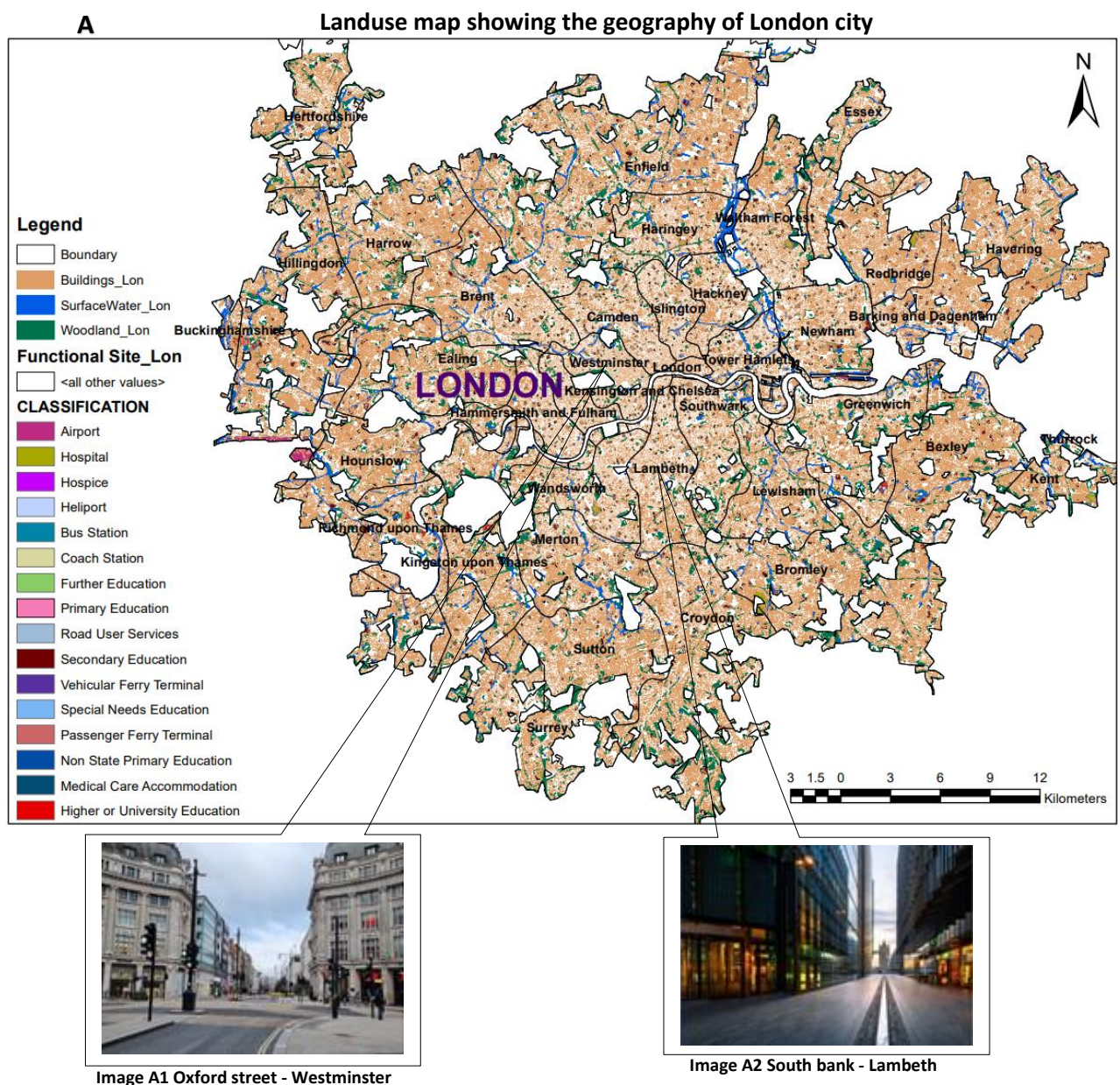
The positive skewness for London ( $S = 0.3$ ) indicates a modest ‘tail’ of the distributions at high values of emitted energy, as also indicated by  $(\chi_{90} - \chi_{50}) > (\chi_{50} - \chi_{10})$  and illustrated in Figure 5.1a. For Sheffield and Milton Keynes, the strongly negative values for skewness (-0.7 and -0.6, respectively)

indicate long tails of the distribution on the low side of the median, as indicated by  $(\chi_{90} - \chi_{50}) \ll (\chi_{50} - \chi_{10})$  (see also Figure 5.1b, c).

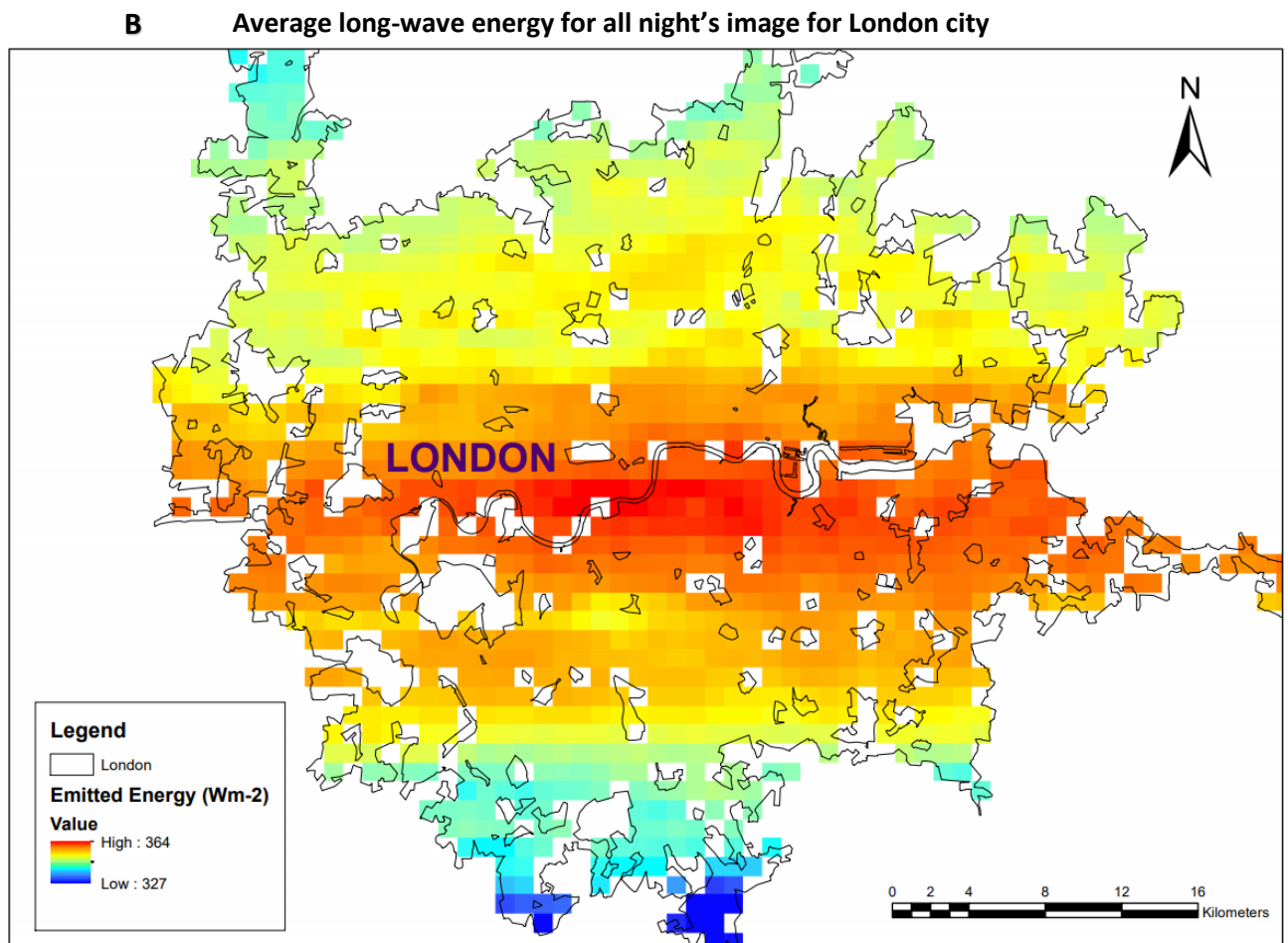
The distributions of emitted energy for the 3 cities on the given night are only very roughly symmetrical (Fig. 5.1a, b, and c). The distributions for London and Sheffield appear to be bimodal with mode values ( $310 \text{ W m}^{-2}$ ,  $322 \text{ W m}^{-2}$ , for London and  $307 \text{ W m}^{-2}$ ,  $314.5 \text{ W m}^{-2}$  for Sheffield), and Milton Keynes looks multimodal with mode values ( $302 \text{ W m}^{-2}$ ,  $304 \text{ W m}^{-2}$ ,  $307 \text{ W m}^{-2}$ ). The mean values are close to the median values for the 3 sample cities (Table 5.1). This type of distribution is quite different from the normal distribution or the bell curve. The median (50<sup>th</sup> percentile) is the more robust measure of central tendency in this case, because the distribution is not normal or symmetrical (Swanson et al., 2011; Frost, 2018). The cities demonstrate relatively similar kurtosis on the sample night, though London is somewhat different (kurtosis = 3.6, compared to 3.1 and 3.2 for Sheffield and Milton Keynes) (see Table 5.1).

Figures 5.2 – 5.4, below, show the spatial distributions (i.e., the ‘maps’) underlying the histograms and fitted distributions as per figure 5.1, for the 3 sample cities in the selected sample night (2<sup>nd</sup> January 2017). Figures 5.2 – 5.4 show different spatial distributions of the average long-wave energy. For London, the hotspot is in the centre of the city and along the river (Fig. 5.2B) which is characterized by tall commercial and residential buildings (e.g., Westminster - oxford street - image A1 panel 5.2A; Tower Hamlets, Lambeth - south bank- image A2 panel 5.2A) and to the east in Docklands, an area of dense high-rise urban regeneration results in a sky view factor (SVF) effect - (the calculated proportion of sky to buildings or vegetation and it varies between 1 - 0) (Unger, 2009). Other major influences include the density and population of the conurbation and its associated anthropogenic heat releases (these areas are called functional site - classification from the land use map legend (fig. 5.2A) – e.g., bus and coach stations, hospitals, primary and secondary education, airport, etc.). All these coupled with other land uses and vegetation cover affect albedo – (the reflection of short-wave radiation), emissivity – (the release of heat or long-wave radiation from the surface), and surface roughness –

(influence on the vertical mixing between the surface and the air) which in turn result in a maximum UHI intensity in the city. Similar results showing concentric regions of urban heating have been obtained from previous studies at city scale: Tomlinson et al. (2012) analysed the SUHI across Birmingham city during a heatwave event in 2006 and identified a record of cold spot in the conurbation – a surface temperature of up to 7°C lower than the city centre; Watkins et al. (2002) analysis of summer air temperatures across London – Findings indicates that the thermal centre is in the city of London which is characterized by tall buildings and anthropogenic heat emissions; the Gedzelman et al. (2003) analysis of urban heat Island around New York city; and the Jackson et al. (2010) analysis at global scale.





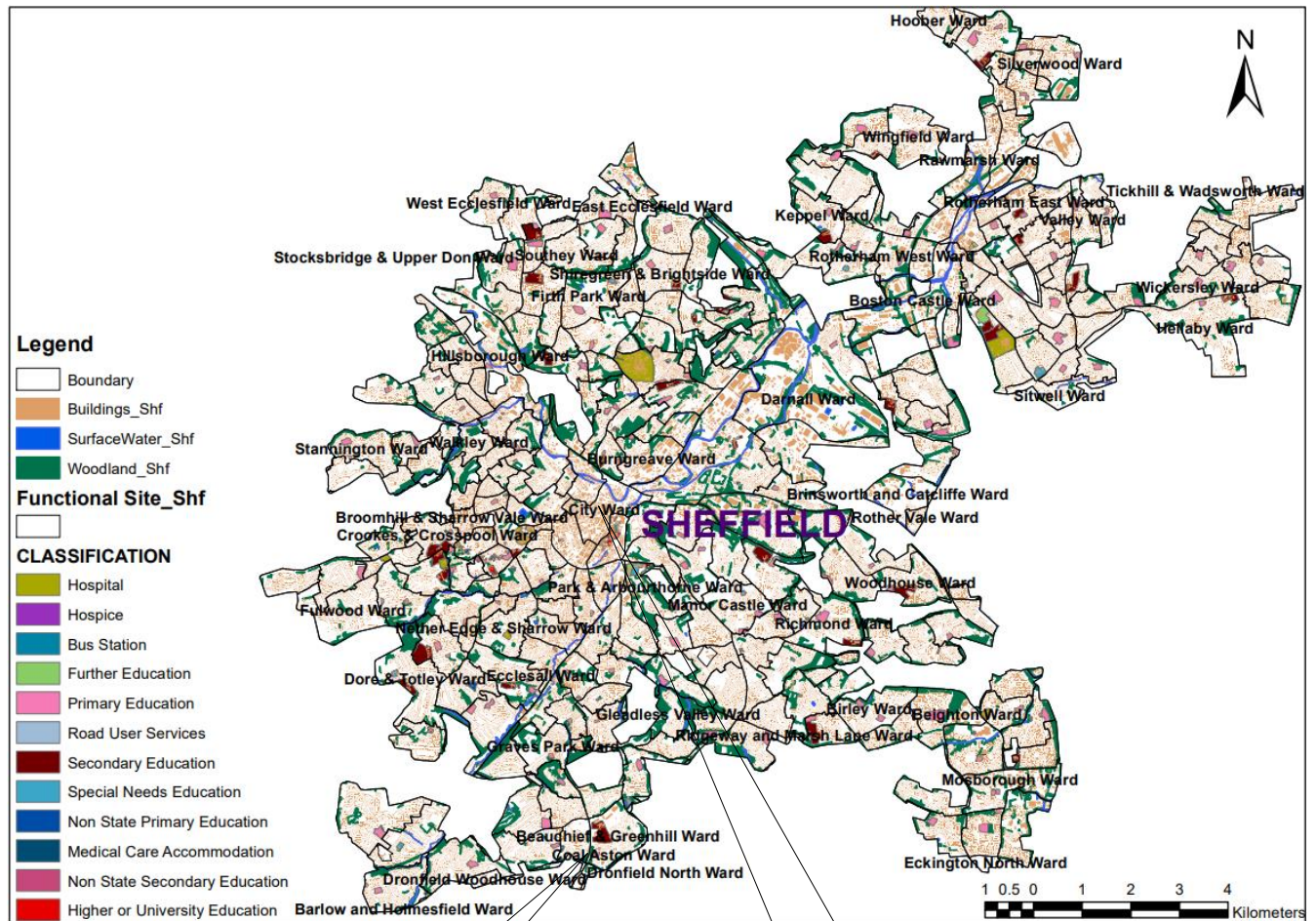


*Figure 5.2 Landuse map showing city geography (plate A - top) and gridded code (interpolation- kriging) long-wave energy translated to city schematic map with magnitude indicating pattern of urban emission (plate B) for an average of all night's sample for London city. Data where sourced from MODIS (Earthdata, 2017), Ordnance survey (meridian2 data – DLUA) and Digimap (<https://digimap.edina.ac.uk/>). ArcGIS 10.4 tool were used to plot the maps*

The long-wave energy magnitude for Sheffield city is concentrated at the centre up to the upper west and far north of the conurbation and from the city ward (image C2 – Sheffield city centre ) as well as up and around the Walkley ward of the conurbation (Fig. 5.3 – panel D). This can be attributed to the concentration of built forms (e.g., hospitals, primary and secondary education, higher or university education etc.) around the city ward and up towards East Ecclesfield ward as well as anthropogenic activities (e.g., bus stations, road users, etc.) along the areas as indicated in the landuse map (Fig. 5.3 - panel C). These built forms and pavements are made from concrete fabrics which retain heat from radiation and emit it at night. The effect of these long-wave not only influences the energy demand for cooling (air conditioning) but has significant effect on the health and thermal comfort of the people living in urban areas. Areas with lower emission are having abundance of woodland or forest (e.g.,

Beighton and Mosborough wards, Coal Aston ward - image C1 - Cliffe park) as shown from the landuse map (Fig. 5.3 – panel C).

**C** Landuse map showing the geography of Sheffield city



**Image C1 - Cliffe park – Coal Aston**



**Image C2 - Sheffield City Centre**

D

Average long-wave energy for all night's image for Sheffield city

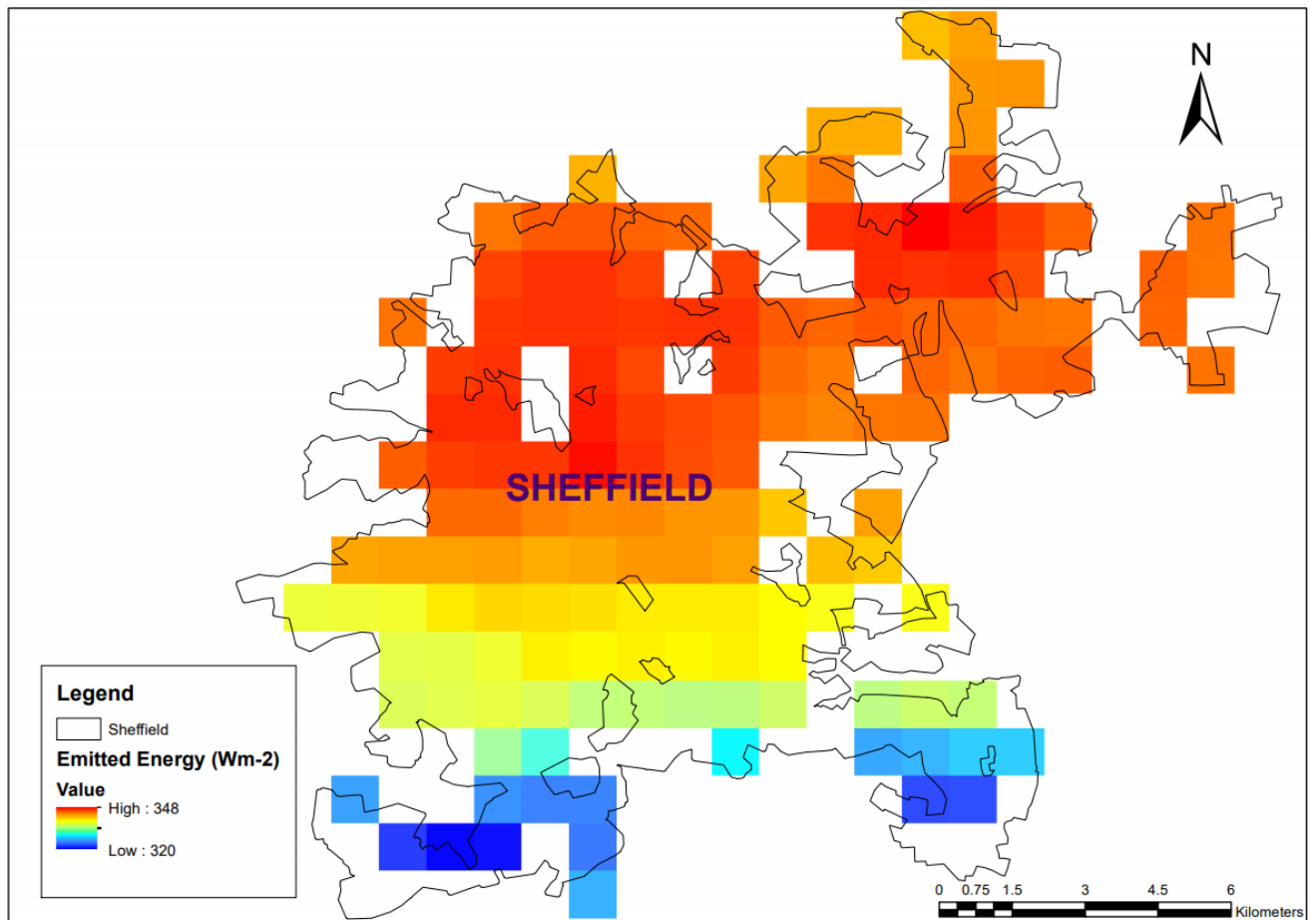
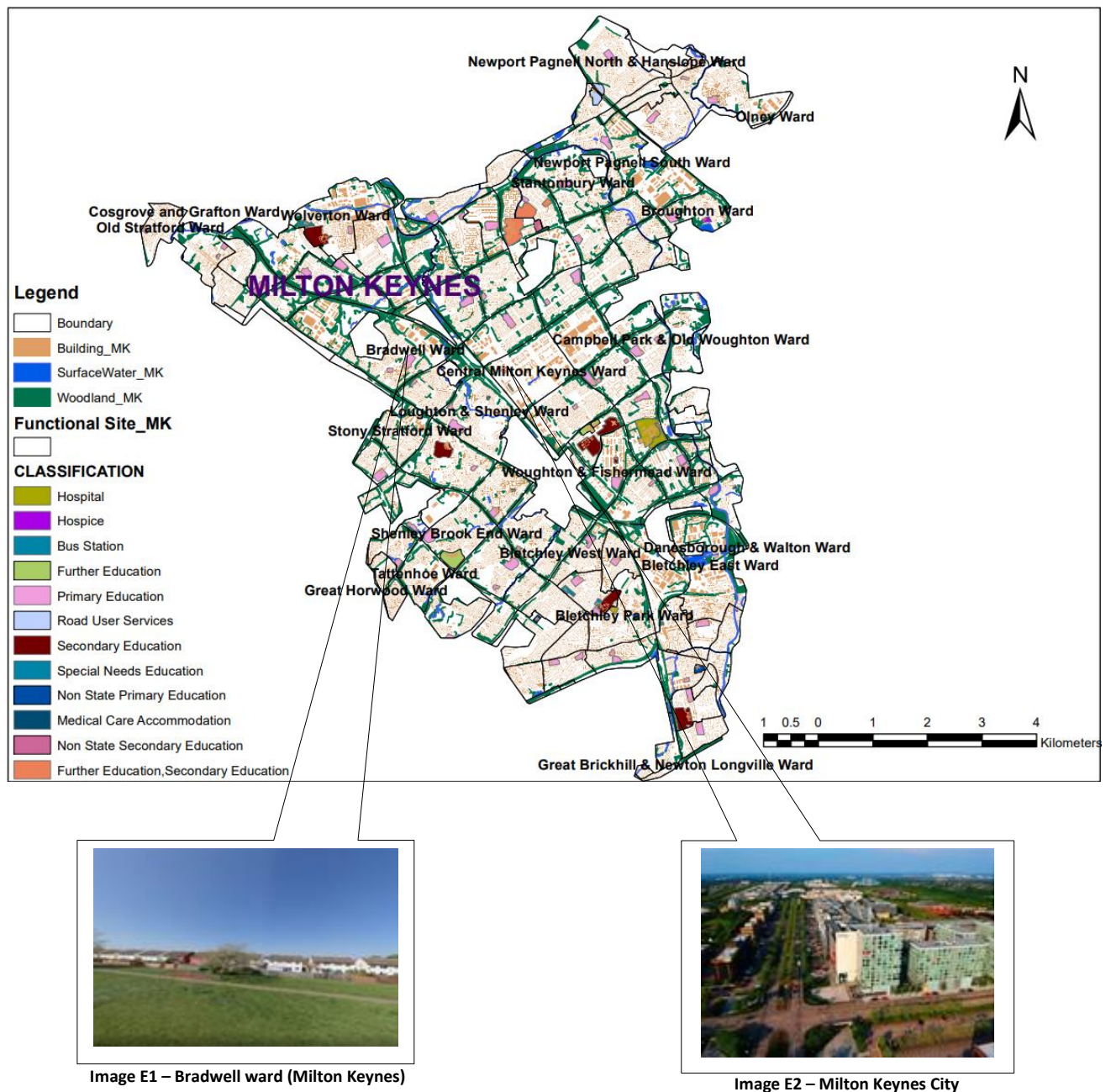


Figure 5.3 Landuse map showing city geography (left panel) and gridded code (interpolation- kriging) long-wave energy translated to city schematic map with magnitude indicating pattern of urban emission (lower panel D) for an average of all night's sample for Sheffield city. Data where sourced from MODIS (Earthdata, 2017), Ordnance survey (meridian2 data – DLUA) and Digimap (<https://digimap.edina.ac.uk/> ). ArcGIS 10.4 tool were used to plot the maps

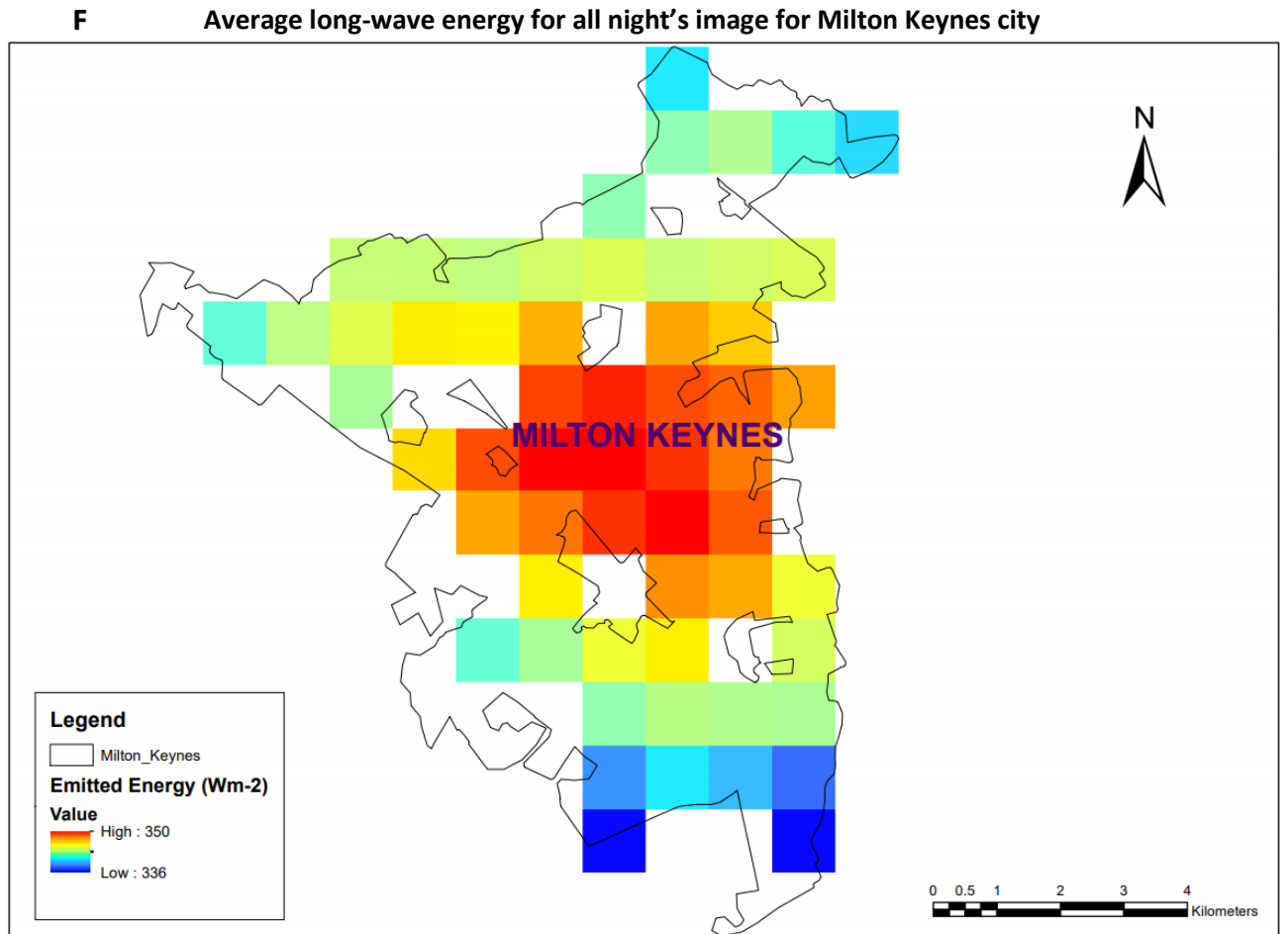


E

## Landuse map showing the geography of Milton Keynes city



The spatial pattern of long-wave energy emission is centred around the central Milton Keynes conurbation and Woughton & Fishermead ward (see Fig. 5.4 – panel F ) where built forms are predominant – e.g., Central Milton Keynes ward – image E2. Another area is Stantonbury down to Broughton wards and as well various man-made activities (e.g., education both primary and secondary, hydrography, bus stations, hospitals, road users, etc.,) as shown from the landuse map. Areas with lower emission have an abundance of woodlands (e.g., Old Stratford down to Bradwell (image E1) wards as shown from the landuse map (Fig. 5.4 – panel E).



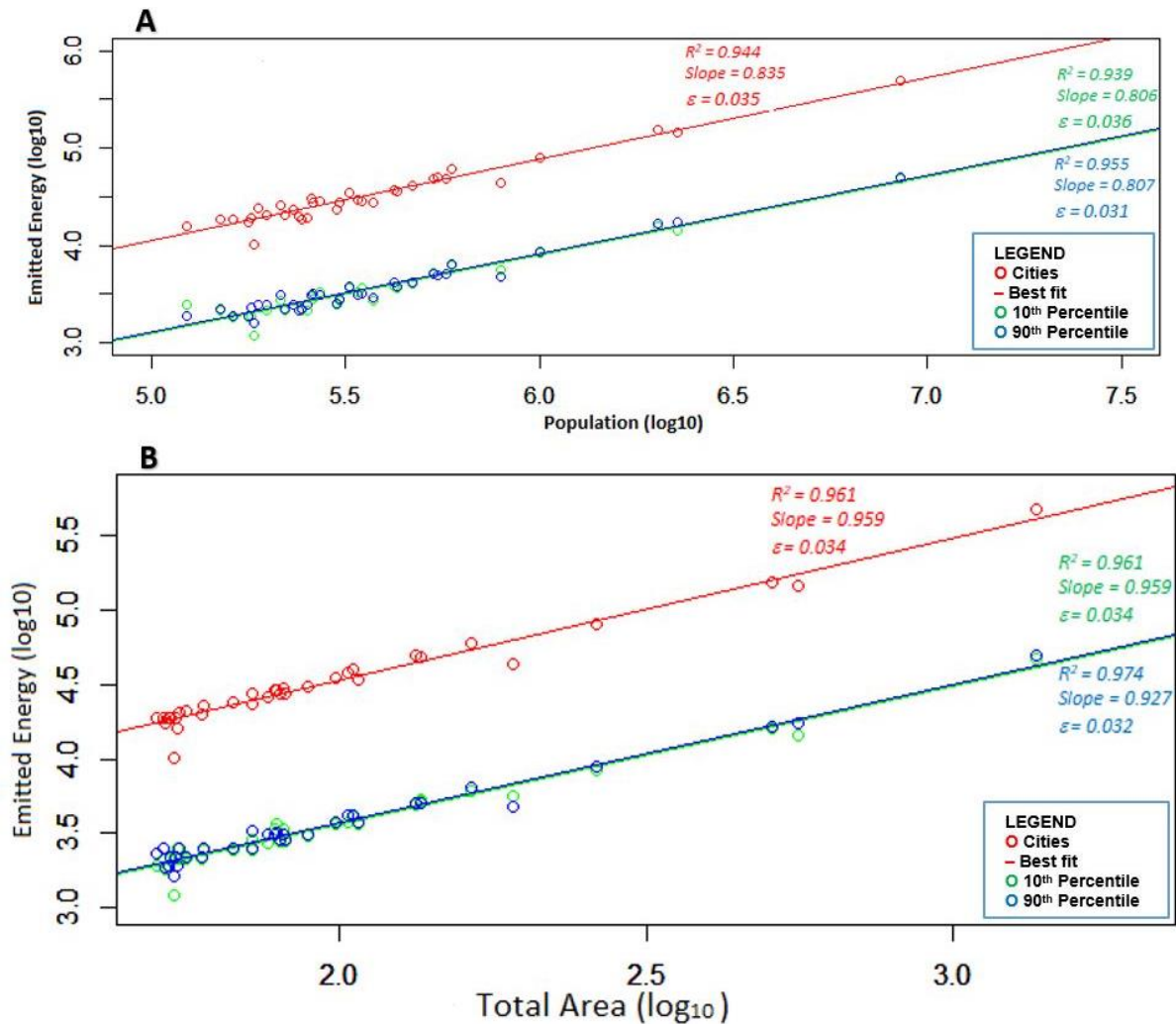
*Figure 5.4 Landuse map showing city geography (left panel) and gridded code (interpolation- kriging) long-wave energy translated to city schematic map with magnitude indicating pattern of urban emission (lower panel F) for an average of all night's sample for Milton Keynes city. Data where sourced from MODIS (Earthdata, 2017), Ordnance survey (meridian2 data – DLUA) and Digimap (<https://digimap.edina.ac.uk/>). ArcGIS 10.4 tool were used to plot the maps*

### 5.3.2 Allometry of emission

Considering a larger population of UK towns and cities, Figures 5.5 – 5.7 below show allometry and statistical measures to extend the study in chapter 3. The sum measure from chapter 3 is compared to statistics for the sum below 10<sup>th</sup> percentile ( $[\chi_{min}, \chi_{10}]$ ) and the sum above 90<sup>th</sup> percentile ( $[\chi_{90}, \chi_{max}]$ ) for all cities in the selected sample night (2<sup>nd</sup> January 2017).

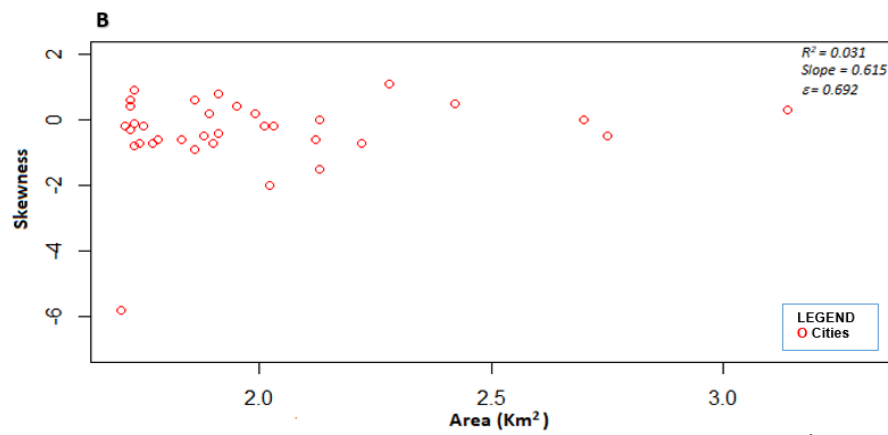
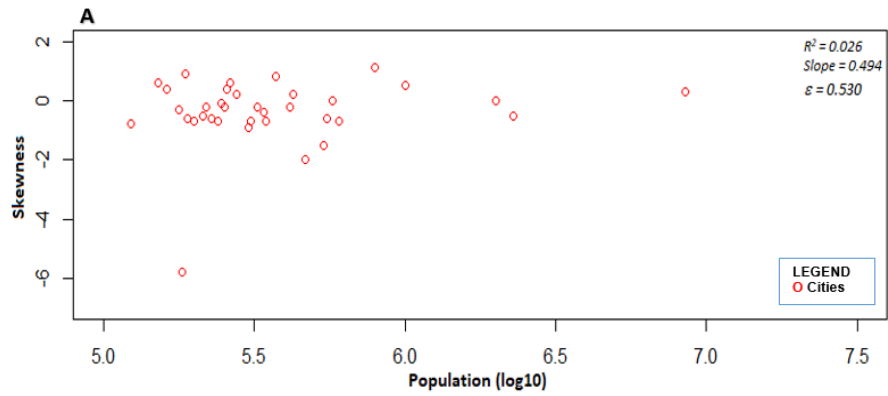
Figure 5.5A presents evidence of strong correlations present on the selected sample night, all regressions having  $R^2 > 0.93$ . All regressions have slopes  $\sim 0.8 \pm 0.03$  that are not statistically distinguishable, although there is a suggestion that the allometries of the extremes have slopes somewhat smaller than that for the whole summed areas. The correlations suggest that population is a good predictor variable for total emitted energy, despite the differences in urban form of the UK cities, as discussed previously in chapter 3. That the correlations for the high and low extremes of the

distributions are not different from that of the sum measure falsifies our hypothesis that “The allometry of the tails of the distribution will not be the same as that of the summed energy”. The positive trend in total energy emitted with population is of the same sign, but much larger than the analysis of (Oke, 1973; Oke, 2002) on city population and the UHI (see chapter 3). As discussed in chapter 3, a major part of the scaling of emitted energy with population is accounted for by the scaling of urban area with population, so that the allometric scalings of the various emitted energy measures with respect to urban area are nearly linear ( $0.93 < \text{slope} < 0.96$ ; fig. 5.5B). The very slightly smaller slope of the allometric scaling of  $[\chi_{min}, \chi_{10}]$  with respect to area may indicate that cooler areas increase more slowly than hotter areas (and their summed emissions) as city size increases.

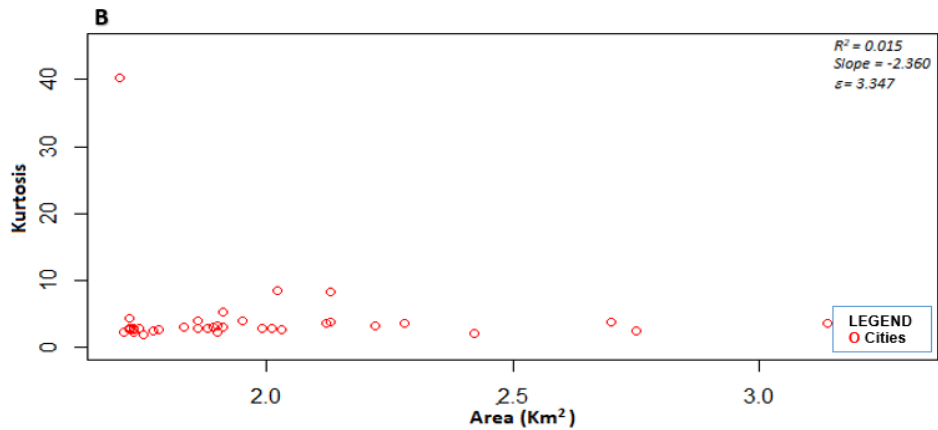
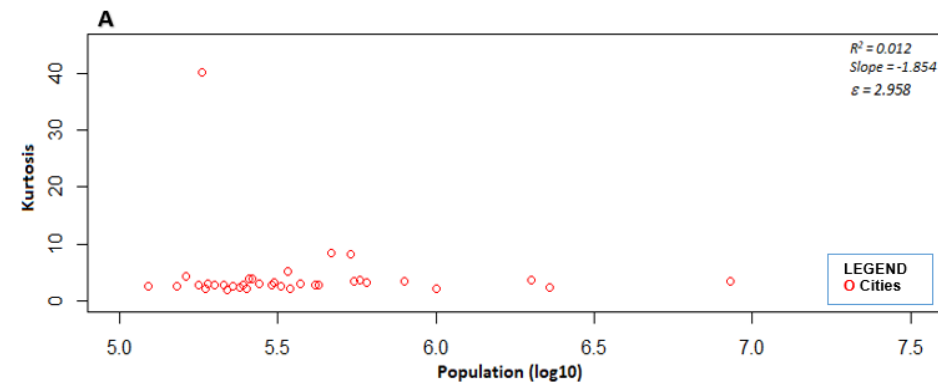


**Figure 5.5** Total emitted energy Versus total population (red), sum below 10<sup>th</sup> (green) and sum above 90<sup>th</sup> (blue) percentiles for all cities on a selected sample night (2<sup>nd</sup> January 2017)(B) Total emitted energy Versus Log<sub>10</sub>(total Area) (red), sum below 10<sup>th</sup> (green) and sum above 90<sup>th</sup> (blue) percentiles for all cities on a selected sample night (2<sup>nd</sup> January 2017). Slope, error on slope ( $\varepsilon$ ) and  $R^2$  are reported on the panels.

Figure 5.6 shows the skewness distribution with population for all cities in chapter 3 on the selected sample night (2<sup>nd</sup> January 2017). The skewness measures for the cities are clustered around zero. Aberdeen appears to be an outlier for both skewness and kurtosis from the plots (Figs. 5.6A & 5.7A) and is discussed further in section 4.0, below. Table 5.2 ranks the cities by their skewness, ranging between 1.1 (Liverpool) and -5.8 (Aberdeen). Eight of the top ten most positively skewed distributions are for coastal towns and cities (Liverpool, Birkenhead, Portsmouth, Gateshead, Swansea/Abertawe, Glasgow, Middlesbrough, and London) and seven of the ten most negatively skewed distributions are for inland towns and cities (Derby, Sheffield, Bradford, Northampton, Telford, Coventry, Leeds). The groupings are not exclusive; inland areas (Weybridge, Leicester) appear amongst the most positively skewed and the coastal cities of Edinburgh and Aberdeen are the most negatively skewed. For kurtosis, the range is from 40.2 (Aberdeen) to 1.9 (Plymouth) (Table 5.2). Omitting Aberdeen, the cities cluster around a kurtosis of  $3 \pm 1.4$ , i.e. the value expected of a normal distribution (Friedman, 1962), albeit with significant variability. The three cities with most negative skew have the largest kurtosis — Leeds, Edinburgh, and Aberdeen — but otherwise little systematic variation is evident. Our three particular case study cities — London, Sheffield, Milton Keynes — do not appear unusual in terms of skewness or kurtosis. The trend is indistinguishable when the skewness and kurtosis distributions were measured against area respectively (Fig. 5.6B and 5.7B).



**Figure 5.6** Skewness versus population for all cities on a clear sample night (2<sup>nd</sup> January 2017). (B) Skewness versus area for all cities on a clear sample night (2<sup>nd</sup> January 2017). Slope, error on slope ( $\varepsilon$ ) and  $R^2$  are reported on the panels



**Figure 5.7** Kurtosis versus population for all cities on a clear sample night (2<sup>nd</sup> January 2017). (B) Kurtosis versus area for all cities on a clear sample night (2<sup>nd</sup> January 2017). Slope, error on slope ( $\varepsilon$ ) and  $R^2$  are reported on the panels.



**Table 5.2 All cities ranked by skewness for selected sample night 2<sup>nd</sup> January 2017**

Rank	Name of City	Population (log10)	Skewness	Kurtosis
1	LIVERPOOL	5.9	1.1	3.5
2	BIRKENHEAD	5.27	0.9	2.2
3	PORTSMOUTH	5.57	0.8	3.1
4	GATESHEAD	5.42	0.6	4
5	SWANSEA / ABERTAWE	5.18	0.6	2.6
6	GLASGOW	6	0.5	2.1
7	WEYBRIDGE	5.41	0.4	4
8	MIDDLESBROUGH	5.21	0.4	4.4
9	LONDON	6.93	0.3	3.6
10	LEICESTER	5.63	0.2	2.9
11	READING	5.44	0.2	3
12	MANCHESTER	6.3	0	3.7
13	BRISTOL	5.76	0	3.7
14	SOUTHAMPTON	5.39	-0.1	2.9
15	STOKE-ON-TRENT	5.51	-0.2	2.6
16	NEWCASTLE UPON TYNE	5.62	-0.2	2.9
17	PLYMOUTH	5.34	-0.2	1.9
18	LUTON	5.4	-0.2	2.3
19	NORWICH	5.25	-0.3	2.9
20	CARDIFF / CAERDYDD	5.53	-0.4	5.2
21	BIRMINGHAM	6.36	-0.5	2.4
22	ALDERSHOT	5.33	-0.5	2.9
23	NOTTINGHAM	5.74	-0.6	3.5
24	MILTON KEYNES	5.28	-0.6	3.1
25	DERBY	5.36	-0.6	2.7
26	SHEFFIELD	5.78	-0.7	3.2
27	BOURNEMOUTH	5.49	-0.7	3.2
28	BRADFORD	5.54	-0.7	2.2
29	SOUTHEND-ON-SEA	5.38	-0.7	2.5
30	NORTHAMPTON	5.3	-0.7	2.9
31	TELFORD	5.09	-0.8	2.6
32	COVENTRY	5.48	-0.9	2.8
33	LEEDS	5.73	-1.5	8.2
34	EDINBURGH	5.67	-2	8.4
35	ABERDEEN	5.26	-5.8	40.2

### 5.3.3 Temporal Variability of emission distributions

Turning to the temporal variation in the within-city distributions of emitted energy, we focus again only on three cities: London, Sheffield, and Milton Keynes. Appendices A – C shows the within-city emission distributions for these three cities for the twelve summer and twelve winter dates discussed

in chapter 3. Note that London passes the cloud-clear threshold on fewer nights, so is sampled on only seventeen nights (Table 5.3). Figure 5.9, 5.12, and 5.15 (appendices A-C) plot  $[\chi_{min}, \chi_{10}]$  (red) and  $[\chi_{90}, \chi_{max}]$  (blue) for all sample nights for London, Sheffield, and Milton Keynes, respectively.

**Table 5.3 Emission Distribution in London for all sample nights (dates) discussed in chapter 3**

Rank	DATE(Nights)	$\chi_{50} - \chi_{10}$ , W m <sup>-2</sup>	Median ( $\chi_{50}$ ), W m <sup>-2</sup>	$\chi_{90} - \chi_{50}$ , W m <sup>-2</sup>	Skewness (S)	Kurtosis (X)	Cloud free area (km <sup>2</sup> )	Mean, W m <sup>-2</sup>	Mode Count	Integrative measures: $\log_{10}(\langle(E_{j,k})[\chi_1, \chi_2]\rangle)$		
										$[\chi_{min}, \chi_{max}]$	$[\chi_{min}, \chi_{10}]$	$[\chi_{90}, \chi_{max}]$
1	30th Nov. 2016	5	308	8	0.5	3.0	1581	308	2	5.595	4.596	4.613
2	02nd Jan. 2017	4	310	4	0.3	3.6	1560	310	2	5.765	4.754	4.803
3	15th Feb. 2016	3	318	4	0.3	2.9	1465	318	3	5.771	4.760	4.788
4	27th Jun. 2010	10	417	17	0.2	2.4	1144	419	4	5.728	4.722	4.766
5	22nd Feb. 2003	5	323	5	0.0	3.2	1589	323	4	5.710	4.723	4.743
6	28th Aug. 2001	11	376	9	0.0	2.6	1572	375	2	5.716	4.711	4.724
7	13th Jul. 2002	10	384	6	-0.1	3.1	1394	384	4	5.759	4.775	4.795
8	07th Jul. 2007	9	384	8	-0.1	2.8	1460	384	4	5.785	4.777	4.808
9	13th Feb. 2017	3	322	2	-0.4	3.5	1588	322	3	5.726	4.729	4.767
10	10th Jun. 2003	6	383	5	-0.4	2.9	1356	383	2	5.748	4.738	4.764
11	16th Aug. 2016	9	389	6	-0.6	3.2	1548	388	4	5.718	4.713	4.743
12	09th Jul. 2006	8	396	4	-0.6	2.9	1542	395	3	5.680	4.673	4.708
13	01st Jan. 2007	5	336	3	-0.7	3.1	1589	335	4	5.669	4.675	4.703
14	26th Dec. 2009	7	333	4	-0.9	4.3	1575	332	5	5.778	4.765	4.803
15	30th Aug. 2005	9	404	5	-1.2	5.9	1427	402	4	5.688	4.696	4.707
16	06th Jun. 2000	12	370	6	-1.8	8.3	1583	368	4	5.685	4.680	4.694
17	29th Feb. 2000	4	335	3	-3.3	25.0	1177	334	5	5.708	4.722	4.724

Note: X – axis is represented by Rank = Date (Nights) in figures 9, 10, and 11; The sample dates in the table are ranked by skewness values

Nights (dates) are ranked according to skewness in tables 5.3-5.5. On 11 of the 17 sample nights, the distribution of emitted energy within London exhibits negative skew with the rate of change of  $|S|$  increasing towards the bottom of the rank order: 29<sup>th</sup> February 2000 (Fig. 5.9 in Appendix A). The skewness pattern is similar for Sheffield (Fig. 5.12), but the nights showing the most skew are different, and even in different seasons. Sixteen of the 24 nights show negative skew, with the rate of change of  $|S|$  increasing towards the bottom of the rank order: 10<sup>th</sup> June 2003. Milton Keynes shows a very different skewness pattern (Fig. 5.15): for 19 of the 24 nights sampled  $S \approx -0.5$ , for three nights  $-0.5 < S < 0.5$ , and for two nights  $S < -1.5$ . The two large negative deviations are for winter nights;

the positive deviations are for two summer nights and one winter night. There is no obvious pattern in skewness with regards to seasonality in the sample nights for the 3 cities (Tables 5.3-5.5).

There are few obvious patterns in the kurtosis values for the different nights and for each city (Tables 5.3-5.5; Figs. 5.11, 5.14, 5.17). Like the kurtosis for all cities on 2<sup>nd</sup> January 2017 (section 5.3.2, above), kurtosis for the three test-case cities over all nights sampled tends to cluster at  $X \approx 3$ , but with a number of significant deviations away from that value on particular occasions. The largest kurtosis values coincide with the most negative skewness for each city, but the dates and seasons vary.

The high and low percentiles of the distributions, for all sample dates, vary only slightly and contribute a similar amount to the total on each day. We might expect, therefore, just as for 2<sup>nd</sup> January 2017 (Fig. 5.2), the allometric scaling for the extremes of the distribution will be closely parallel to that for the sum measure, for the other days studied in chapter 3.

The number of modes in the distribution can be used to describe spatial patterns of the distribution of emitted energy inside the city boundary in which there is more than one central tendency. Tables 5.3-5.5 show that some distributions have up to 5 modes. No strong patterns are apparent for the number of modes in terms of season or of other statistical metrics. The variability of mode number in tables 5.3-5.5 argues against our hypothesis – “The number of modes in a city’s emitted energy distribution will not vary and can be identified with distinct urban forms”.

**Table 5.4 Emission Distribution in Sheffield for all sample nights (dates) discussed in chapter 3**

Rank	DATE(Nights)	$\chi_{50} - \chi_{10'}$ W m <sup>-2</sup>	Median ( $\chi_{50}$ ), W m <sup>-2</sup>	$\chi_{90} - \chi_{50'}$ W m <sup>-2</sup>	Skewness (S)	Kurtosis (X)	Cloud free area (km <sup>2</sup> )	Mean, W m <sup>-2</sup>	Mode Count	Integrative measures: $\log_{10}((E_{j,k})[\chi_1, \chi_2])$		
										$[\chi_{min}, \chi_{max}]$	$[\chi_{min}, \chi_{10}]$	$[\chi_{90}, \chi_{max}]$
1	15th Feb. 2016	3	298	3	0.3	4.0	193	298	2	4.782	3.786	3.797
2	18th Feb. 2006	3	314	4	0.3	2.6	191	314	3	4.847	3.854	3.865
3	29th Feb. 2000	3	325	4	0.2	2.7	186	325	1	4.596	3.609	3.625
4	16th Aug. 2016	8	378	7	0.1	3.4	180	378	4	4.782	3.831	3.802
5	13th Jul. 2002	6	376	6	0.1	2.2	105	376	3	4.800	3.791	3.833
6	20th Jan. 2011	2	298	3	0.1	2.7	193	298	2	4.818	3.827	3.895
7	30th Aug. 2005	4	389	5	0.0	1.9	102	389	2	4.599	3.625	3.709
8	07th Jul. 2007	8	371	8	0.0	2.6	192	370	3	4.778	3.793	3.826
9	22nd Feb. 2003	4	313	3	-0.2	2.6	194	312	2	4.831	3.814	3.862
10	26th Dec. 2009	7	315	5	-0.2	1.7	167	314	2	4.798	3.797	3.823
11	27th Jun. 2010	7	392	5	-0.3	2.5	128	392	3	4.852	3.858	3.881
12	05th Jan. 2005	3	339	2	-0.5	2.8	194	339	2	4.522	3.546	3.722
13	08th Aug. 2012	6	384	4	-0.6	2.7	168	383	2	4.592	3.683	3.608
14	02nd Jan. 2017	4	314	2	-0.7	3.2	194	313	2	4.720	3.809	3.785
15	06th Jun. 2000	4	363	3	-0.7	3.0	194	363	2	4.700	3.789	3.804
16	17th Dec. 2011	3	312	2	-0.7	2.8	193	311	3	4.760	3.792	3.780
17	30th Nov. 2016	4	336	2	-0.9	3.7	76	336	2	4.779	3.850	3.798
18	13th Feb. 2017	1	313	1	-1.1	4.7	14	313	4	4.809	3.806	3.845
19	25th Feb. 2009	5	326	3	-1.1	3.7	102	326	3	4.760	3.769	3.860
20	03rd Aug. 2017	10	379	5	-1.4	4.7	168	378	3	4.833	3.820	3.846
21	28th Aug. 2009	15	365	4	-1.7	5.1	108	362	3	4.407	3.474	3.433
22	09th Jul. 2006	7	377	5	-1.7	6.5	180	376	3	4.784	3.790	3.802
23	01st Jan. 2007	10	329	3	-1.9	7.4	192	327	4	3.642	2.794	2.799
24	10th Jun. 2003	5	374	4	-3.0	18.5	169	373	4	4.802	3.789	3.908

Note: X – axis is represented by Rank = Date (Nights) in figures 12, 13, and 14; The sample dates in the table are ranked by skewness values

**Table 5.5 Emission Distribution in Milton Keynes for all sample nights (dates) discussed in chapter 3**

Rank	DATE(Nights)	$\chi_{50} - \chi_{10'}$ W m <sup>-2</sup>	Median ( $\chi_{50}$ ), W m <sup>-2</sup>	$\chi_{90} - \chi_{50'}$ W m <sup>-2</sup>	Skewness (S)	Kurtosis (X)	Cloud free area (km <sup>2</sup> )	Mean, W m <sup>-2</sup>	Mode Count	Integrative measures: $\log_{10}((E_{j,k})[\chi_1, \chi_2])$		
										$[\chi_{min}, \chi_{max}]$	$[\chi_{min}, \chi_{10}]$	$[\chi_{90}, \chi_{max}]$
1	03rd Aug. 2017	3	342	41	0.4	1.3	73	356	2	4.456	3.457	3.473
2	28th Aug. 2009	3	364	6	0.3	1.8	47	365	2	4.456	3.457	3.475
3	22nd Feb. 2003	3	314	3	0.1	2.1	78	314	3	4.399	3.466	3.426
4	13th Jul. 2002	6	374	7	-0.3	2.1	67	374	2	4.389	3.492	3.405
5	15th Feb. 2016	3	310	2	-0.4	2.2	78	310	2	4.319	3.327	3.363
6	27th Jun. 2010	6	393	6	-0.4	2.6	53	393	3	4.424	3.431	3.489
7	28th Aug. 2001	6	367	5	-0.4	2.5	78	367	2	4.441	3.422	3.454
8	05th Jan. 2005	2	340	2	-0.4	2.5	78	340	2	4.389	3.391	3.581
9	17th Dec. 2011	4	317	1	-0.4	2.0	74	316	2	4.483	3.488	3.550
10	20th Jan. 2009	2	311	2	-0.5	4.5	68	311	4	4.412	3.418	3.426
11	16th Aug. 2016	4	376	6	-0.5	2.2	33	377	2	4.460	3.460	3.479
12	08th Aug. 2012	6	387	4	-0.5	2.6	74	387	2	4.325	3.333	3.342
13	13th Dec. 2010	3	263	1	-0.5	3.3	33	263	3	4.058	3.069	3.225
14	02nd Jan. 2017	3	307	2	-0.6	3.1	78	307	3	4.235	3.335	3.268
15	09th Jul. 2006	5	391	2	-0.6	2.5	78	390	2	4.404	3.459	3.419
16	13th Feb. 2017	2	314	1	-0.6	3.6	78	314	3	4.319	3.364	3.380
17	01st Jan. 2007	3	331	2	-0.7	2.3	78	331	2	3.938	3.016	3.201
18	07th Jul. 2007	9	371	5	-0.7	2.7	78	370	2	4.369	3.398	3.406

19	18th Feb. 2006	5	314	3	-0.7	2.6	78	314	3	4.457	3.482	3.635
20	10th Jun. 2003	17	374	7	-0.7	2.8	56	372	3	4.383	3.441	3.397
21	06th Jun. 2000	7	367	3	-0.8	2.8	78	366	2	4.095	3.169	3.485
22	30th Aug. 2005	18	397	7	-0.8	2.6	70	395	2	4.379	3.385	3.393
23	25th Feb. 2009	38	332	4	-1.7	4.0	35	326	4	4.389	3.396	3.403
24	26th Dec. 2009	3	326	1	-2.7	12.8	78	325	4	4.415	3.432	3.487
Note: X – axis is represented by Rank = Date (Nights) in figures 15, 16, and 17; The sample dates in the table are ranked by skewness values												

## 5.4 Discussion

The results shown in figure 5.1, and presented in table 5.1, which motivated our study, are in-line with results for the same cities on other days (appendices A, B, and C) but there is considerable variability, with little discernible pattern, in all the statistical metrics we have looked at.

The frequency distribution of upwelling thermal energy emitted is a climatic parameter of considerable importance and is expected to mirror the spatial patterns of urban form in each of the sample cities (see Figs. 5.2B; 5.3D & 5.4F – lower panels and appendices A-C). The landuse maps figures 5.2A; 5.3C and 5.4E (upper panels) established a spatial pattern of the city's urban morphology e.g., the built forms i.e., residential and work places (high-rise, medium and low-rise); roads; surface water and hydrography (rivers, canal, lakes, and ponds); land cover (parks and fields); landform (hills); woodlands; populated places (restaurants/eateries, parks, shops/super markets etc.); functional sites (hospitals, education institutes, airports, bus stops, coach stations, etc.). All these factors translated to anthropogenic emission which is apparent on the energy emitted maps coupled with the coastal position (Figs 5.2B; and 5.3D & 5.4F – lower panels). For instance, London's estuarine position imparts a strong microscale component to the long-wave energy emission. The built form in Sheffield, landform, and anthropogenic activities (populated places) is indicative and responsible for the pattern of long-wave emissions in the city. The populated places and hydrography location along the coastal area, in addition to anthropogenic activities in Milton Keynes clearly indicates the high magnitude spots on the emission map.

The tails of the distribution (i.e.,  $[\chi_{min}, \chi_{10}]$  and  $[\chi_{90}, \chi_{max}]$ ) capture the hottest and coolest parts of the urban landscape (Figure 5.1). The shape of the emitted energy distributions in the region of the tails varies greatly day to day and city to city (appendices A-C).

Given the variability and the lack of any discernible pattern in the occurrence of modes in the distributions (Tables 5.3-5.5), we were not able to confirm the hypothesis that ‘the number of modes in a city’s emitted energy distribution will not vary and can be identified with distinct urban form’. One advantage of using the mode is that it is easily identified in a dataset and in a discrete frequency distribution and that it tests for the presence of multiple, overlapping, populations.

Four nights (including 2<sup>nd</sup> January 2017) out of 17 nights for London city have 2 modes (two in summer and two in winter). Three nights are having 3 modes (one in summer and two in winter). The most frequent in the distribution is the one having 8 nights with 4 modes (six in summer and 2 in winter), and finally 2 nights (all in winter) in the distribution with 5 modes. For Sheffield city, 10 nights out of the total of 24 have two modes (three in summer, seven in winter). Next most frequent are distributions with three modes, on nine nights (six in summer, three in winter). Four-mode distributions occur on four nights (two in summer, two in winter), and a single night (29<sup>th</sup> February 2000) has a unimodal distribution. For Milton Keynes, bimodal distributions occur on 14 nights (ten nights in summer and four in winter). A total of seven nights (two in summer, five in winter) have three modes in the distribution, and three nights (all winter) have four modes. Overall, for the nights sampled, upwelling thermal emissions from London have  $3.5 \pm 1$  mode, those from Sheffield have  $2.5 \pm 1$  mode, and those from Milton Keynes have  $2.5 \pm 0.5$  modes.

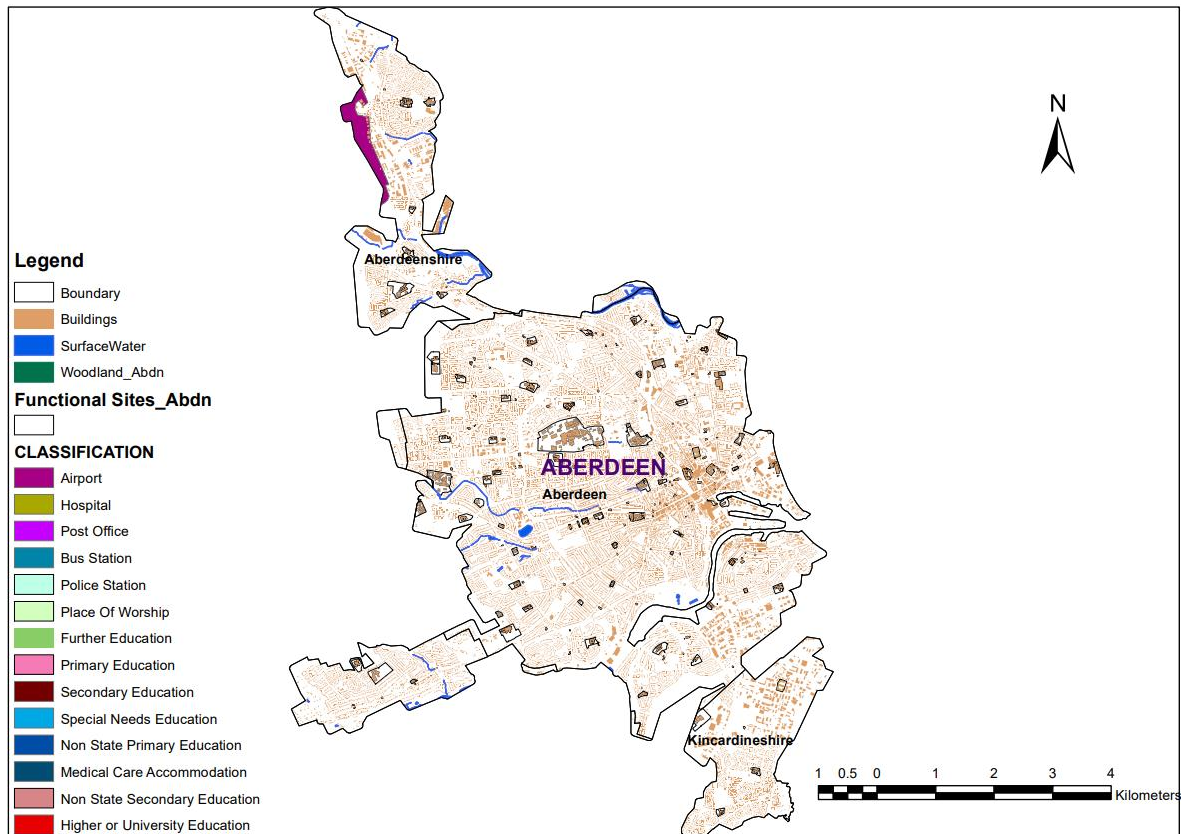
For all the statistical measures tested, the results do not reveal any obvious pattern with regards to seasonality for all the sample nights for the 3 cities (Tables 5.3, 5.4 and 5.5) respectively.

It is possible that the relatively small sample size weakens the statistical testing of our hypotheses. From the discussion above, we expect that, to drive the standard deviation of the mode analysis for

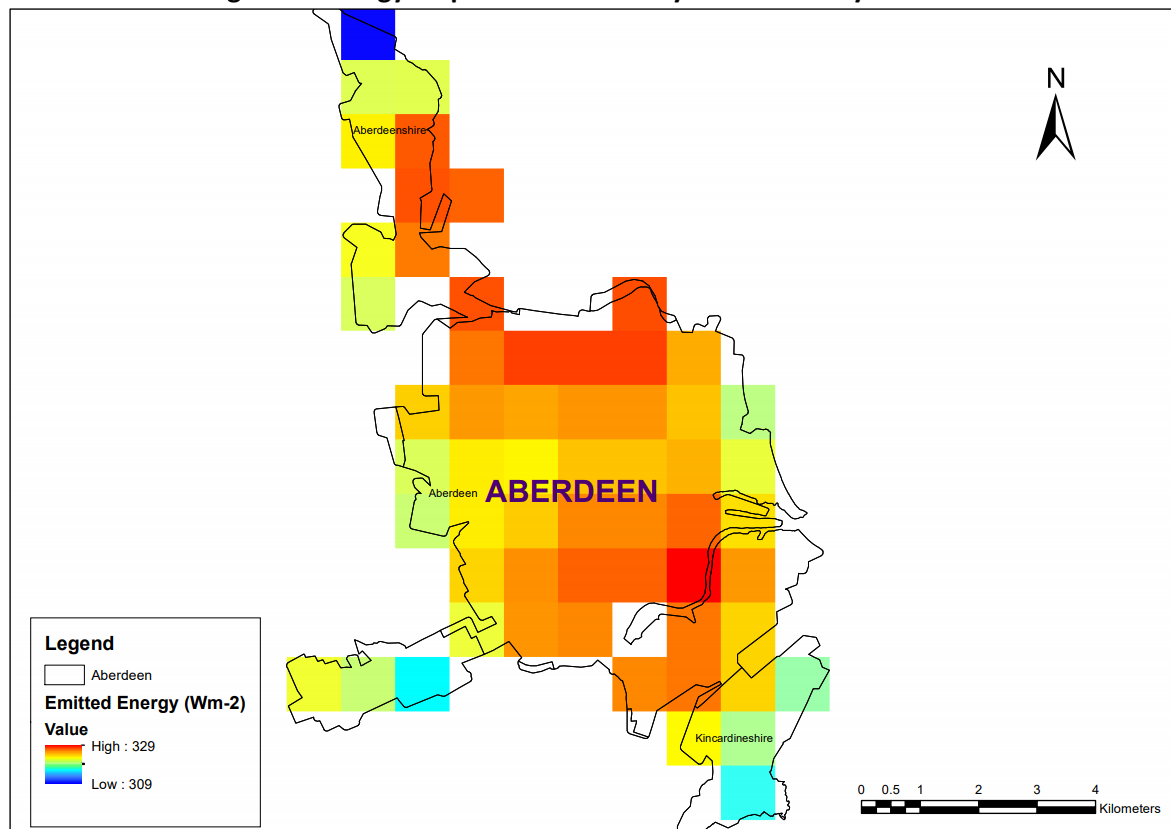
London to about 10% of the mean would require over 270 samples if the standard deviation around the mean varies by  $1/\sqrt{n}$ , where  $n$  is the sample number. Such a large sample was, unfortunately, outside the scope of the present study.

The city of Aberdeen appears as an outlier in the results above, having the most negative skewness ( $S = -5.8$ ) and by far the biggest kurtosis ( $X = 40.2$ ; table 2). Aberdeen is situated at the coast in the northeast of Scotland with an area of 50.27 km<sup>2</sup> and a population of 181,027 (Office for National Statistics, 2017). The climate of Aberdeen is oceanic with a daily average January temperature of 0.6°C and a July daily average temperature of 10°C (Met Office, 2020). Its position in the northeast makes it the coldest city in the UK. The city's morphology, orientation, and intensity of anthropogenic activities may be the key factors of its thermal behaviour. Figure 5.8 below shows the spatial pattern of long-wave energy emission centred towards the upper north and towards the lower south of Aberdeen conurbation (see lower panel ) where various built forms are predominant and other anthropogenic activities ( e.g., education both primary and secondary) and hydrography as indicated from the landuse map (upper panel). The long-wave energy is highest along the coastal areas of the conurbation and lowest around the airport area as illustrated in the landuse map (upper panel).

**Landuse map showing the geography of Aberdeen city**



**Long-wave energy map for Aberdeen city on 2<sup>nd</sup> January 2017**



**Figure 5.8** Landuse map showing city geography (left plate) and gridded code (interpolation-kriging) long-wave energy translated to city schematic map with magnitude indicating pattern of urban emission (lower plate) for Aberdeen on a selected sample night (2<sup>nd</sup> January 2017). Data were sourced from MODIS (Earthdata, 2017), Ordnance survey (meridian2 data – DLUA) and Digimap (<https://digimap.edina.ac.uk/>). ArcGIS 10.6 tools were used to plot the maps



The general observation for table 5.3-5.5 above, shows that from all night samples, London city recorded 10 nights having positive skewness out of the 17 nights. Sheffield recorded 16 nights having positive skewness out of 24 nights, and Milton Keynes recorded 21 nights having positive skewness out of 24 nights. This observation tells us the distribution is far from Gaussian/Normal and predominantly skewed towards high emissions. This also gives us an idea of urban morphology and land cover characteristics in relation to the formation of UHI in the cities.

## 5.5 Conclusion

In this chapter we have investigated how the spatial distribution of night-time emitted thermal energy inside the city boundary is affected by the urban form and whether any generalized patterns emerge. We use fitted distributions and the high and low percentiles of the distribution of emitted energy and landuse map within a city as the basis of comparisons across cities and time. The high and low percentiles provide information about the hottest and coldest spots in the distribution of emitted energy for a given city on a given night.

The study aims to examine whether the hottest and coldest parts of the distribution of emitted energy within UK cities vary with population in the same way as the sum measure discussed in chapter 3. A sample of three cities of very different size and character (London, Sheffield, and Milton Keynes) were focussed on as it is not possible to carry out an exhaustive study in the present analysis. The study looked at the variability of emitted energy distributions in the three case-study cities over 24 nights, in both summer and winter, from 2000 to 2017. In addition, all 35 cities from chapter 3 were studied for one night: 2<sup>nd</sup> January 2017.

The spatial distributions of cities' upwelling emitted long-wave energy were assessed using several statistical metrics: sum measures below the 10<sup>th</sup> percentile ( $[\chi_{min}, \chi_{10}]$ ) and above the 90<sup>th</sup> percentile ( $[\chi_{90}, \chi_{max}]$ ); mode counts; skewness; and kurtosis. We found that cities geography, built form and ultimately man-made activities account for modifications to the distribution of emitted energy (figs.

5.2A, 5.3D & 5.4F – lower panels). Allometric scaling, with population, of  $[\chi_{min}, \chi_{10}]$  and  $[\chi_{90}, \chi_{max}]$  were consistent with the allometry calculated for the sum of the entire distribution ( $[\chi_{min}, \chi_{max}]$ ) calculated in the previous study (Abdulrasheed et al., 2020). There is very tentative evidence for cold spots becoming less prevalent as city size increases.

The skewness, kurtosis, and the 10<sup>th</sup> percentile and 90<sup>th</sup> percentile of the emitted energy distributions for all nights in the 3 sample cities are not affected by season. The only patterns discerned in the results are (i) a general tendency for positive skew, and (ii) a tendency for coastal cities to have the most positive skew. Further work is required to attribute this pattern more robustly, and to establish the most meaningful and robust metrics which best capture the relationships between within-city urban thermal budgets and neighbourhood-scale urban form.

## **6.0 Chapter 6**

### **Overall Synthesis and Conclusions**

The overall aim of this thesis was to evaluate/investigate the implication of spatial settlement patterns on the urban climate using a combination of observational analyses and modelling. This is a broad aim that can only ever be incompletely addressed within the scope of a single PhD thesis. In this chapter, I will discuss the degree to which my chosen research strategy succeeded in addressing the thesis aim, will bring forward the limitations in the approach, and will point to future research directions. Allometric scaling has been utilized in this thesis as the principal lens through which to examine the potential impacts of urban form on surface atmosphere exchange of heat (energy budget). The scaling analysis was then extended by examining the distribution of emitted energy inside particular urban areas. This chapter summarizes findings from the results' chapters (3-5), including the assessment of thermal properties (emitted energy) in relation to cities' urban form. By focusing on an allometric perspective, the work has, in the end, looked more at the overall influence of population rather than the detail of settlement pattern.

Although the principal approach used in this thesis focuses on the bulk properties of cities, I argue that the outcomes of this study — particularly the focus on residuals that remain once the dominant allometric scaling has been removed — will help to contribute to the understanding of urban climate in cities at neighbourhood and regional scale. Together, the allometry, the study of the residuals, and the examination of city emission PDFs, should deliver to decision- and policy-makers, urban planners, and related sectors, perspectives that will help define decisions for the future design of the urban environment

### **6.1 Fulfilment of aims of the thesis**

This thesis had three primary objectives, introduced in section 1.4. The objectives are reiterated below, along with a short discussion given as a summary of findings in relation to this thesis.

## **1. Using appropriate scaling techniques to explore the relationship between urban morphology and the bulk thermal properties (emitted energy) of cities in the UK**

This section of the thesis measured the allometric scaling of emitted energy of selected sample cities in the UK (chapter 3). The work resulted in allometric scaling of night-time clear-sky upwelling long-wave thermal surfaces for 35 largest cities in the UK, derived from MODIS remotely sensed land surface temperature data at 1km resolution. Total (area-summed) emitted energy per overpass per city was shown to correlate closely ( $R^2 \geq 0.79$ ) with population on a log-log 'allometry' plot. This area-summed night-time emitted energy is found to scale sub-linearly with population on both summer and winter nights, with a mean slope over all overpasses sampled of  $0.84 \pm 0.06$ , implying an 'economy (or parsimony) of scale' of about 21% (i.e.  $100(2 - 10^{0.84 \log(2)})$ ) for each doubling of city population. City area showed a very similar economy of scale, so that the scaling of night-time emitted energy with urban area is close to linear ( $1.0 \pm 0.05$ ). This linearity with area indicated that the urban forms used in UK cities to accommodate people more efficiently per unit area as the urban population grows, do not have a large effect on the thermal output per unit area in each city. Although often appearing superficially very different, UK cities appear to be similar in terms of the components of urban form that dictate thermal properties. The difference between the scaling of the heat source and a literature report of the scaling of urban-rural air temperature difference (UHI) is very marked, suggesting that the other factors affecting the UHI act to strongly decrease the scaling with population

## **2. Translate the (allometric scaling) methodology into the developing world within a different context of settlement, urban morphology, and planning constraints**

Using the approaches developed earlier in the thesis, the applicability of the technique in a different environment to the UK was evaluated (i.e., Nigeria). As per the UK, the study used images from MODIS satellite, covering the period between 2000 and 2017, sampled out to examine the seasonal variability of night-time clear-sky upwelling long-wave energy for 33 largest cities across Nigeria. The relationship between total urban population and total emitted energy was found to be sub-linear, again indicating

a thermal ‘parsimony of scale’ with respect to population. Findings also showed that the relationship between total urban area and total emitted energy was linear for Nigeria’s cities, again consistent with what had been shown previously for UK cities even despite UK and Nigeria’s cities being very different morphologically. The common linear scaling of emitted energy with area in UK and Nigerian cities suggests that the changed energy budget of cities, compared to the rural land cover they replace, is driven mostly by the thermal properties of built impervious surfaces rather than the distribution of urban morphological settings. A preliminary investigation of Local Climate Zones, as a means of interpreting the allometry residuals, provided a useful tool to provide insights into both these elements.

### **3. Explore how the spatial distribution of emitted energy within UK cities provides additional information regarding the unique urban form beyond that of a city-scale analysis**

The earlier work in the UK was revisited to investigate whether the spatial distribution of emitted energy within UK cities provides information complementary to the sum measure discussed in the earlier chapters. It is clear that the distribution of emitted energy inside cities is related to local landuse / climate zone, and this will result in localised hot spots and cold spots which will vary as a function of city size. This led to the hypothesis that the allometry of extreme percentiles of the distribution will not conform to that of the sum measure. Indeed, the use of percentiles for this purpose provides an intuitive way to understand where a value falls within a distribution of values. The exploratory study focused on three UK cities of very different size and characteristics; London, Sheffield, and Milton Keynes. However, the findings showed that the allometric scaling at both tails of the distribution are nearly identical to that using the sum measure for the whole of each city. This indicates the presence of local hot spots and cold spots (i.e., parks) has a limited impact on the thermal characteristics of the city as a whole. Rather the cities geographic context, built form and ultimately anthropogenic activities account for modifications to the distribution of emitted energy. Examination of the probability density functions — for each of the study cities for each of the study nights —

showed few clear patterns with respect to the number of modes in the distribution, and the higher-order moments of the distributions (skewness and kurtosis).

## **6.2 Critique of thesis**

This thesis has highlighted a number of uncertainties in, and limitations of, the methodologies used. These have been discussed throughout the thesis but are summarised here. Most of the shortcomings are addressed in the discussion of future work (section 6.3). The methodologies used in this thesis have been designed to be broadly universally applicable. Although the focus was on UK and Nigerian settlements, the findings are applicable to cities elsewhere, and the approaches used (MODIS, LCZ, and allometry – using GIS as a tool) are all standard across the world and therefore allow comparisons to be made. As discussed further below, the biggest challenges for translation are data availability/interoperability between countries and regions.

### ***6.2.1 Remote Sensing: Moderate Resolution Imaging Spectro-radiometer (MODIS)***

Satellite remote sensing approaches are by their nature consistent across the world. This study used the MODIS/Terra V006 composite products (MOD11A1) – MODIS/Terra Land Surface Temperature and Emissivity Daily L3 Global 1km Grid SIN V006. Land Surface Temperature (LST) from MODIS were retrieved from clear sky observations at daytime and night-time with the aid of generalized split-window algorithm (Wan and Dozier, 1996; Wan, 2008). Several studies have affirmed the importance of MODIS LST product for its global coverage, high resolution and accurate calibration in multiple thermal infrared band design for retrievals of LST and atmospheric properties (Wan and Dozier, 1996; Wan et al., 2002; Wan, 2008). This study only uses images from Terra satellite, even though the MODIS sensor is carried by both Aqua and Terra satellites. The night image (obtained from Terra satellite) used in this thesis, gives more accurate LST calculation due to the absence of solar radiation to change the surface radiation balance, and the temperature gradient of night-time images would be expected to be less steep than daytime images (Rigo et al., 2006).

Because of its robust data pipeline, this thesis has used MOD11A1 LST data 'as is', only converting it into emitted energy using the Stefan-Boltzmann law (equation 3.3, chapter 3) so that it can be summed straightforwardly. No account has been taken of the change of viewing angle across the satellite swath. Information on the emissivity of each pixel and the view angle is available in the MOD11A1 data files. Future work should investigate whether using the available metadata alters the allometry. Another limitation, associated with all satellite studies of the ground surface, is obscuration of the surface by cloud. Stringent measures were put in place to avoid bias resulting from cloud by reporting the results only for scenes that passed a 50% cloud-clear threshold. To test the impact of the 50% threshold, the analysis was repeatedly increasing the requirement for inclusion of an urban area in the analysis to 75% cloud-free (see tables 3S3 and 4S3 in supplementary section). Although all the study cities were very seldom available on any given night, the allometric scaling observed was reassuringly consistent.

### ***6.2.2 Allometric Scaling Approach (using GIS as a tool)***

An earlier definition of geographic Information systems (GIS) by Calkins and Tomlinson (1977) cited in (Weng, 2010) states; "It is an integrated software package specifically designed for use with geographic data that performs a comprehensive range of data handling tasks, e.g., data input, storage, retrieval and output". GIS has been defined as an enabling technology because of its vast application in a variety of discipline as a tool. The GIS tool is used extensively by researchers; however, there are challenges to its effective use especially with respect to obtaining data. Specific problem areas include obtaining accurate data on the subject matter and how it is translated and reported, for instance basic climate (e.g., MODIS data) and urban extent (e.g., OS and SEDAC) data used in the study were downloaded and converted into various shapefiles and scales for compatibility with the tool. This presented a large challenge in this work as each country operates to different standards meaning that processing varied between UK and Nigeria. The standards between different datasets also vary and the representation of the extent of an 'urban' area in the UK was different to that in Nigeria. Where this makes little difference at a country scale (as the definition is consistent), this does pose a challenge

when comparing across countries. This will be more so, should future research broaden the approach to include multiple countries (section 6.3).

### ***6.2.3 Local Climate Zone (LCZ)***

The issue of data availability and the application of urban climate models to planning problems is of great importance to any UHI research. This research is not excluded from this circumstance and especially cities around the economically developing world lack the necessary data to delineate its surface extent, vegetation cover, land and building covers/series, and as well the technical know-how of overlaying atmosphere in and around the city. To that end, the concept of LCZ developed by Stewart and Oke, (2012) provides a means to standardize the methods used to describe urban form and its thermal performance in UHI studies. The approach has the ability to classify areas of a settlement into zones of the same capacity to modify the local climate, rather than the conventional “urban and rural” classes. The use of the LCZ approach was examined in relation to the energy budget as standards are necessary for meaningful and consistent exchange of data between regions and across the globe. The applicability of the LCZ scheme by urban climatologist, GIS experts and urban planners demonstrates its appeal across multidisciplinary fields. The scheme is regarded as the first fully comprehensive approach with the inclusion of non-urban sites. The concept is however not completely exhausted in this study for instance the aspects of non-urban zone. This will merit future research. One limitation of this approach is inability of the metadata used for classification to exactly match with the original Stewards and Oke’s (2012) standards, which may be due to physical development planning patterns of the study area. Skills judgement and knowledge of study sites are usually applied in this case as a process in selecting ‘best fit’ zones. Another limitation is subject to certain assumptions, for instance in land use (urban function) may vary between neighbourhoods – e.g., a set of high-rise building may be used for residential blocks (LCZ 1) and another set of high-rise building for commercial purpose (LCZ 1), and meanwhile the built form (morphological characteristics) could be similar, the expectation would be the time spent (occupancy ratio), energy and water usage are radically different, hence would affect the urban energy balance. However, the applications of Local Climate Zones is fast



becoming a standard approach and there is a large amount of research underway to provide standardised tools for application across the world (e.g., <http://www.wudapt.org/>)

### **6.3 Future work**

Further studies, which help to take these limitations into account, will need to be undertaken as pointed out in conclusions within individual chapters (see sections 3.5; 4.5; and 5.5).

In line with the results outcome presented in this thesis, there is scope for many further studies on allometry to explore underlying mechanisms. Earlier in this study, the allometry approach was used to examine the extent and rate of emitted long-wave energy with population in temperate and tropical cities for MODIS/Terra V006 composite product (MOD11 A1). The study investigated the influence of the city characteristics – (e.g., buildings morphology, population, and long-wave emission). The results of this investigation are also an excellent qualitative agreement with those presented in Oke, 1973 and Oke 1982. The results also produced a well-documented aspect such as the potentials for understanding the role of urban form in heat storage and emission in built environment and the uniqueness of British and Nigeria's urban form manifestation in the residuals for each city. However, the study has not found any simple guidelines that would allow predicting the size of the residual from its geographical context (including climate). Further research is required to provide greater insight into the effects of this mechanism.

Fundamentally, the universal nature of the approach (provided, the limitations with data can be overcome) lends itself to a truly global study enabling the impacts of differences in morphology to be quantified on an intercontinental scale. Allometric studies provide a means to achieve this even if there is some debate in the literature on such a bulk properties approach (Martilli et al., 2020)(Manoli et al., 2020). However, there is a general paucity of urban climate studies in developing nations, especially across Africa, and the ease of this approach provides an excellent entry point into more detailed investigations. A future research agenda could focus on the need for improved low latitude urban climate studies. Most of the developing world is experiencing rapid urbanization over the last

50 years. Climate change intensifies the impact of urban microclimate on tropical environments and makes city residents and infrastructure more vulnerable. Future urban climate studies in these regions need to consider impact at city level and as well its risk assessments. Bio-degradation and environmental problems in the tropical regions is clearly on the increase, e.g., air pollution, heat stress which impact on the health and comfort of the people living in the region.

The study of allometry applied to temperature variation, rather than to emitted energy, is appearing with increasing frequency in urban climate studies. Also, the inclusion of cloud and topographic impact into climate studies would permit investigation and full analysis of different weather conditions for cities at different scale.

At the opposite scale, there is scope to expand on the work in Chapter 5 investigating the spatial distribution of emitted long-wave energy within individual cities. This will help researchers to find new and better ways of statistical and quantitative interpretation of urban land use land cover (LULC) / LCZ versus LST relationships and evaluate spatial patterns of hot- and cold-spots.

Finally, it would also be interesting to expand the analyses to other variables such as the scaling of air pollution in relation to urban form around the globe, building on MacKenzie et al. (2019) and utilizing the much-improved pollution detection capabilities of the new generation of satellites, such as the Sentinel series.

Overall, the simplicity and universal applicability of the approach, not just in space, but also in time and for any variable could lead to a renaissance in the use of allometry as an entry level study for the investigation of a range of urban environmental problems.

## References

- Abdulasheed, M., MacKenzie, A.R., Whyatt, J.D., Chapman, L., 2020. Allometric scaling of thermal infrared emitted from UK cities and its relation to urban form. *City Environ. Interact.* 100037. <https://doi.org/10.1016/j.cacint.2020.100037>
- Adams, J.S., 1970. Residential Structure of Midwestern Cities. *Ann. Assoc. Am. Geogr.* 60, 37–62. <https://doi.org/10.1111/j.1467-8306.1970.tb00703.x>
- Adefolalu, D.O., 1984. On bioclimatological aspects of Harmattan dust haze in Nigeria. *Arch. Meteorol. Geophys. Bioclimatol. Ser. B* 33, 387–404. <https://doi.org/10.1007/BF02274004>
- Adelekan, I.O., 2010. Vulnerability of poor urban coastal communities to flooding in Lagos, Nigeria. *Environ. Urban.* 22, 433–450. <https://doi.org/10.1177/0956247810380141>
- Adole, T., Dash, J., Atkinson, P.M., 2018. Major trends in the land surface phenology (LSP) of Africa, controlling for land-cover change. *Int. J. Remote Sens.* 39, 8060–8075. <https://doi.org/10.1080/01431161.2018.1479797>
- Aguado, E., Burt, J.E., 2015. Understanding Weather and Climate [WWW Document]. URL <https://www.pearson.com/us/higher-education/product/Aguado-Understanding-Weather-and-Climite-7th-Edition/9780321987303.html> (accessed 12.17.18).
- Ahmed, K.S., 2003. Comfort in urban spaces: defining the boundaries of outdoor thermal comfort for the tropical urban environments. *Energy Build.* 35, 103–110. [https://doi.org/10.1016/S0378-7788\(02\)00085-3](https://doi.org/10.1016/S0378-7788(02)00085-3)
- Akpodiogaga-a, P., Odjugo, O., 2010. General Overview of Climate Change Impacts in Nigeria. *J. Hum. Ecol.* 29, 47–55. <https://doi.org/10.1080/09709274.2010.11906248>
- Alavipanah, S., Wegmann, M., Qureshi, S., Weng, Q., Koellner, T., 2015. The Role of Vegetation in Mitigating Urban Land Surface Temperatures: A Case Study of Munich, Germany during the Warm Season. *Sustainability* 7, 4689–4706. <https://doi.org/10.3390/su7044689>
- Alexander, A., 2009. Britain's New Towns: Garden Cities to Sustainable Communities. Routledge.
- Aliyu, A.A., Amadu, L., 2017. Urbanization, Cities, and Health: The Challenges to Nigeria – A Review. *Ann. Afr. Med.* 16, 149–158. [https://doi.org/10.4103/aam.aam\\_1\\_17](https://doi.org/10.4103/aam.aam_1_17)
- Alonzo, M., Bookhagen, B., McFadden, J.P., Sun, A., Roberts, D.A., 2015. Mapping urban forest leaf area index with airborne lidar using penetration metrics and allometry. *Remote Sens. Environ.* 162, 141–153. <https://doi.org/10.1016/j.rse.2015.02.025>
- Amundsen, H., Berglund, F., Westskog, H., 2010. Overcoming Barriers to Climate Change Adaptation—A Question of Multilevel Governance? *Environ. Plan. C Gov. Policy* 28, 276–289. <https://doi.org/10.1068/c0941>
- Anderson, J.R., 1976. A Land Use and Land Cover Classification System for Use with Remote Sensor Data. U.S. Government Printing Office.
- Anderson, W.P., Kanaroglou, P.S., Miller, E.J., 1996. Urban Form, Energy and the Environment: A Review of Issues, Evidence and Policy. *Urban Stud.* 33, 7–35. <https://doi.org/10.1080/00420989650012095>
- Anguelovski, I., Chu, E., Carmin, J., 2014. Variations in approaches to urban climate adaptation: Experiences and experimentation from the global South. *Glob. Environ. Change* 27, 156–167. <https://doi.org/10.1016/j.gloenvcha.2014.05.010>
- Anukwonke, C., 2015. Urbanization Processes and Environment.
- Arifwidodo, S.D., Tanaka, T., 2015. The Characteristics of Urban Heat Island in Bangkok, Thailand. *Procedia - Soc. Behav. Sci., World Conference on Technology, Innovation and Entrepreneurship* 195, 423–428. <https://doi.org/10.1016/j.sbspro.2015.06.484>
- Arimah, B.C., Adeagbo, D., 2000. Compliance with urban development and planning regulations in Ibadan, Nigeria. *Habitat Int.* 24, 279–294. [https://doi.org/10.1016/S0197-3975\(99\)00043-0](https://doi.org/10.1016/S0197-3975(99)00043-0)
- Arnfield, A.J., 2003. Two decades of urban climate research: a review of turbulence, exchanges of energy and water, and the urban heat island. *Int. J. Climatol.* 23, 1–26. <https://doi.org/10.1002/joc.859>

- Arnfield, A.J., Grimmond, C.S.B., 1998. An urban canyon energy budget model and its application to urban storage heat flux modeling. *Energy Build.* 27, 61–68. [https://doi.org/10.1016/S0378-7788\(97\)00026-1](https://doi.org/10.1016/S0378-7788(97)00026-1)
- Ayanlade, A., 2017. Variations in urban surface temperature: an assessment of land use change impacts over Lagos metropolis. *Weather* 72, 315–319. <https://doi.org/10.1002/wea.2925>
- Ayanlade, A., 2016a. Seasonality in the daytime and night-time intensity of land surface temperature in a tropical city area. *Sci. Total Environ.* 557–558, 415–424. <https://doi.org/10.1016/j.scitotenv.2016.03.027>
- Ayanlade, A., 2016b. Variation in diurnal and seasonal urban land surface temperature: landuse change impacts assessment over Lagos metropolitan city. *Model. Earth Syst. Environ.* 2, 193. <https://doi.org/10.1007/s40808-016-0238-z>
- Ayanlade, A., 2015. Evaluation of the intensity of the daytime surface urban heat island: how can remote sensing help?: *International Journal of Image and Data Fusion: Vol 6, No 4* [WWW Document]. URL <https://www.tandfonline.com/doi/full/10.1080/19479832.2014.985618> (accessed 7.26.19).
- Azevedo, J.A., Chapman, L., Muller, C.L., 2016. Quantifying the Daytime and Night-Time Urban Heat Island in Birmingham, UK: A Comparison of Satellite Derived Land Surface Temperature and High Resolution Air Temperature Observations. *Remote Sens.* 8, 153. <https://doi.org/10.3390/rs8020153>
- Bahi, H., Rhinane, H., Bensalmia, A., Fehrenbach, U., Scherer, D., 2016. Effects of Urbanization and Seasonal Cycle on the Surface Urban Heat Island Patterns in the Coastal Growing Cities: A Case Study of Casablanca, Morocco. *Remote Sens.* 8, 829. <https://doi.org/10.3390/rs8100829>
- Ball, M., Maginn, P.J., 2005. Urban Change and Conflict: Evaluating the Role of Partnerships in Urban Regeneration in the UK. *Hous. Stud.* 20, 9–28. <https://doi.org/10.1080/0267303042000308705>
- Balling, R.C., Cervený, R.S., 2003. Vertical dimensions of seasonal trends in the diurnal temperature range across the central United States. *Geophys. Res. Lett.* 30. <https://doi.org/10.1029/2003GL017776>
- Balogun, I.A., Balogun, A.A., 2014. Urban heat island and bioclimatological conditions in a hot-humid tropical city: The example of Akure, Nigeria. *Erde* 145, 3–15. <https://doi.org/10.12854/erde-145-2>
- Balogun, I.A., Balogun, A.A., Adeyewa, Z.D., 2012. Observed urban heat island characteristics in Akure, Nigeria. *Afr. J. Environ. Sci. Technol.* 6, 1–8–8. <https://doi.org/10.5897/AJEST11.084>
- Bao, Y., 2013. On Sample Skewness and Kurtosis. *Econom. Rev.* 32, 415–448. <https://doi.org/10.1080/07474938.2012.690665>
- Basu, R., Samet, J.M., 2002. Relation between Elevated Ambient Temperature and Mortality: A Review of the Epidemiologic Evidence. *Epidemiol. Rev.* 24, 190–202. <https://doi.org/10.1093/epirev/mxf007>
- Batty, M., 2008. The Size, Scale, and Shape of Cities. *Science* 319, 769–771. <https://doi.org/10.1126/science.1151419>
- Bauman, J.F., Muller, E.K., 2006. Before Renaissance: Planning in Pittsburgh, 1889–1943. University of Pittsburgh Pre.
- Beale, C.L., 1975. The Revival of Population Growth in Nonmetropolitan America.
- Bechtel, B., Alexander, P., Böhner, J., Ching, J., Conrad, O., Feddema, J., Mills, G., See, L., Stewart, I., 2015. Mapping Local Climate Zones for a Worldwide Database of the Form and Function of Cities. *ISPRS Int. J. Geo-Inf.* 4, 199–219. <https://doi.org/10.3390/ijgi4010199>
- Belcher, S.E., Jerram, N., Hunt, J.C.R., 2003. Adjustment of a turbulent boundary layer to a canopy of roughness elements. *J. Fluid Mech.* 488, 369–398. <https://doi.org/10.1017/S0022112003005019>

- Bettencourt, L., West, G., 2010. A unified theory of urban living. *Nature* 467, 912–913.  
<https://doi.org/10.1038/467912a>
- Bettencourt, L.M.A., 2013. The Origins of Scaling in Cities. *Science* 340, 1438–1441.  
<https://doi.org/10.1126/science.1235823>
- Bettencourt, L.M.A., Lobo, J., 2016. Urban scaling in Europe | *Journal of The Royal Society Interface* [WWW Document]. URL <http://rsif.royalsocietypublishing.org/content/13/116/20160005> (accessed 12.13.17).
- Bettencourt, L.M.A., Lobo, J., Helbing, D., Kühnert, C., West, G.B., 2007. Growth, innovation, scaling, and the pace of life in cities. *Proc. Natl. Acad. Sci.* 104, 7301–7306.  
<https://doi.org/10.1073/pnas.0610172104>
- Bettencourt, L.M.A., Lobo, J., Strumsky, D., West, G.B., 2010. Urban Scaling and Its Deviations: Revealing the Structure of Wealth, Innovation and Crime across Cities. *PLOS ONE* 5, e13541.  
<https://doi.org/10.1371/journal.pone.0013541>
- Bibby, P., Brindley, P., 2013. Urban and Rural Area Definitions for Policy Purposes in England and Wales: Methodology (v1.0) 36.
- Bohnenstengel, S.I., Hamilton, I., Davies, M., Belcher, S.E., 2014. Impact of anthropogenic heat emissions on London's temperatures. *Q. J. R. Meteorol. Soc.* 140, 687–698.  
<https://doi.org/10.1002/qj.2144>
- Bokaie, M., Zarkesh, M.K., Arasteh, P.D., Hosseini, A., 2016. Assessment of Urban Heat Island based on the relationship between land surface temperature and Land Use/ Land Cover in Tehran. *Sustain. Cities Soc.* 23, 94–104. <https://doi.org/10.1016/j.scs.2016.03.009>
- Bongaarts, J., 2009. Human population growth and the demographic transition. *Philos. Trans. R. Soc. B Biol. Sci.* 364, 2985–2990. <https://doi.org/10.1098/rstb.2009.0137>
- Bornstein, R.D., 1968. Observations of the Urban Heat Island Effect in New York City. *J. Appl. Meteorol.* 7, 575–582. [https://doi.org/10.1175/1520-0450\(1968\)007<0575:OOTUHI>2.0.CO;2](https://doi.org/10.1175/1520-0450(1968)007<0575:OOTUHI>2.0.CO;2)
- Bounoua, L., DeFries, R.S., Imhoff, M.L., Steininger, M.K., 2004. Land use and local climate: A case study near Santa Cruz, Bolivia. *Meteorol. Atmospheric Phys.* 86, 73–85.  
<https://doi.org/10.1007/s00703-003-0616-8>
- Bourne, L.S., 1982. Internal Structure of Cities 7 Lembar | *City* [WWW Document]. Scribd. URL <https://www.scribd.com/document/382973520/Bourne-L-S-1982-Internal-Structure-of-Cities-7-Lembar> (accessed 1.14.20).
- Bremner, J., Frost, A., Haub, C., Mather, M., Ringheim, K., Zuehlke, E., 2010. World population highlights: Key findings from PRB's 2010 world population data sheet. *Popul. Bull.* 65, 1–12.
- Briney, A., Am, a B., geographer, a B. is a professional, writer, Degrees, S. with T.U., GIS, an advanced certificate in, 2019. How the United Kingdom Became an Island Nation [WWW Document]. ThoughtCo. URL <https://www.thoughtco.com/geography-of-the-united-kingdom-1435710> (accessed 9.4.19).
- Brousse, O., Martilli, A., Foley, M., Mills, G., Bechtel, B., 2016. WUDAPT, an efficient land use producing data tool for mesoscale models? Integration of urban LCZ in WRF over Madrid. *Urban Clim.* 17, 116–134. <https://doi.org/10.1016/j.uclim.2016.04.001>
- Brown, R., 2011. Ameliorating the effects of climate change: Modifying microclimates through design. *Landsc. Urban Plan. - Landsc. URBAN PLAN* 100, 372–374.  
<https://doi.org/10.1016/j.landurbplan.2011.01.010>
- Buhaug, H., Urdal, H., 2013. An urbanization bomb? Population growth and social disorder in cities. *Glob. Environ. Change* 23, 1–10. <https://doi.org/10.1016/j.gloenvcha.2012.10.016>
- Burnett, J., 1986. Social History of Housing by Burnett - AbeBooks [WWW Document]. URL <https://www.abebooks.co.uk/book-search/title/social-history-of-housing/author/burnett/> (accessed 9.28.19).
- Carlos, B.K., Paul, O., Alan, H.P., Matthias, I., 2017. Mapping Local Climate Zones for urban morphology classification based on airborne remote sensing data [WWW Document]. URL

- [https://www.researchgate.net/publication/314286458\\_Mapping\\_Local\\_Climate\\_Zones\\_for\\_urban\\_morphology\\_classification\\_based\\_on\\_airborne\\_remote\\_sensing\\_data](https://www.researchgate.net/publication/314286458_Mapping_Local_Climate_Zones_for_urban_morphology_classification_based_on_airborne_remote_sensing_data) (accessed 1.4.20).
- Carmin, J., Anguelovski, I., Roberts, D., 2012. Urban Climate Adaptation in the Global South: Planning in an Emerging Policy Domain. *J. Plan. Educ. Res.* 32, 18–32.  
<https://doi.org/10.1177/0739456X11430951>
- Carmon, N., 1999. Three generations of urban renewal policies: analysis and policy implications. *Geoforum* 30, 145–158. [https://doi.org/10.1016/S0016-7185\(99\)00012-3](https://doi.org/10.1016/S0016-7185(99)00012-3)
- Carroll, M.L., DiMiceli, C.M., Townshend, J.R.G., Sohlberg, R.A., Elders, A.I., Devadiga, S., Sayer, A.M., Levy, R.C., 2017. Development of an operational land water mask for MODIS Collection 6, and influence on downstream data products. *Int. J. Digit. Earth* 10, 207–218.  
<https://doi.org/10.1080/17538947.2016.1232756>
- Carroll, M.L., Townshend, J.R., DiMiceli, C.M., Noojipady, P., Sohlberg, R.A., 2009. A new global raster water mask at 250 m resolution. *Int. J. Digit. Earth* 2, 291–308.  
<https://doi.org/10.1080/17538940902951401>
- Castán Broto, V., 2017. Urban Governance and the Politics of Climate change. *World Dev.* 93, 1–15.  
<https://doi.org/10.1016/j.worlddev.2016.12.031>
- CEDA, 2011. CEDA Data Server, Index of /badc/ukcp09/data/gridded-land-obs/gridded-land-obs-averages-5km/grid/netcdf/mean-temperature/ [WWW Document]. URL <http://data.ceda.ac.uk/badc/ukcp09/data/gridded-land-obs/gridded-land-obs-averages-5km/grid/netcdf/mean-temperature/> (accessed 10.2.18).
- Chadchan, J., Shankar, R., 2009. Emerging Urban Development Issues in the Context of Globalization 9.
- Chadwick, E., 1842. Edwin Chadwick's Report on the sanitary conditions of the labouring population of Great Britain was published | Policy Navigator [WWW Document]. URL <https://navigator.health.org.uk/content/edwin-chadwicks-report-sanitary-conditions-labouring-population-great-britain-was-published> (accessed 12.22.18).
- Chandler, T.J., 1966. The climate of London. By T. J. Chandler. London (Hutchinson), 1965. Pp. 292 : 86 Figures; 98 Tables; 5 Appendix Tables. £3. 10s. 0d. *Q. J. R. Meteorol. Soc.* 92, 320–321.  
<https://doi.org/10.1002/qj.49709239230>
- Chandler, T.J., 1962. London's Urban Climate. *Geogr. J.* 128, 279–298.  
<https://doi.org/10.2307/1794042>
- Chang, K., 1962. A Typology of Settlement and Community Patterns in Some Circumpolar Societies. *Arct. Anthropol.* 1, 28–41.
- Changnon, S.A., 1992. Inadvertent Weather Modification in Urban Areas: Lessons for Global Climate Change. *Bull. Am. Meteorol. Soc.* 73, 619–627. [https://doi.org/10.1175/1520-0477\(1992\)073<0619:IWMIUA>2.0.CO;2](https://doi.org/10.1175/1520-0477(1992)073<0619:IWMIUA>2.0.CO;2)
- Changnon, S.A., Kunkel, K.E., Reinke, B.C., 1996. Impacts and Responses to the 1995 Heat Wave: A Call to Action. *Bull. Am. Meteorol. Soc.* 77, 1497–1506. [https://doi.org/10.1175/1520-0477\(1996\)077<1497:IARTTH>2.0.CO;2](https://doi.org/10.1175/1520-0477(1996)077<1497:IARTTH>2.0.CO;2)
- Chapman, L., Bell, S.J., 2018. High-Resolution Monitoring of Weather Impacts on Infrastructure Networks Using the Internet of Things. *Bull. Am. Meteorol. Soc.* 99, 1147–1154.  
<https://doi.org/10.1175/BAMS-D-17-0214.1>
- Chapman, L., Thornes, J.E., 2006. A geomatics-based road surface temperature prediction model. *Sci. Total Environ., Urban Environmental Research in the UK: The Urban Regeneration and the Environment (NERC URGENT) Programme and associated studies.* 360, 68–80.  
<https://doi.org/10.1016/j.scitotenv.2005.08.025>
- Chapman, L., Thornes, J.E., 2004. Real-Time Sky-View Factor Calculation and Approximation: *Journal of Atmospheric and Oceanic Technology: Vol 21, No 5* [WWW Document]. URL <https://journals.ametsoc.org/doi/full/10.1175/1520-0426%282004%29021%3C0730%3ARSFCAA%3E2.0.CO%3B2> (accessed 8.21.19).

- Chapman, L., Thornes, J.E., 2003. The use of geographical information systems in climatology and meteorology. *Prog. Phys. Geogr. Earth Environ.* 27, 313–330.  
<https://doi.org/10.1191/0309133303pp384ra>
- Chen, L., Wang, H.-Y., Wang, T.-S., Kou, C.-H., 2019. Remote Sensing for Detecting Changes of Land Use in Taipei City, Taiwan. *J. Indian Soc. Remote Sens.* 47, 1847–1856.  
<https://doi.org/10.1007/s12524-019-01031-4>
- Chen, Y., 2010. Characterizing Growth and Form of Fractal Cities with Allometric Scaling Exponents [WWW Document]. *Discrete Dyn. Nat. Soc.* <https://doi.org/10.1155/2010/194715>
- Christen, A., Vogt, R., 2004. Energy and radiation balance of a central European city. *Int. J. Climatol.* 24, 1395–1421. <https://doi.org/10.1002/joc.1074>
- Chrysanthou, A., van der Schrier, G., van den Besselaar, E.J.M., Klein Tank, A.M.G., Brandsma, T., 2014. The effects of urbanization on the rise of the European temperature since 1960. *Geophys. Res. Lett.* 41, 7716–7722. <https://doi.org/10.1002/2014GL061154>
- Chudnovsky, A., Ben-Dor, E., Saaroni, H., 2004. Diurnal thermal behavior of selected urban objects using remote sensing measurements. *Energy Build.* 36, 1063–1074.  
<https://doi.org/10.1016/j.enbuild.2004.01.052>
- Cohen, B., 2006. Urbanization in developing countries: Current trends, future projections, and key challenges for sustainability. *Technol. Soc., Sustainable Cities* 28, 63–80.  
<https://doi.org/10.1016/j.techsoc.2005.10.005>
- Cohen, J.E., 2003. Human Population: The Next Half Century. *Science* 302, 1172–1175.  
<https://doi.org/10.1126/science.1088665>
- Cottineau, C., Hatna, E., Arcaute, E., Batty, M., 2017. Diverse cities or the systematic paradox of Urban Scaling Laws. *Comput. Environ. Urban Syst., Spatial analysis with census data: emerging issues and innovative approaches* 63, 80–94.  
<https://doi.org/10.1016/j.compenvurbsys.2016.04.006>
- CPRE, 2018. Campaign to Protect Rural England | 38 Degrees [WWW Document]. URL <https://you.38degrees.org.uk/partnerships/campaign-to-protect-rural-england> (accessed 9.28.19).
- Cui, L., Shi, J., 2012. Urbanization and its environmental effects in Shanghai, China. *Urban Clim.* 2, 1–15. <https://doi.org/10.1016/j.uclim.2012.10.008>
- Daramola, A., Ibem, E.O., 2010. Urban Environmental Problems in Nigeria Implications for Sustainable Development. *J. Sustain. Dev. Afr.* 12, 124–145.
- Davoudi, S., 2014. Climate Change, Securitisation of Nature, and Resilient Urbanism. *Environ. Plan. C Gov. Policy* 32, 360–375. <https://doi.org/10.1068/c12269>
- Davoudi, S., 2012. Climate Risk and Security: New Meanings of “the Environment” in the English Planning System. *Eur. Plan. Stud.* 20, 49–69. <https://doi.org/10.1080/09654313.2011.638491>
- Davoudi, S., Crawford, J., Mehmood, A., 2009. Planning for climate change: strategies for mitigation and adaptation for spatial planners. Earthscan.
- Dawson, R.J., Thompson, D., Johns, D., Wood, R., Darch, G., Chapman, L., Hughes, P.N., Watson, G.V.R., Paulson, K., Bell, S., Gosling, S.N., Powrie, W., Hall, J.W., 2018. A systems framework for national assessment of climate risks to infrastructure. *Philos. Transact. A Math. Phys. Eng. Sci.* 376. <https://doi.org/10.1098/rsta.2017.0298>
- Dissanayake, D., Morimoto, T., Murayama, Y., Ranagalage, M., Handayani, H.H., 2019. Impact of Urban Surface Characteristics and Socio-Economic Variables on the Spatial Variation of Land Surface Temperature in Lagos City, Nigeria. *Sustainability* 11, 25.  
<https://doi.org/10.3390/su11010025>
- Donnay, J.-P., Barnsley, M.J., Longley, P.A., 2014. Remote Sensing and Urban Analysis: GISDATA 9. CRC Press.
- Douglas, I., Alam, K., Maghenda, M., McDonnell, Y., Mclean, L., Campbell, J., 2008. Unjust waters: climate change, flooding and the urban poor in Africa. *Environ. Urban.* 20, 187–205.  
<https://doi.org/10.1177/0956247808089156>

- Duckworth, F.S., Sandberg, J.S., 1954. The Effect of Cities upon Horizontal and Vertical Temperature Gradients. *Bull. Am. Meteorol. Soc.* 35, 198–207.
- Eagleman, J.R., 1974. A comparison of urban climatic modifications in three cities. *Atmospheric Environ.* 1967 8, 1131–1142. [https://doi.org/10.1016/0004-6981\(74\)90047-X](https://doi.org/10.1016/0004-6981(74)90047-X)
- Earthdata, 2017. LP DAAC - Homepage [WWW Document]. URL <https://lpdaac.usgs.gov/> (accessed 10.16.19).
- EDINA, 2018. Digimap [WWW Document]. URL <https://digimap.edina.ac.uk/> (accessed 11.29.19).
- Eliasson, I., 1996. Urban nocturnal temperatures, street geometry and land use. *Atmos. Environ., Conference on the Urban Thermal Environment Studies in Tohwa* 30, 379–392. [https://doi.org/10.1016/1352-2310\(95\)00033-X](https://doi.org/10.1016/1352-2310(95)00033-X)
- Ellis, C., 2014. History Of Cities And City Planning [WWW Document]. URL <http://www.art.net/~hopkins/Don/simcity/manual/history.html> (accessed 3.26.20).
- Eludoyin, O.M., Adelekan, I.O., Webster, R., Eludoyin, A.O., 2014. Air temperature, relative humidity, climate regionalization and thermal comfort of Nigeria. *Int. J. Climatol.* 34, 2000–2018. <https://doi.org/10.1002/joc.3817>
- Emilsson, T., Ode Sang, Å., 2017. Impacts of Climate Change on Urban Areas and Nature-Based Solutions for Adaptation, in: Kabisch, N., Korn, H., Stadler, J., Bonn, A. (Eds.), *Nature-Based Solutions to Climate Change Adaptation in Urban Areas: Linkages between Science, Policy and Practice, Theory and Practice of Urban Sustainability Transitions*. Springer International Publishing, Cham, pp. 15–27. [https://doi.org/10.1007/978-3-319-56091-5\\_2](https://doi.org/10.1007/978-3-319-56091-5_2)
- Emmanuel, R., Krüger, E., 2012. Urban heat island and its impact on climate change resilience in a shrinking city: The case of Glasgow, UK. <https://doi.org/10.1016/J.BUILDENV.2012.01.020>
- Endsjö, P.-C., 1973. Urbanization in Nigeria. *Nor. Geogr. Tidsskr. - Nor. J. Geogr.* 27, 207–219. <https://doi.org/10.1080/00291957308551958>
- Enquist, B.J., Brown, J.H., West, G.B., 1998. Allometric scaling of plant energetics and population density. *Nature* 395, 163–165. <https://doi.org/10.1038/25977>
- Equere, V., Mirzaei, P.A., Riffat, S., 2020. Definition of a new morphological parameter to improve prediction of urban heat island. *Sustain. Cities Soc.* 56, 102021. <https://doi.org/10.1016/j.scs.2020.102021>
- Fan, F., Wang, Y., Qiu, M., Wang, Z., 2009. Evaluating the Temporal and Spatial Urban Expansion Patterns of Guangzhou from 1979 to 2003 by Remote Sensing and GIS Methods. *Int. J. Geogr. Inf. Sci.* 23, 1371–1388. <https://doi.org/10.1080/13658810802443432>
- Fichera, C.R., Modica, G., Pollino, M., 2012. Land Cover classification and change-detection analysis using multi-temporal remote sensed imagery and landscape metrics. *Eur. J. Remote Sens.* 45, 1–18. <https://doi.org/10.5721/EuJRS20124501>
- Fluschnik, T., Kriewald, S., García Cantú Ros, A., Zhou, B., Reusser, D.E., Kropp, J.P., Rybski, D., 2016. The Size Distribution, Scaling Properties and Spatial Organization of Urban Clusters: A Global and Regional Percolation Perspective. *ISPRS Int. J. Geo-Inf.* 5, 110. <https://doi.org/10.3390/ijgi5070110>
- Friedl, M.A., Mclver, D.K., Hodges, J.C.F., Zhang, X.Y., Muchoney, D., Strahler, A.H., Woodcock, C.E., Gopal, S., Schneider, A., Cooper, A., Baccini, A., Gao, F., Schaaf, C., 2002. Global land cover mapping from MODIS: algorithms and early results. *Remote Sens. Environ., The Moderate Resolution Imaging Spectroradiometer (MODIS): a new generation of Land Surface Monitoring* 83, 287–302. [https://doi.org/10.1016/S0034-4257\(02\)00078-0](https://doi.org/10.1016/S0034-4257(02)00078-0)
- Friedman, G.M., 1962. On Sorting, Sorting Coefficients, and the Lognormality of the Grain-Size Distribution of Sandstones. *J. Geol.* 70, 737–753. <https://doi.org/10.1086/jg.70.6.30066373>
- Frost, J., 2018. Measures of Variability: Range, Interquartile Range, Variance, and Standard Deviation. *Stat. Jim.* URL <http://statisticsbyjim.com/basics/variability-range-interquartile-variance-standard-deviation/> (accessed 2.11.20).



- Frumkin, H., 2002. Urban Sprawl and Public Health [WWW Document]. ResearchGate. URL [https://www.researchgate.net/publication/11035517\\_Urban\\_Sprawl\\_and\\_Public\\_Health](https://www.researchgate.net/publication/11035517_Urban_Sprawl_and_Public_Health) (accessed 3.8.20).
- Fujii, H., Iwata, K., Managi, S., 2017. How do urban characteristics affect climate change mitigation policies? *J. Clean. Prod.* 168, 271–278. <https://doi.org/10.1016/j.jclepro.2017.08.221>
- Gandrud, C., 2013. Reproducible Research with R and R Studio. CRC Press.
- Gedzelman, S.D., Austin, S., Cermak, R., Stefano, N., Partridge, S., Quesenberry, S., Robinson, D.A., 2003. Mesoscale aspects of the Urban Heat Island around New York City. *Theor. Appl. Climatol.* 75, 29–42. <https://doi.org/10.1007/s00704-002-0724-2>
- Goist, P.D., 1974. Patrick Geddes and the City. *J. Am. Inst. Plann.* 40, 31–37. <https://doi.org/10.1080/01944367408977444>
- Golden, J.S., 2004. The Built Environment Induced Urban Heat Island Effect in Rapidly Urbanizing Arid Regions – A Sustainable Urban Engineering Complexity. *Environ. Sci.* 1, 321–349. <https://doi.org/10.1080/15693430412331291698>
- Goldstein, G., 1990. Urbanization, Health and Well-Being: A Global Perspective. *J. R. Stat. Soc. Ser. Stat.* 39, 121–133. <https://doi.org/10.2307/2348533>
- Gould, S.J., 1966. Allometry and Size in Ontogeny and Phylogeny. *Biol. Rev.* 41, 587–638. <https://doi.org/10.1111/j.1469-185X.1966.tb01624.x>
- Griend, A.A.V.D., Owe, M., 1993. On the relationship between thermal emissivity and the normalized difference vegetation index for natural surfaces. *Int. J. Remote Sens.* 14, 1119–1131. <https://doi.org/10.1080/01431169308904400>
- Grimmond, C.S.B., Roth, M., Oke, T.R., 2010. Climate and More Sustainable Cities: Climate Information for Improved Planning and Management of Cities (Producers/Capabilities Perspective) - ScienceDirect [WWW Document]. URL <https://www.sciencedirect.com/science/article/pii/S1878029610000174> (accessed 1.4.20).
- Grimmond, S., 2007. Urbanization and global environmental change: local effects of urban warming. *Geogr. J.* 173, 83–88. [https://doi.org/10.1111/j.1475-4959.2007.232\\_3.x](https://doi.org/10.1111/j.1475-4959.2007.232_3.x)
- Guo, H., Xu, M., Hu, Q., 2011. Changes in near-surface wind speed in China: 1969–2005. *Int. J. Climatol.* 31, 349–358. <https://doi.org/10.1002/joc.2091>
- Han, J.-Y., Baik, J.-J., Lee, H., 2013. Urban impacts on precipitation. *Asia-Pac. J. Atmospheric Sci.* 50. <https://doi.org/10.1007/s13143-014-0016-7>
- Haregeweyn, N., Tesfaye, S., Tsunekawa, A., Tsubo, M., Meshesha, D.T., Adgo, E., Elias, A., 2014. Dynamics of land use and land cover and its effects on hydrologic responses: case study of the Gilgel Tekeze catchment in the highlands of Northern Ethiopia. *Environ. Monit. Assess.* 187, 4090. <https://doi.org/10.1007/s10661-014-4090-1>
- Hartz, D.A., Prashad, L., Hedquist, B.C., Golden, J., Brazel, A.J., 2006. Linking satellite images and hand-held infrared thermography to observed neighborhood climate conditions. *Remote Sens. Environ., Thermal Remote Sensing of Urban Areas* 104, 190–200. <https://doi.org/10.1016/j.rse.2005.12.019>
- Hasegawa, J., 2013. The attitudes of the Ministry of Town and Country Planning towards blitzed cities in 1940s Britain. *Plan. Perspect.* 28, 271–289. <https://doi.org/10.1080/02665433.2013.737712>
- Heaviside, C., Cai, X.-M., Vardoulakis, S., 2015. The effects of horizontal advection on the urban heat island in Birmingham and the West Midlands, United Kingdom during a heatwave. *Q. J. R. Meteorol. Soc.* 141, 1429–1441. <https://doi.org/10.1002/qj.2452>
- Heaviside, C., Vardoulakis, S., Cai, X.-M., 2016. Attribution of mortality to the urban heat island during heatwaves in the West Midlands, UK. *Environ. Health* 15. <https://doi.org/10.1186/s12940-016-0100-9>
- Hendrickson, T.P., Nikolic, M., Rakas, J., 2016. Selecting climate change mitigation strategies in urban areas through life cycle perspectives. *J. Clean. Prod.* 135, 1129–1137. <https://doi.org/10.1016/j.jclepro.2016.06.075>

- Herold, M., Goldstein, N.C., Clarke, K.C., 2003. The spatiotemporal form of urban growth : measurement , analysis and modeling [WWW Document]. URL /paper/The-spatiotemporal-form-of-urban-growth-%3A-%2C-and-Herold-Goldstein/c814f8dd54d6cf89874753ca662c5e244198c284 (accessed 8.20.18).
- Hillier, W.R.G., Hanson, J., Peponis, J., 1987. Syntactic Analysis of Settlements. *Archit. Comport. Behav.* 3, 217–231.
- Ho, J.C., Ren, C., Ng, E., 2015. A review of studies on the relationship between urban morphology and urban climate towards better urban planning and design in (sub)tropical regions 6.
- Hollow, M., 2012. Utopian urges: visions for reconstruction in Britain, 1940–1950'. *Plan. Perspect.* 27, 569–585. <https://doi.org/10.1080/02665433.2012.705126>
- Hondula, D.M., Balling, R.C., Vanos, J.K., Georgescu, M., 2015. Rising Temperatures, Human Health, and the Role of Adaptation. *Curr. Clim. Change Rep.* 1, 144–154. <https://doi.org/10.1007/s40641-015-0016-4>
- Hoornweg, D., Lorraine Sugar, Claudia Lorena Trejos Gómez, 2011. Cities and greenhouse gas emissions: moving forward. *Environ. Urban.* 23, 207–227. <https://doi.org/10.1177/0956247810392270>
- Hopkins, M.I.W., 2012. The ecological significance of urban fringe belts [WWW Document]. ResearchGate. URL [https://www.researchgate.net/publication/279625709\\_The\\_ecological\\_significance\\_of\\_urban\\_fringe\\_belts](https://www.researchgate.net/publication/279625709_The_ecological_significance_of_urban_fringe_belts) (accessed 7.7.20).
- Horton, N.J., Kleinman, K., 2015. Using R and RStudio for Data Management, Statistical Analysis, and Graphics. CRC Press.
- Howard, L., 1833. The Climate of London 285.
- Howard, L., 1818. The Climate of London 285.
- Huang, L., Li, J., Zhao, D., Zhu, J., 2008. A fieldwork study on the diurnal changes of urban microclimate in four types of ground cover and urban heat island of Nanjing, China. *Build. Environ.* 43, 7–17. <https://doi.org/10.1016/j.buildenv.2006.11.025>
- Ibrahim, A.A., Nduka, I.C., Iguisi, E.O., Ati, O.F., 2011. An Assesment of the Impact of Sky View Factor (SVF) on the Micro-climate of Urban Kano. [WWW Document]. ResearchGate. URL [https://www.researchgate.net/publication/266025961\\_An\\_Assesment\\_of\\_the\\_Impact\\_of\\_Sky\\_View\\_Factor\\_SVF\\_on\\_the\\_Micro-climate\\_of\\_Urban\\_Kano](https://www.researchgate.net/publication/266025961_An_Assesment_of_the_Impact_of_Sky_View_Factor_SVF_on_the_Micro-climate_of_Urban_Kano) (accessed 8.8.19).
- Ichinose, T., Shimodozono, K., Hanaki, K., 1999. Impact of anthropogenic heat on urban climate in Tokyo. *Atmos. Environ.* 33, 3897–3909. [https://doi.org/10.1016/S1352-2310\(99\)00132-6](https://doi.org/10.1016/S1352-2310(99)00132-6)
- Imhoff, M.L., Zhang, P., Wolfe, R.E., Bounoua, L., 2010. Remote sensing of the urban heat island effect across biomes in the continental USA. *Remote Sens. Environ.* 114, 504–513. <https://doi.org/10.1016/j.rse.2009.10.008>
- Inikori, J.E., 2002. A Historiography of the First Industrial Revolution [WWW Document]. *Afr. Ind. Revolut. Engl. Study Int. Trade Econ. Dev.* <https://doi.org/10.1017/CBO9780511583940.004>
- IPCC, 2014. AR5 Climate Change 2014: Impacts, Adaptation, and Vulnerability — IPCC. URL <https://www.ipcc.ch/report/ar5/wg2/> (accessed 3.4.20).
- Jabareen, Y.R., 2006. Sustainable Urban Forms: Their Typologies, Models, and Concepts. *J. Plan. Educ. Res.* 26, 38–52. <https://doi.org/10.1177/0739456X05285119>
- Jackson, T.L., Feddema, J.J., Oleson, K.W., Bonan, G.B., Bauer, J.T., 2010. Parameterization of Urban Characteristics for Global Climate Modeling. *Ann. Assoc. Am. Geogr.* 100, 848–865. <https://doi.org/10.1080/00045608.2010.497328>
- Jacobs, J., 1962. Defends Urbanism in 1960s New York City Planning | WNYC | New York Public Radio, Podcasts, Live Streaming Radio, News [WWW Document]. WNYC. URL <https://www.wnyc.org/story/192689-jane-jacobs/> (accessed 1.14.20).
- Jones, A.R., 1975. Density-size Rule, a further Note. *Urban Stud.* 12, 225–228.
- Juju films, 2018. juju films - Google Search [WWW Document]. URL [https://www.google.com/search?q=juju+films&rlz=1C1CHBF\\_enGB909GB909&sxsrf=ALeKk0](https://www.google.com/search?q=juju+films&rlz=1C1CHBF_enGB909GB909&sxsrf=ALeKk0)

- 2TLQWM8r0rGBb2BzJjOC0srwsiqg:1595607195164&source=lnms&tbn=isch&sa=X&ved=2ahUKEwjksaApObqAhVTsSAKHxhNCU0Q\_AUoAnoECA8QBA&biw=1280&bih=610 (accessed 7.24.20).
- Justice, C.O., Townshend, J.R.G., Vermote, E.F., Masuoka, E., Wolfe, R.E., Saleous, N., Roy, D.P., Morisette, J.T., 2002. An overview of MODIS Land data processing and product status. *Remote Sens. Environ.*, The Moderate Resolution Imaging Spectroradiometer (MODIS): a new generation of Land Surface Monitoring 83, 3–15. [https://doi.org/10.1016/S0034-4257\(02\)00084-6](https://doi.org/10.1016/S0034-4257(02)00084-6)
- Kafi, K.M., Shafri, H.Z.M., Shariff, A.B.M., 2014. An analysis of LULC change detection using remotely sensed data\$\\mathsemicolon\$ A Case study of Bauchi City. *IOP Conf. Ser. Earth Environ. Sci.* 20, 012056. <https://doi.org/10.1088/1755-1315/20/1/012056>
- Karl, T.R., Diaz, H.F., Kukla, G., 1988. Urbanization: Its Detection and Effect in the United States Climate Record. *J. Clim.* 1, 1099–1123. [https://doi.org/10.1175/1520-0442\(1988\)001<1099:UIDAEI>2.0.CO;2](https://doi.org/10.1175/1520-0442(1988)001<1099:UIDAEI>2.0.CO;2)
- Karp, M., 2013. A Very Old Book: The Case for Eric Hobsbawm’s Age of Revolution. *The Junto*. URL <https://earlyamericanists.com/2013/02/07/a-very-old-book-the-case-for-eric-hobsbawms-age-of-revolution/> (accessed 12.29.18).
- Kennedy, J., Dunn, R., McCarthy, M., Titchner, H., Morice, C., 2017. Global and regional climate in 2016. *Weather* 72, 219–225. <https://doi.org/10.1002/wea.3042>
- Kotharkar, R., Bagade, A., 2018. Evaluating urban heat island in the critical local climate zones of an Indian city. *Landsc. Urban Plan.* 169, 92–104. <https://doi.org/10.1016/j.landurbplan.2017.08.009>
- Krayenhoff, E.S., Moustauoui, M., Broadbent, A.M., Gupta, V., Georgescu, M., 2018. Diurnal interaction between urban expansion, climate change and adaptation in US cities. *Nat. Clim. Change* 8, 1097. <https://doi.org/10.1038/s41558-018-0320-9>
- LaBarbera, M., 1989. Analyzing Body Size as a Factor in Ecology and Evolution. *Annu. Rev. Ecol. Syst.* 20, 97–117. <https://doi.org/10.1146/annurev.es.20.110189.000525>
- Landsberg, H.E., 1981. *The Urban Climate*. Academic Press.
- Lee, D.O., 1984. Urban climates. *Prog. Phys. Geogr. Earth Environ.* 8, 1–31. <https://doi.org/10.1177/030913338400800101>
- Lee, D.O., 1977. Urban Influence on Wind Directions Over London. *Weather* 32, 162–170. <https://doi.org/10.1002/j.1477-8696.1977.tb04544.x>
- Lee, H.-Y., 1993. An application of NOAA AVHRR thermal data to the study of urban heat islands. *Atmospheric Environ. Part B Urban Atmosphere* 27, 1–13. [https://doi.org/10.1016/0957-1272\(93\)90041-4](https://doi.org/10.1016/0957-1272(93)90041-4)
- Lee, Y., 1989. An Allometric Analysis of the US Urban System: 1960 – 80. *Environ. Plan. Econ. Space* 21, 463–476. <https://doi.org/10.1068/a210463>
- Lehoczky, A., Sobrino, J.A., Skoković, D., Aguilar, E., 2017. The Urban Heat Island Effect in the City of Valencia: A Case Study for Hot Summer Days. *Urban Sci.* 1, 9. <https://doi.org/10.3390/urbansci1010009>
- Lemmen, D.S., Warren, F.J., 2004. Climate change impacts and adaptation: a Canadian perspective.
- Li, D., Liao, W., Rigden, A.J., Liu, X., Wang, D., Malyshev, S., Shevliakova, E., 2019. Urban heat island: Aerodynamics or imperviousness? *Sci. Adv.* 5, eaau4299. <https://doi.org/10.1126/sciadv.aau4299>
- Li, M., Shi, J., Guo, J., Cao, J., Niu, J., Xiong, M., 2015. Climate Impacts on Extreme Energy Consumption of Different Types of Buildings. *PLOS ONE* 10, e0124413. <https://doi.org/10.1371/journal.pone.0124413>
- Lillesand, T., Kiefer, R.W., Chipman, J., 2015. *Remote Sensing and Image Interpretation*. John Wiley & Sons.

- Longley, P., Batty, M., Shepherd, J., Sadler, G., 1992. Do Green Belts Change the Shape of Urban Areas? A Preliminary Analysis of the Settlement Geography of South East England. *Reg. Stud.* 26, 437–452. <https://doi.org/10.1080/00343409212331347101>
- Longley, P.A., Batty, M., Shepherd, J., 1991. The Size, Shape and Dimension of Urban Settlements. *Trans. Inst. Br. Geogr.* 16, 75–94. <https://doi.org/10.2307/622907>
- Lu, Y., Wang, H., Wang, Q., Zhang, Y., Yu, Y., Qian, Y., 2017. Global anthropogenic heat emissions from energy consumption, 1965–2100. *Clim. Change* 145, 459–468. <https://doi.org/10.1007/s10584-017-2092-z>
- Ludwig, F., Scheltinga, C.T.H.M.T.V., Verhagen, J., Kruijt, B., Ierland, E.C. van, Dellink, R.B., Bruin, K. de, Bruin, K.C. de, Kabat, P., 2007. Climate change impacts on Developing Countries - EU Accountability (No. PE 393.511). European Parliament, Brussels.
- Mabogunje, A.L., 1992. New initiatives in urban planning and management in Nigeria. *Habitat Int.*, Special Issue Urban Development Over Three Decades: Practitioners' Perspective on Policy, Planning and Management, 1960–1990 16, 73–88. [https://doi.org/10.1016/0197-3975\(92\)90038-Z](https://doi.org/10.1016/0197-3975(92)90038-Z)
- Mabogunje, A.L., 1990. Urban Planning and the Post-Colonial State in Africa: A Research Overview. *Afr. Stud. Rev.* 33, 121–203. <https://doi.org/10.2307/524471>
- MacKenzie, A.R., Whyatt, J.D., Barnes, M.J., Davies, G., Hewitt, C.N., 2019. Urban form strongly mediates the allometric scaling of airshed pollution concentrations. *Environ. Res. Lett.* 14, 124078. <https://doi.org/10.1088/1748-9326/ab50e3>
- MacKenzie, R., Barnes, M., Whyatt, D., Hewitt, N., 2019. Allometric scaling of UK urban emissions: interpretation and implications for air quality management. Presented at the EGU General Assembly Conference Abstracts, pp. EPSC2016-8112.
- Mackey, C.W., Lee, X., Smith, R.B., 2012. Remotely sensing the cooling effects of city scale efforts to reduce urban heat island. *Build. Environ.* 49, 348–358. <https://doi.org/10.1016/j.buildenv.2011.08.004>
- Manoli, G., Fatichi, S., Schlöpfer, M., Yu, K., Crowther, T.W., Meili, N., Burlando, P., Katul, G., Zeid, E.B., 2020. Reply to Martilli et al. (2020): Summer average urban-rural surface temperature differences do not indicate the need for urban heat reduction (preprint). *Open Science Framework*. <https://doi.org/10.31219/osf.io/mwpna>
- Manoli, G., Fatichi, S., Schlöpfer, M., Yu, K., Crowther, T.W., Meili, N., Burlando, P., Katul, G.G., Bou-Zeid, E., 2019. Magnitude of urban heat islands largely explained by climate and population. *Nature* 573, 55–60. <https://doi.org/10.1038/s41586-019-1512-9>
- Mao, K., Yuan, Z., Zuo, Z., Xu, T., Shen, X., Gao, C., 2019. Changes in Global Cloud Cover Based on Remote Sensing Data from 2003 to 2012. *Chin. Geogr. Sci.* 29, 306–315. <https://doi.org/10.1007/s11769-019-1030-6>
- Martilli, A., Roth, M., Chow, W.T.L., Demuzere, M., Lipson, M., Krayenhoff, E.S., Sailor, D., Nazarian, N., Voogt, J., Wouters, H., Middel, A., Stewart, I.D., Bechtel, B., Christen, A., Hart, M.A., 2020. Summer average urban-rural surface temperature differences do not indicate the need for urban heat reduction (preprint). *Open Science Framework*. <https://doi.org/10.31219/osf.io/8gnbf>
- Martins, P.B., 2000. Urbanizing World [WWW Document]. URL <http://www.prb.org/Publications/Reports/2000/AnUrbanizingWorldPDF619KB.aspx> (accessed 11.26.17).
- Massion, K., 2017. What Is an Urban Settlement? [WWW Document]. Bizfluent. URL <https://bizfluent.com/info-7890851-urban-settlement.html> (accessed 7.4.18).
- McCarthy, M.P., Best, M.J., Betts, R.A., 2010. Climate change in cities due to global warming and urban effects. *Geophys. Res. Lett.* 37. <https://doi.org/10.1029/2010GL042845>
- McCoy, D.T., Eastman, R., Hartmann, D.L., Wood, R., 2017. The Change in Low Cloud Cover in a Warmed Climate Inferred from AIRS, MODIS, and ERA-Interim. *J. Clim.* 30, 3609–3620. <https://doi.org/10.1175/JCLI-D-15-0734.1>

- McGranahan, G., Satterthwaite, D., 2003. Urban Centers: An Assessment of Sustainability. *Annu. Rev. Environ. Resour.* 28, 243–274.  
<https://doi.org/10.1146/annurev.energy.28.050302.105541>
- Memon, R.A., Leung, D.Y.C., Chunho, L., 2008. A review on the generation, determination and mitigation of urban heat island. *J. Environ. Sci. China* 20, 120–128.  
[https://doi.org/10.1016/s1001-0742\(08\)60019-4](https://doi.org/10.1016/s1001-0742(08)60019-4)
- Met Office, 2020. Weather and climate change [WWW Document]. Met Off. URL <https://www.metoffice.gov.uk/> (accessed 6.29.20).
- Middel, A., Krayerhoff, E.S., 2019. Micrometeorological determinants of pedestrian thermal exposure during record-breaking heat in Tempe, Arizona: Introducing the MaRTy observational platform. *Sci. Total Environ.* 687, 137–151.  
<https://doi.org/10.1016/j.scitotenv.2019.06.085>
- Miller, J.D., Hutchins, M., 2017. The impacts of urbanisation and climate change on urban flooding and urban water quality: A review of the evidence concerning the United Kingdom. *J. Hydrol. Reg. Stud.* 12, 345–362. <https://doi.org/10.1016/j.ejrh.2017.06.006>
- Mills, G., 2007. Cities as agents of global change. *Int. J. Climatol.* 27, 1849–1857.  
<https://doi.org/10.1002/joc.1604>
- Mishra, A.K., 2019. Investigating changes in cloud cover using the long-term record of precipitation extremes. *Meteorol. Appl.* 26, 108–116. <https://doi.org/10.1002/met.1745>
- Mohan, M., Kikegawa, Y., Gurjar, B.R., Bhati, S., Kolli, N.R., 2013. Assessment of urban heat island effect for different land use–land cover from micrometeorological measurements and remote sensing data for megacity Delhi | SpringerLink [WWW Document]. URL <https://link.springer.com/article/10.1007/s00704-012-0758-z> (accessed 7.26.19).
- Morisette, J.T., Privette, J.L., Justice, C.O., 2002. A framework for the validation of MODIS Land products. *Remote Sens. Environ., The Moderate Resolution Imaging Spectroradiometer (MODIS): a new generation of Land Surface Monitoring* 83, 77–96.  
[https://doi.org/10.1016/S0034-4257\(02\)00088-3](https://doi.org/10.1016/S0034-4257(02)00088-3)
- Morris, A.E.J., 1974. History of Urban Form by A E J Morris - AbeBooks [WWW Document]. URL <https://www.abebooks.co.uk/book-search/title/history-of-urban-form/author/a-e-j-morris/> (accessed 7.6.20).
- Mundia, C.N., Aniya, M., 2005. Analysis of land use/cover changes and urban expansion of Nairobi city using remote sensing and GIS. *Int. J. Remote Sens.* 26, 2831–2849.  
<https://doi.org/10.1080/01431160500117865>
- Murray, V., Ebi, K.L., 2012. IPCC Special Report on Managing the Risks of Extreme Events and Disasters to Advance Climate Change Adaptation (SREX). *J. Epidemiol Community Health* 66, 759–760. <https://doi.org/10.1136/jech-2012-201045>
- Mushore, T.D., Dube, T., Manjowe, M., Gumindoga, W., Chemura, A., Rousta, I., Odindi, J., Mutanga, O., 2019. Remotely sensed retrieval of Local Climate Zones and their linkages to land surface temperature in Harare metropolitan city, Zimbabwe. *Urban Clim.* 27, 259–271.  
<https://doi.org/10.1016/j.uclim.2018.12.006>
- MyGuide, 2017. Nigeria Travel Guide [WWW Document]. My Guide Niger. URL <https://www.myguidenigeria.com/> (accessed 7.24.20).
- Nairaland, 2018. Nairaland Forum [WWW Document]. URL <https://www.nairaland.com/> (accessed 7.24.20).
- Naroll, R.S., Bertalanffy, L. von, 1956. The principle of allometry in biology and the social sciences. *Gen. Syst. Yearb.*
- Nduka, I.C., Abdulhamed, A.I., 2011. Classifying Urban Climate Field Sites by “Thermal Climate Zones” the Case of Onitsha Metropolis [WWW Document]. ResearchGate. URL [https://www.researchgate.net/publication/267549851\\_Classifying\\_Urban\\_Climate\\_Field\\_Sites\\_by\\_Thermal\\_Climate\\_Zones\\_the\\_Case\\_of\\_Onitsha\\_Metropolis](https://www.researchgate.net/publication/267549851_Classifying_Urban_Climate_Field_Sites_by_Thermal_Climate_Zones_the_Case_of_Onitsha_Metropolis) (accessed 8.8.19).

- Neteler, M., 2010. Estimating Daily Land Surface Temperatures in Mountainous Environments by Reconstructed MODIS LST Data. *Remote Sens.* 2, 333–351.  
<https://doi.org/10.3390/rs1020333>
- Neuman, M., Smith, S., 2010. City Planning and Infrastructure: Once and Future Partners. *J. Plan. Hist.* 9, 21–42. <https://doi.org/10.1177/1538513209355373>
- Newman, P., Kenworthy, J., 1999. *Sustainability and Cities: Overcoming Automobile Dependence.* Island Press.
- Ng, E., Yuan, C., Chen, L., Ren, C., Fung, J.C.H., 2011. Improving the wind environment in high-density cities by understanding urban morphology and surface roughness: A study in Hong Kong. *Landsc. Urban Plan.* 101, 59–74. <https://doi.org/10.1016/j.landurbplan.2011.01.004>
- Nichol, J., Wong, M.S., 2005. Modeling urban environmental quality in a tropical city. *Landsc. Urban Plan.* 73, 49–58. <https://doi.org/10.1016/j.landurbplan.2004.08.004>
- Nordbeck, S., 1971. Urban Allometric Growth. *Geogr. Ann. Ser. B Hum. Geogr.* 53, 54–67.  
<https://doi.org/10.2307/490887>
- NPCN, 2018. National Population Commission of Nigeria | GHDx [WWW Document]. URL <http://ghdx.healthdata.org/organizations/national-population-commission-nigeria> (accessed 7.11.19).
- Nunez, M., Oke, T.R., 1977. The Energy Balance of an Urban Canyon. *J. Appl. Meteorol.* 16, 11–19.  
[https://doi.org/10.1175/1520-0450\(1977\)016<0011:TEBOAU>2.0.CO;2](https://doi.org/10.1175/1520-0450(1977)016<0011:TEBOAU>2.0.CO;2)
- OECD, 2014. OECD and Bloomberg Philanthropies: Cities and Climate... - Google Scholar [WWW Document]. URL [https://scholar.google.com/scholar\\_lookup?title=Cities%20and%20Climate%20Change%3A%20National%20Governments%20Enabling%20Local%20Action&publication\\_year=2014&author=OECD](https://scholar.google.com/scholar_lookup?title=Cities%20and%20Climate%20Change%3A%20National%20Governments%20Enabling%20Local%20Action&publication_year=2014&author=OECD) (accessed 4.27.19).
- Ofem, B., 2012. A Review of the Criteria for Defining Urban Areas in Nigeria.  
<https://doi.org/10.1080/09709274.2012.11906461>
- Office for National Statistics, 2017. Population estimates - Office for National Statistics [WWW Document]. URL <https://www.ons.gov.uk/peoplepopulationandcommunity/populationandmigration/populationestimates> (accessed 12.9.17).
- Ogunjobi, K.O., Oluleye, A., Ajayi, V.O., 2012. A long-term record of aerosol index from TOMS observations and horizontal visibility in sub-Saharan West Africa. *Int. J. Remote Sens.* 33, 6076–6093. <https://doi.org/10.1080/01431161.2012.676689>
- Ojeh, V.N., Balogun, A.A., Okhimamhe, A.A., 2016. Urban-Rural Temperature Differences in Lagos. *Climate* 4, 29. <https://doi.org/10.3390/cli4020029>
- Oke, T.R., 2006. *Instrument and Observing Methods Report No. 81* 51.
- Oke, T.R., 2002. *Boundary Layer Climates.* Routledge.
- Oke, T. R., 1995. The Heat Island of the Urban Boundary Layer: Characteristics, Causes and Effects, in: *Wind Climate in Cities, NATO ASI Series.* Springer, Dordrecht, pp. 81–107.  
[https://doi.org/10.1007/978-94-017-3686-2\\_5](https://doi.org/10.1007/978-94-017-3686-2_5)
- Oke, T.R., 1995. Classics in physical geography revisited: Sundborg, Å. 1951: Climatological studies in Uppsala with special regard to the temperature conditions in the urban area. *Geographica* 22. *Prog. Phys. Geogr. Earth Environ.* 19, 107–113.  
<https://doi.org/10.1177/030913339501900105>
- Oke, T.R., 1982. The energetic basis of the urban heat island. *Q. J. R. Meteorol. Soc.* 108, 1–24.  
<https://doi.org/10.1002/qj.49710845502>
- Oke, T.R., 1981. Canyon geometry and the nocturnal urban heat island: Comparison of scale model and field observations. *J. Climatol.* 1, 237–254. <https://doi.org/10.1002/joc.3370010304>
- Oke, T.R., 1973. City size and the urban heat island. *Atmospheric Environ.* 1967 7, 769–779.  
[https://doi.org/10.1016/0004-6981\(73\)90140-6](https://doi.org/10.1016/0004-6981(73)90140-6)

- Oke, T.R., 1970. The temperature profile near the ground on calm clear nights. *Q. J. R. Meteorol. Soc.* 96, 14–23. <https://doi.org/10.1002/qj.49709640703>
- Oke, T.R., Maxwell, G.B., 1975. Urban heat island dynamics in Montreal and Vancouver. *Atmospheric Environ.* 1967 9, 191–200. [https://doi.org/10.1016/0004-6981\(75\)90067-0](https://doi.org/10.1016/0004-6981(75)90067-0)
- Oliveira, V., 2016. *Urban Morphology: An Introduction to the Study of the Physical Form of Cities*. Springer.
- Oloyede, M.A., Akinbode, A., 2010. Towards Effective Physical Planning in Local Governments in Nigeria | Michael Oloyede Al [WWW Document]. ResearchGate. URL [https://www.researchgate.net/publication/250303778\\_Towards\\_Effective\\_Physical\\_Planning\\_in\\_Local\\_Governments\\_in\\_Nigeria](https://www.researchgate.net/publication/250303778_Towards_Effective_Physical_Planning_in_Local_Governments_in_Nigeria) (accessed 7.19.19).
- Omofonmwan, S.I., Osa-Edoh, G.I., 2008. The Challenges of Environmental Problems in Nigeria. *J. Hum. Ecol.* 23, 53–57. <https://doi.org/10.1080/09709274.2008.11906054>
- Omole, F.K., Akinbamijo, O.B., 2012. Land Development and Planning Laws in Nigeria: The Historical Account. *J. Law Policy Glob.* 8, 25–31–31.
- Os, B., Aa, A., 2016. Change Detection in Land Surface Temperature and Land Use Land Cover over Lagos Metropolis, Nigeria. *J. Remote Sens. GIS* 5, 1–7. <https://doi.org/10.4172/2469-4134.1000171>
- Qşqba, S.O., 1969. THE PHENOMENON OF LABOUR MIGRATION IN THE ERA OF BRITISH COLONIAL RULE: A NEGLECTED ASPECT OF NIGERIA'S SOCIAL HISTORY. *J. Hist. Soc. Niger.* 4, 515–538.
- Ouahabi, M.H., Benabdelouahab, F., Khamlichi, A., 2017. Analyzing wind speed data and wind power density of Tetouan city in Morocco by adjustment to Weibull and Rayleigh distribution functions. *Wind Eng.* 41, 174–184. <https://doi.org/10.1177/0309524X17709908>
- Pal, S., Ziaul, Sk., 2017. Detection of land use and land cover change and land surface temperature in English Bazar urban centre. *Egypt. J. Remote Sens. Space Sci.* 20, 125–145. <https://doi.org/10.1016/j.ejrs.2016.11.003>
- Palumbo, A., Mazzarella, A., 1980. Rainfall Statistical Properties in Naples. *Mon. Weather Rev.* 108, 1041–1045. [https://doi.org/10.1175/1520-0493\(1980\)108<1041:RSPIN>2.0.CO;2](https://doi.org/10.1175/1520-0493(1980)108<1041:RSPIN>2.0.CO;2)
- Pasquini, L., 2019. The urban governance of climate change adaptation in least-developed African countries and in small cities: the engagement of local decision-makers in Dar es Salaam, Tanzania, and Karonga, Malawi. *Clim. Dev.* 0, 1–12. <https://doi.org/10.1080/17565529.2019.1632166>
- Patz, J.A., Campbell-Lendrum, D., Holloway, T., Foley, J.A., 2005. Impact of regional climate change on human health. *Nature* 438, 310–317. <https://doi.org/10.1038/nature04188>
- Payton, N.I., 1995. The machine in the garden city: Patrick Geddes' plan for Tel Aviv. *Plan. Perspect.* 10, 359–381. <https://doi.org/10.1080/02665439508725829>
- Peng, S., Piao, S., Ciais, P., Friedlingstein, P., Ottle, C., Bréon, F.-M., Nan, H., Zhou, L., Myneni, R.B., 2012. Surface Urban Heat Island Across 419 Global Big Cities. *Environ. Sci. Technol.* 46, 696–703. <https://doi.org/10.1021/es2030438>
- Peterson, T.C., 2003. Assessment of Urban Versus Rural In Situ Surface Temperatures in the Contiguous United States: No Difference Found. *J. Clim.* 16, 2941–2959. [https://doi.org/10.1175/1520-0442\(2003\)016<2941:AOUVRI>2.0.CO;2](https://doi.org/10.1175/1520-0442(2003)016<2941:AOUVRI>2.0.CO;2)
- Piault, M.-H., 1963. Family and Social Change in an African City. *Homme* 3, 121–124.
- Pielke, R.A., 2013. *Mesoscale Meteorological Modeling: Chapter 13. Examples of Mesoscale Models*. Elsevier Inc. Chapters.
- Puseerit, J., Beringer, A.L., Inmuong, Y., Kaomuangnoi, K., 2019. Understanding Urban Vulnerabilities to Climate Change Impacts in Khon Kaen and Mukdahan in Thailand. *Community Univ. Engagem. J.* 1, 1–13.
- Qihao, W., 2012. *An Introduction to Contemporary Remote Sensing* [WWW Document]. eBooks.com. URL <https://www.ebooks.com/en-gb/book/883325/an-introduction-to-contemporary-remote-sensing/qihao-weng/> (accessed 3.4.21).

- Qu, J.J., Gao, W., Kafatos, M., Murphy, R.E., Salomonson, V.V., 2007. *Earth Science Satellite Remote Sensing: Vol.1: Science and Instruments*. Springer Science & Business Media.
- Quattrochi, D.A., Goodchild, M.F., 1997. Scale in remote sensing and GIS. <https://doi.org/10.5860/choice.35-1541>
- Rabin, R.M., Martin, D.W., 1996. Satellite observations of shallow cumulus coverage over the central United States: An exploration of land use impact on cloud cover. *J. Geophys. Res. Atmospheres* 101, 7149–7155. <https://doi.org/10.1029/95JD02891>
- Ragatoa, D.S., Ogunjobi, K.O., Klutse, N.A.B., Okhimamhe, A.A., Eichie, J.O., 2019. A change comparison of heat wave aspects in climatic zones of Nigeria. *Environ. Earth Sci.* 78, 111. <https://doi.org/10.1007/s12665-019-8112-8>
- Rigo, G., Parlow, E., Oesch, D., 2006. Validation of satellite observed thermal emission with in-situ measurements over an urban surface. *Remote Sens. Environ., Thermal Remote Sensing of Urban Areas* 104, 201–210. <https://doi.org/10.1016/j.rse.2006.04.018>
- Rizwan, A.M., Dennis, L.Y.C., Liu, C., 2008. A review on the generation, determination and mitigation of Urban Heat Island. *J. Environ. Sci.* 20, 120–128. [https://doi.org/10.1016/S1001-0742\(08\)60019-4](https://doi.org/10.1016/S1001-0742(08)60019-4)
- Robine, J.-M., Cheung, S.L.K., Le Roy, S., Van Oyen, H., Griffiths, C., Michel, J.-P., Herrmann, F.R., 2008. Death toll exceeded 70,000 in Europe during the summer of 2003. *C. R. Biol., Dossier : Nouveautés en cancérogenèse / New developments in carcinogenesis* 331, 171–178. <https://doi.org/10.1016/j.crvi.2007.12.001>
- Rohat, G., Flacke, J., Dosio, A., Dao, H., Maarseveen, M.V., 2019. Projections of Human Exposure to Dangerous Heat in African Cities Under Multiple Socioeconomic and Climate Scenarios - Rohat - 2019 - *Earth's Future* - Wiley Online Library [WWW Document]. URL <https://agupubs.onlinelibrary.wiley.com/doi/full/10.1029/2018EF001020> (accessed 1.3.20).
- Rose, M.H., 2001. Review of The Sanitary City: Urban Infrastructure in America from Colonial Times to the Present. *Environ. Hist.* 6, 478–480. <https://doi.org/10.2307/3985668>
- Rosenzweig, C., Solecki, W.D., Hammer, S.A., Mehrotra, S., 2011. *Climate Change and Cities: First Assessment Report of the Urban Climate Change Research Network*. Cambridge University Press.
- Rubin, N.H., 2009. The changing appreciation of Patrick Geddes: a case study in planning history. *Plan. Perspect.* 24, 349–366. <https://doi.org/10.1080/02665430902933986>
- Rybski, D., Reusser, D.E., Winz, A.-L., Fichtner, C., Sterzel, T., Kropp, J.P., 2017. Cities as nuclei of sustainability? *Environ. Plan. B Urban Anal. City Sci.* 44, 425–440. <https://doi.org/10.1177/0265813516638340>
- Sachindra, D.A., Ng, A.W.M., Muthukumaran, S., Perera, B.J.C., 2016. Impact of climate change on urban heat island effect and extreme temperatures: a case-study. *Q. J. R. Meteorol. Soc.* 142, 172–186. <https://doi.org/10.1002/qj.2642>
- Salomonson, V.V., Barnes, W.L., Maymon, P.W., Montgomery, H.E., Ostrow, H., 1989. MODIS: advanced facility instrument for studies of the Earth as a system. *IEEE Trans. Geosci. Remote Sens.* 27, 145–153. <https://doi.org/10.1109/36.20292>
- Santamouris, M., 2013. *Energy and Climate in the Urban Built Environment*. Routledge. <https://doi.org/10.4324/9781315073774>
- Sarkar, S., Phibbs, P., Simpson, R., Wasnik, S., 2018. The scaling of income distribution in Australia: Possible relationships between urban allometry, city size, and economic inequality. *Environ. Plan. B Urban Anal. City Sci.* 45, 603–622. <https://doi.org/10.1177/0265813516676488>
- Satterthwaite, D., 2007. *Adapting to Climate Change in Urban Areas: The Possibilities and Constraints in Low- and Middle-income Nations*. IIED.
- Schmidt-Nielsen, K., 1984. *Scaling: Why is Animal Size So Important?* Cambridge University Press.
- Schneider, A., Friedl, M.A., Potere, D., 2009. A new map of global urban extent from MODIS satellite data. *Environ. Res. Lett.* 4, 044003. <https://doi.org/10.1088/1748-9326/4/4/044003>



- Schwarz, N., Lautenbach, S., Seppelt, R., 2011. Exploring indicators for quantifying surface urban heat islands of European cities with MODIS land surface temperatures. *Remote Sens. Environ.* 115, 3175–3186. <https://doi.org/10.1016/j.rse.2011.07.003>
- Schwarz, N., Manceur, A.M., 2015. Analyzing the Influence of Urban Forms on Surface Urban Heat Islands in Europe. *J. Urban Plan. Dev. Div. ASCE* 141, A4014003. [https://doi.org/10.1061/\(ASCE\)UP.1943-5444.0000263](https://doi.org/10.1061/(ASCE)UP.1943-5444.0000263)
- SEDAC, 2017. EarthData | SEDAC [WWW Document]. URL <https://sedac.ciesin.columbia.edu/search/data?contains=population+data> (accessed 1.25.20).
- Seto, K.C., Güneralp, B., Hutyrá, L.R., 2012. Global forecasts of urban expansion to 2030 and direct impacts on biodiversity and carbon pools. *Proc. Natl. Acad. Sci.* 109, 16083–16088. <https://doi.org/10.1073/pnas.1211658109>
- Seto, K.C., Sánchez-Rodríguez, R., Fragkias, M., 2010. The New Geography of Contemporary Urbanization and the Environment. *Annu. Rev. Environ. Resour.* 35, 167–194. <https://doi.org/10.1146/annurev-environ-100809-125336>
- Shalaby, A., Tateishi, R., 2007. Remote sensing and GIS for mapping and monitoring land cover and land-use changes in the Northwestern coastal zone of Egypt. *Appl. Geogr.* 27, 28–41. <https://doi.org/10.1016/j.apgeog.2006.09.004>
- Sheng, L., Tang, X., You, H., Gu, Q., Hu, H., 2017. Comparison of the urban heat island intensity quantified by using air temperature and Landsat land surface temperature in Hangzhou, China. *Ecol. Indic.* 72, 738–746. <https://doi.org/10.1016/j.ecolind.2016.09.009>
- Short, J.R., 1982. *Housing in Britain: The Post-war Experience*. Routledge, London ; New York.
- Small, C.G., 2012. *The Statistical Theory of Shape*. Springer Science & Business Media.
- Smith, C.L., Webb, A., Levermore, G.J., Lindley, S.J., Beswick, K., 2011. Fine-scale spatial temperature patterns across a UK conurbation. *Clim. Change* 109, 269–286. <https://doi.org/10.1007/s10584-011-0021-0>
- SolarGIS, 2019. Global Solar Atlas [WWW Document]. URL <https://globalsolaratlas.info/support/release-notes> (accessed 1.25.20).
- Solomon, S., Intergovernmental Panel on Climate Change, Intergovernmental Panel on Climate Change (Eds.), 2007. *Climate change 2007: the physical science basis: contribution of Working Group I to the Fourth Assessment Report of the Intergovernmental Panel on Climate Change*. Cambridge University Press, Cambridge ; New York.
- Stefanovic, J.O., Yang, H., Zhou, Y., Kamali, B., Ogalleh, S.A., 2019. Adaption to climate change: a case study of two agricultural systems from Kenya. *Clim. Dev.* 11, 319–337. <https://doi.org/10.1080/17565529.2017.1411241>
- Stewart, I., Oke, T.R., 2010. Thermal differentiation of local climate zones using temperature observations from urban and rural field sites [WWW Document]. ResearchGate. URL [https://www.researchgate.net/publication/228420685\\_Thermal\\_differentiation\\_of\\_local\\_climate\\_zones\\_using\\_temperature\\_observations\\_from\\_urban\\_and\\_rural\\_field\\_sites](https://www.researchgate.net/publication/228420685_Thermal_differentiation_of_local_climate_zones_using_temperature_observations_from_urban_and_rural_field_sites) (accessed 11.8.19).
- Stewart, I.D., Oke, T., 2009a. A New Classification System for Urban Climate Sites. *Bull. Am. Meteorol. Soc. Boston* 90, 922–923.
- Stewart, I.D., Oke, T.R., 2012. Local Climate Zones for Urban Temperature Studies. *Bull. Am. Meteorol. Soc.* 93, 1879–1900. <https://doi.org/10.1175/BAMS-D-11-00019.1>
- Stewart, I.D., Oke, T.R., 2009b. Newly Developed “Thermal Climate Zones” for Defining and Measuring Urban Heat Island “Magnitude” in the Canopy Layer [WWW Document]. ResearchGate. URL [https://www.researchgate.net/publication/254774486\\_Newly\\_Developed\\_Thermal\\_Climate\\_Zones\\_for\\_Defining\\_and\\_Measuring\\_Urban\\_Heat\\_Island\\_Magnitude\\_in\\_the\\_Canopy\\_Layer](https://www.researchgate.net/publication/254774486_Newly_Developed_Thermal_Climate_Zones_for_Defining_and_Measuring_Urban_Heat_Island_Magnitude_in_the_Canopy_Layer) (accessed 8.12.19).

- Stewart, I.D., Oke, T.R., Kravynhoff, E.S., 2014. Evaluation of the 'local climate zone' scheme using temperature observations and model simulations. *Int. J. Climatol.* 34, 1062–1080. <https://doi.org/10.1002/joc.3746>
- Swanson, D.A., Tayman, J., Bryan, T.M., 2011. MAPE-R: a rescaled measure of accuracy for cross-sectional subnational population forecasts. *J. Popul. Res.* 28, 225–243. <https://doi.org/10.1007/s12546-011-9054-5>
- Terjung, W.H., Louie, S.S.-F., 1974. A Climatic Model of Urban Energy Budgets. *Geogr. Anal.* 6, 341–367. <https://doi.org/10.1111/j.1538-4632.1974.tb00519.x>
- Tizot, J.-Y., 2018. Ebenezer Howard's Garden City Idea and the Ideology of Industrialism. *Cah. Victoriens Edouardiens* 87. <https://doi.org/10.4000/cve.3605>
- Tomlinson, C.J., Chapman, L., Thornes, J.E., Baker, C.J., 2012. Derivation of Birmingham's summer surface urban heat island from MODIS satellite images. *Int. J. Climatol.* 32, 214–224. <https://doi.org/10.1002/joc.2261>
- Toomey, D., 2017. Investigating the Enigma of Clouds and Climate Change [WWW Document]. Yale E360. URL <https://e360.yale.edu/features/investigating-the-enigma-of-clouds-and-climate-change> (accessed 3.1.21).
- Torok, S.J., Morris, C.J.G., Skinner, C., Plummer, N., 2001. Urban heat island features of southeast Australian towns. *Aust. Meteorol. Mag.* 14.
- Tran, H., Uchiyama, D., Ochi, S., Yasuoka, Y., 2006. Assessment with satellite data of the urban heat island effects in Asian mega cities. *Int. J. Appl. Earth Obs. Geoinformation* 8, 34–48.
- Tsai, Y.-H., 2005. Quantifying Urban Form: Compactness versus "Sprawl." *Urban Stud.* 42, 141–161. <https://doi.org/10.1080/0042098042000309748>
- Tsubaki, T., 2000. Planners and the public: British popular opinion on housing during the second world war. *Contemp. Br. Hist.* 14, 81–98. <https://doi.org/10.1080/13619460008581573>
- Turner, B., Moss, R.H., Skole, D.L., 1993. Relating land use and global land-cover change. No Source Inf. Available.
- Turner, J.C., 1968. Housing Priorities, Settlement Patterns, and Urban Development in Modernizing Countries. *J. Am. Inst. Plann.* 34, 354–363. <https://doi.org/10.1080/01944366808977562>
- UN 2010, 2010. World Urbanization Prospects 2009 Revision (United Nations 2010) | Urban Area | Urbanization [WWW Document]. Scribd. URL <https://www.scribd.com/document/78681125/World-Urbanization-Prospects-2009-Revision-United-Nations-2010> (accessed 11.14.17).
- UNDP, 2010. Human Development Report 2010 | Human Development Reports [WWW Document]. URL <http://hdr.undp.org/en/content/human-development-report-2010> (accessed 6.28.19).
- Unger, J., 2009. Connection between urban heat island and sky view factor approximated by a software tool on a 3D urban database. *Int. J. Environ. Pollut.* 36, 59. <https://doi.org/10.1504/IJEP.2009.021817>
- Unger, J., 2006. Modelling of the annual mean maximum urban heat island using 2D and 3D surface parameters. *Clim. Res.* 30, 215–226. <https://doi.org/10.3354/cr030215>
- Unger, J., Savic, S., Gal, T., 2011. Modelling of the Annual Mean Urban Heat Island Pattern for Planning of Representative Urban Climate Station Network [WWW Document]. URL [https://www.researchgate.net/publication/215620072\\_Modelling\\_of\\_the\\_Annual\\_Mean\\_Urban\\_Heat\\_Island\\_Pattern\\_for\\_Planning\\_of\\_Representative\\_Urban\\_Climate\\_Station\\_Network](https://www.researchgate.net/publication/215620072_Modelling_of_the_Annual_Mean_Urban_Heat_Island_Pattern_for_Planning_of_Representative_Urban_Climate_Station_Network) (accessed 6.1.20).
- United Nations, Department of Economic and Social Affairs, Population Division, 2019. World urbanization prospects: the 2018 revision.
- Urban, J., Holušová, K., Menšík, L., Čermák, J., Kantor, P., 2013. Tree allometry of Douglas fir and Norway spruce on a nutrient-poor and a nutrient-rich site. *Trees* 27, 97–110. <https://doi.org/10.1007/s00468-012-0771-y>
- Usman, S.U., Abdulhamed, I.A., Ibrahim, M., Iguisi, E.O., Azare, I.M., Ati, O.F., 2016. Classifying Urban Climate Field Sites by Local Climate Zones of Kaduna Metropolis Nigeria 6.

- Vancutsem, C., Ceccato, P., Dinku, T., Connor, S.J., 2010. Evaluation of MODIS land surface temperature data to estimate air temperature in different ecosystems over Africa. *Remote Sens. Environ.* 114, 449–465. <https://doi.org/10.1016/j.rse.2009.10.002>
- Verburg, P.H., Erb, K.-H., Mertz, O., Espindola, G., 2013. Land System Science: between global challenges and local realities. *Curr. Opin. Environ. Sustain.* 5, 433–437. <https://doi.org/10.1016/j.cosust.2013.08.001>
- Vining, D.R.J., Kontuly, T., 1978. Population Dispersal from Major Metropolitan Regions: An International Comparison. *Int. Reg. Sci. Rev.* 3, 49–73. <https://doi.org/10.1177/016001767800300102>
- Voogt, J.A., Oke, T.R., 2003. Thermal remote sensing of urban climates. *Remote Sens. Environ., Urban Remote Sensing* 86, 370–384. [https://doi.org/10.1016/S0034-4257\(03\)00079-8](https://doi.org/10.1016/S0034-4257(03)00079-8)
- Voogt, J.A., Oke, T.R., 1997. Complete Urban Surface Temperatures. *J. Appl. Meteorol.* 36, 1117–1132. [https://doi.org/10.1175/1520-0450\(1997\)036<1117:CUST>2.0.CO;2](https://doi.org/10.1175/1520-0450(1997)036<1117:CUST>2.0.CO;2)
- Wamsler, C., Brink, E., Rivera, C., 2013. Planning for climate change in urban areas: from theory to practice. *J. Clean. Prod.* 50, 68–81.
- Wan, Z., 2008. New refinements and validation of the MODIS Land-Surface Temperature/Emissivity products. *Remote Sens. Environ.* 112, 59–74. <https://doi.org/10.1016/j.rse.2006.06.026>
- Wan, Z., Dozier, J., 1996. A generalized split-window algorithm for retrieving land-surface temperature from space. *IEEE Trans. Geosci. Remote Sens.* 34, 892–905. <https://doi.org/10.1109/36.508406>
- Wan, Z., Zhang, Y., Zhang, Q., Li, Z., 2002. Validation of the land-surface temperature products retrieved from Terra Moderate Resolution Imaging Spectroradiometer data. *Remote Sens. Environ., The Moderate Resolution Imaging Spectroradiometer (MODIS): a new generation of Land Surface Monitoring* 83, 163–180. [https://doi.org/10.1016/S0034-4257\(02\)00093-7](https://doi.org/10.1016/S0034-4257(02)00093-7)
- Wan, Z., Zhang, Y., Zhang, Q., Li, Z.-L., 2004. Quality assessment and validation of the MODIS global land surface temperature. *Int. J. Remote Sens.* 25, 261–274. <https://doi.org/10.1080/0143116031000116417>
- Wan, Z.S.H., 2015. MOD11A1 MODIS/Terra Land Surface Temperature/Emissivity Daily L3 Global 1km SIN Grid V006. <https://doi.org/10.5067/MODIS/MOD11A1.006>
- Wang, ran, Ren, C., Xu, Y., Shi, Y., 2017. Mapping the local climate zones of urban areas by GIS-based and WUDAPT methods: A case study of Hong Kong [WWW Document]. ResearchGate. URL [https://www.researchgate.net/publication/320368260\\_Mapping\\_the\\_local\\_climate\\_zones\\_of\\_urban\\_areas\\_by\\_GIS-based\\_and\\_WUDAPT\\_methods\\_A\\_case\\_study\\_of\\_Hong\\_Kong](https://www.researchgate.net/publication/320368260_Mapping_the_local_climate_zones_of_urban_areas_by_GIS-based_and_WUDAPT_methods_A_case_study_of_Hong_Kong) (accessed 8.8.19).
- Wang, C., Middel, A., Myint, S.W., Kaplan, S., Brazel, A.J., Lukasczyk, J., 2018. Assessing local climate zones in arid cities: The case of Phoenix, Arizona and Las Vegas, Nevada. *ISPRS J. Photogramm. Remote Sens.* 141, 59–71. <https://doi.org/10.1016/j.isprsjprs.2018.04.009>
- Wang, R., Cai, M., Ren, C., Bechtel, B., Xu, Y., Ng, E., 2019. Detecting multi-temporal land cover change and land surface temperature in Pearl River Delta by adopting local climate zone. *Urban Clim.* 28, 100455. <https://doi.org/10.1016/j.uclim.2019.100455>
- Wang, Y., Berardi, U., Akbari, H., 2016. Comparing the effects of urban heat island mitigation strategies for Toronto, Canada. <https://doi.org/10.1016/J.ENBUILD.2015.06.046>
- Wang, Y., Li, Y., Sabatino, S.D., Martilli, A., Chan, P.W., 2018. Effects of anthropogenic heat due to air-conditioning systems on an extreme high temperature event in Hong Kong. *Environ. Res. Lett.* 13, 034015. <https://doi.org/10.1088/1748-9326/aaa848>
- Watkins, R., Palmer, J., Kolokotroni, M., Littlefair, P., 2002. The London Heat Island: results from summertime monitoring. *Build. Serv. Eng. Res. Technol.* 23, 97–106. <https://doi.org/10.1191/0143624402bt0310a>

- Webb, M.S., 2018. Local responses to the protection of medieval buildings and archaeology in British post-war town reconstruction: Southampton and Coventry. *Urban Hist.* 45, 635–659. <https://doi.org/10.1017/S0963926818000019>
- Weng, Q., 2011. *Advances in Environmental Remote Sensing: Sensors, Algorithms, and Applications*. CRC Press.
- Weng, Q., 2010. *Remote sensing and GIS integration theories, methods, and applications*. McGraw-Hill, New York.
- Weng, Q., 2009. Thermal infrared remote sensing for urban climate and environmental studies: Methods, applications, and trends. *ISPRS J. Photogramm. Remote Sens.* 64, 335–344. <https://doi.org/10.1016/j.isprsjprs.2009.03.007>
- Weng, Q., Lu, D., 2008. A sub-pixel analysis of urbanization effect on land surface temperature and its interplay with impervious surface and vegetation coverage in Indianapolis, United States. *Int. J. Appl. Earth Obs. Geoinformation* 10, 68–83. <https://doi.org/10.1016/j.jag.2007.05.002>
- West, G.B., Brown, J.H., 2005. The origin of allometric scaling laws in biology from genomes to ecosystems: towards a quantitative unifying theory of biological structure and organization. *J. Exp. Biol.* 208, 1575–1592. <https://doi.org/10.1242/jeb.01589>
- White, R., Engelen, G., 1993. Cellular Automata and Fractal Urban Form: A Cellular Modelling Approach to the Evolution of Urban Land-Use Patterns. *Environ. Plan. A* 25, 1175–1199. <https://doi.org/10.1068/a251175>
- Whitehand, J.W.R., 2001. The Physical Form of Cities: A Historico-Geographical Approach, in: *Handbook of Urban Studies*. SAGE Publications Ltd, London, pp. 69–87. <https://doi.org/10.4135/9781848608375>
- Whitehand, J.W.R., Whitehand, S.M., 1983. The Study of Physical Change in Town Centres: Research Procedures and Types of Change. *Trans. Inst. Br. Geogr.* 8, 483–507. <https://doi.org/10.2307/621964>
- Whitehand, J.W.R., Whitehand, S.M.R., 1984. The Physical Fabric of Town Centres: The Agents of Change. *Trans. Inst. Br. Geogr.* 9, 231. <https://doi.org/10.2307/622170>
- Wiedenhofer, D., Lenzen, M., Steinberger, J.K., 2013. Energy requirements of consumption: Urban form, climatic and socio-economic factors, rebounds and their policy implications. *Energy Policy* 63, 696–707. <https://doi.org/10.1016/j.enpol.2013.07.035>
- Wikipedia, 2020. Geography of Sheffield. Wikipedia.
- Wilks, D.S., 1995. *Statistical Methods in the Atmospheric Sciences, Volume 59 - 1st Edition* [WWW Document]. URL <https://www.elsevier.com/books/statistical-methods-in-the-atmospheric-sciences/wilks/978-0-12-751965-4> (accessed 4.28.21).
- Winsborough, H.H., 1962. City Growth and City Structure†. *J. Reg. Sci.* 4, 35–49. <https://doi.org/10.1111/j.1467-9787.1962.tb00903.x>
- Wouters, H., De Ridder, K., Poelmans, L., Willems, P., Brouwers, J., Hosseinzadehtalaei, P., Tabari, H., Vanden Broucke, S., van Lipzig, N.P.M., Demuzere, M., 2017. Heat stress increase under climate change twice as large in cities as in rural areas: A study for a densely populated midlatitude maritime region. *Geophys. Res. Lett.* 44, 8997–9007. <https://doi.org/10.1002/2017GL074889>
- Wright, A.J., Young, A.N., Natarajan, S., 2016. Dwelling temperatures and comfort during the August 2003 heat wave: Build. Serv. Eng. Res. Technol. <https://doi.org/10.1191/0143624405bt136oa>
- Wu, J., Jones, K., Li, H., Loucks, O., 2006. *Scaling and Uncertainty Analysis in Ecology: Methods and Applications*.
- Wu, X., Zhang, L., Zang, S., 2019. Examining seasonal effect of urban heat island in a coastal city. *PLOS ONE* 14, e0217850. <https://doi.org/10.1371/journal.pone.0217850>
- Xu, Y., Pu, L., Zhang, L., 2014. Spatial Pattern and the Process of Settlement Expansion in Jiangsu Province from 1980 to 2010, Eastern China. *Sustainability* 6, 8180–8194. <https://doi.org/10.3390/su6118180>

- Yamamoto, Y., 2006. Measures to Mitigate Urban Heat Islands 19.
- Yang, J., Wong, M.S., Menenti, M., Nichol, J., 2015. Modeling the effective emissivity of the urban canopy using sky view factor. *ISPRS J. Photogramm. Remote Sens.* 105, 211–219. <https://doi.org/10.1016/j.isprsjprs.2015.04.006>
- Yuan, F., Bauer, M.E., 2007. Comparison of impervious surface area and normalized difference vegetation index as indicators of surface urban heat island effects in Landsat imagery. *Remote Sens. Environ.* 106, 375–386. <https://doi.org/10.1016/j.rse.2006.09.003>
- Zhang, H., Qi, Z., Ye, X., Cai, Y., Ma, W., Chen, M., 2013. Analysis of land use/land cover change, population shift, and their effects on spatiotemporal patterns of urban heat islands in metropolitan Shanghai, China. *Appl. Geogr.* 44, 121–133. <https://doi.org/10.1016/j.apgeog.2013.07.021>
- Zhang, Q., Seto, K.C., 2011. Mapping urbanization dynamics at regional and global scales using multi-temporal DMSP/OLS nighttime light data. *Remote Sens. Environ.* 115, 2320–2329. <https://doi.org/10.1016/j.rse.2011.04.032>
- Zhang, Z., Xiao, R., Shortridge, A., Wu, J., 2014. Spatial Point Pattern Analysis of Human Settlements and Geographical Associations in Eastern Coastal China — A Case Study. *Int. J. Environ. Res. Public Health* 11, 2818–2833. <https://doi.org/10.3390/ijerph110302818>
- Zhao, L., Lee, X., Smith, R.B., Oleson, K., 2014. Strong contributions of local background climate to urban heat islands. *Nature* 511, 216–219. <https://doi.org/10.1038/nature13462>
- Zhou, B., Rybski, D., Kropp, J.P., 2017. The role of city size and urban form in the surface urban heat island. *Sci. Rep.* 7, 1–9. <https://doi.org/10.1038/s41598-017-04242-2>
- Zhou, B., Rybski, D., Kropp, J.P., 2013. On the statistics of urban heat island intensity. *Geophys. Res. Lett.* 40, 5486–5491. <https://doi.org/10.1002/2013GL057320>
- Zhou, D., Zhao, S., Liu, S., Zhang, L., Zhu, C., 2014. Surface urban heat island in China's 32 major cities: Spatial patterns and drivers. *Remote Sens. Environ.* 152, 51–61. <https://doi.org/10.1016/j.rse.2014.05.017>

## Data Sources

Meridian\_data, 2017

[https://digimap.edina.ac.uk/webhelp/os/data\\_information/os\\_products/meridian\\_2.htm](https://digimap.edina.ac.uk/webhelp/os/data_information/os_products/meridian_2.htm), data downloaded on 31st January 2017

MODIS/Terra Land Surface Temperature and Emissivity Daily L3 Global 1km Grid SIN V006

<https://search.earthdata.nasa.gov/search>, Data downloaded on 23<sup>rd</sup> August 2017. (Earthdata, 2017).

For a description of the dataset, see <https://lpdaac.usgs.gov/products/mod11a1v006/>

UK Planning history: <https://www.planninghelp.cpre.org.uk/planning-explained/history-of-the-planning-system>, last accessed 26th 825 September 20

SEDAC, 2017. EarthData | SEDAC [WWW Document]. URL

<https://sedac.ciesin.columbia.edu/search/data> ?contains=population + data (accessed 1.25.20).

MODIS/ Terra Land Surface Temperature and Emissivity Daily L3 Global 1km Grid SIN V006

<https://search.earthdata.nasa.gov/search>, Data downloaded on 06<sup>th</sup> November 2017 (Earthdata, 2017). For a description of the dataset, see <https://lpdaac.usgs.gov/products/mod11a1v006/>

Landuse map for London, Sheffield, Milton Keynes, and Aberdeen (ordnance survey data) (EDINA, 2018) Data downloaded on 19<sup>th</sup> July 2020 <https://digimap.edina.ac.uk/>

## **Supplementary Materials**

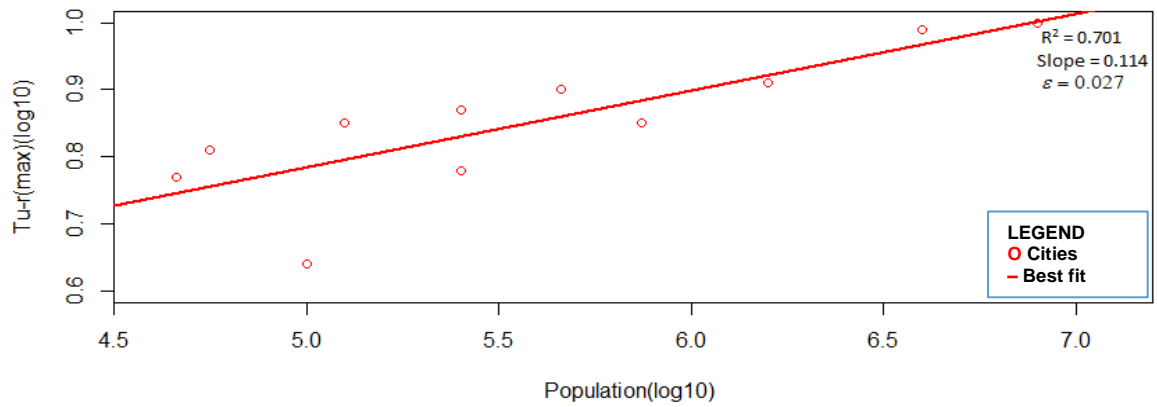
## Supplementary 3SI

### (Materials for chapter 3)

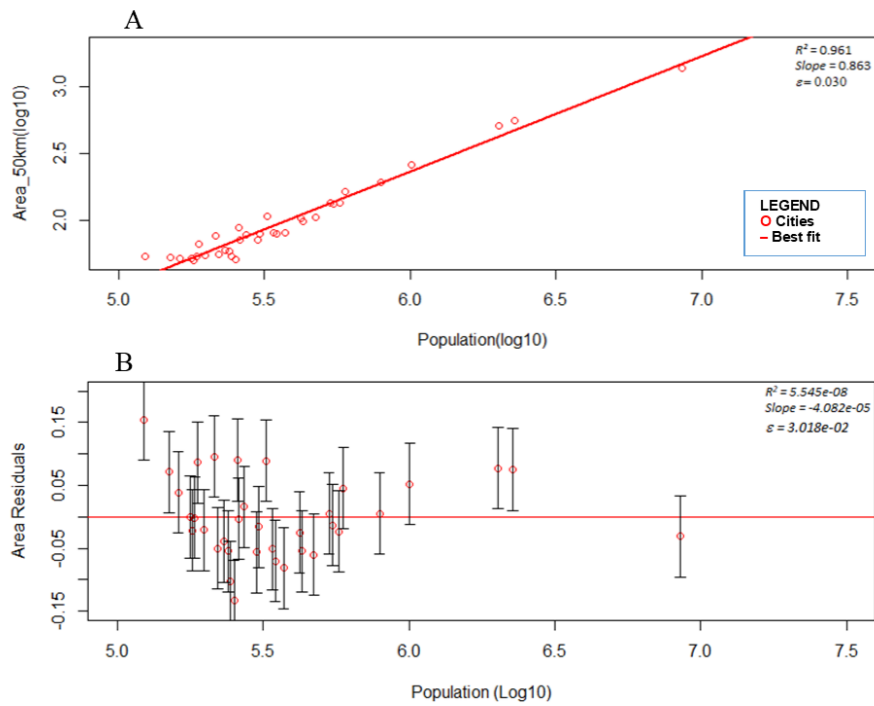
*Table 3S1. Hierarchical population distribution and area for 35 biggest cities in Great Britain (50km<sup>2</sup> and above; source: Meridian data 2017)*

NAME OF CITY	POPULATION	AREA (km <sup>2</sup> )
London	8519128	1,365.43
Birmingham	2273321	558.07
Manchester	2018064	506.06
Glasgow	1006585	261.85
Liverpool	792665	191.28
Sheffield	596456	164.23
Bristol	573382	135.52
Nottingham	546720	133.02
Leeds	531516	135.50
Edinburgh	472217	105.28
Leicester	429753	98.25
Newcastle Upon Tyne	420710	103.31
Portsmouth	371300	81.52
Bradford	347653	78.96
Cardiff / Caerdydd	339746	80.84
Stoke-On-Trent	323762	107.18
Bournemouth	305788	80.08
Coventry	300924	71.98
Reading	272658	78.04
Gateshead	260779	71.95
Weybridge	259047	88.69
Luton	251115	51.56
Southampton	243807	53.91
Southend-On-Sea	239424	59.37
Derby	231497	59.78
Plymouth	220942	55.91
Aldershot	214691	76.37
Northampton	198564	54.55
Milton Keynes	188643	66.86
Birkenhead	184461	53.58
Aberdeen	181027	50.27
Norwich	177619	51.98
Middlesbrough	161596	52.43
Swansea / Abertawe	150201	53.01
Telford	123416	54.26

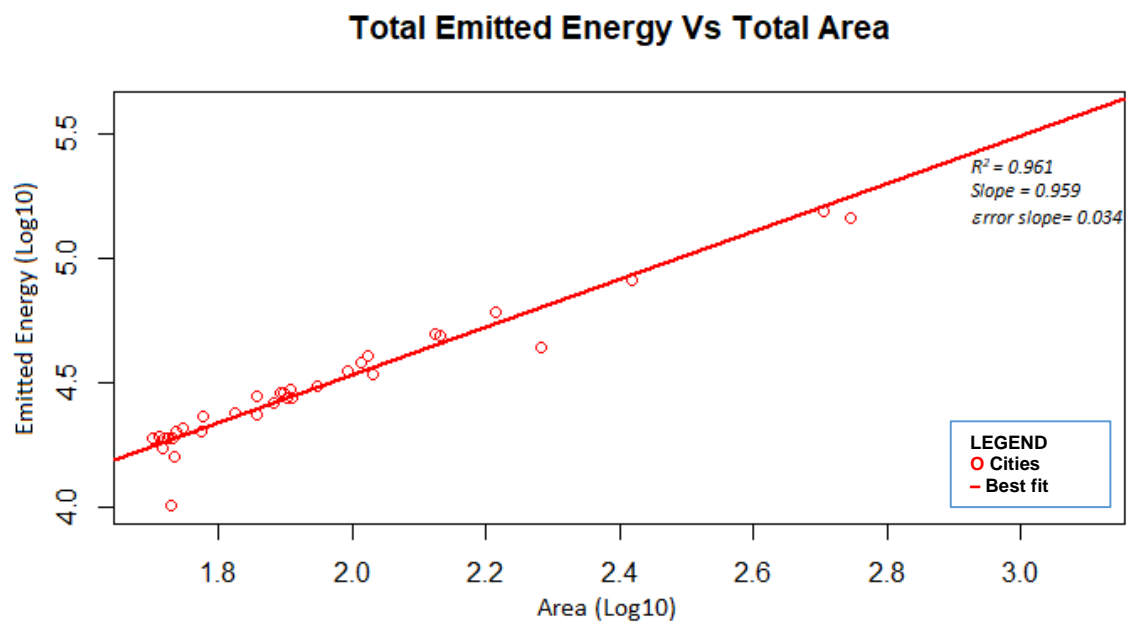




**Fig. 3S1.** As for Figure 1 of the main text but re-drawn on log-log axes to show the power-law scaling. Reported on the graph (top right) are the Coefficient of Determination ( $R^2$ ) for the best-fit regression, the slope of the regression, and the error on the slope ( $\varepsilon$ ).



**Fig. 3S2.** (A) Relationship between total city area and total population for 35 cities in Great Britain. The allometric regression relationship shown has a coefficient of determination ( $R^2 = 0.961$ ) and slope =  $0.86 \pm 0.03$ . (B) Residuals (equation 2, main text) of city area plotted against city population. The best-fit regression values are reported but are not significant.



**Fig 3S3.** Relationship between emitted energy and urban area for 35 cities in Great Britain. Reported on the graph (top right) are the Coefficient of Determination ( $R^2$ ) for the best-fit regression, the slope of the regression, and the error on the slope ( $\epsilon$ ).

**Table 3S2. Residuals for Emitted Energy and surface area for 35 biggest cities in Great Britain (cities are ranked by emitted energy residuals)**

NAME OF CITY	EMITTED ENERGY RESIDUAL ( $\text{W m}^{-2}$ )	AREA RESIDUAL ( $\text{km}^2$ )
Telford	0.146	0.155
Stoke-On-Trent	0.086	0.089
Weybridge	0.075	0.090
Birmingham	0.074	0.075
Milton Keynes	0.073	0.087
Swansea / Abertawe	0.062	0.071
Reading	0.052	0.016
Aldershot	0.051	0.096
Glasgow	0.050	0.052
Middlesbrough	0.038	0.039
Manchester	0.038	0.078
Gateshead	0.025	-0.003
Bournemouth	0.012	-0.016
Nottingham	0.008	-0.013
Sheffield	0.001	0.045
Bristol	0.001	-0.023
Northampton	-0.002	-0.021
Leeds	-0.004	0.005
Plymouth	-0.005	-0.050
Newcastle Upon Tyne	-0.005	-0.025
Aberdeen	-0.014	-0.022
London	-0.017	-0.031
Birkenhead	-0.024	-0.001
Liverpool	-0.029	0.005
Derby	-0.030	-0.039
Cardiff / Caerdydd	-0.033	-0.051
Edinburgh	-0.046	-0.060
Norwich	-0.049	0.000
Leicester	-0.049	-0.055
Portsmouth	-0.073	-0.081
Bradford	-0.076	-0.070
Coventry	-0.077	-0.056
Southampton	-0.080	-0.103
Southend-On-Sea	-0.087	-0.054
Luton	-0.114	-0.133

**Table 3S3. Summary of night-time emitted energy scalings for thirty-five (35) UK large Cities on 28 selected summer and winter nights between 2000 and 2017. Results are ranked by the strength ( $R^2$ ) of the log-log correlation between emitted energy and population, for a threshold for inclusion of a city in the scatter plot of 75% cloud-free pixels. The table reports the allometry slope, error on slope ( $\epsilon$ ), intercept, and sample size at 50% and 75% cloud free pixels**

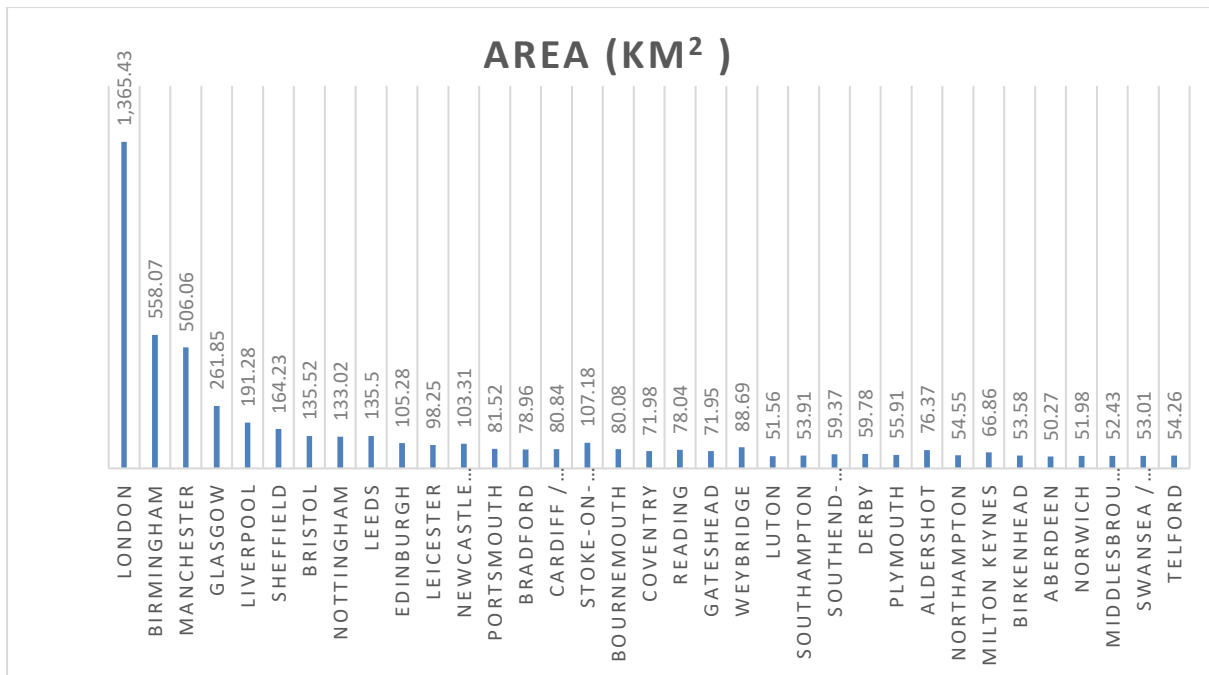
RANK	DATE	NUMBER OF CITIES	NUMBER *OF CITIES	$R^2$	* $R^2$	SLOPE ( $\alpha$ )	SLOPE *( $\alpha$ )	ERROR ON SLOPE ( $\epsilon$ )	ERROR ON *SLOPE ( $\epsilon$ )	INTERCEPT	*INTERCEPT
1	13th Feb. 2017	26	25	0.97	0.97	0.86	0.84	0.03	0.03	-0.23	-0.15
2	02nd Jan. 2017	35	33	0.94	0.97	0.84	0.83	0.04	0.03	-0.13	-0.09
3	15th Feb. 2016	25	25	0.96	0.96	0.85	0.85	0.03	0.03	-0.18	-0.18
4	06th Jun. 2000	33	32	0.96	0.96	0.85	0.88	0.03	0.03	-0.13	-0.28
5	29th Feb. 2000	21	19	0.92	0.96	0.83	0.78	0.05	0.04	-0.08	0.19
6	22nd Feb. 2003	28	28	0.96	0.96	0.88	0.88	0.04	0.04	-0.37	-0.37
7	07th Jul. 2007	34	34	0.96	0.96	0.84	0.84	0.03	0.03	-0.08	-0.08
8	01st Jan. 2007	32	32	0.96	0.96	0.85	0.85	0.03	0.03	-0.16	-0.16
9	20th Jan. 2011	22	17	0.88	0.95	0.74	0.82	0.06	0.05	0.33	-0.06
10	09th Jul. 2006	34	30	0.88	0.95	0.88	0.84	0.06	0.04	-0.31	-0.04
11	30th Aug. 2005	22	18	0.90	0.95	0.82	0.84	0.06	0.05	0.00	-0.06
12	20th Jan. 2009	18	14	0.88	0.94	0.83	0.80	0.08	0.06	-0.18	0.01
13	28th Aug. 2001	25	23	0.91	0.94	0.88	0.86	0.06	0.05	-0.30	-0.18
14	10th Jun. 2003	27	20	0.87	0.94	0.81	0.82	0.06	0.05	-0.02	-0.02
15	16th Aug. 2016	35	34	0.92	0.94	0.89	0.87	0.04	0.04	-0.31	-0.21
16	27th Jun. 2010	32	31	0.93	0.94	0.80	0.81	0.04	0.04	0.16	0.13
17	17th Dec. 2011	26	20	0.83	0.93	0.92	0.94	0.09	0.06	-0.65	-0.74
18	25th Feb. 2009	26	19	0.85	0.93	0.91	0.97	0.08	0.06	-0.62	-0.89
19	26th Dec. 2009	24	24	0.93	0.93	0.81	0.81	0.05	0.05	0.03	0.03
20	05th Jan. 2005	34	30	0.88	0.93	0.80	0.86	0.05	0.05	0.06	-0.25
21	13th Jul. 2002	28	22	0.87	0.92	0.77	0.80	0.06	0.05	0.22	0.14
22	30th Nov. 2016	20	17	0.92	0.92	0.86	0.82	0.06	0.06	-0.30	-0.08
23	18th Feb. 2006	25	23	0.79	0.92	0.84	0.86	0.09	0.06	-0.15	-0.21
24	01st Jan. 2012	24	24	0.92	0.92	0.89	0.89	0.06	0.06	-0.43	-0.43
25	08th Aug. 2012	25	20	0.88	0.89	0.83	0.99	0.06	0.08	-0.07	-0.95
26	03rd Aug. 2017	22	18	0.86	0.86	0.82	0.84	0.07	0.09	-0.06	-0.17
27	13th Dec. 2010	17	15	0.92	0.84	0.73	0.91	0.06	0.11	0.35	-0.62
28	28th Aug. 2009	30	21	0.84	0.82	0.81	0.88	0.07	0.09	-0.02	-0.36
	Mean					0.84	0.86	0.06	0.05	-0.13	-0.22
	Median					0.83	0.85				

\*= 75% cloud free pixels

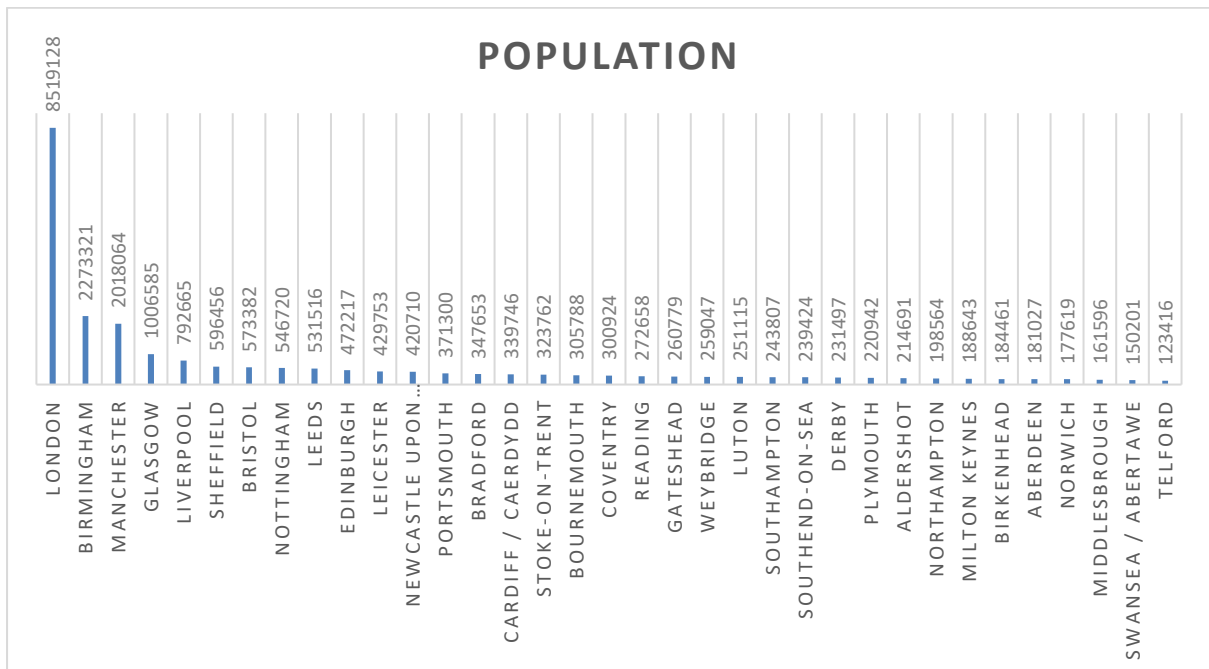
**Table 3S4. Summary of night-time emitted energy for UK large Cities with populations >250,000 and >500,000 on selected summer and winter nights. Results are ranked by the strength ( $R^2$  [%]) of the log-log correlation between emitted energy and population, for which the slope, error on slope ( $\epsilon$ ), and intercept are reported**

RANK	DATE	NUMBER OF CITIES	NUMBER OF *CITIES	$R^2$	* $R^2$	SLOPE ( $\alpha$ )	SLOPE *( $\alpha$ )	ERROR ON SLOPE ( $\epsilon$ )	ERROR ON SLOPE *( $\epsilon$ )	INTERCEPT	*INTERCEPT
1	15th Feb. 2016	16	7	0.98	0.99	0.86	0.85	0.04	0.04	-0.23	-0.19
2	13th Feb. 2017	16	7	0.97	0.97	0.82	0.84	0.04	0.06	-0.02	-0.10
3	16th Aug. 2016	22	9	0.97	0.98	0.87	0.89	0.03	0.04	-0.22	-0.32
4	07th Jul. 2007	22	9	0.97	0.98	0.85	0.86	0.03	0.05	-0.13	-0.16
5	01st Jan. 2007	21	8	0.97	0.98	0.85	0.87	0.04	0.06	-0.17	-0.30
6	29th Feb. 2000	15	7	0.97	0.96	0.81	0.78	0.04	0.07	0.03	0.24
7	02nd Jan. 2017	22	9	0.96	0.96	0.83	0.84	0.04	0.06	-0.07	-0.14
8	06th Jun. 2000	21	8	0.96	0.96	0.83	0.82	0.04	0.07	-0.02	0.06
9	22nd Feb. 2003	19	8	0.95	0.98	0.88	0.87	0.05	0.05	-0.35	-0.27
10	28th Aug. 2001	15	4	0.95	0.99	0.89	0.84	0.06	0.07	-0.38	0.01
11	09th Jul. 2006	22	9	0.95	0.95	0.82	0.85	0.04	0.08	0.05	-0.15
12	30th Nov. 2016	11	2	0.95	1.00	0.90	0.84	0.07	NA	-0.52	-0.10
13	26th Dec. 2009	13	5	0.94	0.98	0.84	0.92	0.07	0.07	-0.14	-0.68
14	01st Jan. 2012	16	7	0.93	0.95	1.02	0.98	0.07	0.10	-1.15	-0.93
15	13th Dec. 2010	10	5	0.92	0.93	0.66	0.58	0.07	0.09	0.81	1.31
16	05th Jan. 2005	21	9	0.92	0.90	0.81	0.65	0.05	0.08	0.03	1.01
17	27th Jun. 2010	20	8	0.92	0.95	0.81	0.87	0.06	0.08	0.14	-0.25
18	20th Jan. 2011	16	7	0.90	0.98	0.69	0.55	0.06	0.04	0.66	1.52
19	30th Aug. 2005	15	6	0.90	0.94	0.79	0.88	0.07	0.11	0.18	-0.38
20	20th Jan. 2009	12	4	0.89	0.88	0.90	0.85	0.10	0.22	-0.58	-0.29
21	03rd Aug. 2017	14	6	0.87	0.83	0.85	0.74	0.09	0.17	-0.21	0.47
22	28th Aug. 2009	20	8	0.87	0.92	0.88	0.80	0.08	0.09	-0.43	0.12
23	10th Jun. 2003	16	6	0.87	0.93	0.83	0.97	0.09	0.13	-0.11	-0.99
24	08th Aug. 2012	17	7	0.87	0.84	0.84	0.85	0.08	0.16	-0.16	-0.20
25	13th Jul. 2002	15	5	0.86	0.99	0.79	1.00	0.09	0.05	0.13	-1.20
26	25th Feb. 2009	16	7	0.85	0.88	1.02	0.93	0.11	0.16	-1.27	-0.72
27	18th Feb. 2006	16	6	0.82	0.98	1.02	0.98	0.13	0.08	-1.20	-0.92
28	17th Dec. 2011	16	6	0.79	0.76	0.92	0.83	0.13	0.23	-0.67	-0.12
	<b>Mean</b>					<b>0.85</b>	<b>0.84</b>	<b>0.07</b>	<b>0.09</b>	<b>-0.21</b>	<b>-0.13</b>
	<b>Median</b>					<b>0.84</b>	<b>0.85</b>				

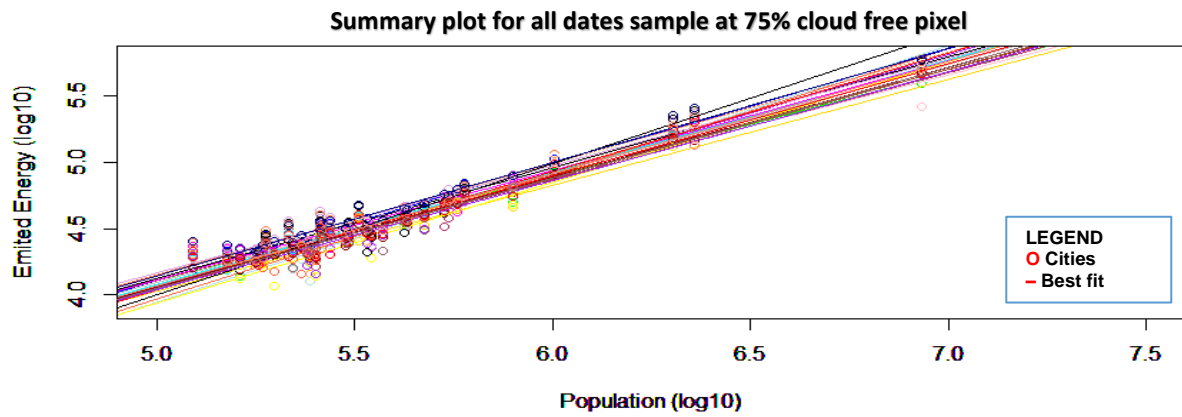
\* = Population >500,000



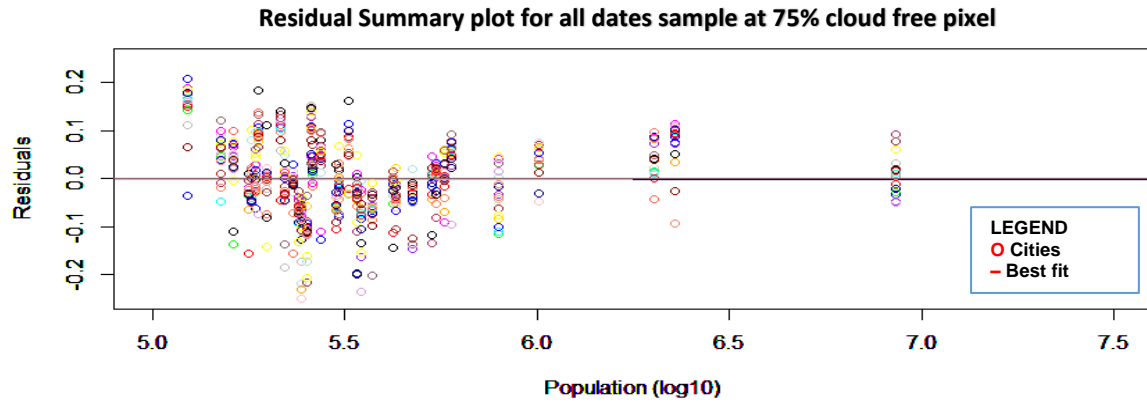
**Fig. 354** Hierarchical Area distribution for the 35 biggest cities in Great Britain



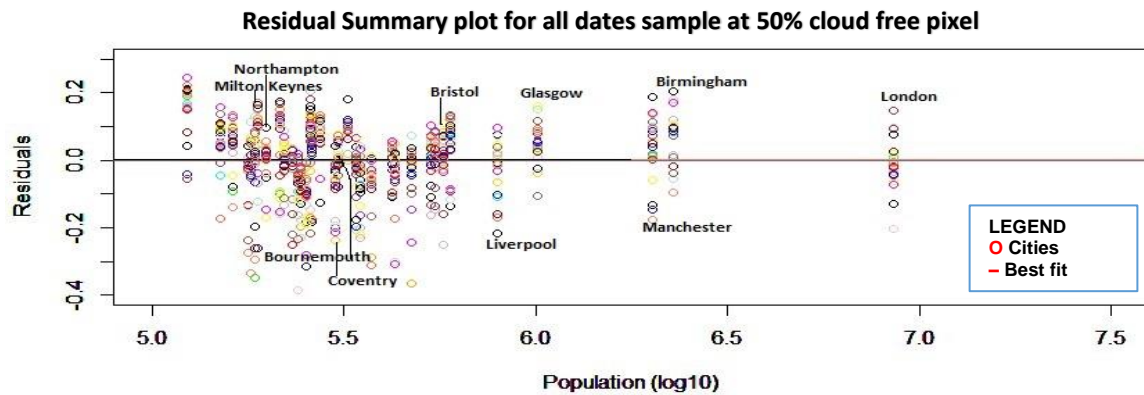
**Fig. 355** Hierarchical population distribution for the 35 biggest cities in Great Britain



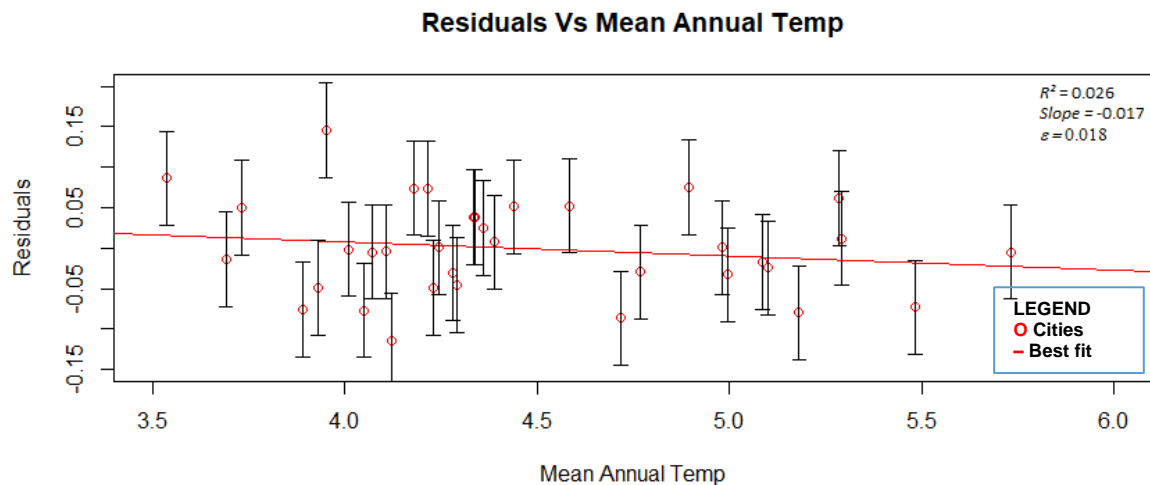
**Fig. 356** Relationship between total emitted energy and total population across Cities in Great Britain for selected nights, listed in Table 3. Each colour represents a different night. Allometric regressions are plotted for each night, the equations for which are reported in Table 3. The overall best straight line through the data is



**Fig. 357** Residual Summary plot for all dates sample at 75% cloud free pixel

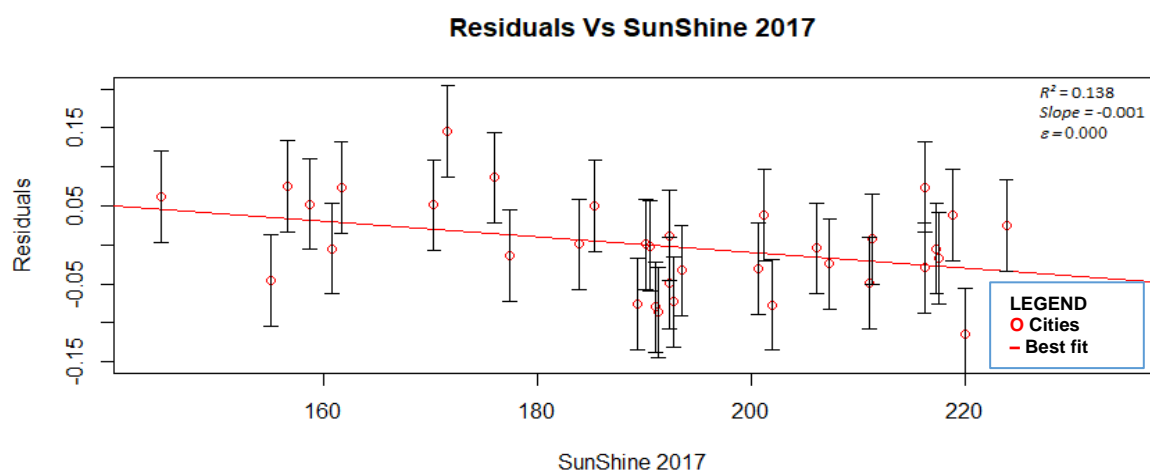


**Fig. 358** Residual Summary plot for all dates sample at 50% cloud free pixel



**Fig. 359**

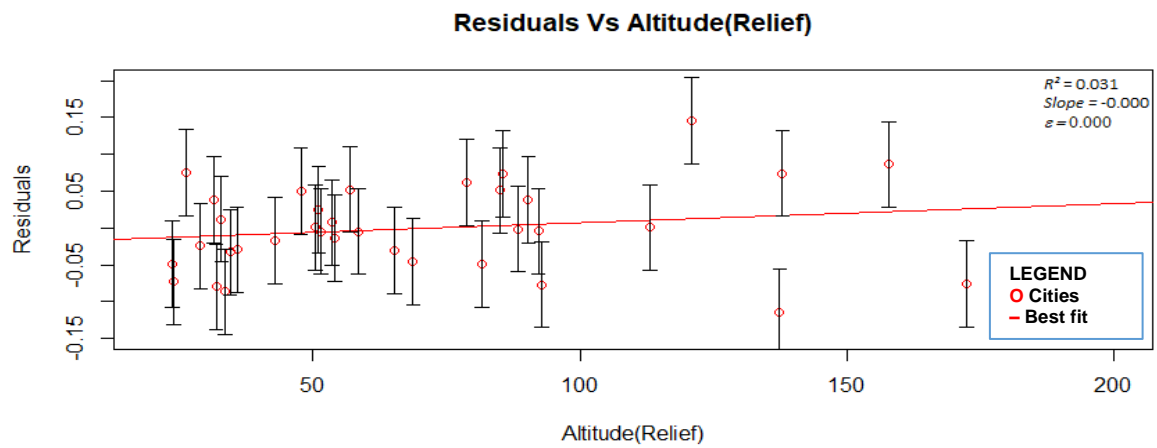
**Mean Residuals plots Vs Mean Annual Temperature**



**Fig. 3510**

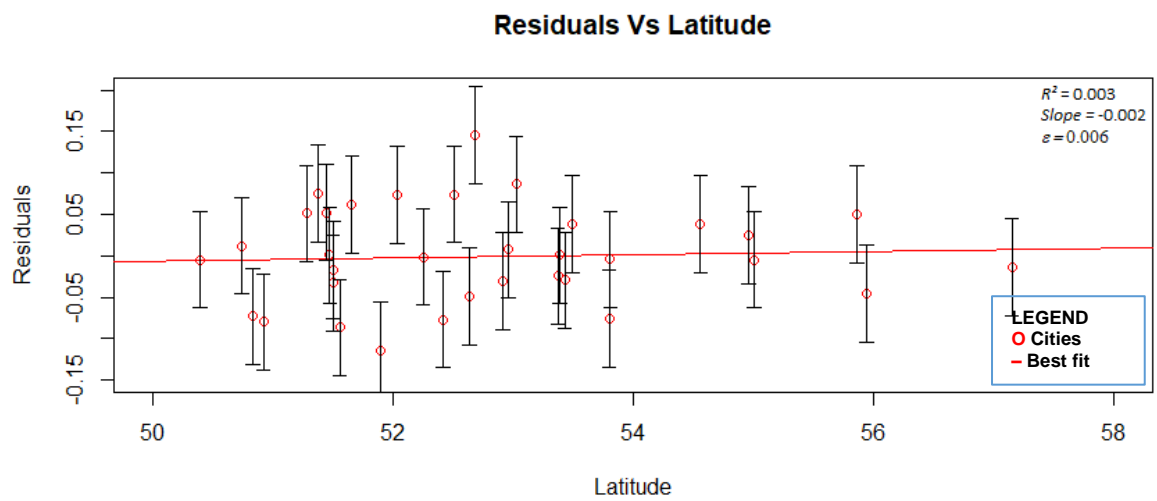
**Mean Residuals plots Vs Hours of Sunshine**





**Fig. 3S11**

**Mean Residuals plots Vs Altitude**



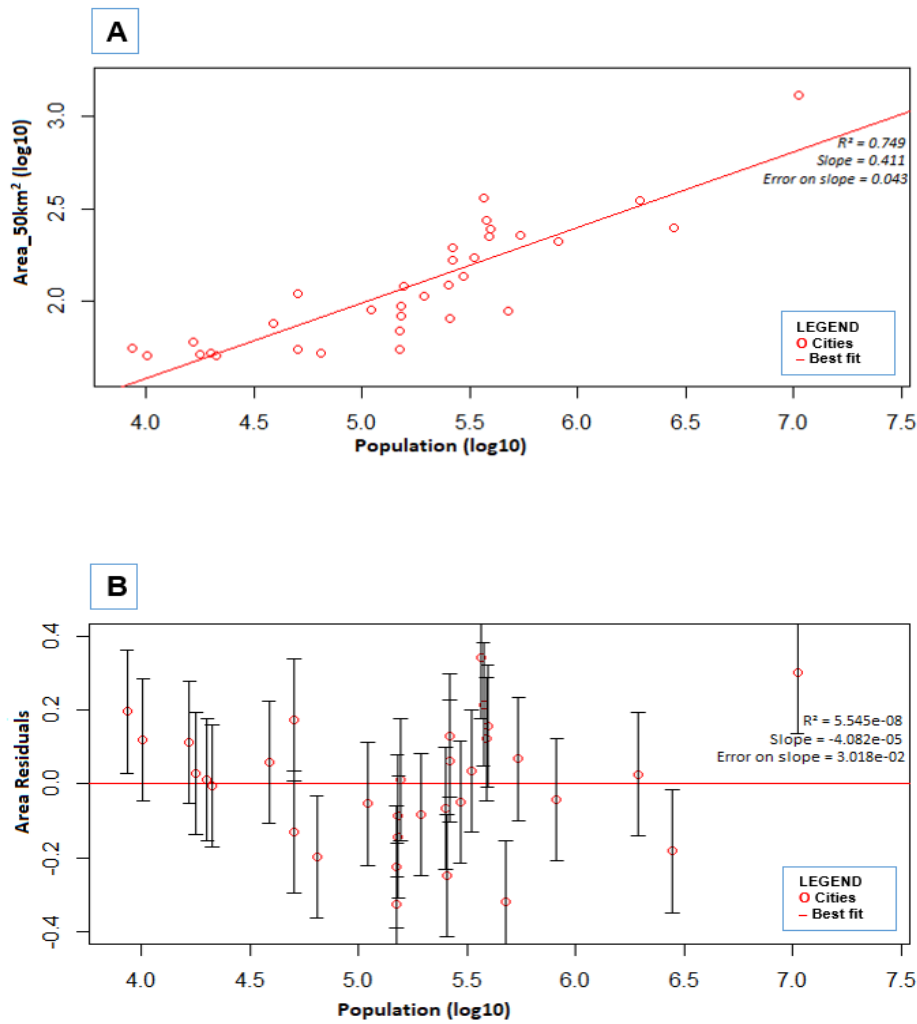
**Fig. 3S12** **Mean Residuals plots Vs Latitude.** The regression is not significantly different from zero and explain 0.3% of the variance.

## Supplementary 4SI

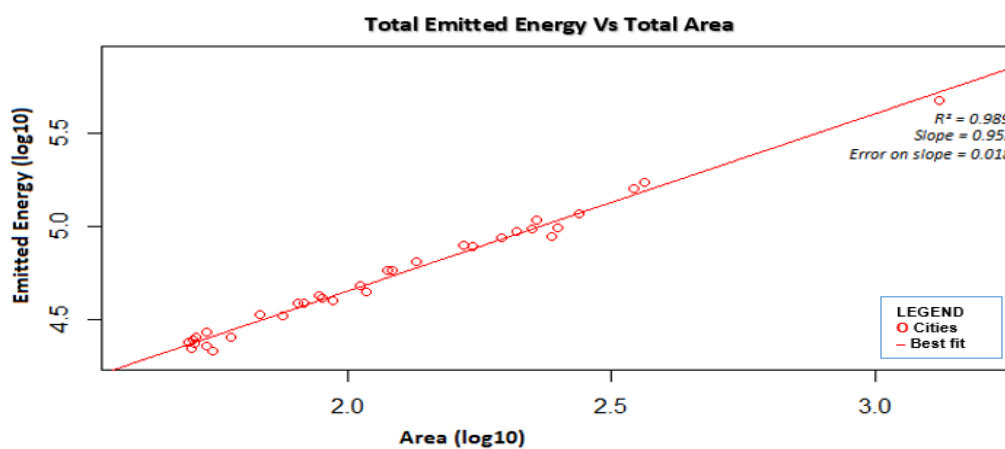
### (Materials for chapter 4)

**Table 4S1. Hierarchical population distribution and area for 33 biggest cities across Nigeria (cities within the limit of 50km<sup>2</sup> and above. (Source: (SEDAC, 2017))**

NAME OF CITY	POPULATION	AREA (km <sup>2</sup> )
Lagos	10472436	1314.62
Fct_Abuja	366849	363.95
Ibadan	1945397	349.33
Edo	375130	274.46
Kano	2780321	250.15
Maiduguri	391719	243.60
Port_Harcourt	544308	227.46
Owerri	386591	223.79
Kaduna	816209	208.53
Jos	263239	195.44
Enugu	329910	172.45
Osogbo	261571	166.04
Ilorin	292856	135.31
Anambra	250292	121.54
Ilesha	155509	119.49
Yola	50191	108.87
Onisha	193431	105.40
Zaria	150452	93.99
Umuahia	110319	89.35
Aba	476770	88.56
Uvwie_Warri	152496	82.94
Abeokuta	255975	80.59
Makurdi	38635	75.41
Minna	149638	68.29
Kebbi	16597	60.14
Akko_Gombe	8552	55.53
Akure	50163	54.28
Katsina	150012	54.18
Kogi	20045	51.70
Eket_A_Ibom	64112	51.50
Ebonyi	17826	50.98
Jalingo	21084	50.68
Ife_North	10153	50.02



**Fig. 4S1 Relationship between total areas and total population across Cities in Nigeria. The allometric regression relationship shown has a coefficient of determination ( $R^2 = 0.749$ ) and slope =  $0.41 \pm 0.04$ . (B) Residuals of urban areas plotted against urban population. The best-fit regression values are reported but are not significant**



**Fig. 4S2 Relationship between total emitted energy and total area across 33 cities in Nigeria. Reported on the graph (top right) are the Coefficient of Determination ( $R^2$ ) for the best-fit regression, the slope of the regression, and the error on the slope ( $\pm$ )**

**Table 4S2. Distribution of Emitted energy and area for 33 biggest cities across Nigeria**

<b>NAME OF CITY</b>	<b>AREA_50km<sup>2</sup> (log10)</b>	<b>EMITTED ENERGY (log10)</b>
Lagos	3.12	5.68
Fct_Abuja	2.56	5.24
Ibadan	2.54	5.21
Edo	2.44	5.07
Kano	2.40	4.99
Maiduguri	2.39	4.95
Port_Harcourt	2.36	5.03
Owerri	2.35	4.99
Kaduna	2.32	4.97
Jos	2.29	4.94
Enugu	2.24	4.89
Osogbo	2.22	4.90
Ilorin	2.13	4.81
Anambra	2.08	4.77
Ilesha	2.08	4.76
Yola	2.04	4.65
Onisha	2.02	4.68
Zaria	1.97	4.60
Umuahia	1.95	4.62
Aba	1.95	4.63
Uvwie_Warri	1.92	4.59
Abeokuta	1.91	4.59
Makurdi	1.88	4.52
Minna	1.83	4.53
Kebbi	1.78	4.41
Akko_Gombe	1.74	4.34
Akure	1.73	4.43
Katsina	1.73	4.36
Kogi	1.71	4.41
Eket_A_Ibom	1.71	4.38
Ebonyi	1.71	4.40
Jalingo	1.70	4.35
Ife_North	1.70	4.38

**Table 4S3. Summary of night-time emitted energy for thirty-three (33) large Cities across Nigeria on 23 selected nights between 2000 and 2017. Results are ranked by the strength ( $R^2$  [50%]) of the log-log correlation between emitted energy and population, for a threshold for inclusion of a city in the scatter plot of 75% cloud-free pixels. The table reports the allometry slope, error on slope ( $\epsilon$ ), intercept and sample size at 50% and 75% cloud free pixels**

RANK	DATE	NUMBER OF CITIES(n)	NUMBER *OF CITIES (n)	$R^2$ (50%)	* $R^2$ (75%)	SLOPE ( $\alpha$ )	SLOPE *( $\alpha$ )	ERROR ON SLOPE ( $\epsilon$ )	ERROR ON*SLOPE ( $\epsilon$ )	INTERCEPT	*INTERCEPT
1	15th Feb. 2008	29	25	0.81	0.84	0.43	0.42	0.04	0.04	2.47	2.55
2	12th Dec. 2003	23	22	0.80	0.80	0.39	0.40	0.04	0.04	2.67	2.66
3	07th Feb. 2006	31	31	0.79	0.79	0.41	0.41	0.04	0.04	2.65	2.65
4	16th Nov. 2004	19	18	0.79	0.79	0.44	0.44	0.06	0.06	2.47	2.47
5	02nd Jan. 2017	32	29	0.78	0.76	0.43	0.43	0.04	0.05	2.52	2.53
6	11th Apr. 2005	28	27	0.78	0.72	0.38	0.37	0.04	0.05	2.80	2.86
7	17th Nov. 2005	33	33	0.77	0.77	0.42	0.42	0.04	0.04	2.60	2.60
8	25th Dec. 2000	33	33	0.77	0.77	0.42	0.42	0.04	0.04	2.58	2.58
9	20th Dec. 2013	31	31	0.76	0.76	0.43	0.43	0.04	0.04	2.52	2.52
10	06th Feb. 2009	17	16	0.76	0.67	0.38	0.37	0.06	0.07	2.75	2.81
11	03rd Jan. 2012	32	32	0.76	0.76	0.41	0.41	0.04	0.04	2.58	2.58
12	29th Nov. 2016	30	28	0.75	0.75	0.43	0.41	0.05	0.05	2.49	2.58
13	26th Jan. 2001	31	31	0.73	0.73	0.40	0.40	0.05	0.05	2.65	2.65
14	05th Jan. 2013	29	29	0.72	0.72	0.42	0.42	0.05	0.05	2.54	2.54
15	25th Nov. 2003	22	18	0.71	0.74	0.42	0.43	0.06	0.06	2.54	2.50
16	20th Jan. 2016	28	26	0.69	0.76	0.39	0.43	0.05	0.05	2.71	2.51
17	02nd Jan. 2007	30	29	0.68	0.75	0.39	0.43	0.05	0.05	2.68	2.47
18	05th Jan. 2005	33	31	0.67	0.69	0.41	0.40	0.05	0.04	2.60	2.69
19	05th Feb. 2002	27	25	0.67	0.84	0.41	0.42	0.06	0.04	2.60	2.58
20	05th Jan. 2004	16	15	0.61	0.60	0.33	0.32	0.07	0.07	2.99	3.07
21	11th Apr. 2014	23	22	0.59	0.59	0.30	0.31	0.05	0.06	3.16	3.13
22	28th Feb. 2000	20	14	0.48	0.45	0.31	0.26	0.08	0.08	3.00	3.32
23	10th Jan. 2005	32	31	0.41	0.67	0.25	0.36	0.06	0.05	3.36	2.81
	Mean			0.71	0.73	0.39	0.40	0.05	0.05		
	Median					0.41	0.41				

\*=75% cloud free pixels

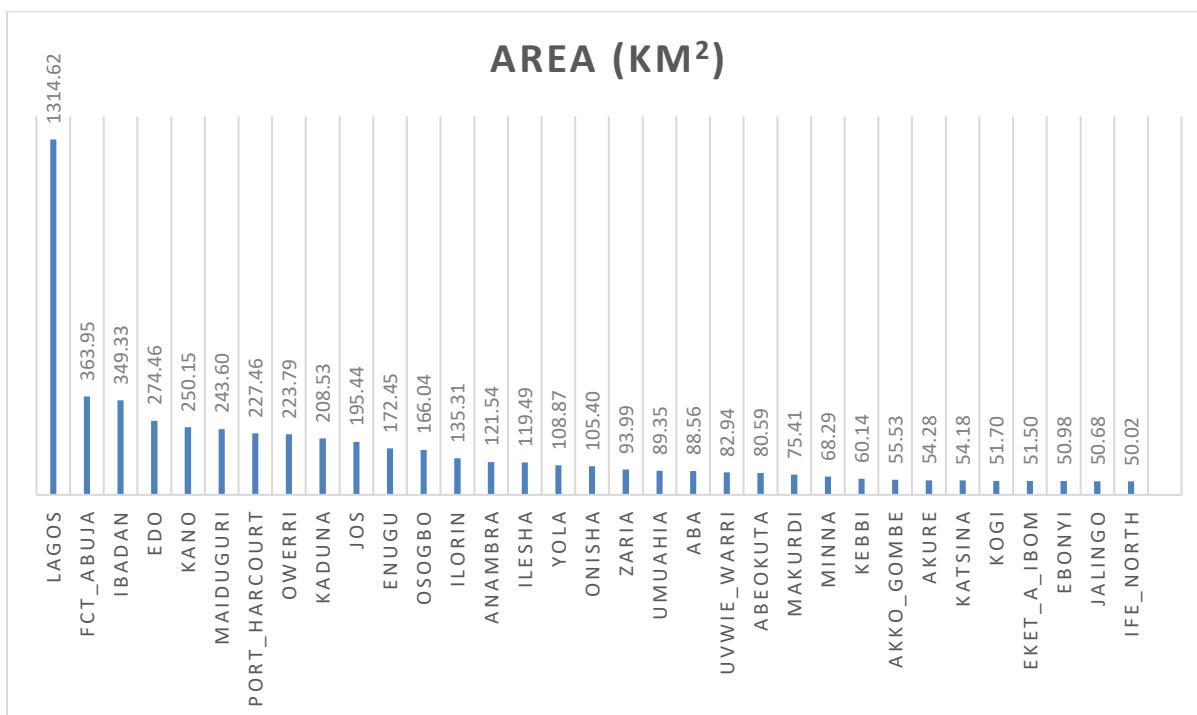
**Table 4S4. Summary of night-time emitted energy for Nigeria's large Cities with populations >250,000 and >500,000 on selected nights. Results are ranked by the strength (\*R<sup>2</sup>) of the log-log correlation between emitted energy and population, for which the slope, error on slope (ε), and intercept are reported**

DATE	NUMBER OF CITIES(n)	NUMBER *OF CITIES (n)	R <sup>2</sup> >250,000	*R <sup>2</sup> >500,000	(α) SLOPE	*(α) SLOPE	ERROR ON SLOPE (ε)	ERROR ON *SLOPE (ε)	INTERCEPT	*INTERCEPT
11th Apr. 2014	9	2	0.07	1.00	0.18	0.01	0.24	NA	3.89	5.06
28th Feb. 2000	9	2	0.11	1.00	0.24	-0.31	0.26	NA	3.46	6.96
15th Feb. 2008	14	4	0.78	0.90	0.57	0.48	0.09	0.11	1.69	2.31
16th Nov. 2004	9	3	0.66	0.80	0.55	0.45	0.14	0.22	1.87	2.60
05th Feb. 2002	12	3	0.64	0.76	0.56	0.47	0.13	0.26	1.75	2.40
10th Jan. 2005	16	5	0.03	0.71	-0.08	-0.44	0.12	0.16	5.38	7.69
25th Nov. 2003	12	3	0.62	0.68	0.56	0.37	0.14	0.26	1.71	3.06
12th Dec. 2003	10	4	0.70	0.67	0.43	0.42	0.10	0.21	2.52	2.58
29th Nov. 2016	13	5	0.63	0.51	0.49	0.33	0.11	0.19	2.19	3.25
05th Jan. 2004	7	3	0.01	0.47	-0.04	-0.23	0.16	0.24	5.23	6.40
25th Dec. 2000	16	5	0.60	0.47	0.48	0.33	0.11	0.20	2.23	3.28
17th Nov. 2005	16	5	0.59	0.45	0.47	0.33	0.10	0.21	2.33	3.29
03rd Jan. 2012	15	5	0.60	0.44	0.48	0.33	0.11	0.22	2.24	3.26
07th Feb. 2006	15	5	0.65	0.43	0.46	0.31	0.09	0.20	2.42	3.41
02nd Jan. 2017	16	5	0.58	0.42	0.48	0.32	0.11	0.22	2.24	3.28
11th Apr. 2005	13	5	0.58	0.40	0.35	0.21	0.09	0.15	2.99	3.95
05th Jan. 2005	16	5	0.55	0.40	0.42	0.26	0.10	0.18	2.59	3.68
20th Dec. 2013	16	5	0.58	0.39	0.46	0.31	0.11	0.23	2.34	3.34
05th Jan. 2013	14	5	0.56	0.38	0.46	0.31	0.12	0.23	2.33	3.38
26th Jan. 2001	15	5	0.45	0.21	0.37	0.21	0.11	0.24	2.81	3.89
02nd Jan. 2007	15	5	0.44	0.1978	0.42	0.26	0.13	0.31	2.50	3.57
20th Jan. 2016	13	5	0.38	0.19	0.38	0.25	0.15	0.30	2.79	3.66
06th Feb. 2009	7	3	0.48	0.16	0.24	0.11	0.11	0.26	3.71	4.56
Mean					0.39	0.22		0.22		
Median					0.46	0.31		0.22		

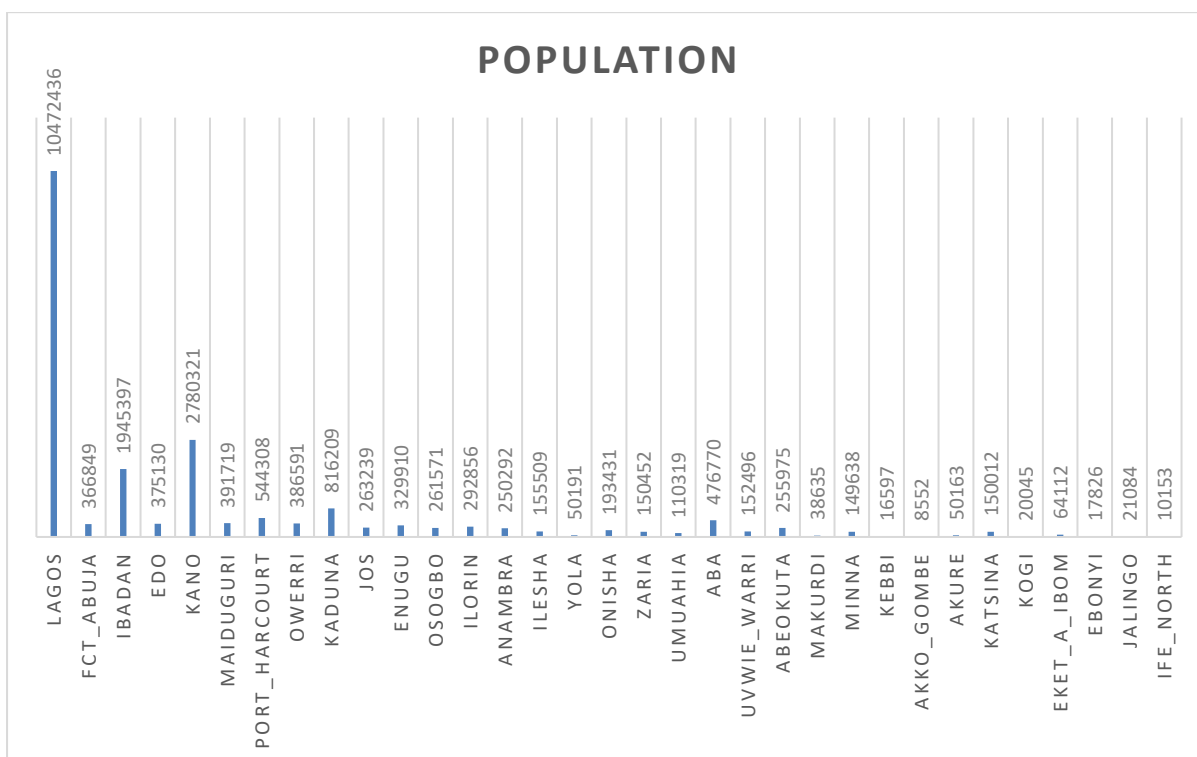
\* = Population >500,000

**Table 4S5. Residuals for Emitted Energy and surface area for 33 biggest cities in Nigeria (cities are ranked by emitted energy residuals)**

NAME OF CITY	EMITTED ENERGY RESIDUALS (W m <sup>-2</sup> )	AREA RESIDUALS (km <sup>2</sup> )
Fct_Abuja	0.372	0.342
Lagos	0.212	0.302
Edo	0.199	0.215
Jos	0.138	0.131
Ife_North	0.135	0.119
Yola	0.121	0.172
Akko_Gombe	0.112	0.195
Owerri	0.099	0.121
Osogbo	0.091	0.061
Port_Harcourt	0.089	0.067
Kebbi	0.080	0.112
Maiduguri	0.068	0.156
Enugu	0.046	0.036
Makurdi	0.045	0.059
Ebonyi	0.045	0.027
Ilesha	0.044	0.011
Ibadan	0.039	0.026
Kogi	0.036	0.012
Ilorin	-0.011	-0.048
Kaduna	-0.022	-0.043
Jalingo	-0.034	-0.005
Anambra	-0.042	-0.066
Umuahia	-0.046	-0.054
Onisha	-0.072	-0.082
Akure	-0.091	-0.130
Zaria	-0.105	-0.087
Uvwie_Warri	-0.134	-0.144
Minna	-0.183	-0.225
Eket_A_Ibom	-0.194	-0.197
Kano	-0.202	-0.182
Abeokuta	-0.221	-0.249
Aba	-0.279	-0.319
Katsina	-0.296	-0.326

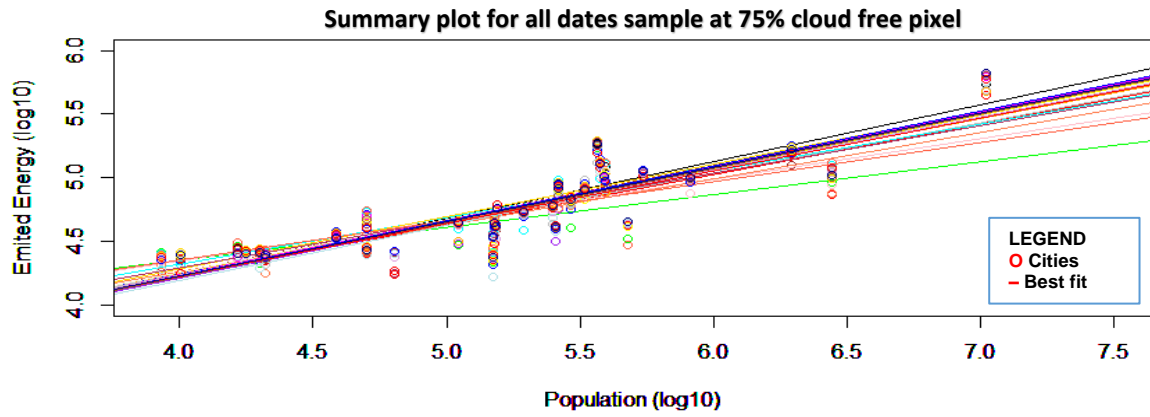


**Fig. 4S3 Hierarchical Area distribution for the 33 biggest cities in Nigeria**

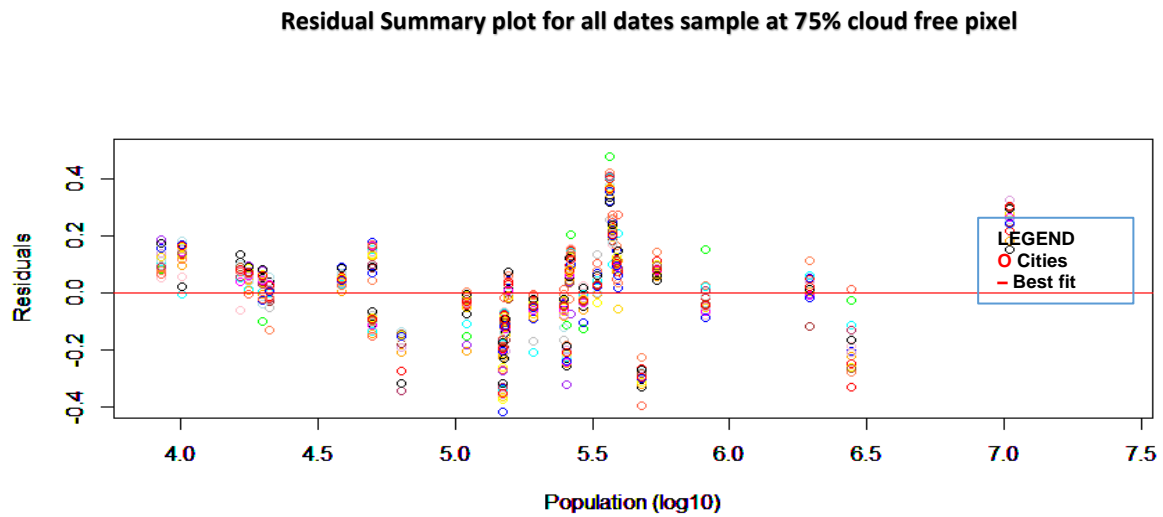


**Fig. 4S4 Hierarchical population distribution for the 33 biggest cities in Nigeria**

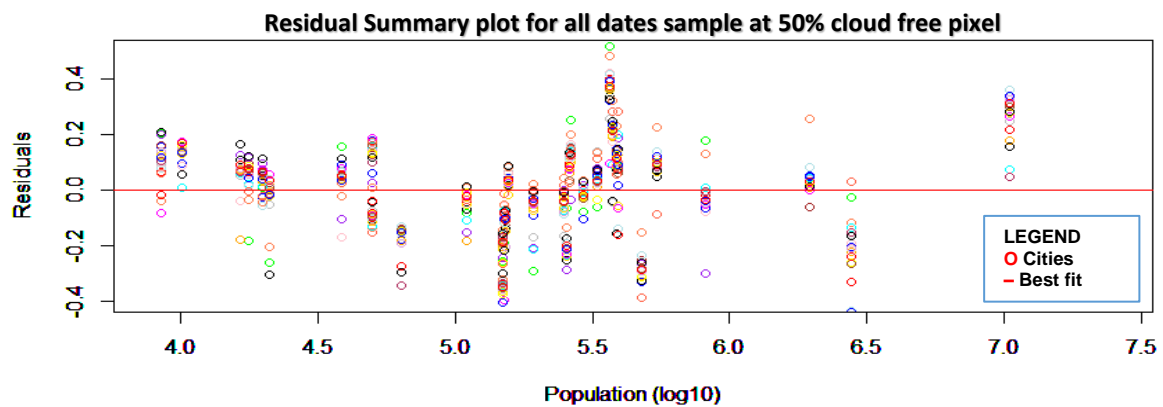










**Fig. 4S5** Relationship between total emitted energy and total population across Cities in Nigeria for selected nights, listed in Table 1. Each colour represents a different night. Allometric regressions are plotted for each night, the equations for which are reported in Table 1. The overall best straight line through the data is  $0.40 \pm 0.05$ .





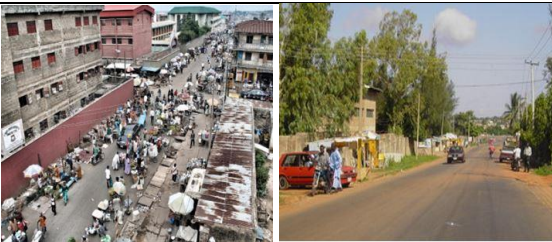


**Fig. 4S6** Residual Summary plot for all dates sample at 75% cloud free pixel










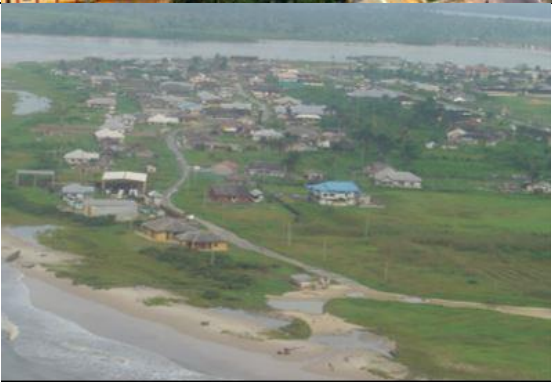
**Fig. 4S7** Residual Summary plot for all dates sample at 50% cloud free pixel

Name of City	Image Illustration	Landscape Description	LCZ Classification
Lagos a.		Busy coastal area along the commercial axis of Lagos with scattered evergreen trees and mid-rise buildings. Large open water body	LCZ2
b.		Dense mix of low-rise and tall buildings scattered with featureless landscape of rock	LCZ3 – LCZ4
c.		Spatially spaced array of tall buildings with abundance of impervious land cover and few trees	LCZ4 - LCZ5
d.		Dense mix low-rise and single-story buildings with few or no trees	LCZ7
e.		Dense mix of midrise buildings with no trees and densely populated	LCZ3
f.		Medium density buildings/ industries sparsely arranged with few trees and abundance of impervious/pervious land covers	LCZ9 – LCZ10





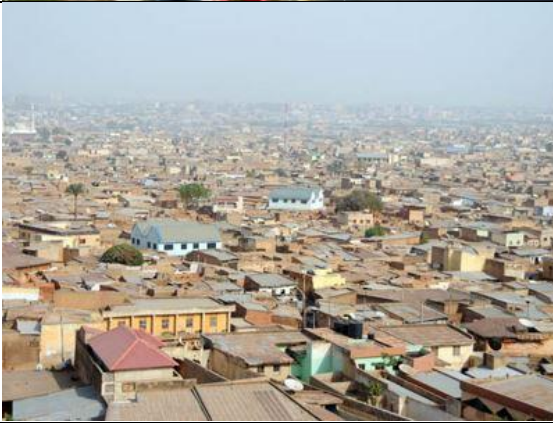

Abuja a.		Sparsely array of tall buildings with abundance of impervious land cover and trees	LCZ4
Akko/Gombe a.		Medium density of buildings spatially arranged with pervious and impervious land cover	LCZ5
b.		High density mix of low-rise buildings with few trees and mostly paved land cover	LCZ3
Kaduna a.		<ul style="list-style-type: none"> <li>- Commercial area along the central business district with dense solid buildings made up of heavy fabrics.</li> <li>- Narrow inner street and heavy traffic in part of the area with few or no vegetation</li> </ul>	LCZ2 – LCZ3
b		<ul style="list-style-type: none"> <li>- Mid-rise buildings with few or no trees.</li> <li>- Low-rise residential layout buildings with light traffic and abundance of vegetation</li> </ul>	LCZ2 – LCZ7


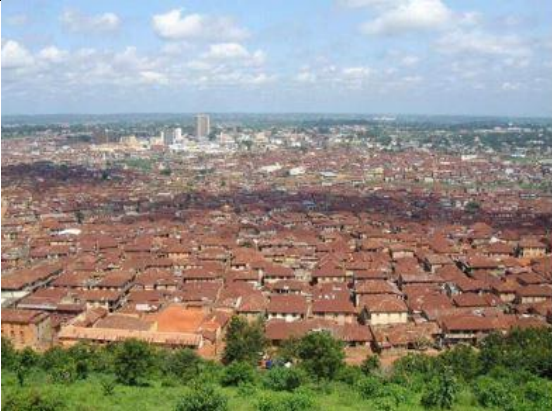




Port Harcourt a.		Dense mix low-rise buildings along the coastal area with large open water bodies. Scattered tree and abundance of pervious land cover	LCZ7
b.		Commercial centre having sparsely mid-rise solid buildings with medium traffic flow. Scattered tree and abundance of impervious land cover	LCZ2 – LCZ6
c.		Sky view of residential and commercial suburbs with plants and trees scattered. Abundance of pervious and impervious land cover	LCZ3 – LCZ7
d.		Industrial area with abundance of natural surface cover and scarce vegetation. Low traffic flow.	LCZ10
e.		Medium density buildings sparsely arranged with trees and abundance of pervious land cover. Medium traffic density	LCZ2 – LCZ4





Warri (Uvwie) a.		Wetland and uncultivated field on the outskirts of the city. Low plant cover with no traffic flow	LCZ6
A/Ibom (Eket) a.		Residential and commercial areas having sparsely mid-rise solid buildings with medium traffic flow. Scattered trees and abundance of pervious and impervious land cover	LCZ3 – LCZ7
		Wetland and uncultivated field on the outskirts of the city. Low plant cover with no traffic flow	LCZ6




Onitsha a.		Array of low-rise buildings. Densely populated with high traffic flow. Few or no trees and abundance of impervious land cover	LCZ3
b.		Dense mix of midrise building with few or no trees and medium traffic flow. Abundance of bare soil or sand	LCZ2 – LCZ5
c.		Compact mid-rise residential buildings with few or no trees. Abundance of pervious land cover and no traffic	LCZ2 – LCZ5
Kano a.		Commercial centre having sparsely mid-rise solid buildings with medium traffic flow. Scattered tree and abundance of impervious land cover	LCZ4 – LCZ6
b.		Dense mix low-rise and single-story buildings with few or no trees	LCZ7
c.		Dense mix of midrise building with few trees and medium traffic flow. Abundance of pervious and impervious land cover	LCZ5

d.		Dense mix of midrise solid buildings with few or no trees and medium traffic flow. Abundance of impermeable surface	LCZ5
Ibadan		Dense mix low-rise and few tall buildings with abundance of plants and trees.	LCZ3 – LCZ7
		Dense mix of midrise building with few or no trees and medium traffic flow. Abundance of impervious land cover	LCZ5
		Dense mix of midrise building with few or no trees and medium traffic flow. Abundance of bare paved surface	LCZ5



Akure a.		Commercial centre having sparsely mid-rise solid buildings with medium traffic flow. Scattered tree and abundance of impervious land cover	LCZ4 – LCZ6
b.		Medium mix array of low-rise buildings with light or no traffic flow. Shrubs and grasses, mostly pervious.	LCZ6
c.		Dense mix of midrise building with few or no trees and high traffic flow. Abundance of impervious land cover	LCZ5
d.		Low-rise residential layout buildings with light or no traffic and abundance of vegetation	LCZ6



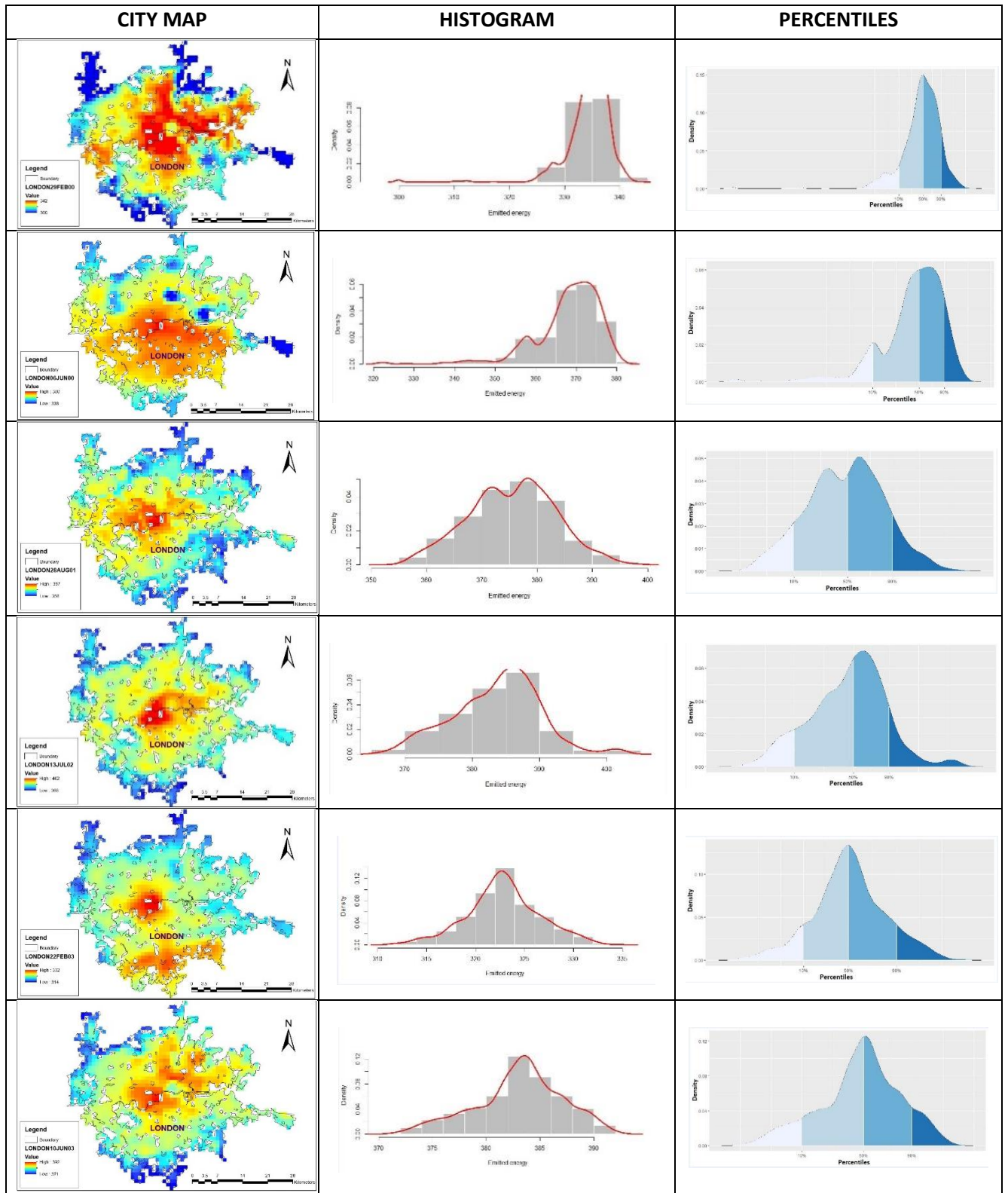
e.		Spatially dense mix of midrise buildings with abundance of trees and medium traffic flow. Permeable and impermeable surface.	LCZ5

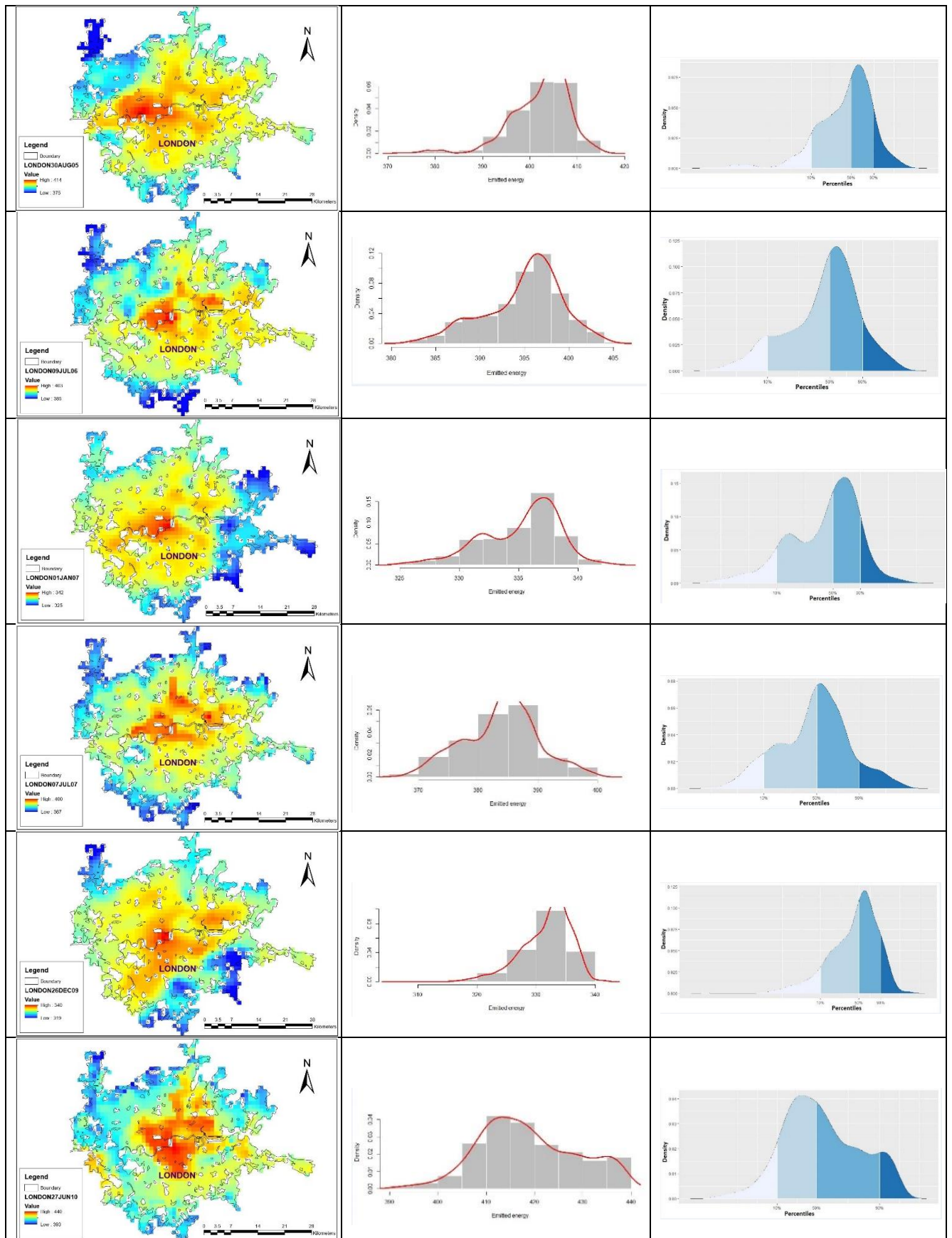
**Fig. 4S8 Classification of field sites by local climate zone (LCZ) according to some selected cities in Nigeria (Sources: (Nduka and Abdulhamed, 2011); (Balogun et al., 2012); (Usman et al., 2016); (MyGuide, 2017); (Juju films, 2018); (Nairaland, 2018))**

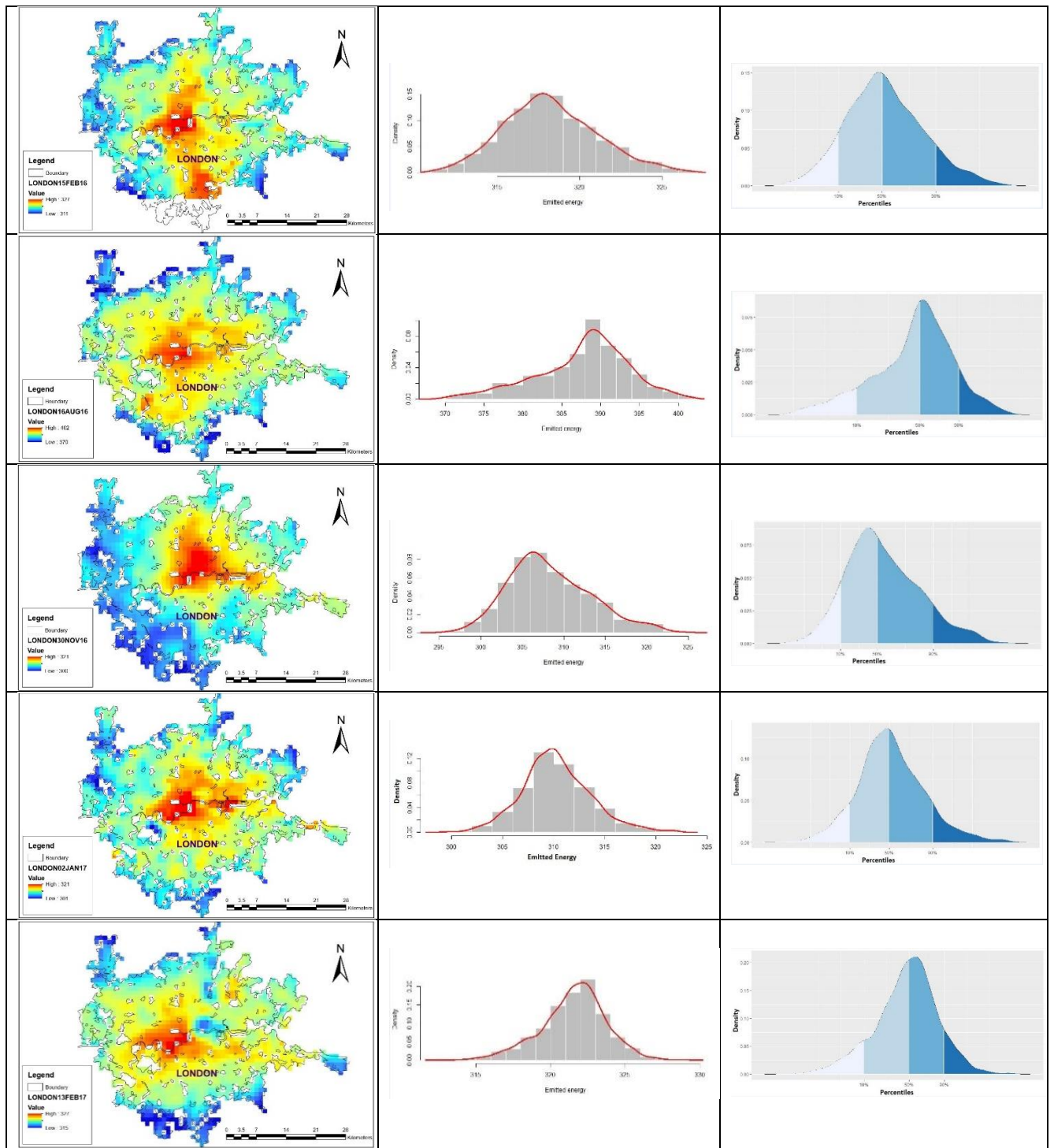
## **Appendices**

# Appendix A

## LONDON







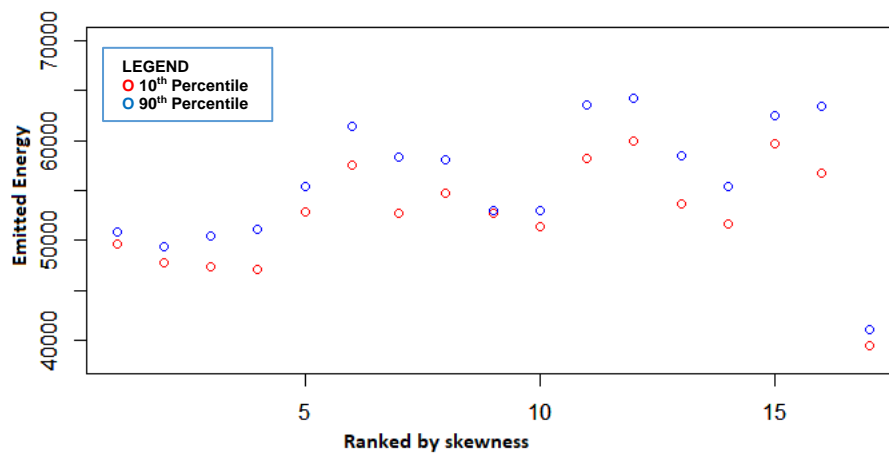


Fig. 5.9 The sum below 10<sup>th</sup> (red) and the sum above 90<sup>th</sup> (blue) percentiles for all sample nights in London city

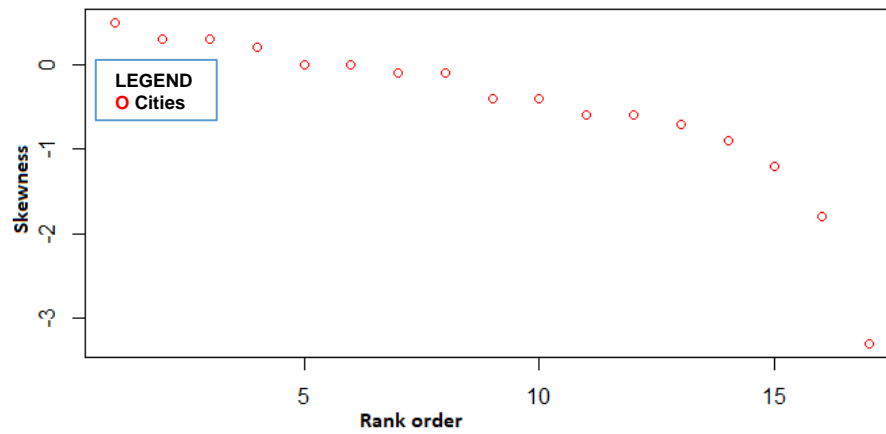


Fig. 5.10 Skewness for all sample nights in London city

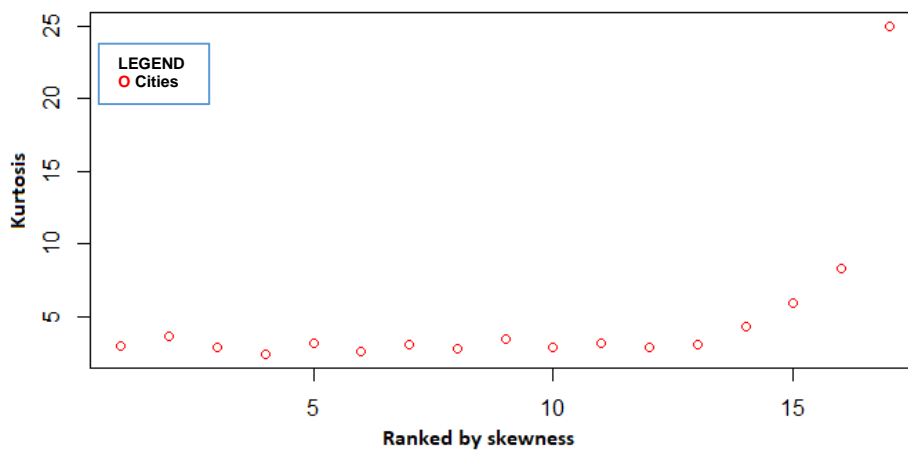
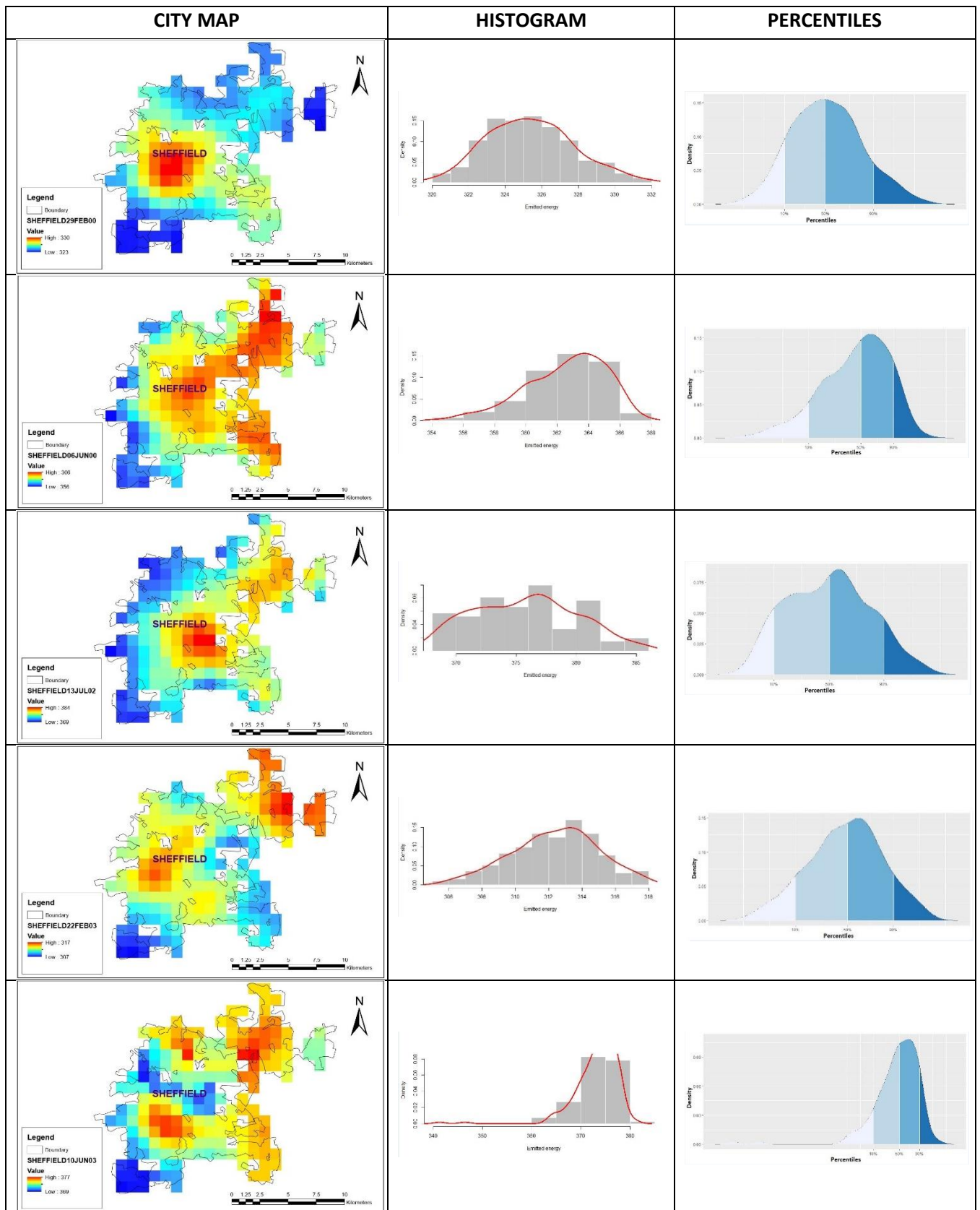


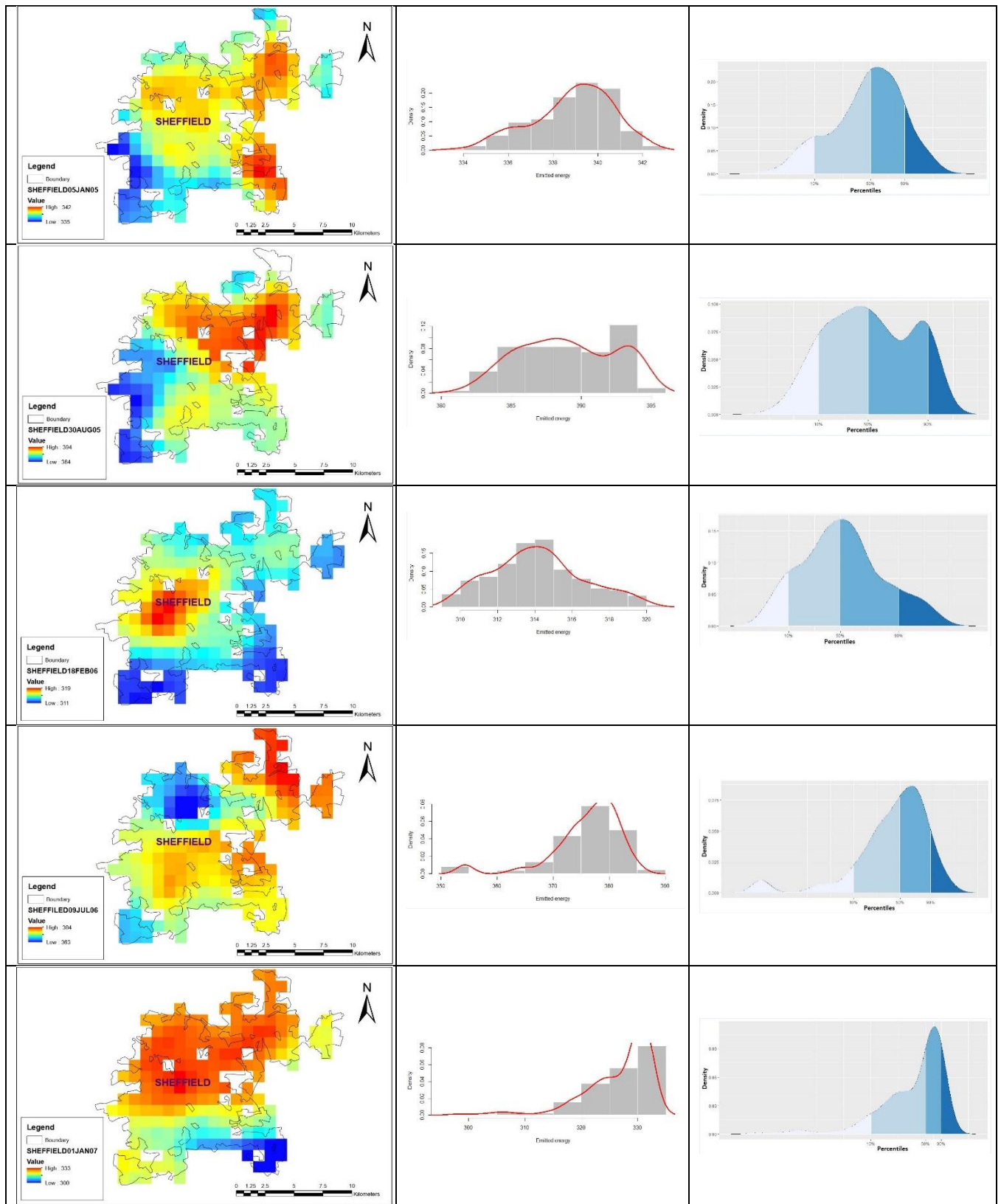
Fig. 5.11 Kurtosis for all sample nights in London city



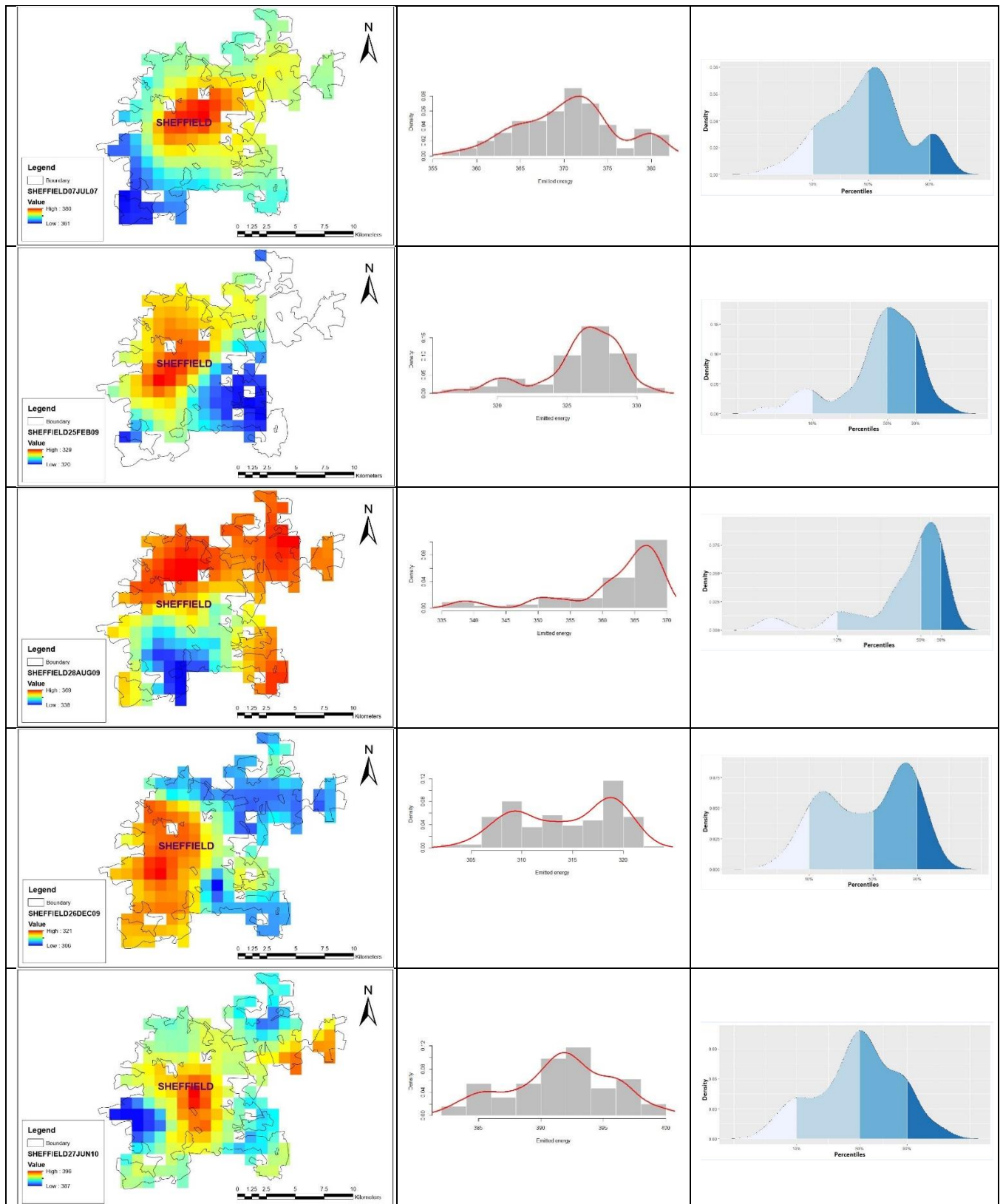
## Appendix B

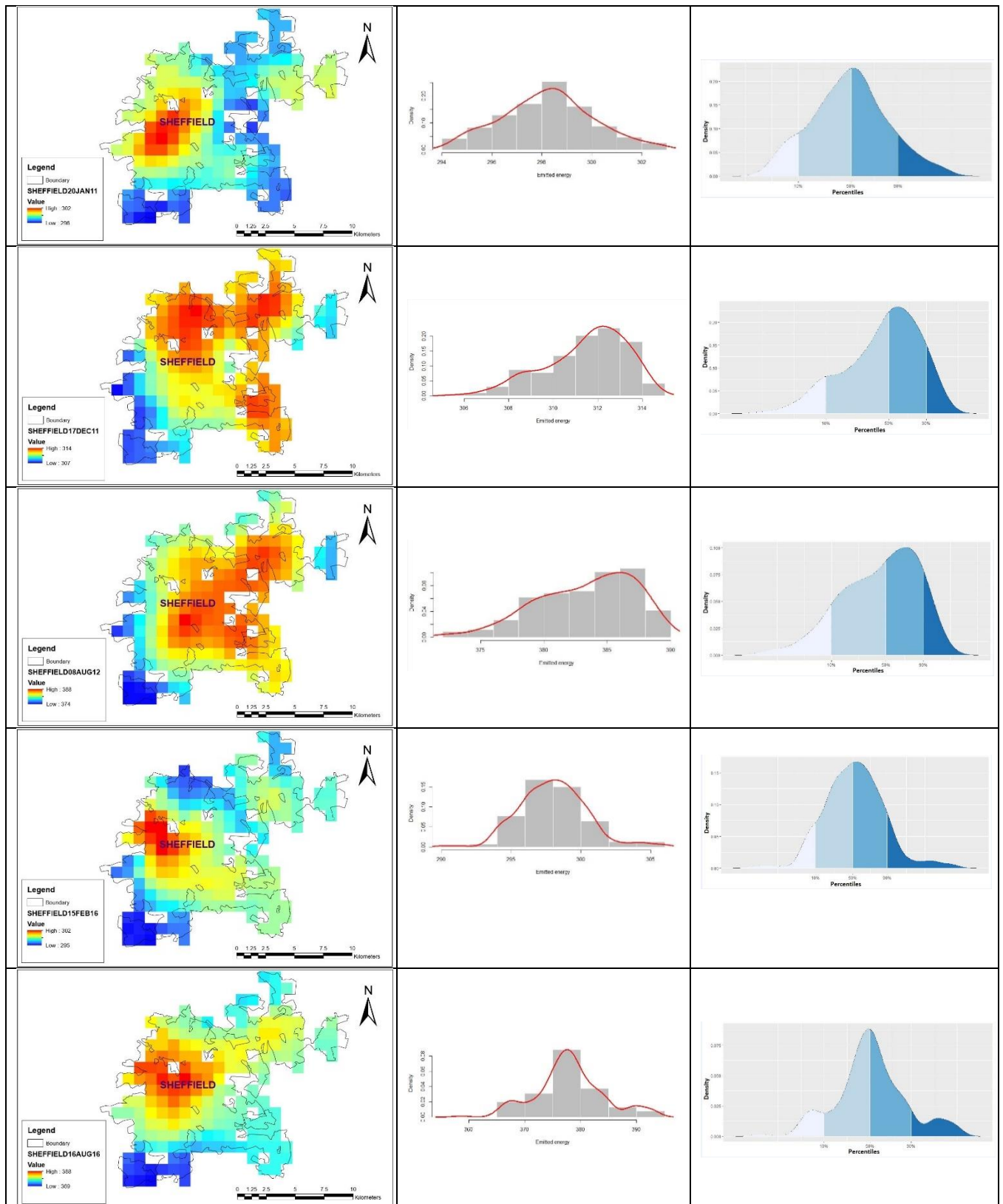
### SHEFFIELD

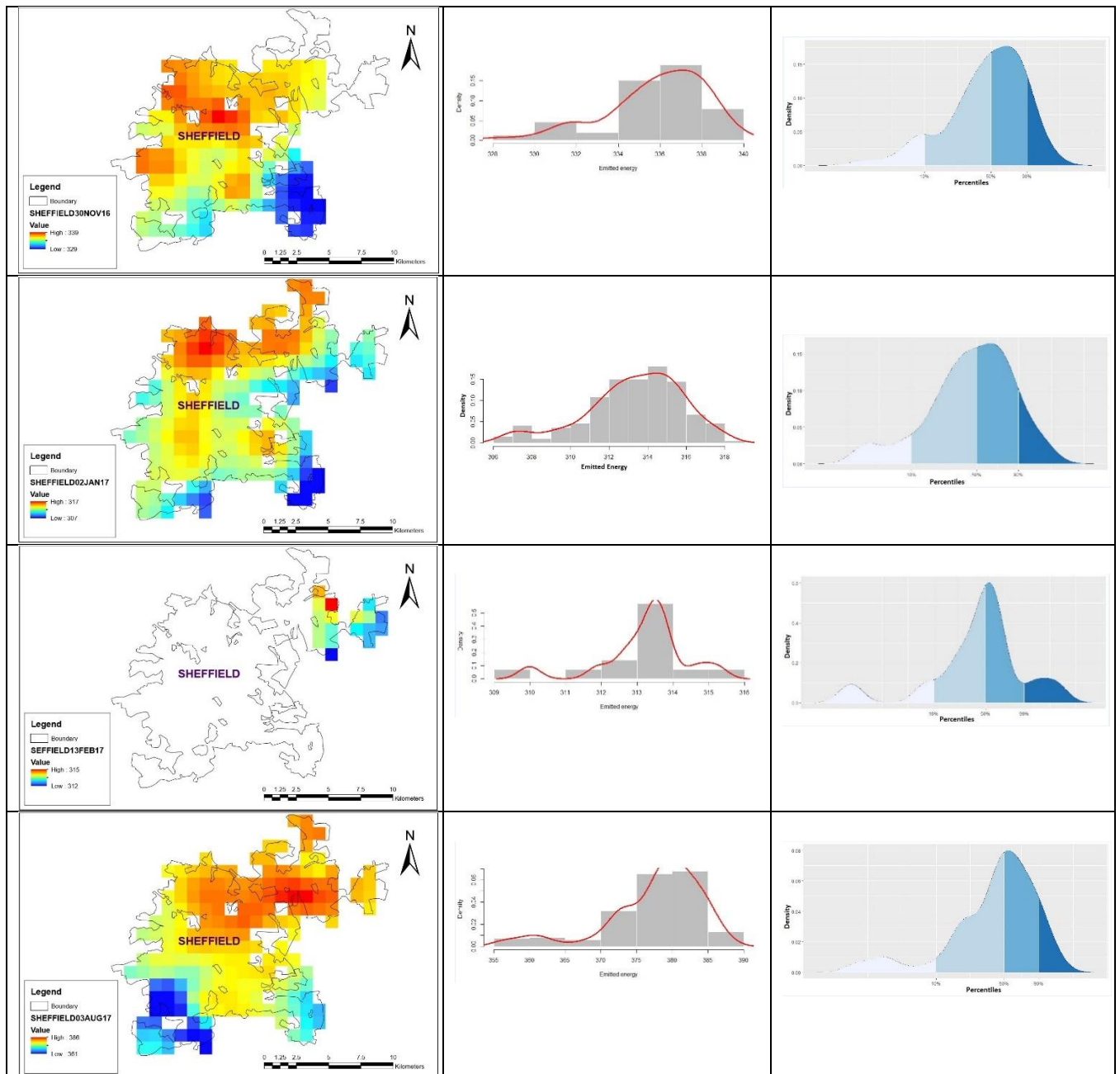












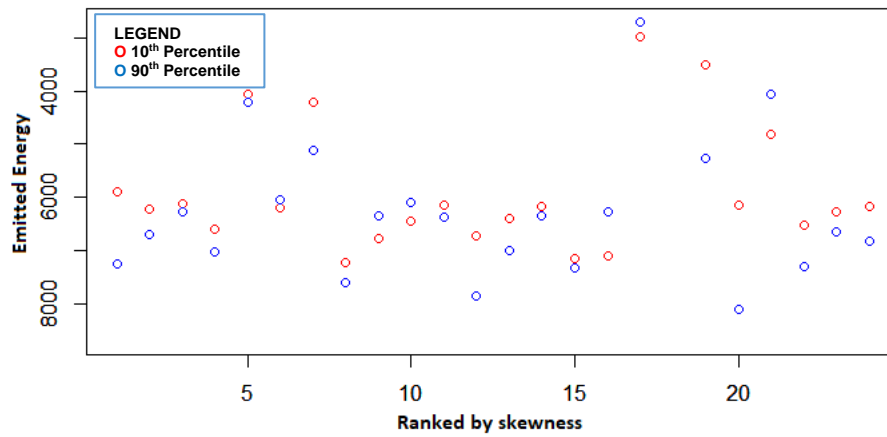


Fig. 5.12 The sum below 10<sup>th</sup> (red) and the sum above 90<sup>th</sup> (blue) percentiles for all sample nights in Sheffield city

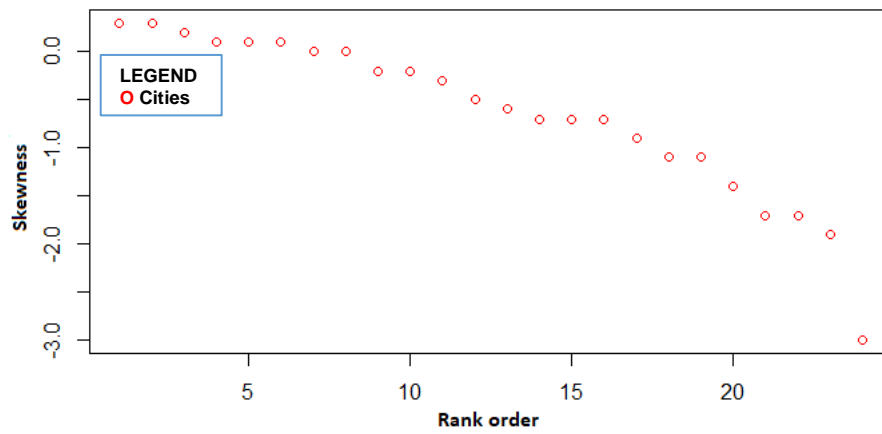


Fig. 5.13 Skewness for all sample nights in Sheffield city

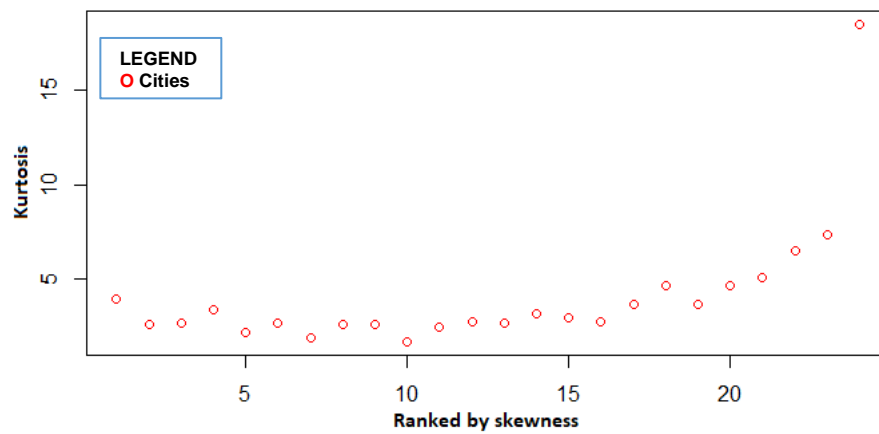
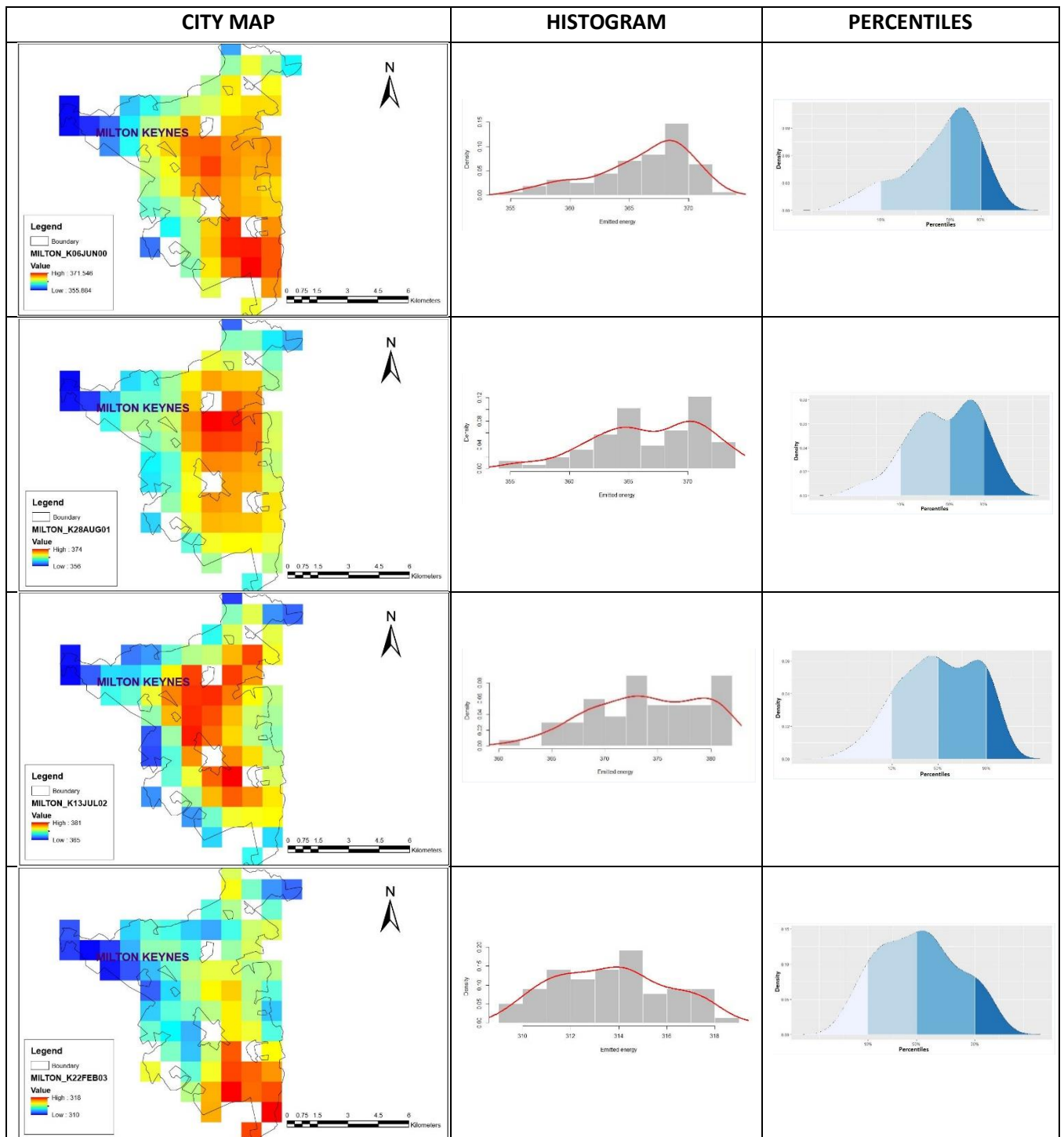


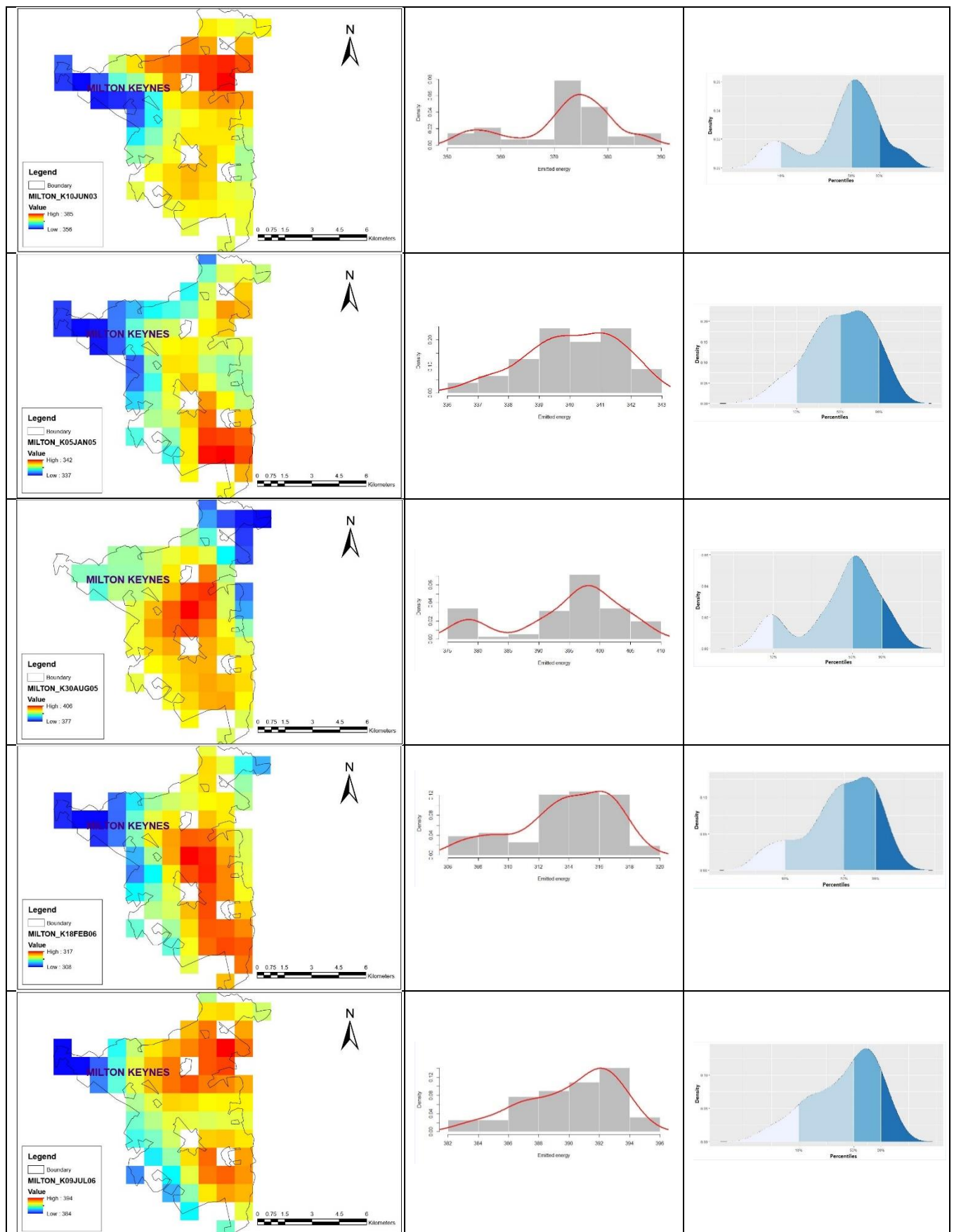
Fig. 5.14 Kurtosis for all sample nights in Sheffield city

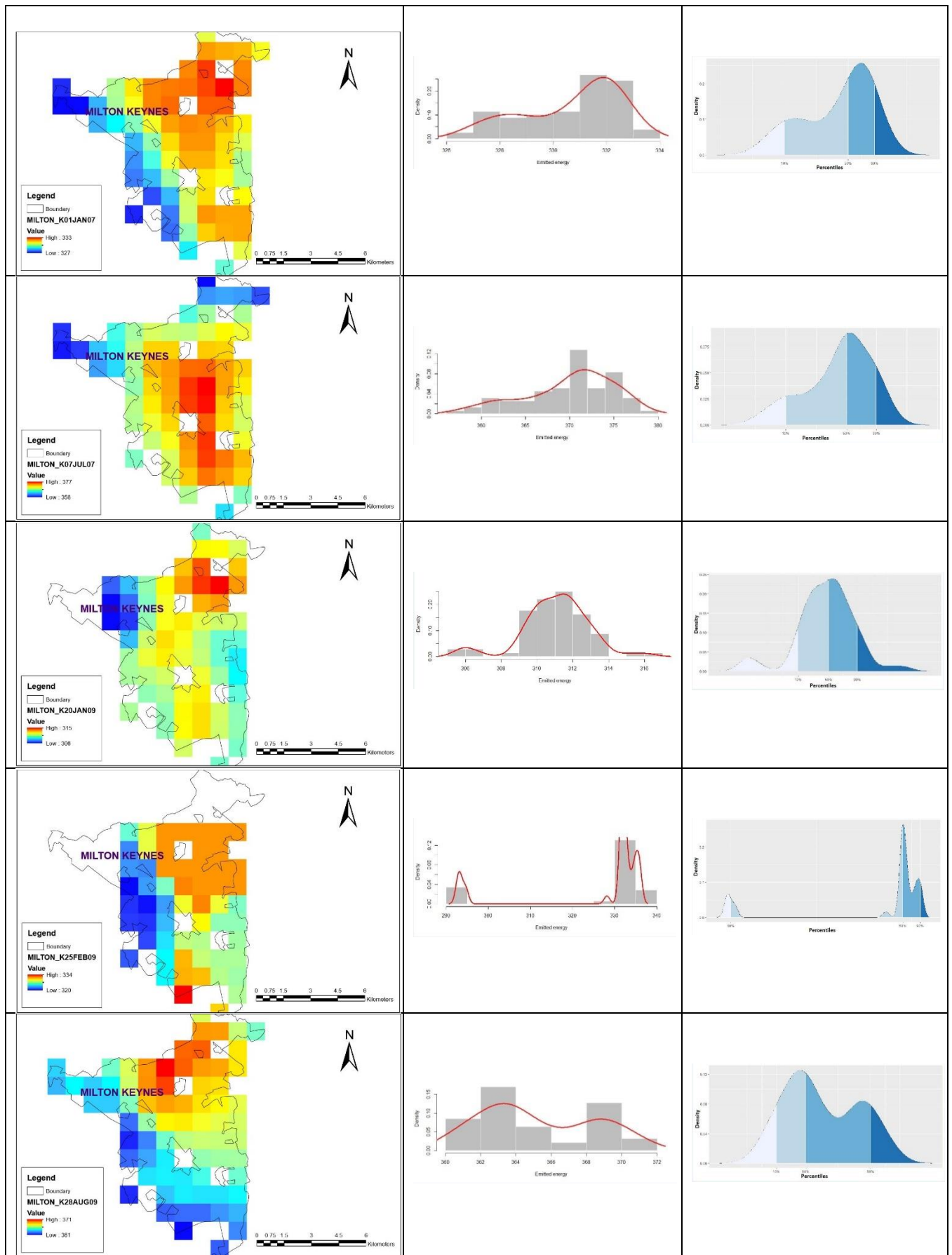
## Appendix C

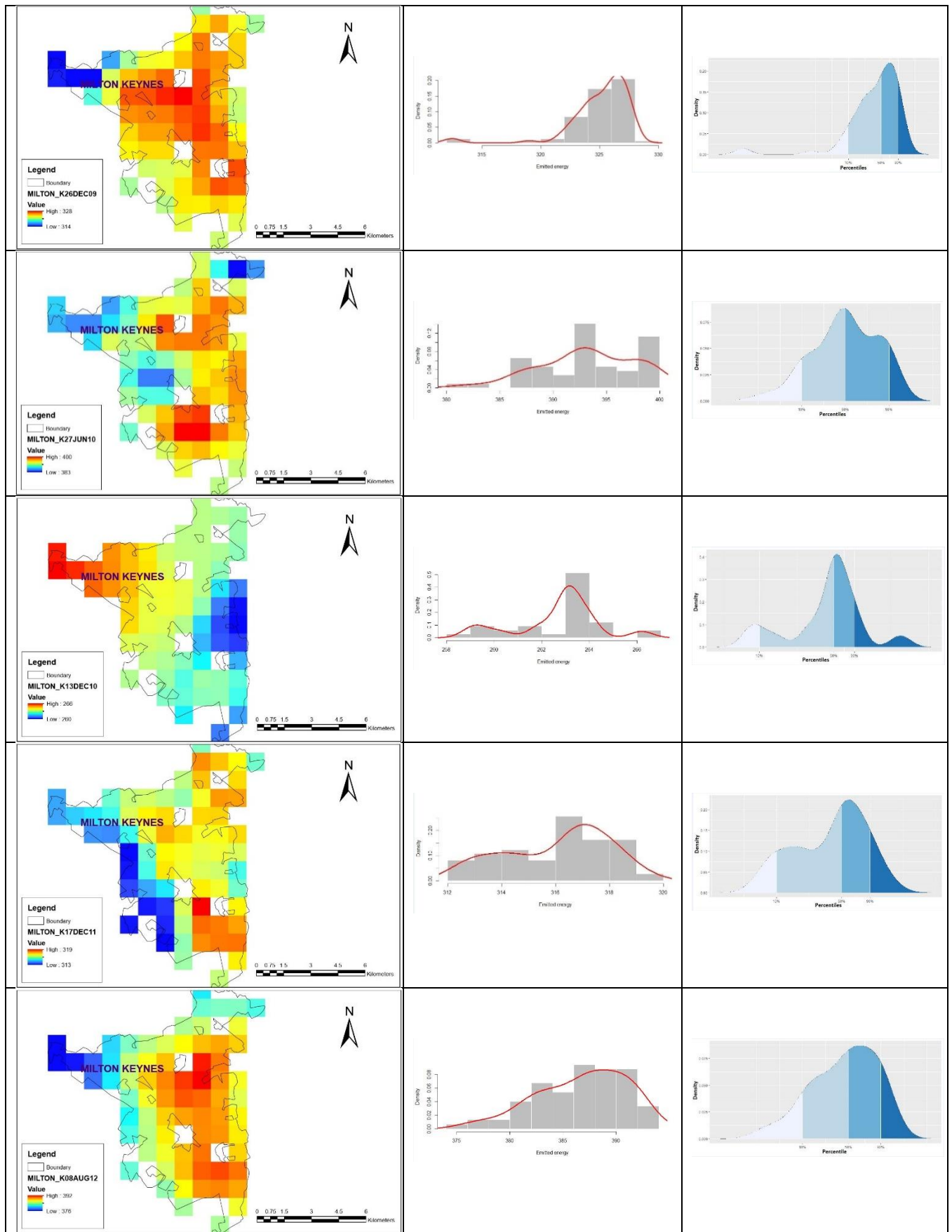
### MILTON KEYNES



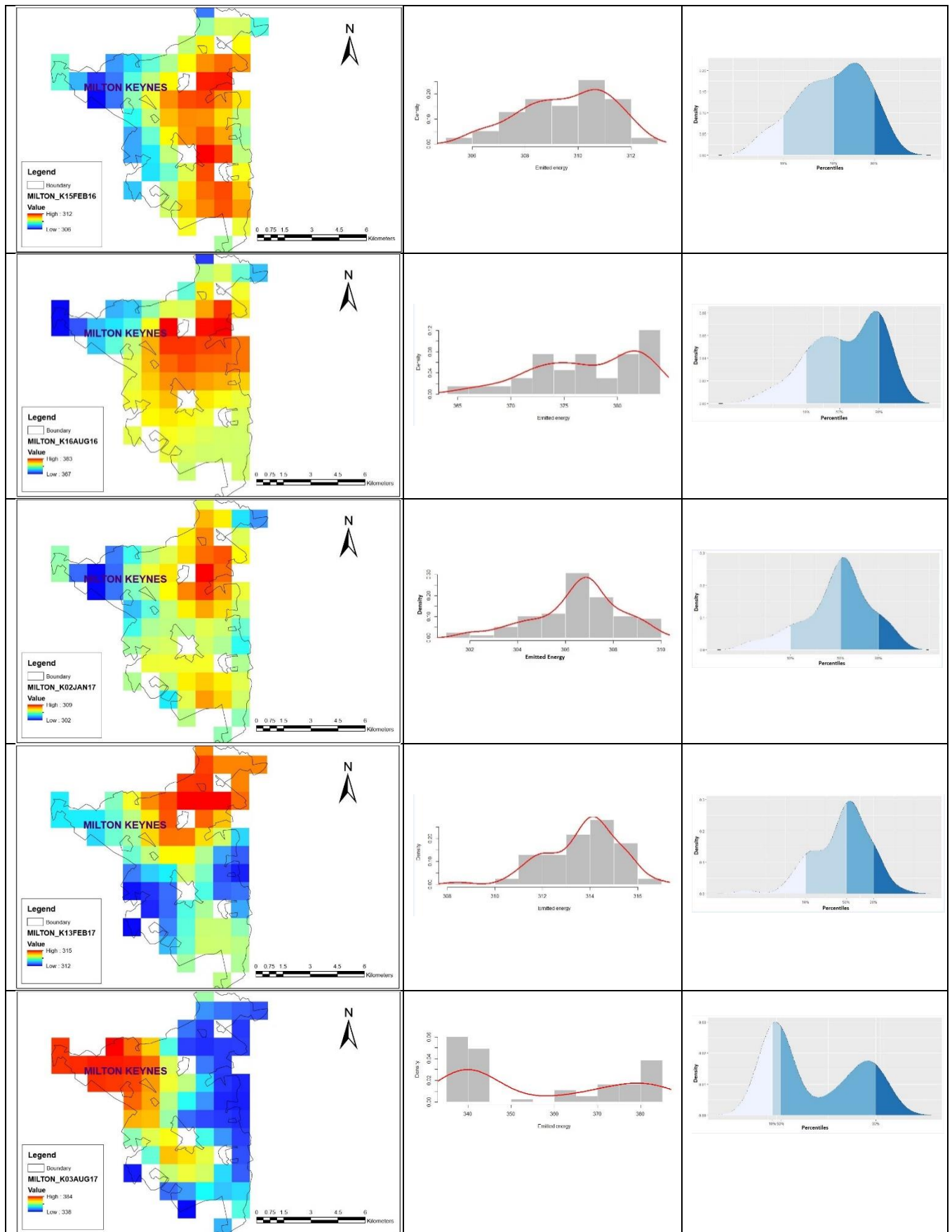












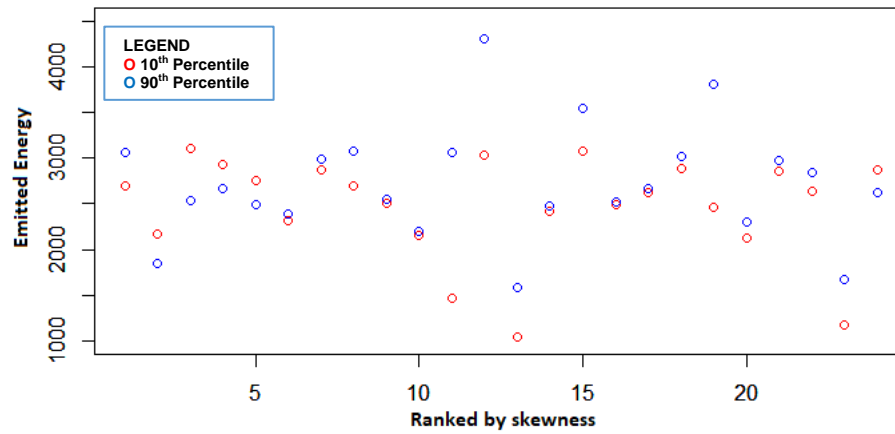


Fig. 5.15 The sum below 10<sup>th</sup> (red) and the sum above 90<sup>th</sup> (blue) percentiles for all sample nights in Milton Keynes city

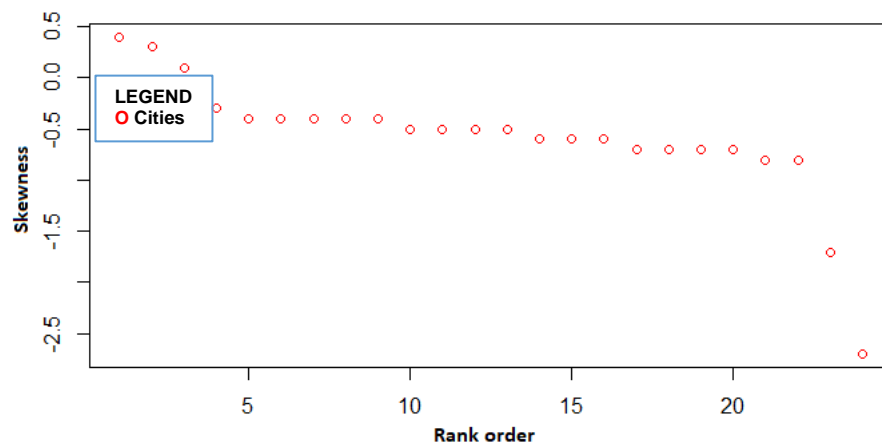


Fig. 5.16 Skewness for all sample nights in Milton Keynes

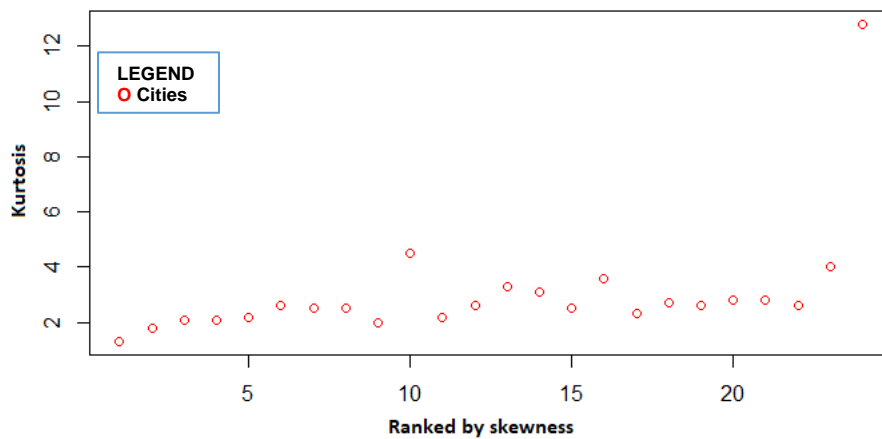


Fig. 5.17 Kurtosis for all sample nights in Milton Keynes city

## Appendix D

### Published paper

City and Environment Interactions 5 (2020) 100037



Contents lists available at ScienceDirect

## City and Environment Interactions

journal homepage: [www.elsevier.com/locate/cacint](http://www.elsevier.com/locate/cacint)



### Allometric scaling of thermal infrared emitted from UK cities and its relation to urban form



M. Abdulrasheed<sup>a</sup>, A.R. MacKenzie<sup>a,b,\*</sup>, J.D. Whyatt<sup>c</sup>, L. Chapman<sup>a</sup>

<sup>a</sup> School of Geography, Earth and Environmental Science, University of Birmingham, Edgbaston, B15 2TT Birmingham, UK

<sup>b</sup> Birmingham Institute of Forest Research, University of Birmingham, Edgbaston, B15 2TT Birmingham, UK

<sup>c</sup> Lancaster Environment Centre, Lancaster University, Lancaster LA1 4YQ, UK

#### ARTICLE INFO

##### Article history:

Received 25 February 2020

Received in revised form 27 May 2020

Accepted 30 May 2020

Available online 03 June 2020

##### Keywords:

Urban Heat Island (UHI)

Land Surface Temperature (LST)

Allometry

Urban size and population

Geographic information system (GIS)

MODIS and emitted energy

#### ABSTRACT

As a result of differences in heat absorption and release between urban and rural landscapes, cities develop a climate different from their surroundings. The rise in global average surface temperature and high rates of urbanization, make it important to understand the energy balance of cities, including whether any energy-balance-related patterns emerge as a function of city size. In this study, images from the Moderate Resolution Imaging Spectro-radiometer (MODIS) satellite instrument, covering the period between 2000 and 2017, were sampled to examine the seasonal (winter and summer) night-time clear-sky upwelling long-wave energy for 35 UK cities. Total (area-summed) emitted energy per overpass per city is shown to correlate closely ( $R^2 \geq 0.79$ ) with population on a log-log 'allometry' plot. The production of emitted energy from the larger cities is smaller than would be produced from a constellation of smaller cities housing the same population. The mean allometry slope over all overpasses sampled is  $0.84 \pm 0.06$ , implying an 'economy (or parsimony) of scale' (i.e., a less-than-proportional increase) of about 21% (i.e.  $100(2-10^{0.84 \log(2)})$ ) for each doubling of city population. City area shows a very similar economy of scale, so that the scaling of night-time emitted energy with urban area is close to linear ( $1.0 \pm 0.05$ ). This linearity with area indicates that the urban forms used in UK cities to accommodate people more efficiently per unit area as the urban population grows, do not have a large effect on the thermal output per unit area in each city. Although often appearing superficially very different, UK cities appear to be similar in terms of the components of urban form that dictate thermal properties. The difference between the scaling of the heat source and literature reports of the scaling of urban-rural air (or surface) temperature difference is very marked, suggesting that the other factors affecting the temperature difference act to decrease strongly its scaling with population.

# Allometric scaling of thermal infrared emitted from UK cities and its relation to urban form

M. Abdulrasheed<sup>1</sup>, A.R. MacKenzie<sup>1, 2\*</sup>, J.D. Whyatt<sup>3</sup>, L. Chapman<sup>1</sup>

1. School of Geography, Earth and Environmental Science, University of Birmingham, Edgbaston, B15 2TT, Birmingham, UK

2. Birmingham Institute of Forest Research, University of Birmingham, Edgbaston, B15 2TT, Birmingham, UK

3. Lancaster Environment Centres, Lancaster University, Lancaster LA1 4YQ UK

\* Corresponding author

## ABSTRACT

As a result of differences in heat absorption and release between urban and rural landscapes, cities develop a climate different from their surroundings. The rise in global average surface temperature and high rates of urbanization, make it important to understand the energy balance of cities, including whether any energy-balance-related patterns emerge as a function of city size. In this study, images from the Moderate Resolution Imaging Spectro-radiometer (MODIS) satellite instrument, covering the period between 2000 and 2017, were sampled to examine the seasonal (winter and summer) night-time clear-sky upwelling long-wave energy for 35 UK cities. Total (area-summed) emitted energy per overpass per city is shown to correlate closely ( $R^2 \geq 0.79$ ) with population on a log-log 'allometry' plot. This area-summed night-time emitted energy is found to scale sub-linearly with population on both summer and winter nights, with a mean slope over all overpasses sampled of  $0.84 \pm 0.06$ , implying an 'economy (or parsimony) of scale' of about 21% (i.e.  $100(2 - 10^{0.84 \log(2)})$ ) for each doubling of city population. City area shows a very similar economy of scale, so that the scaling of night-time emitted energy with urban area is close to linear ( $1.0 \pm 0.05$ ). This linearity with area indicates that the urban forms used in UK cities to accommodate people more efficiently per unit area as the urban population grows, do not have a large effect on the thermal output per unit area in each city. Although often appearing superficially very different, UK cities appear to be similar in terms of the components of urban form that dictate thermal properties. The difference between the scaling of the heat source and a literature report of the scaling of urban-rural air temperature difference (UHI) is very marked, suggesting that the other factors affecting the UHI act to decrease strongly the scaling with population.

## HIGHLIGHTS

- MODIS was used to assess the clear-sky upwelling long-wave energy for the thirty-five (35) most populous UK urban areas;
- A robust, sub-linear, scaling relationship between total urban population and total emitted energy demonstrates a thermal 'economy (or parsimony) of scale' with respect to population.
- The scaling relationships with population for city area and for emitted energy suggest a testable hypothesis regarding the similarity of energy budgets across urban areas of very different sizes.

**Keywords:** Urban Heat Island (UHI); Land Surface Temperature (LST); Allometry; Urban size and population; Geographic Information System (GIS); MODIS and Emitted energy

## 1.0 INTRODUCTION

Urbanization is accelerating across the world, especially in developing countries across Africa and Asia (Martins, 2000; Cohen, 2006). Current projections indicate that by 2050, the global urban population will increase by 2.4 billion, i.e., about half the current population of 4.22 billion (United Nation, 2019) (Seto et al., 2012; Buhaug and Urdal, 2013; Bremner et al., 2010; Bongaarts, 2009). The change of land surface characteristics caused by urbanisation leads, amongst other things, to changes in the local energy balance that must be taken into account when determining long-term temperature trends (Chrysanthou et al., 2014). This change in thermal climate in urban areas, leads to the urban heat island (UHI), which is the tendency of an urban area to have warmer near-surface air temperatures than its rural surroundings (Bornstein, 1968; Landsberg, 1981; Oke, 1995; Sheng et al., 2017). Related phenomena include: urban thermal plumes (Oke, 1995; Heaviside et al., 2015) and urban precipitation anomalies (Han et al., 2013).

Recent conceptual UHI models have emphasised the importance of different land uses within cities (Stewart and Oke, 2012; Tomlinson et al., 2012), highlighting the prospect that urban planning choices can be used to mitigate adverse urban climate trends (Davoudi, 2012; Davoudi, 2014). Implicit in most studies of UHI, from Howard (1818) on, is that local, one-dimensional (i.e., vertical), energy budgets for urban land uses, combine through the action of fluid stirring and mixing, to produce a three-dimensional dome of urban heating over a city — see, for example, the very widely reproduced

cross-sections of UHI through an idealised city (e.g., Lemmon and Warren, 2004).

We hypothesise that gross changes in urban form as the size of cities increase affect the storage of solar heating. We focus on night-time, clear-sky, emitted long-wave as a primary measure of heat storage, and we use population as our yardstick of city size. We use an extensive property — total emitted energy (in Megawatts) per city per night — rather than intensive property such as temperature or emission per unit area, to permit direct comparisons with other extensive properties such as urban area, and to explore the extent to which the behaviour of intensive properties, particularly UHI, differ from the behaviour of the extensive properties.

### 1.1 Urban Form and urban heat

The urban form of a city is the result of its social, economic, and environmental context. We focus on UK cities in this study; further work will focus on a different setting in order to try and distinguish the general from that dependent on UK context (Abdulrasheed, 2020). A recognised system of UK urban planning mostly originates from the industrial revolution, prior to which most people lived and worked in the countryside (Inikori, 2002; CPRE, 2018). As industries grew, people migrated to towns and cities in search of better wages, opportunities, and livelihood (Karp, 2013) leading to rapid growth in town and cities. Many decrees and ordinances were issued to manage this growth, including, at the beginning of the 20<sup>th</sup> century, the Town Planning Act 1909, which was introduced to ensure that local authorities prepared schemes of town planning. This was followed by the Housing Act 1919, which required the

design of houses to be approved by the Ministry of Health, and the Housing Act 1930, which required clearance of high-density 'slums', which were considered unsanitary (Carmon, 1999). The post-war 1940s was a period of uncertainty for the architects and town planners tasked with rebuilding Britain's bomb-damaged cities (Tsubaki, 2000; Ball and Maginn, 2005; Hollow, 2012). Residential rebuilding in this period often involved the replacement of low-rise private dwellings with fewer, but larger, high-rise public buildings (Carmon, 1999), sometimes with an intermediate period of low-rise prefabricated structures (Short, 1982). Cities across the UK such as Bristol, Coventry, Hull, Portsmouth, Southampton and Plymouth were very severely damaged during World War II (Hasegawa, 2013), and so were subject to significant post-war changes. For those neighbourhoods, which, by the 1960s and 1970s, had escaped slum clearance or destruction in wartime, the tendency was for renewal rather than replacement of low-rise and mid-rise residential buildings (Carmon, 1999). In the subsequent decades, and until the present day, a more laissez-faire approach has dominated, with renewal and replacement of housing and commercial buildings through private-public cost sharing of various kinds (Carmon, 1999; Hasegawa, 2013; Webb, 2018) .

Emerging in parallel, from the latter part of the nineteenth century and through the first part of the 20<sup>th</sup> century, was the Garden Cities movement, which advocated public health improvement by planning to build cities with more, and more accessible, green spaces, see e.g., (Burnett, 1986). This advocacy eventually led to the New Towns movement and New Towns

Act 1946 (Goist, 1974; Rubin, 2009; Alexander, 2009; Tizot, 2018) which resulted in towns such as Telford, Letchworth and Milton Keynes. All the 20<sup>th</sup>-century housing and town planning policies in the UK led to notable changes in the urban form from the scale of individual dwellings, through neighbourhood scale land-use, to the patterns of use across whole urban areas.

The nature and patterns of urban form (i.e. building geometry, pervious surface fraction, building and tree densities, soil permeability etc.) determine the thermal characteristics of place. Such characteristics can be used to define local climate zones (LCZ)(Stewart et al., 2014), which may vary over time as a result of planned or unplanned changes. For example, slum clearance often re-shaped low-rise, close-packed, terraced housing into a sparse array of high-rise towers e.g., (Carmon, 1999). Suburban extension of cities replaced farm field (or, often, filled in parkland estates around large houses) with semi-detached two storey housing in wide boulevards (shifting from linear form to cul-de-sac mid-century). Infilling (building in what had previously been back gardens) became prominent towards the end of the 20<sup>th</sup> century (Whitehand and Whitehand, 1983).

As cities grow, green space — trees and vegetation — are replaced with grey space, i.e., buildings and transport and utility infrastructure. The magnitude and nature of the change is often sporadic and patchy, and results in a wide variety of urban forms (Morris, 1974; Hopkins, 2012). In terms of the surface energy balance, changing from rural to urban land results, in general, in the absorption of a higher fraction of incoming solar radiation and a decrease in the Bowen ratio (i.e., the ratio of sensible

to latent heat emission) (Arnfield, 2003; Aguado and Burt, 2015). Energy absorption and emission at the ground surface is therefore a key driver of urban climate, strongly influencing the near surface air temperature and the radiant fluxes relevant for health effects (e.g., Basu and Samet, 2002; Middel and Krayenhoff, 2019). Satellite based studies report thermal emission as land-surface temperature (or 'skin' temperature), from which surface UHI intensity (SUHI) can be derived (e.g., Peng et al., 2012; Zhou D. et al., 2014; Zhou B. et al., 2017). In-situ sensing reports air temperature directly. Near-surface air temperature UHI and SUHI do not always correspond for a variety of physical reasons (Voogt and Oke, 1998; 2003; Arnfield, 2003; Schwarz et al., 2011; Sheng et al., 2017) but both are driven by absorption and emission of energy at the ground surface. The fundamental role of surface energy exchange motivates us to investigate how surface energy parameters vary for a set of cities of very different size and urban form, in order to understand this foundational driver of both the UHI and SUHI.

Buildings also slow the wind near the surface, retaining the heat released from vehicles and buildings (Golden, 2004; Arifwidodo and Tanaka, 2015). Energy removed from the mean wind is lost to the surfaces or transformed into turbulent kinetic energy, affecting the dissipation of scalars such as temperature and trace-gas pollutants e.g., (Belcher et al., 2003). Dense building arrangements decrease the sky-view factor (Chapman and Thornes, 2004; Grimmond, 2007; Yang et al., 2015). The net result of all these changes is the increased storage of heat, which is the root cause of the UHI effect. Increased heat storage can lead to a number of issues such

as human health risk (Basu and Samet, 2002; Rosenzweig et al., 2011; Murray and Ebi, 2012; Smith et al., 2011; Patz et al., 2005; Hondula et al., 2015; Wouters et al., 2017; Krayenhoff et al., 2018; Middel and Krayenhoff, 2019), environmental hazard (e.g., Chapman and Thornes, 2006), and infrastructure failure (Chapman and Bell, 2018; Dawson et al., 2018), which themselves often require further energy consumption to offset (Li et al., 2015).

Researchers have long studied the effects of urban form on climate change, and the impacts of climate change on urban environment, as reviewed in (Mills, 2007) and (Seto et al., 2010). Urban planning responses to urban heat and climate change, including both mitigation and adaptation strategies, continue to evolve, especially with respect to sustainable urban development in cities (Jabareen, 2006 ; Rybski et al., 2017; Davoudi et al., 2009; Hendrickson et al., 2016; Castán Broto, 2017; Fujii et al., 2017). Urban climate adaptation focuses on reducing vulnerability and promoting resilience of people and properties (Amundsen et al., 2010; Carmin et al., 2012; Anguelovski et al., 2014). Microclimate planning and design modification to outdoor environment can also enhance thermal comfort, e.g., neighbourhood streets trees, green spaces and parks, (Brown, 2011; OECD, 2014). We expect that planning responses to urban heat will manifest in the relationship of urban form to city size.

## 1.2 Allometry and urban heat

Allometry is originally a concept from biology, relating morphological and physiological aspects of organism biology

to some more easily measured parameters such as body mass (Schmidt-Nielsen, 1984; Gould, 1966; Lee, 1989; Small, 2012). Allometric approaches were introduced to urban studies (e.g. West and Brown, 2005; Naroll and Bertalanffy, 1956; Nordbeck, 1971) and used to model the relationship between a set of cities and the largest city within a geographical region (Small, 2012). Urban allometry studies have sought to elucidate decadal evolution of urbanized area (Lee, 1989; Longley et al., 1991), fractal spatial patterning (Chen, 2010), income inequality (Sarkar et al., 2018), and between urban form and growth (Bettencourt et al., 2007). Interpretations drawn from urban allometry include growth by innovation driven by economies of scale (Batty, 2008), and urban form as a hierarchy of clusters, (Bettencourt, 2013).

In general, for urban studies, allometric scaling relates aspects of urban material, energy, or economic flows to the size of cities as determined by their population (Bettencourt, 2013; Batty, 2008; Lee, 1989; Longley et al., 1992). Because it focuses on the relative rate of change of properties with size, referred to as ‘scaling’ below, allometry lends itself to comparative studies of properties of very different character (Bettencourt and West, 2010). In our previous study of air pollutant emissions and concentrations, we found it informative to compare the scaling of an intensive property (urban air concentrations) with the scaling of extensive properties (area-summed pollutant emissions and urban area) (MacKenzie et al., 2019).

Allometric scaling recognises that the many microscopic interactions within a complex system often collapse to a simple pattern (Cottineau et al., 2017). Scaling, therefore, allows us a synthesising

perspective on cities (Batty, 2008), by searching for simple patterns without becoming overwhelmed by details of local context.

Allometric patterns, where they exist, conform closely to an equation of the form:

$$Y = \beta X^\alpha \quad (1a)$$

The power law, equation (1a), describes a straight-line relationship between the X and Y variables when the function is plotted on a double logarithmic coordinate system, i.e.

$$\log(Y) = \log(\beta) + \alpha \cdot \log(X) \quad (1b)$$

where  $\log(\beta)$  is a constant offset and  $\alpha$  is the rate of relative growth (the allometric scaling factor or, simply, slope). Below, we will refer to  $\alpha$  as defining the ‘scaling’ of Y with respect to X.

Using allometry, this study seeks a quantitative scaling relationship between population and clear-sky upwelling emitted energy, in order to determine whether and how the many detailed processes affecting this part of the urban energy budget combine at the city-scale. The study evaluates whether simplicity emerges from urban complexity with respect to emitted long-wave. We compare our findings on clear-sky upwelling long-wave to a classical result in the literature of urban heat islands.

The empirical relationship between the UHI and structure of a city arises from the fact that tall, close-packed, concrete and brick buildings store solar energy in day time and emit it at night more slowly than a flat surface (Duckworth and Sandberg, 1954). The thermal infrared energy emitted from a surface is acted on by wind



and radiation transfer processes; structural elements of a city affecting wind and radiative transfer will therefore influence UHI (Oke, 1973). Since structural elements of cities are often laid out block by block, one approach to analysing a city is to determine its energy budget and surface temperature explicitly on a block-by-block basis (Terjung and Louie, 1974; Chandler, 1966). Land-use categories and urban morphology types offer useful approaches to determining modifications to the surface energy budget that will produce a nocturnal urban heat Island (Oke, 1981; Landsberg, 1981; Eliasson, 1996). Other urban climate studies focus on the effect of the urban surface at the neighbourhood scale, using land-use classifications to generalise results (e.g. Arnfield, 2003; Stewart and Oke, 2012). At city scale the number of studies are fewer: (Landsberg, 1981) for North American settlements; (Lee, 1993) for Korea; (Eagleman, 1974) for Kansas city; and (Oke and Maxwell, 1975) for Montreal and Vancouver.

Several studies in the urban climate literature offer an allometric perspective (Oke, 1982; Torok et al., 2001), and many other comparative studies show that UHI or SUHI increases with some measure of the size of the city (e.g. Zhou B., et al., 2013; 2017; Schwarz and Manceur, 2015) or focus on the largest cities because the UHI is assumed to be largest there (e.g., Peng et al., 2012; Zhou D., et al., 2014). Oke (1973; 1982) presented the relationship between a measure of maximum UHI ( $\Delta T_{u-r}(\max)$ ) and population for European settlements (fig.1) and supports the hypothesis that the canopy air temperature,  $\Delta T_{u-r}$ , is a function of city size, with the absolute UHI increasing by about 0.6 °C (i.e.  $1.975 \cdot \log_{10}(2)$ ) for every

doubling in population. Zhou et al. (2013) fitted a sigmoidal curve to the log-linear relationship of SUHI to urban area. The sigmoidal function is approximately linear for urban clusters with areas between 2 and 200 km<sup>2</sup> with SUHI increasing by ~0.3°C for an area doubling (Zhou et al., their Figure 2). Zhou et al. (2017) plot SUHI against  $\log_e(\text{urban area})$  similarly to find a log-linear regression in which SUHI increases by about 0.4 °C (i.e.  $0.55 \cdot \log_e(2)$ ) for an area doubling.

Fig S1 in the Supplementary Information presents the Oke (1973) data in a power-law log-log graph. Regressing on  $\log_{10}(\Delta T_{u-r}(\max))$  gives more weight to the smaller cities, but a strong relationship is still found. The scaling of  $\Delta T_{u-r}$  in Fig S1 is small,  $0.11 \pm 0.03$ , but significantly different from zero — and equivalent to an increase of just 8% (i.e.  $100(10^{0.11 \cdot \log(2)} - 1)$ ) in UHI for a population doubling. Such a modest scaling with population has implications, such as that ‘densification’ of population into large urban centres presents a rather modest increased contribution of air temperature to thermal discomfort and associated health risk, at least to the extent that this can be gauged by the UHI of the 20<sup>th</sup> century city forms in Oke’s (1973; 1982) sample.

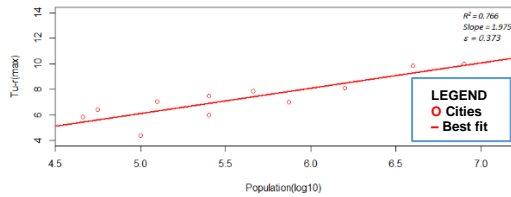
Having identified the best-fit scaling relationship, the residual offset from this best-fit for any individual city is also informative (Bettencourt et al., 2010). The residual for any city on any night,  $r_{j,k}$ , is calculated as the vertical distance of the datum for that city to the best-fit line:

$$r_{j,k} = \log(Y_{j,k}) - \{\log(\beta_k) + \alpha_k \cdot \log(X_j)\} \quad (2)$$

where  $Y_{j,k}$  is the measured value of dependent variable (in our case, the summed emitted energy of city,  $j$ , on a

given night,  $k$ ),  $X_j$  is the population, of city  $j$ , and the parameters  $\alpha_k$  and  $\beta_k$  define the allometric scaling relationship. In Oke's scaling data (Figs 1 and S1), the largest-magnitude residual is a large negative deviation (i.e. less heat island than expected) for the UK town of Reading (Oke, 1973).

**Fig 1**



**Fig.1. Relation between maximum air temperature heat island intensity ( $\Delta T_{u-r} (max)$ , degrees Celsius) and population ( $P$ ) for European Settlements (redrawn from Oke, 1982). Sources of  $\Delta T_{u-r} (max)$  are literature and private communications dating from 1927–1972. It is not clear in Oke (1973; 1982) if the population data used is matched in time to the date for  $\Delta T_{u-r} (max)$ . Reported on the graph (top right) are the Coefficient of Determination ( $R^2$ ) for the best-fit regression, the slope of the regression, and the error on the slope ( $\epsilon$ ).**

Since both the canopy air temperature UHI, and the surface temperature SUHII result from heat storage, the scaling of emitted energy (with population or urban area) will be an important contributor to the scaling of UHI and SUHII. When the observed scaling of emitted energy is larger than that for UHI or SUHII, other factors must be acting to dampen the overall scaling.

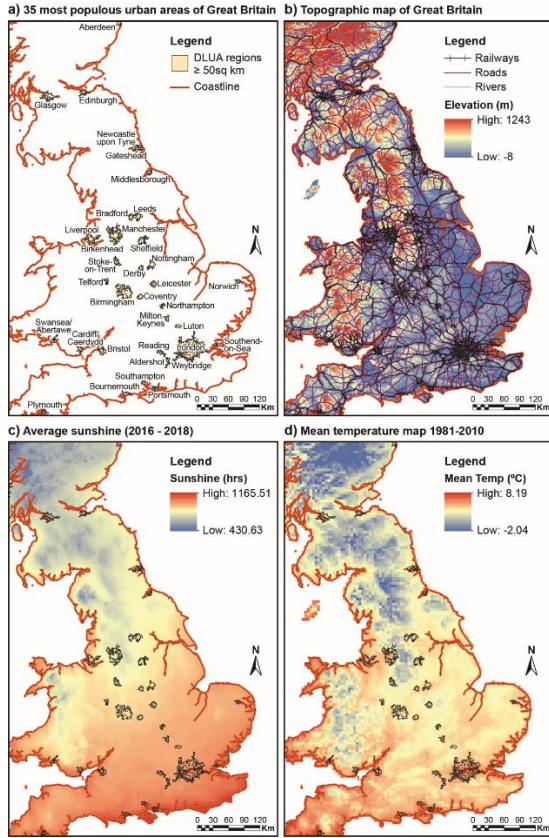
## 2.0 METHODOLOGY

### 2.1 The study area

According to the Office for National Statistics (ONS), the population of UK as at 30<sup>th</sup> June 2016 is estimated to be 65,648,000, concentrated in urban areas in the southern half of the country (Figure 2a), and with a rate

of increase of 0.8% (538,000) per annum (Office for National Statistics, 2017). The climate of UK is temperate, but variable, particularly because of altitude and distance from the coast (Figure 2b). Average temperature is 4°C January (winter) and 15°C in July (summer) (Kennedy et al., 2017; Briney, 2019). Mean climate data are shown in figure 2. This study focuses on the thirty-five (35) most populous settlements in the Great British mainland of the UK (see fig. 2a below and table S1 and fig S5 in supplementary section SI).

Boundaries for the cities were extracted from medium scale Ordnance Survey digital map data (Meridian2; see Data Sources, below) and represent contiguous Developed Land Use Areas (DLUA) rather than administrative demarcations. UHI, SUHII, and urban allometry studies are sensitive to the choice of urban boundary and this should be borne in mind in the comparisons discussed below. The urban boundary used to define population in Oke (1973) is likely administrative; the urban cluster areas used in Zhou et al. (2013, 2017) are similar to our contiguous DLUA. Population counts were retrieved from the Office of National Statistics (2017) at the lowest level of geographical aggregation (output area) and attributed to the contiguous DLUAs.



**Fig. 2 (a) 35 most populous urban areas in Great Britain (urban boundaries are contiguous Developed Land Use Areas from Meridian2 data); (b) Topographic map of central Great Britain with cities and major roads; (c) Average Sunshine of central Great Britain; (d) Mean 2m Temperature map of central Great Britain. The data were sourced from Centre for Environmental Data Analysis (CEDA, 2011), (SolarGIS, 2019), and ArcGIS tool were used to plot the maps.**

## 2.2 Data collection and analysis

This study uses MODIS/Terra V006 composite products (MOD11A1) – MODIS/Terra Land Surface Temperature and Emissivity Daily L3 Global 1km Grid SIN V006 (Wan et al., 2015). This product is useful because it is gridded, has high resolution, is cloud-cleared, is quality-controlled and quality-assured, and has accurate calibration in multiple thermal infrared bands designed for retrievals of Land Surface Temperature (LST) and atmospheric properties (Wan and Dozier, 1996; Wan et al., 2015). LST from MODIS are retrieved from

clear sky observations at daytime and night-time with the aid of a generalized split-window algorithm (Wan and Dozier, 1996; Wan, 2008). Satellite sensors looking in the nadir oversample horizontal urban surfaces and undersample vertical surfaces (Voogt and Oke, 1998; Arnfield, 2003). This sampling will tend to overemphasise both day-time heating and night-time cooling. The extent to which horizontal and vertical surface contribute to any given radiance varies with the angle of view. Angle of view also affects the native spatial resolution of the satellite radiances; interpolation in the MOD11A1 processing pipeline brings the dataset to a uniform 1-km grid. The MOD11A1 dataset contains information on view angle but we have not implemented any correction for off-nadir view geometries. For simplicity, only night-time overpasses (0130h local time) are considered for the present study.

Area-summed clear-sky night-time long-wave upwelling emitted energy (hereafter ‘emitted energy’) for mainland Great Britain was derived for selected days from 2000-2017. We interpret emitted energy in preference to LST because it gives proper weighting to radiance from the highest temperatures and provides a sum in physically meaningful units. The LST data used was selected to have as much clear sky over the region as possible. LST data for each pixel,  $i$ , within the city,  $j$ , on night,  $k$ , was converted to emitted energy,  $\epsilon_{i,j}$  in  $\text{W m}^{-2}$ , using the Boltzmann law:

$$\epsilon_{i,j,k} = \sigma T_{i,j,k}^4 \quad (3)$$

where,  $\sigma$  is the Stefan-Boltzmann constant =  $5.67 \times 10^{-8} \text{ W m}^{-2} \text{ K}^{-4}$ , and  $T_{i,j,k}$  is the LST in Kelvin. The effect of varying surface emissivity is not taken into account. Area-summed emitted energy,  $\langle E_j \rangle$  in MW, for each city on each night, was then calculated by summing the  $p$  unobscured land-surface pixels inside the city boundary:

$$\langle E_{j,k} \rangle = \sum_{i=0}^p \epsilon_{i,j,k} \Delta a \quad (4)$$

where  $\Delta a = 1 \text{ km}^2$  and the factor of  $10^6$  converting  $\text{km}^2$  into  $\text{m}^2$  is accommodated in the units of  $\langle E_j \rangle$ . A default 50% threshold of clear sky was set for each city on each image based on the assumption that adequate coverage of the study region can be achieved by sampling a large enough set of imagery. The threshold was implemented in ArcGIS simply by comparing the maximum area of each city as given by the Meridian dataset (Table S1) with the area inside the city containing valid LST (i.e.  $p \cdot \Delta a$ ) from the satellite dataset. The effect of using a 75% clear-sky threshold is discussed below.

### 2.3 Scaling Study Methodology

35 cities were selected for study using an arbitrary threshold of city area greater than  $50 \text{ km}^2$ , from which population and emitted energy were derived (table S3 in SI). Clear-sky nights were selected based on the prevalent synoptic meteorology (i.e., fog-free anticyclone conditions in the absence of fronts). A total of 28 nights was selected: 15 in winter (30 November – 28 February) and 13 in summer (1 June -31 August) in the period 2000 – 2017.

## 3.0 RESULTS

Area-summed emitted energy varies over 1.5 orders of magnitude for cities with populations ranging over 2 orders of magnitude (Figure 3a). Although the exact slope varies from night to night (Figure 3b), the tight log-log correlation is always present. Strong correlations are present on both summer and winter nights (table 1) with no obvious pattern. The correlations suggest that population is a good predictor variable for total emitted energy, despite substantial differences in urban form of British cities. Figure 3b shows the plots for all dates sampled in this study. Slopes are

similar, varying between  $0.73 \pm 0.06$  (13 December 2010; Table 1) and  $0.92 \pm 0.09$  (17 December 2011) and are ranked in Table 1 by their  $R^2$  value when using a 50% cloud-free threshold. Standard error on the slope increases as  $R^2$  decreases but there is no obvious trend in the value of the slope.

The derived regression equation for the averaged allometry over 28 nights is:

$$\log(\bar{Y}) = \log(\bar{\beta}) \bar{\alpha} \cdot \log(\langle \bar{E}_j \rangle), \quad (5)$$

Where

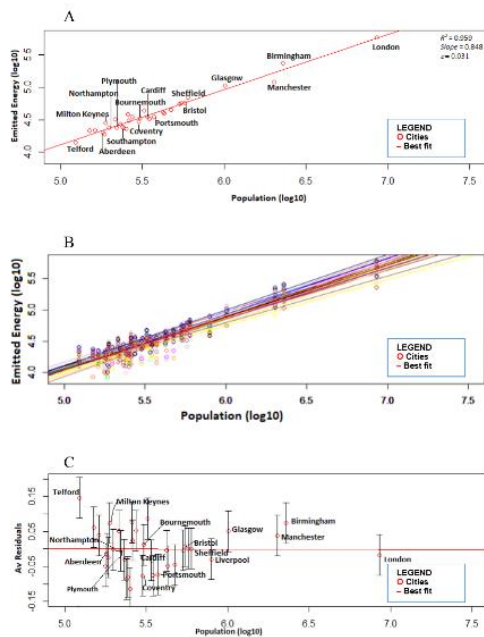
$$\langle \bar{E}_j \rangle = \frac{\sum_{k=0}^n E_{j,k}}{n}. \quad (6)$$

That is,  $\langle \bar{E}_j \rangle$  is the average emitted energy (in MW) over all nights for city,  $j$ , and  $n$  is the number of nights = 28.

Although the two extreme values of the allometric slope are statistically different (i.e., the means are further apart than the sum of the standard errors, Table S3, Supplementary SI), Figure 3a does not show any clustering of the regression slopes in the sample. It is assumed, therefore, that, to a first approximation at least, the results indicate that a single overall allometric scaling of total emitted energy with population of  $0.84 \pm 0.06$  is plausible (fig.3b). If this assumption is justified, the variation observed in the regression slope must derive from difficult-to-quantify errors in the retrieval of the emitted energies, including the effect of partially obscured urban areas on the slope.

To test the impact of partial cloud obscuring, the analysis was repeated increasing the threshold for inclusion of an urban area in the analysis to 75% cloud-free (see table S3 and fig. S6 in supplementary SI). The scaling of emitted energy with population under this more stringent condition has a slope of  $0.86 \pm 0.05$  (Table S3 in Supplementary SI), which is, within

error, indistinguishable from the mean slope from Table 1.



**Fig. 3: (A) An example of allometric scaling of night-time emitted energy  $\text{Log}_{10}\langle E_j \rangle$ , in MW) against urban population for the 35 largest cities in Great Britain. Reported on the graph (top right) are the Coefficient of Determination ( $R^2$ ) for the best-fit regression, the slope of the regression, and the error on the slope ( $\epsilon$ ). (B) The ensemble of allometric relationships derived for the nights studied (Table 1). (C) Residual emitted energy (mean and standard deviation of  $\text{Log}_{10}\langle E_j \rangle$  in MW) for urban areas with respect to the allometric scalings shown in (B).**

**Table 1. Night-time emitted energy for thirty-five (35) UK large Cities on selected summer and winter nights. Results are ranked by the strength ( $R^2$ ) of the log-log correlation between emitted energy and population, for which the slope, and error on slope are reported at 50% cloud free pixels**

Rank	DATE	Number of CITIES	$R^2$	SLOPE ( $\alpha$ )	ERROR ON SLOPE
1	13 <sup>th</sup> Feb. 2017	26	0.97	0.86	0.03
2	15 <sup>th</sup> Feb. 2016	25	0.96	0.85	0.03
3	06 <sup>th</sup> Jun. 2000	33	0.96	0.85	0.03
4	22 <sup>nd</sup> Feb. 2003	28	0.96	0.88	0.04
5	07 <sup>th</sup> Jul. 2007	34	0.96	0.84	0.03
6	01 <sup>st</sup> Jan. 2007	32	0.96	0.85	0.03
7	02 <sup>nd</sup> Jan. 2017	35	0.94	0.84	0.04
8	26 <sup>th</sup> Dec. 2009	24	0.93	0.81	0.05
9	27 <sup>th</sup> Jun. 2010	32	0.93	0.80	0.04
10	16 <sup>th</sup> Aug. 2016	35	0.92	0.89	0.04
11	29 <sup>th</sup> Feb. 2000	21	0.92	0.83	0.05
12	01 <sup>st</sup> Jan. 2012	24	0.92	0.89	0.06
13	30 <sup>th</sup> Nov. 2016	20	0.92	0.86	0.06
14	13 <sup>th</sup> Dec. 2010	17	0.92	0.73	0.06

15	28 <sup>th</sup> Aug. 2001	25	0.91	0.88	0.06
16	30 <sup>th</sup> Aug. 2005	22	0.90	0.82	0.06
17	20 <sup>th</sup> Jan. 2009	18	0.88	0.83	0.08
18	09 <sup>th</sup> Jul. 2006	34	0.88	0.88	0.06
19	20 <sup>th</sup> Jan. 2011	22	0.88	0.74	0.06
20	08 <sup>th</sup> Aug. 2012	25	0.88	0.83	0.06
21	05 <sup>th</sup> Jan. 2005	34	0.88	0.80	0.05
22	10 <sup>th</sup> Jun. 2003	27	0.87	0.81	0.06
23	13 <sup>th</sup> Jul. 2002	28	0.87	0.77	0.06
24	03 <sup>rd</sup> Aug. 2017	22	0.86	0.82	0.07
25	25 <sup>th</sup> Feb. 2009	26	0.85	0.91	0.08
26	28 <sup>th</sup> Aug. 2009	30	0.84	0.81	0.07
27	17 <sup>th</sup> Dec. 2011	26	0.83	0.92	0.09
28	18 <sup>th</sup> Feb. 2006	25	0.79	0.84	0.09
Mean				0.84	0.06
Median				0.83	

Table S4 (supplementary SI) tests the effect of a population threshold by comparing the correlations for cities with populations greater than 250,000 and greater than 500,000. The mean slope of the regression is not significantly different for both subsets of cities.

#### 4.0 DISCUSSION

The findings from this study indicate that population is a good predictor variable for total emitted energy despite the differences in the urban form of UK cities. This study finds a much more significant scaling for upwelling clear-sky long-wave with population than was found for  $\Delta T_{u-r} (max)$  by Oke (1973; 1982) (i.e., Fig. S1 in SI). Energy emitted from the surface is acted on by turbulent and radiative transfer processes, the net result of which is  $\Delta T_{u-r} (max)$  (Oke, 1982). Although it is plausible that turbulent transfer processes scale with city size (as discussed in (MacKenzie et al., 2019)), it appears that the overall effect on the energy budget is to dampen very significantly the scaling of  $\Delta T_{u-r} (max)$  compared to the scaling of emitted energy. The difference in the scalings of the heat source and the final temperature difference is very marked. Investigating this further will require a detailed investigation of the scaling of each aspect of the urban energy budget, which is outside the scope of the present study.

The scaling of emitted energy with population is very similar to that of total urban area with

population (Fig S2A in the SI). Hence, emitted energy varies linearly with urban area for the 35 cities in our study (Fig S3), even though that area becomes increasingly densely populated as city population increases. The implication is that, on average, there is no structural change of relevance to the total emitted energy between a single city the size of London or ten cities each a tenth of the area (i.e., roughly the size of Bristol). This quantitative scaling without qualitative structural change may be consistent with Oke's 1973 study on city size and the urban heat Island, and with his study in 1981 on canyon geometry and the nocturnal urban heat Island, in which he cited Chandler's 1967 observation on the similarities of London and Leicester temperature on the same night, despite their difference in size and population (Oke, 1973; 1981). Non-linearities may become more important when smaller urban centres are included, as in the study of Zhou et al. (2013).

Further information pertaining to the urban form can be derived by inspection of the residuals, i.e., the distances of each urban area from the line of best fit (Fig 3c). We postulate that differences in urban form across Great British cities will be evident in both the magnitude and sign of the residuals. Firstly, however, we discount geographical and climate factors. Comparisons between mean emitted-energy residuals and each of altitude, latitude, mean hours of sunshine, and mean annual temperature for each city showed no significant correlations (see figs. S9, S10, S11 and S12 in supplementary SI).

The magnitude of residual can be interpreted as the degree to which an individual city deviates positively or negatively from the value expected for a city of its size (Bettencourt et al., 2010). For the case of emitted thermal energy, positive anomalies correspond to cities with warmer surfaces than expected and negative anomalies correspond to surfaces cooler than

expected based on the best-fit population-based allometry. There is a tendency for the magnitude of residuals to be larger for the smaller urban areas (Fig 3c). For example, the residual for Telford is positive and about 4% of its mean area-summed emission, whereas, for London, the residual is about 0.2% of the mean area-summed emission.

The cities of Coventry and Plymouth, which were reconstructed post-war (Hasegawa et al., 2013) have large negative residuals (-0.075 and -0.004 y-axis units ( $\log_{10}(\langle E_j \rangle$  in MW)), Fig 3c), whereas the New Town 'Garden Cities' of Milton Keynes and Telford both have large positive residuals (0.08 and 0.15 units). These unexpected results do not seem to arise from sampling issues affecting the overall allometry because the residuals are robust for the various nights studied (variation bars in Fig 3c). Instead, the results may arise from a greater area of impervious, low albedo, surface per person in the lower density Garden Cities. Residuals for the area allometry for each city are reported in (table S2 supplementary SI). Milton Keynes and Telford have large positive residuals compared to their expected area (0.087 and 0.155 units, respectively), whilst Coventry and Plymouth have large negative residuals (-0.056 and -0.050 units). So, the Garden cities emit more than expected for their populations but spread that emission over a wider surface area than expected, whereas Coventry and Plymouth emit much less than expected from their population but spread that emission over a smaller-than-expected area.

Northampton, situated about 60 miles (97km) north-west of London and 45 miles (72km) south-east of Birmingham, had a population of 212,100 at the 2011 census. Northampton is predominantly a post-war settlement in which growth was limited until it was nominated as a New Town in 1968 (Whitehand and Whitehand, 1984). Its mean energy emission

residual is close to zero, similar to Bristol (fig. 3c), despite being radically different in terms of population and their histories of urban development. The residuals for urban area are also similar for Northampton and Bristol. However, Milton Keynes, the city closest to Northampton in population (table 1, supplementary SI), similarly situated (about 50 miles (80km) north-west of London), and also a classic post-war New Town, has a large positive mean emitted energy residual (fig 3c) and large positive area residual.

City configuration, street patterns and orientation, structure of buildings and density, and ultimately the intensity of human activities are key factors that determine thermal behaviour in the city. In summary, the residuals (fig. 3c) allow an assessment of the similarities and differences in emitted energy, relative to that expected by the best-fit line, for settlements of very different size.

## 5.0 CONCLUSION

This study aimed at evaluating the extent and rate of clear-sky emitted long-wave energy with population in the cities for MODIS/Terra V006 composite products (MOD11 A1). This was achieved by assessing the night-time emitted energy across cities in Great Britain for 28 night-time samples across summer (JJA) and winter (DJF) between 2000 and 2017. British cities show a strong and consistent sub-linear allometric scaling of total emitted energy with population. That is, there is a substantial ‘economy (or parsimony) of scale’ in terms of nocturnal heat production in British cities: the production from the larger cities is smaller than would be produced from a constellation of smaller cities housing the same population. This uniformity of scaling occurs despite of the obvious differences in architecture and urban form in settlements with Medieval centres (e.g. Aberdeen), predominantly commercial/military (e.g. Southampton) or

residential (Bournemouth) coastal settlements, and post-second world-war planned settlements (e.g., Milton Keynes).

The scaling of emitted energy with population is much larger than reported in the previous literature of the scaling of air temperature urban heat island (UHI) with population (Oke, 1973; Oke, 1982). It is possible to compare these scalings even though emitted energy and UHI have different units because the logarithmic scaling produces a dimensionless slope quantifying relative changes. Since long-wave emissions from the relatively warm urban surface are the source of the nocturnal UHI and SUHI, turbulent and radiative transfer in the atmosphere must act to dampen significantly the scaling signal for heat island metrics. The concentration of population into larger urban areas, rather than spread out over more, smaller, cities, has only a marginal worsening effect on the risk to health arising from air temperature UHI but a much larger effect arising from radiant flux (cf., e.g., Middel and Krayenhoff, 2019).

The scaling of total emitted energy with population has a similar slope, within statistical error, as the scaling of urban area with population. This equality of scaling suggests that energy emitted per unit area averages out to be approximately the same everywhere in cities at the granularity of the current analysis. This ‘emergent simplicity’ in the scaling of emitted energy for urban areas of different sizes seems counter intuitive given our understanding of the role of urban form in heat storage and emission in the built environment (Arnfield and Grimmond, 1998; Nunez and Oke, 1977). Instead, the particularities of British urban form seem to manifest in the residuals for each city, i.e., the magnitude of the difference in emitted energy measured from that predicted by the best-fit line. As yet, we have not been able to find any simple rules that would allow us to predict the size of the



residual from its geographical context (including climate) or from its development history but we believe this merit further study.

## CRediT authorship contribution statement

M. Abdulrasheed: Investigation, Writing - original draft. A.R. MacKenzie: Conceptualization, Supervision, Writing - review & editing. J.D. Whyatt: Investigation, Writing - review & editing. L. Chapman:

Conceptualization, developed from earlier work by JDW and ARMK, Supervision, Writing - review & editing.

## Acknowledgements

We very gratefully acknowledge the substantial work of the referees and editor to improve the manuscript. ARMK and LC acknowledge support from the WM Air project of the Natural Environment Research Council (NE/ S003487/1). MA gratefully acknowledges support from the Petroleum Technology Development Fund.

## REFERENCES

- Abdulrasheed, M., 2020. The Effect of Spatial Settlement Patterns on Urban Climatology. PhD Thesis, University of Birmingham, Birmingham, UK.
- Abdulrasheed, M., MacKenzie, A.R., Whyatt, J.D., Chapman, L., 2020. Allometric scaling of thermal infrared emitted from UK cities and its relation to urban form. *City Environ. Interact.* 100037. <https://doi.org/10.1016/j.cacint.2020.100037>
- Adams, J.S., 1970. Residential Structure of Midwestern Cities. *Ann. Assoc. Am. Geogr.* 60, 37–62. <https://doi.org/10.1111/j.1467-8306.1970.tb00703.x>
- Adefolalu, D.O., 1984. On bioclimatological aspects of Harmattan dust haze in Nigeria. *Arch. Meteorol. Geophys. Bioclimatol. Ser. B* 33, 387–404. <https://doi.org/10.1007/BF02274004>
- Adelekan, I.O., 2010. Vulnerability of poor urban coastal communities to flooding in Lagos, Nigeria. *Environ. Urban.* 22, 433–450. <https://doi.org/10.1177/0956247810380141>
- Adole, T., Dash, J., Atkinson, P.M., 2018. Major trends in the land surface phenology (LSP) of Africa, controlling for land-cover change. *Int. J. Remote Sens.* 39, 8060–8075. <https://doi.org/10.1080/01431161.2018.1479797>
- Aguado, E., Burt, J.E., 2015. Understanding Weather and Climate [WWW Document]. URL <https://www.pearson.com/us/higher-education/product/Aguado-Understanding-Weather-and-Climete-7th-Edition/9780321987303.html> (accessed 12.17.18).
- Ahmed, K.S., 2003. Comfort in urban spaces: defining the boundaries of outdoor thermal comfort for the tropical urban environments. *Energy Build.* 35, 103–110. [https://doi.org/10.1016/S0378-7788\(02\)00085-3](https://doi.org/10.1016/S0378-7788(02)00085-3)
- Akpodiogaga-a, P., Odjugo, O., 2010. General Overview of Climate Change Impacts in Nigeria. *J. Hum. Ecol.* 29, 47–55. <https://doi.org/10.1080/09709274.2010.11906248>
- Alavipanah, S., Wegmann, M., Qureshi, S., Weng, Q., Koellner, T., 2015. The Role of Vegetation in Mitigating Urban Land Surface Temperatures: A Case Study of Munich, Germany during the Warm Season. *Sustainability* 7, 4689–4706. <https://doi.org/10.3390/su7044689>
- Alexander, A., 2009. Britain's New Towns: Garden Cities to Sustainable Communities. Routledge.



- Aliyu, A.A., Amadu, L., 2017. Urbanization, Cities, and Health: The Challenges to Nigeria – A Review. *Ann. Afr. Med.* 16, 149–158.  
[https://doi.org/10.4103/aam.aam\\_1\\_17](https://doi.org/10.4103/aam.aam_1_17)
- Alonzo, M., Bookhagen, B., McFadden, J.P., Sun, A., Roberts, D.A., 2015. Mapping urban forest leaf area index with airborne lidar using penetration metrics and allometry. *Remote Sens. Environ.* 162, 141–153.  
<https://doi.org/10.1016/j.rse.2015.02.025>
- Amundsen, H., Berglund, F., Westskog, H., 2010. Overcoming Barriers to Climate Change Adaptation—A Question of Multilevel Governance? *Environ. Plan. C Gov. Policy* 28, 276–289.  
<https://doi.org/10.1068/c0941>
- Anderson, J.R., 1976. A Land Use and Land Cover Classification System for Use with Remote Sensor Data. U.S. Government Printing Office.
- Anderson, W.P., Kanaroglou, P.S., Miller, E.J., 1996. Urban Form, Energy and the Environment: A Review of Issues, Evidence and Policy. *Urban Stud.* 33, 7–35.  
<https://doi.org/10.1080/00420989650012095>
- Anguelovski, I., Chu, E., Carmin, J., 2014. Variations in approaches to urban climate adaptation: Experiences and experimentation from the global South. *Glob. Environ. Change* 27, 156–167.  
<https://doi.org/10.1016/j.gloenvcha.2014.05.010>
- Anukwonke, C., 2015. Urbanization Processes and Environment.
- Arifwidodo, S.D., Tanaka, T., 2015. The Characteristics of Urban Heat Island in Bangkok, Thailand. *Procedia - Soc. Behav. Sci., World Conference on Technology, Innovation and Entrepreneurship* 195, 423–428.  
<https://doi.org/10.1016/j.sbspro.2015.06.484>
- Arimah, B.C., Adeagbo, D., 2000. Compliance with urban development and planning regulations in Ibadan, Nigeria. *Habitat Int.* 24, 279–294.  
[https://doi.org/10.1016/S0197-3975\(99\)00043-0](https://doi.org/10.1016/S0197-3975(99)00043-0)
- Arnfield, A.J., 2003. Two decades of urban climate research: a review of turbulence, exchanges of energy and water, and the urban heat island. *Int. J. Climatol.* 23, 1–26.  
<https://doi.org/10.1002/joc.859>
- Arnfield, A.J., Grimmond, C.S.B., 1998. An urban canyon energy budget model and its application to urban storage heat flux modeling. *Energy Build.* 27, 61–68.  
[https://doi.org/10.1016/S0378-7788\(97\)00026-1](https://doi.org/10.1016/S0378-7788(97)00026-1)
- Ayanlade, A., 2017. Variations in urban surface temperature: an assessment of land use change impacts over Lagos metropolis. *Weather* 72, 315–319.  
<https://doi.org/10.1002/wea.2925>
- Ayanlade, A., 2016a. Seasonality in the daytime and night-time intensity of land surface temperature in a tropical city area. *Sci. Total Environ.* 557–558, 415–424.  
<https://doi.org/10.1016/j.scitotenv.2016.03.027>
- Ayanlade, A., 2016b. Variation in diurnal and seasonal urban land surface temperature: landuse change impacts assessment over Lagos metropolitan city. *Model. Earth Syst. Environ.* 2, 193. <https://doi.org/10.1007/s40808-016-0238-z>
- Ayanlade, A., 2015. Evaluation of the intensity of the daytime surface urban heat island: how can remote sensing help?: *International Journal of Image and Data Fusion: Vol 6, No 4 [WWW Document]*. URL <https://www.tandfonline.com/doi/full/10.1080/19479832.2014.985618> (accessed 7.26.19).
- Azevedo, J.A., Chapman, L., Muller, C.L., 2016. Quantifying the Daytime and Night-Time Urban Heat Island in Birmingham, UK: A Comparison of Satellite Derived Land Surface Temperature and High Resolution Air

- Temperature Observations. *Remote Sens.* 8, 153.  
<https://doi.org/10.3390/rs8020153>
- Bahi, H., Rhinane, H., Bensalmia, A., Fehrenbach, U., Scherer, D., 2016. Effects of Urbanization and Seasonal Cycle on the Surface Urban Heat Island Patterns in the Coastal Growing Cities: A Case Study of Casablanca, Morocco. *Remote Sens.* 8, 829.  
<https://doi.org/10.3390/rs8100829>
- Ball, M., Maginn, P.J., 2005. Urban Change and Conflict: Evaluating the Role of Partnerships in Urban Regeneration in the UK. *Hous. Stud.* 20, 9–28.  
<https://doi.org/10.1080/0267303042000308705>
- Balling, R.C., Cervený, R.S., 2003. Vertical dimensions of seasonal trends in the diurnal temperature range across the central United States. *Geophys. Res. Lett.* 30.  
<https://doi.org/10.1029/2003GL017776>
- Balogun, I.A., Balogun, A.A., 2014. Urban heat island and bioclimatological conditions in a hot-humid tropical city: The example of Akure, Nigeria. *Erde* 145, 3–15.  
<https://doi.org/10.12854/erde-145-2>
- Balogun, I.A., Balogun, A.A., Adeyewa, Z.D., 2012. Observed urban heat island characteristics in Akure, Nigeria. *Afr. J. Environ. Sci. Technol.* 6, 1–8.  
<https://doi.org/10.5897/AJEST11.084>
- Bao, Y., 2013. On Sample Skewness and Kurtosis. *Econom. Rev.* 32, 415–448.  
<https://doi.org/10.1080/07474938.2012.690665>
- Basu, R., Samet, J.M., 2002. Relation between Elevated Ambient Temperature and Mortality: A Review of the Epidemiologic Evidence. *Epidemiol. Rev.* 24, 190–202.  
<https://doi.org/10.1093/epirev/mxf007>
- Batty, M., 2008. The Size, Scale, and Shape of Cities. *Science* 319, 769–771.  
<https://doi.org/10.1126/science.1151419>
- Bauman, J.F., Muller, E.K., 2006. *Before Renaissance: Planning in Pittsburgh, 1889–1943*. University of Pittsburgh Press.
- Beale, C.L., 1975. *The Revival of Population Growth in Nonmetropolitan America*.
- Bechtel, B., Alexander, P., Böhner, J., Ching, J., Conrad, O., Feddema, J., Mills, G., See, L., Stewart, I., 2015. Mapping Local Climate Zones for a Worldwide Database of the Form and Function of Cities. *ISPRS Int. J. Geo-Inf.* 4, 199–219.  
<https://doi.org/10.3390/ijgi4010199>
- Belcher, S.E., Jerram, N., Hunt, J.C.R., 2003. Adjustment of a turbulent boundary layer to a canopy of roughness elements. *J. Fluid Mech.* 488, 369–398.  
<https://doi.org/10.1017/S0022112003005019>
- Bettencourt, L., West, G., 2010. A unified theory of urban living. *Nature* 467, 912–913.  
<https://doi.org/10.1038/467912a>
- Bettencourt, L.M.A., 2013. The Origins of Scaling in Cities. *Science* 340, 1438–1441.  
<https://doi.org/10.1126/science.1235823>
- Bettencourt, L.M.A., Lobo, J., 2016. Urban scaling in Europe | *Journal of The Royal Society Interface* [WWW Document]. URL <http://rsif.royalsocietypublishing.org/content/13/116/20160005> (accessed 12.13.17).
- Bettencourt, L.M.A., Lobo, J., Helbing, D., Kühnert, C., West, G.B., 2007. Growth, innovation, scaling, and the pace of life in cities. *Proc. Natl. Acad. Sci.* 104, 7301–7306.  
<https://doi.org/10.1073/pnas.0610172104>
- Bettencourt, L.M.A., Lobo, J., Strumsky, D., West, G.B., 2010. Urban Scaling and Its Deviations: Revealing the Structure of Wealth, Innovation and Crime across Cities. *PLOS ONE* 5, e13541.  
<https://doi.org/10.1371/journal.pone.0013541>

- Bibby, P., Brindley, P., 2013. Urban and Rural Area Definitions for Policy Purposes in England and Wales: Methodology (v1.0) 36.
- Bohnenstengel, S.I., Hamilton, I., Davies, M., Belcher, S.E., 2014. Impact of anthropogenic heat emissions on London's temperatures. *Q. J. R. Meteorol. Soc.* 140, 687–698. <https://doi.org/10.1002/qj.2144>
- Bokaie, M., Zarkesh, M.K., Arasteh, P.D., Hosseini, A., 2016. Assessment of Urban Heat Island based on the relationship between land surface temperature and Land Use/ Land Cover in Tehran. *Sustain. Cities Soc.* 23, 94–104. <https://doi.org/10.1016/j.scs.2016.03.009>
- Bongaarts, J., 2009. Human population growth and the demographic transition. *Philos. Trans. R. Soc. B Biol. Sci.* 364, 2985–2990. <https://doi.org/10.1098/rstb.2009.0137>
- Bornstein, R.D., 1968. Observations of the Urban Heat Island Effect in New York City. *J. Appl. Meteorol.* 7, 575–582. [https://doi.org/10.1175/1520-0450\(1968\)007<0575:OOTUHI>2.0.CO;2](https://doi.org/10.1175/1520-0450(1968)007<0575:OOTUHI>2.0.CO;2)
- Bounoua, L., DeFries, R.S., Imhoff, M.L., Steiner, M.K., 2004. Land use and local climate: A case study near Santa Cruz, Bolivia. *Meteorol. Atmospheric Phys.* 86, 73–85. <https://doi.org/10.1007/s00703-003-0616-8>
- Bourne, L.S., 1982. Internal Structure of Cities 7 Lembar | City [WWW Document]. Scribd. URL <https://www.scribd.com/document/382973520/Bourne-L-S-1982-Internal-Structure-of-Cities-7-Lembar> (accessed 1.14.20).
- Bremner, J., Frost, A., Haub, C., Mather, M., Ringheim, K., Zuehlke, E., 2010. World population highlights: Key findings from PRB's 2010 world population data sheet. *Popul. Bull.* 65, 1–12.
- Briney, A., Am, a B., geographer, a B. is a professional, writer, Degrees, S. with T.U., GIS, an advanced certificate in, 2019. How the United Kingdom Became an Island Nation [WWW Document]. ThoughtCo. URL <https://www.thoughtco.com/geography-of-the-united-kingdom-1435710> (accessed 9.4.19).
- Brousse, O., Martilli, A., Foley, M., Mills, G., Bechtel, B., 2016. WUDAPT, an efficient land use producing data tool for mesoscale models? Integration of urban LCZ in WRF over Madrid. *Urban Clim.* 17, 116–134. <https://doi.org/10.1016/j.uclim.2016.04.001>
- Brown, R., 2011. Ameliorating the effects of climate change: Modifying microclimates through design. *Landsc. Urban Plan. - Landsc. URBAN PLAN* 100, 372–374. <https://doi.org/10.1016/j.landurbplan.2011.01.010>
- Buhaug, H., Urdal, H., 2013. An urbanization bomb? Population growth and social disorder in cities. *Glob. Environ. Change* 23, 1–10. <https://doi.org/10.1016/j.gloenvcha.2012.10.016>
- Burnett, J., 1986. Social History of Housing by Burnett - AbeBooks [WWW Document]. URL <https://www.abebooks.co.uk/book-search/title/social-history-of-housing/author/burnett/> (accessed 9.28.19).
- Carlos, B.K., Paul, O., Alan, H.P., Matthias, I., 2017. Mapping Local Climate Zones for urban morphology classification based on airborne remote sensing data [WWW Document]. URL [https://www.researchgate.net/publication/314286458\\_Mapping\\_Local\\_Climate\\_Zones\\_for\\_urban\\_morphology\\_classification\\_based\\_on\\_airborne\\_remote\\_sensing\\_data](https://www.researchgate.net/publication/314286458_Mapping_Local_Climate_Zones_for_urban_morphology_classification_based_on_airborne_remote_sensing_data) (accessed 1.4.20).
- Carmin, J., Anguelovski, I., Roberts, D., 2012. Urban Climate Adaptation in the Global South: Planning in an Emerging Policy Domain. *J. Plan. Educ. Res.* 32,

- 18–32.  
<https://doi.org/10.1177/0739456X11430951>
- Carmon, N., 1999. Three generations of urban renewal policies: analysis and policy implications. *Geoforum* 30, 145–158.  
[https://doi.org/10.1016/S0016-7185\(99\)00012-3](https://doi.org/10.1016/S0016-7185(99)00012-3)
- Carroll, M.L., DiMiceli, C.M., Townshend, J.R.G., Sohlberg, R.A., Elders, A.I., Devadiga, S., Sayer, A.M., Levy, R.C., 2017. Development of an operational land water mask for MODIS Collection 6, and influence on downstream data products. *Int. J. Digit. Earth* 10, 207–218.  
<https://doi.org/10.1080/17538947.2016.1232756>
- Carroll, M.L., Townshend, J.R., DiMiceli, C.M., Noojipady, P., Sohlberg, R.A., 2009. A new global raster water mask at 250 m resolution. *Int. J. Digit. Earth* 2, 291–308.  
<https://doi.org/10.1080/17538940902951401>
- Castán Broto, V., 2017. Urban Governance and the Politics of Climate change. *World Dev.* 93, 1–15.  
<https://doi.org/10.1016/j.worlddev.2016.12.031>
- CEDA, 2011. CEDA Data Server, Index of /badc/ukcp09/data/gridded-land-obs/gridded-land-obs-averages-5km/grid/netcdf/mean-temperature/ [WWW Document]. URL <http://data.ceda.ac.uk/badc/ukcp09/data/gridded-land-obs/gridded-land-obs-averages-5km/grid/netcdf/mean-temperature/> (accessed 10.2.18).
- Chadchan, J., Shankar, R., 2009. Emerging Urban Development Issues in the Context of Globalization 9.
- Chadwick, E., 1842. Edwin Chadwick's Report on the sanitary conditions of the labouring population of Great Britain was published | Policy Navigator [WWW Document]. URL <https://navigator.health.org.uk/content/edwin-chadwicks-report-sanitary-conditions-labouring-population-great-britain-was-published> (accessed 12.22.18).
- Chandler, T.J., 1966. The climate of London. By T. J. Chandler. London (Hutchinson), 1965. Pp. 292 : 86 Figures; 98 Tables; 5 Appendix Tables. £3. 10s. 0d. *Q. J. R. Meteorol. Soc.* 92, 320–321.  
<https://doi.org/10.1002/qj.49709239230>
- Chandler, T.J., 1962. London's Urban Climate. *Geogr. J.* 128, 279–298.  
<https://doi.org/10.2307/1794042>
- Chang, K., 1962. A Typology of Settlement and Community Patterns in Some Circumpolar Societies. *Arct. Anthropol.* 1, 28–41.
- Changnon, S.A., 1992. Inadvertent Weather Modification in Urban Areas: Lessons for Global Climate Change. *Bull. Am. Meteorol. Soc.* 73, 619–627.  
[https://doi.org/10.1175/1520-0477\(1992\)073<0619:IWMIUA>2.0.CO;2](https://doi.org/10.1175/1520-0477(1992)073<0619:IWMIUA>2.0.CO;2)
- Changnon, S.A., Kunkel, K.E., Reinke, B.C., 1996. Impacts and Responses to the 1995 Heat Wave: A Call to Action. *Bull. Am. Meteorol. Soc.* 77, 1497–1506. [https://doi.org/10.1175/1520-0477\(1996\)077<1497:IARTTH>2.0.CO;2](https://doi.org/10.1175/1520-0477(1996)077<1497:IARTTH>2.0.CO;2)
- Chapman, L., Bell, S.J., 2018. High-Resolution Monitoring of Weather Impacts on Infrastructure Networks Using the Internet of Things. *Bull. Am. Meteorol. Soc.* 99, 1147–1154.  
<https://doi.org/10.1175/BAMS-D-17-0214.1>
- Chapman, L., Thornes, J.E., 2006. A geomatics-based road surface temperature prediction model. *Sci. Total Environ., Urban Environmental Research in the UK: The Urban Regeneration and the Environment (NERC URGENT) Programme and associated studies.* 360, 68–80.  
<https://doi.org/10.1016/j.scitotenv.2005.08.025>
- Chapman, L., Thornes, J.E., 2004. Real-Time Sky-View Factor Calculation and Approximation: *Journal of*

- Atmospheric and Oceanic Technology: Vol 21, No 5 [WWW Document]. URL <https://journals.ametsoc.org/doi/full/10.1175/1520-0426%282004%29021%3C0730%3ARSFCAA%3E2.O.CO%3B2> (accessed 8.21.19).
- Chapman, L., Thornes, J.E., 2003. The use of geographical information systems in climatology and meteorology. *Prog. Phys. Geogr. Earth Environ.* 27, 313–330.  
<https://doi.org/10.1191/0309133303pp384ra>
- Chen, L., Wang, H.-Y., Wang, T.-S., Kou, C.-H., 2019. Remote Sensing for Detecting Changes of Land Use in Taipei City, Taiwan. *J. Indian Soc. Remote Sens.* 47, 1847–1856.  
<https://doi.org/10.1007/s12524-019-01031-4>
- Chen, Y., 2010. Characterizing Growth and Form of Fractal Cities with Allometric Scaling Exponents [WWW Document]. *Discrete Dyn. Nat. Soc.*  
<https://doi.org/10.1155/2010/194715>
- Christen, A., Vogt, R., 2004. Energy and radiation balance of a central European city. *Int. J. Climatol.* 24, 1395–1421.  
<https://doi.org/10.1002/joc.1074>
- Chrysanthou, A., van der Schrier, G., van den Besselaar, E.J.M., Klein Tank, A.M.G., Brandsma, T., 2014. The effects of urbanization on the rise of the European temperature since 1960. *Geophys. Res. Lett.* 41, 7716–7722.  
<https://doi.org/10.1002/2014GL061154>
- Chudnovsky, A., Ben-Dor, E., Saaroni, H., 2004. Diurnal thermal behavior of selected urban objects using remote sensing measurements. *Energy Build.* 36, 1063–1074.  
<https://doi.org/10.1016/j.enbuild.2004.01.052>
- Cohen, B., 2006. Urbanization in developing countries: Current trends, future projections, and key challenges for sustainability. *Technol. Soc., Sustainable Cities* 28, 63–80.  
<https://doi.org/10.1016/j.techsoc.2005.10.005>
- Cohen, J.E., 2003. Human Population: The Next Half Century. *Science* 302, 1172–1175.  
<https://doi.org/10.1126/science.1088665>
- Cottineau, C., Hatna, E., Arcaute, E., Batty, M., 2017. Diverse cities or the systematic paradox of Urban Scaling Laws. *Comput. Environ. Urban Syst., Spatial analysis with census data: emerging issues and innovative approaches* 63, 80–94.  
<https://doi.org/10.1016/j.compenvurbsys.2016.04.006>
- CPRE, 2018. Campaign to Protect Rural England | 38 Degrees [WWW Document]. URL <https://you.38degrees.org.uk/partnerships/campaign-to-protect-rural-england> (accessed 9.28.19).
- Cui, L., Shi, J., 2012. Urbanization and its environmental effects in Shanghai, China. *Urban Clim.* 2, 1–15.  
<https://doi.org/10.1016/j.uclim.2012.10.008>
- Daramola, A., Ibem, E.O., 2010. Urban Environmental Problems in Nigeria Implications for Sustainable Development. *J. Sustain. Dev. Afr.* 12, 124–145.
- Davoudi, S., 2014. Climate Change, Securitisation of Nature, and Resilient Urbanism. *Environ. Plan. C Gov. Policy* 32, 360–375.  
<https://doi.org/10.1068/c12269>
- Davoudi, S., 2012. Climate Risk and Security: New Meanings of “the Environment” in the English Planning System. *Eur. Plan. Stud.* 20, 49–69.  
<https://doi.org/10.1080/09654313.2011.638491>
- Davoudi, S., Crawford, J., Mehmood, A., 2009. Planning for climate change: strategies for mitigation and adaptation for spatial planners. Earthscan.
- Dawson, R.J., Thompson, D., Johns, D., Wood, R., Darch, G., Chapman, L., Hughes, P.N., Watson, G.V.R., Paulson, K., Bell,

- S., Gosling, S.N., Powrie, W., Hall, J.W., 2018. A systems framework for national assessment of climate risks to infrastructure. *Philos. Transact. A Math. Phys. Eng. Sci.* 376. <https://doi.org/10.1098/rsta.2017.0298>
- Dissanayake, D., Morimoto, T., Murayama, Y., Ranagalage, M., Handayani, H.H., 2019. Impact of Urban Surface Characteristics and Socio-Economic Variables on the Spatial Variation of Land Surface Temperature in Lagos City, Nigeria. *Sustainability* 11, 25. <https://doi.org/10.3390/su11010025>
- Donnay, J.-P., Barnsley, M.J., Longley, P.A., 2014. Remote Sensing and Urban Analysis: GISDATA 9. CRC Press.
- Douglas, I., Alam, K., Maghenda, M., McDonnell, Y., Mclean, L., Campbell, J., 2008. Unjust waters: climate change, flooding and the urban poor in Africa. *Environ. Urban.* 20, 187–205. <https://doi.org/10.1177/0956247808089156>
- Duckworth, F.S., Sandberg, J.S., 1954. The Effect of Cities upon Horizontal and Vertical Temperature Gradients. *Bull. Am. Meteorol. Soc.* 35, 198–207.
- Eagleman, J.R., 1974. A comparison of urban climatic modifications in three cities. *Atmospheric Environ.* 1967 8, 1131–1142. [https://doi.org/10.1016/0004-6981\(74\)90047-X](https://doi.org/10.1016/0004-6981(74)90047-X)
- Earthdata, 2017. LP DAAC - Homepage [WWW Document]. URL <https://lpdaac.usgs.gov/> (accessed 10.16.19).
- EDINA, 2018. Digimap [WWW Document]. URL <https://digimap.edina.ac.uk/> (accessed 11.29.19).
- Eliasson, I., 1996. Urban nocturnal temperatures, street geometry and land use. *Atmos. Environ., Conference on the Urban Thermal Environment Studies in Tohwa* 30, 379–392. [https://doi.org/10.1016/1352-2310\(95\)00033-X](https://doi.org/10.1016/1352-2310(95)00033-X)
- Ellis, C., 2014. History Of Cities And City Planning [WWW Document]. URL <http://www.art.net/~hopkins/Don/simcity/manual/history.html> (accessed 3.26.20).
- Eludoyin, O.M., Adelekan, I.O., Webster, R., Eludoyin, A.O., 2014. Air temperature, relative humidity, climate regionalization and thermal comfort of Nigeria. *Int. J. Climatol.* 34, 2000–2018. <https://doi.org/10.1002/joc.3817>
- Emilsson, T., Ode Sang, Å., 2017. Impacts of Climate Change on Urban Areas and Nature-Based Solutions for Adaptation, in: Kabisch, N., Korn, H., Stadler, J., Bonn, A. (Eds.), *Nature-Based Solutions to Climate Change Adaptation in Urban Areas: Linkages between Science, Policy and Practice, Theory and Practice of Urban Sustainability Transitions*. Springer International Publishing, Cham, pp. 15–27. [https://doi.org/10.1007/978-3-319-56091-5\\_2](https://doi.org/10.1007/978-3-319-56091-5_2)
- Emmanuel, R., Krüger, E., 2012. Urban heat island and its impact on climate change resilience in a shrinking city: The case of Glasgow, UK. <https://doi.org/10.1016/J.BUILDENV.2012.01.020>
- Endsjö, P.-C., 1973. Urbanization in Nigeria. *Nor. Geogr. Tidsskr. - Nor. J. Geogr.* 27, 207–219. <https://doi.org/10.1080/00291957308551958>
- Enquist, B.J., Brown, J.H., West, G.B., 1998. Allometric scaling of plant energetics and population density. *Nature* 395, 163–165. <https://doi.org/10.1038/25977>
- Equere, V., Mirzaei, P.A., Riffat, S., 2020. Definition of a new morphological parameter to improve prediction of urban heat island. *Sustain. Cities Soc.* 56, 102021. <https://doi.org/10.1016/j.scs.2020.102021>
- Fan, F., Wang, Y., Qiu, M., Wang, Z., 2009. Evaluating the Temporal and Spatial Urban Expansion Patterns of Guangzhou from 1979 to 2003 by Remote Sensing and GIS Methods. *Int.*

- J. Geogr. Inf. Sci. 23, 1371–1388.  
<https://doi.org/10.1080/13658810802443432>
- Fichera, C.R., Modica, G., Pollino, M., 2012. Land Cover classification and change-detection analysis using multi-temporal remote sensed imagery and landscape metrics. *Eur. J. Remote Sens.* 45, 1–18.  
<https://doi.org/10.5721/EuJRS20124501>
- Fluschnik, T., Kriewald, S., García Cantú Ros, A., Zhou, B., Reusser, D.E., Kropp, J.P., Rybski, D., 2016. The Size Distribution, Scaling Properties and Spatial Organization of Urban Clusters: A Global and Regional Percolation Perspective. *ISPRS Int. J. Geo-Inf.* 5, 110.  
<https://doi.org/10.3390/ijgi5070110>
- Friedl, M.A., McIver, D.K., Hodges, J.C.F., Zhang, X.Y., Muchoney, D., Strahler, A.H., Woodcock, C.E., Gopal, S., Schneider, A., Cooper, A., Baccini, A., Gao, F., Schaaf, C., 2002. Global land cover mapping from MODIS: algorithms and early results. *Remote Sens. Environ., The Moderate Resolution Imaging Spectroradiometer (MODIS): a new generation of Land Surface Monitoring* 83, 287–302.  
[https://doi.org/10.1016/S0034-4257\(02\)00078-0](https://doi.org/10.1016/S0034-4257(02)00078-0)
- Friedman, G.M., 1962. On Sorting, Sorting Coefficients, and the Lognormality of the Grain-Size Distribution of Sandstones. *J. Geol.* 70, 737–753.  
<https://doi.org/10.1086/jg.70.6.30066373>
- Frost, J., 2018. Measures of Variability: Range, Interquartile Range, Variance, and Standard Deviation. *Stat. Jim.* URL <http://statisticsbyjim.com/basics/variability-range-interquartile-variance-standard-deviation/> (accessed 2.11.20).
- Frumkin, H., 2002. Urban Sprawl and Public Health [WWW Document]. ResearchGate. URL [https://www.researchgate.net/publication/11035517\\_Urban\\_Sprawl\\_and\\_Public\\_Health](https://www.researchgate.net/publication/11035517_Urban_Sprawl_and_Public_Health) (accessed 3.8.20).
- Fujii, H., Iwata, K., Managi, S., 2017. How do urban characteristics affect climate change mitigation policies? *J. Clean. Prod.* 168, 271–278.  
<https://doi.org/10.1016/j.jclepro.2017.08.221>
- Gandrud, C., 2013. Reproducible Research with R and R Studio. CRC Press.
- Gedzelman, S.D., Austin, S., Cermak, R., Stefano, N., Partridge, S., Quesenberry, S., Robinson, D.A., 2003. Mesoscale aspects of the Urban Heat Island around New York City. *Theor. Appl. Climatol.* 75, 29–42.  
<https://doi.org/10.1007/s00704-002-0724-2>
- Goist, P.D., 1974. Patrick Geddes and the City. *J. Am. Inst. Plann.* 40, 31–37.  
<https://doi.org/10.1080/01944367408977444>
- Golden, J.S., 2004. The Built Environment Induced Urban Heat Island Effect in Rapidly Urbanizing Arid Regions – A Sustainable Urban Engineering Complexity. *Environ. Sci.* 1, 321–349.  
<https://doi.org/10.1080/15693430412331291698>
- Goldstein, G., 1990. Urbanization, Health and Well-Being: A Global Perspective. *J. R. Stat. Soc. Ser. Stat.* 39, 121–133.  
<https://doi.org/10.2307/2348533>
- Gould, S.J., 1966. Allometry and Size in Ontogeny and Phylogeny. *Biol. Rev.* 41, 587–638.  
<https://doi.org/10.1111/j.1469-185X.1966.tb01624.x>
- Griend, A.A.V.D., Owe, M., 1993. On the relationship between thermal emissivity and the normalized difference vegetation index for natural surfaces. *Int. J. Remote Sens.* 14, 1119–1131.  
<https://doi.org/10.1080/01431169308904400>
- Grimmond, C.S.B., Roth, M., Oke, T.R., 2010. Climate and More Sustainable Cities: Climate Information for Improved Planning and Management of Cities (Producers/Capabilities Perspective) -

- ScienceDirect [WWW Document]. URL <https://www.sciencedirect.com/science/article/pii/S1878029610000174> (accessed 1.4.20).
- Grimmond, S., 2007. Urbanization and global environmental change: local effects of urban warming. *Geogr. J.* 173, 83–88. [https://doi.org/10.1111/j.1475-4959.2007.232\\_3.x](https://doi.org/10.1111/j.1475-4959.2007.232_3.x)
- Guo, H., Xu, M., Hu, Q., 2011. Changes in near-surface wind speed in China: 1969–2005. *Int. J. Climatol.* 31, 349–358. <https://doi.org/10.1002/joc.2091>
- Han, J.-Y., Baik, J.-J., Lee, H., 2013. Urban impacts on precipitation. *Asia-Pac. J. Atmospheric Sci.* 50. <https://doi.org/10.1007/s13143-014-0016-7>
- Haregeweyn, N., Tesfaye, S., Tsunekawa, A., Tsubo, M., Meshesha, D.T., Adgo, E., Elias, A., 2014. Dynamics of land use and land cover and its effects on hydrologic responses: case study of the Gilgel Tekeze catchment in the highlands of Northern Ethiopia. *Environ. Monit. Assess.* 187, 4090. <https://doi.org/10.1007/s10661-014-4090-1>
- Hartz, D.A., Prashad, L., Hedquist, B.C., Golden, J., Brazel, A.J., 2006. Linking satellite images and hand-held infrared thermography to observed neighborhood climate conditions. *Remote Sens. Environ., Thermal Remote Sensing of Urban Areas* 104, 190–200. <https://doi.org/10.1016/j.rse.2005.12.019>
- Hasegawa, J., 2013. The attitudes of the Ministry of Town and Country Planning towards blitzed cities in 1940s Britain. *Plan. Perspect.* 28, 271–289. <https://doi.org/10.1080/02665433.2013.737712>
- Heaviside, C., Cai, X.-M., Vardoulakis, S., 2015. The effects of horizontal advection on the urban heat island in Birmingham and the West Midlands, United Kingdom during a heatwave. *Q. J. R. Meteorol. Soc.* 141, 1429–1441. <https://doi.org/10.1002/qj.2452>
- Heaviside, C., Vardoulakis, S., Cai, X.-M., 2016. Attribution of mortality to the urban heat island during heatwaves in the West Midlands, UK. *Environ. Health* 15. <https://doi.org/10.1186/s12940-016-0100-9>
- Hendrickson, T.P., Nikolic, M., Rakas, J., 2016. Selecting climate change mitigation strategies in urban areas through life cycle perspectives. *J. Clean. Prod.* 135, 1129–1137. <https://doi.org/10.1016/j.jclepro.2016.06.075>
- Herold, M., Goldstein, N.C., Clarke, K.C., 2003. The spatiotemporal form of urban growth : measurement , analysis and modeling [WWW Document]. URL [/paper/The-spatiotemporal-form-of-urban-growth-%3A-%2C-and-Herold-Goldstein/c814f8dd54d6cf89874753ca662c5e244198c284](http://paper/The-spatiotemporal-form-of-urban-growth-%3A-%2C-and-Herold-Goldstein/c814f8dd54d6cf89874753ca662c5e244198c284) (accessed 8.20.18).
- Hillier, W.R.G., Hanson, J., Peponis, J., 1987. Syntactic Analysis of Settlements. *Archit. Comport. Behav.* 3, 217–231.
- Ho, J.C., Ren, C., Ng, E., 2015. A review of studies on the relationship between urban morphology and urban climate towards better urban planning and design in (sub)tropical regions 6.
- Hollow, M., 2012. Utopian urges: visions for reconstruction in Britain, 1940–1950'. *Plan. Perspect.* 27, 569–585. <https://doi.org/10.1080/02665433.2012.705126>
- Hondula, D.M., Balling, R.C., Vanos, J.K., Georgescu, M., 2015. Rising Temperatures, Human Health, and the Role of Adaptation. *Curr. Clim. Change Rep.* 1, 144–154. <https://doi.org/10.1007/s40641-015-0016-4>
- Hoornweg, D., Lorraine Sugar, Claudia Lorena Trejos Gómez, 2011. Cities and greenhouse gas emissions: moving forward. *Environ. Urban.* 23, 207–227. <https://doi.org/10.1177/0956247810392270>



- Hopkins, M.I.W., 2012. The ecological significance of urban fringe belts [WWW Document]. ResearchGate. URL [https://www.researchgate.net/publication/279625709\\_The\\_ecological\\_significance\\_of\\_urban\\_fringe\\_belts](https://www.researchgate.net/publication/279625709_The_ecological_significance_of_urban_fringe_belts) (accessed 7.7.20).
- Horton, N.J., Kleinman, K., 2015. Using R and RStudio for Data Management, Statistical Analysis, and Graphics. CRC Press.
- Howard, L., 1833. The Climate of London 285.
- Howard, L., 1818. The Climate of London 285.
- Huang, L., Li, J., Zhao, D., Zhu, J., 2008. A fieldwork study on the diurnal changes of urban microclimate in four types of ground cover and urban heat island of Nanjing, China. *Build. Environ.* 43, 7–17. <https://doi.org/10.1016/j.buildenv.2006.11.025>
- Ibrahim, A.A., Nduka, I.C., Iguisi, E.O., Ati, O.F., 2011. An Assessment of the Impact of Sky View Factor (SVF) on the Microclimate of Urban Kano. [WWW Document]. ResearchGate. URL [https://www.researchgate.net/publication/266025961\\_An\\_Assessment\\_of\\_the\\_Impact\\_of\\_Sky\\_View\\_Factor\\_SVF\\_on\\_the\\_Microclimate\\_of\\_Urban\\_Kano](https://www.researchgate.net/publication/266025961_An_Assessment_of_the_Impact_of_Sky_View_Factor_SVF_on_the_Microclimate_of_Urban_Kano) (accessed 8.8.19).
- Ichinose, T., Shimodozono, K., Hanaki, K., 1999. Impact of anthropogenic heat on urban climate in Tokyo. *Atmos. Environ.* 33, 3897–3909. [https://doi.org/10.1016/S1352-2310\(99\)00132-6](https://doi.org/10.1016/S1352-2310(99)00132-6)
- Imhoff, M.L., Zhang, P., Wolfe, R.E., Bounoua, L., 2010. Remote sensing of the urban heat island effect across biomes in the continental USA. *Remote Sens. Environ.* 114, 504–513. <https://doi.org/10.1016/j.rse.2009.10.008>
- Inikori, J.E., 2002. A Historiography of the First Industrial Revolution [WWW Document]. *Afr. Ind. Revolut. Engl. Study Int. Trade Econ. Dev.* <https://doi.org/10.1017/CBO9780511583940.004>
- IPCC, 2014. AR5 Climate Change 2014: Impacts, Adaptation, and Vulnerability — IPCC. URL <https://www.ipcc.ch/report/ar5/wg2/> (accessed 3.4.20).
- Jabareen, Y.R., 2006. Sustainable Urban Forms: Their Typologies, Models, and Concepts. *J. Plan. Educ. Res.* 26, 38–52. <https://doi.org/10.1177/0739456X05285119>
- Jackson, T.L., Feddema, J.J., Oleson, K.W., Bonan, G.B., Bauer, J.T., 2010. Parameterization of Urban Characteristics for Global Climate Modeling. *Ann. Assoc. Am. Geogr.* 100, 848–865. <https://doi.org/10.1080/00045608.2010.497328>
- Jacobs, J., 1962. Defends Urbanism in 1960s New York City Planning | WNYC | New York Public Radio, Podcasts, Live Streaming Radio, News [WWW Document]. WNYC. URL <https://www.wnyc.org/story/192689-jane-jacobs/> (accessed 1.14.20).
- Jones, A.R., 1975. Density-size Rule, a further Note. *Urban Stud.* 12, 225–228.
- Juju films, 2018. juju films - Google Search [WWW Document]. URL [https://www.google.com/search?q=juju+films&rlz=1C1CHBF\\_enGB909GB909&sxsrf=ALeKk02TLQWM8r0rGBb2BzJjOC0srwsiqg:1595607195164&source=lnms&tbn=isch&sa=X&ved=2ahUKEwjrksaApObqAhVTSSAKHXhNCU0Q\\_AUoAnoECA8QBA&biw=1280&bih=610](https://www.google.com/search?q=juju+films&rlz=1C1CHBF_enGB909GB909&sxsrf=ALeKk02TLQWM8r0rGBb2BzJjOC0srwsiqg:1595607195164&source=lnms&tbn=isch&sa=X&ved=2ahUKEwjrksaApObqAhVTSSAKHXhNCU0Q_AUoAnoECA8QBA&biw=1280&bih=610) (accessed 7.24.20).
- Justice, C.O., Townshend, J.R.G., Vermote, E.F., Masuoka, E., Wolfe, R.E., Saleous, N., Roy, D.P., Morisette, J.T., 2002. An overview of MODIS Land data processing and product status. *Remote Sens. Environ., The Moderate Resolution Imaging Spectroradiometer (MODIS): a new generation of Land Surface Monitoring* 83, 3–15.

- [https://doi.org/10.1016/S0034-4257\(02\)00084-6](https://doi.org/10.1016/S0034-4257(02)00084-6)
- Kafi, K.M., Shafri, H.Z.M., Shariff, A.B.M., 2014. An analysis of LULC change detection using remotely sensed data. *Int. J. Remote Sens.* 35, 1205–1220. <https://doi.org/10.1080/01448759.2013.828056>
- Karl, T.R., Diaz, H.F., Kukla, G., 1988. Urbanization: Its Detection and Effect in the United States Climate Record. *J. Clim.* 1, 1099–1123. [https://doi.org/10.1175/1520-0442\(1988\)001<1099:UIDAEI>2.0.CO;2](https://doi.org/10.1175/1520-0442(1988)001<1099:UIDAEI>2.0.CO;2)
- Karp, M., 2013. A Very Old Book: The Case for Eric Hobsbawm's Age of Revolution. *The Junto*. URL <https://earlyamericanists.com/2013/02/07/a-very-old-book-the-case-for-eric-hobsbawms-age-of-revolution/> (accessed 12.29.18).
- Kennedy, J., Dunn, R., McCarthy, M., Titchner, H., Morice, C., 2017. Global and regional climate in 2016. *Weather* 72, 219–225. <https://doi.org/10.1002/wea.3042>
- Kotharkar, R., Bagade, A., 2018. Evaluating urban heat island in the critical local climate zones of an Indian city. *Landsc. Urban Plan.* 169, 92–104. <https://doi.org/10.1016/j.landurbplan.2017.08.009>
- Krayenhoff, E.S., Moustauoi, M., Broadbent, A.M., Gupta, V., Georgescu, M., 2018. Diurnal interaction between urban expansion, climate change and adaptation in US cities. *Nat. Clim. Change* 8, 1097. <https://doi.org/10.1038/s41558-018-0320-9>
- LaBarbera, M., 1989. Analyzing Body Size as a Factor in Ecology and Evolution. *Annu. Rev. Ecol. Syst.* 20, 97–117. <https://doi.org/10.1146/annurev.es.20.110189.000525>
- Landsberg, H.E., 1981. *The Urban Climate*. Academic Press.
- Lee, D.O., 1984. Urban climates. *Prog. Phys. Geogr. Earth Environ.* 8, 1–31. <https://doi.org/10.1177/030913338400800101>
- Lee, D.O., 1977. Urban Influence on Wind Directions Over London. *Weather* 32, 162–170. <https://doi.org/10.1002/j.1477-8696.1977.tb04544.x>
- Lee, H.-Y., 1993. An application of NOAA AVHRR thermal data to the study of urban heat islands. *Atmospheric Environ. Part B Urban Atmosphere* 27, 1–13. [https://doi.org/10.1016/0957-1272\(93\)90041-4](https://doi.org/10.1016/0957-1272(93)90041-4)
- Lee, Y., 1989. An Allometric Analysis of the US Urban System: 1960 – 80. *Environ. Plan. Econ. Space* 21, 463–476. <https://doi.org/10.1068/a210463>
- Lehoczky, A., Sobrino, J.A., Skoković, D., Aguilar, E., 2017. The Urban Heat Island Effect in the City of Valencia: A Case Study for Hot Summer Days. *Urban Sci.* 1, 9. <https://doi.org/10.3390/urbansci1010009>
- Lemmen, D.S., Warren, F.J., 2004. Climate change impacts and adaptation: a Canadian perspective.
- Li, D., Liao, W., Rigden, A.J., Liu, X., Wang, D., Malyshev, S., Shevliakova, E., 2019. Urban heat island: Aerodynamics or imperviousness? *Sci. Adv.* 5, eaau4299. <https://doi.org/10.1126/sciadv.aau4299>
- Li, M., Shi, J., Guo, J., Cao, J., Niu, J., Xiong, M., 2015. Climate Impacts on Extreme Energy Consumption of Different Types of Buildings. *PLOS ONE* 10, e0124413. <https://doi.org/10.1371/journal.pone.0124413>
- Lillesand, T., Kiefer, R.W., Chipman, J., 2015. *Remote Sensing and Image Interpretation*. John Wiley & Sons.
- Longley, P., Batty, M., Shepherd, J., Sadler, G., 1992. Do Green Belts Change the Shape of Urban Areas? A Preliminary Analysis of the Settlement Geography of South East England. *Reg. Stud.* 26,

- 437–452.  
<https://doi.org/10.1080/00343409212331347101>
- Longley, P.A., Batty, M., Shepherd, J., 1991. The Size, Shape and Dimension of Urban Settlements. *Trans. Inst. Br. Geogr.* 16, 75–94.  
<https://doi.org/10.2307/622907>
- Lu, Y., Wang, H., Wang, Q., Zhang, Y., Yu, Y., Qian, Y., 2017. Global anthropogenic heat emissions from energy consumption, 1965–2100. *Clim. Change* 145, 459–468.  
<https://doi.org/10.1007/s10584-017-2092-z>
- Ludwig, F., Scheltinga, C.T.H.M.T.V., Verhagen, J., Kruijt, B., Ierland, E.C. van, Dellink, R.B., Bruin, K. de, Bruin, K.C. de, Kabat, P., 2007. Climate change impacts on Developing Countries - EU Accountability (No. PE 393.511). European Parliament, Brussels.
- Mabogunje, A.L., 1992. New initiatives in urban planning and management in Nigeria. *Habitat Int., Special Issue Urban Development Over Three Decades: Practitioner's Perspective on Policy, Planning and Management*, 1960–1990 16, 73–88.  
[https://doi.org/10.1016/0197-3975\(92\)90038-Z](https://doi.org/10.1016/0197-3975(92)90038-Z)
- Mabogunje, A.L., 1990. Urban Planning and the Post-Colonial State in Africa: A Research Overview. *Afr. Stud. Rev.* 33, 121–203.  
<https://doi.org/10.2307/524471>
- MacKenzie, A.R., Whyatt, J.D., Barnes, M.J., Davies, G., Hewitt, C.N., 2019. Urban form strongly mediates the allometric scaling of airshed pollution concentrations. *Environ. Res. Lett.* 14, 124078.  
<https://doi.org/10.1088/1748-9326/ab50e3>
- MacKenzie, R., Barnes, M., Whyatt, D., Hewitt, N., 2019. Allometric scaling of UK urban emissions: interpretation and implications for air quality management. Presented at the EGU General Assembly Conference Abstracts, pp. EPSC2016-8112.
- Mackey, C.W., Lee, X., Smith, R.B., 2012. Remotely sensing the cooling effects of city scale efforts to reduce urban heat island. *Build. Environ.* 49, 348–358.  
<https://doi.org/10.1016/j.buildenv.2011.08.004>
- Manoli, G., Fatichi, S., Schläpfer, M., Yu, K., Crowther, T.W., Meili, N., Burlando, P., Katul, G., Zeid, E.B., 2020. Reply to Martilli et al. (2020): Summer average urban-rural surface temperature differences do not indicate the need for urban heat reduction (preprint). Open Science Framework.  
<https://doi.org/10.31219/osf.io/mwpna>
- Manoli, G., Fatichi, S., Schläpfer, M., Yu, K., Crowther, T.W., Meili, N., Burlando, P., Katul, G.G., Bou-Zeid, E., 2019. Magnitude of urban heat islands largely explained by climate and population. *Nature* 573, 55–60.  
<https://doi.org/10.1038/s41586-019-1512-9>
- Mao, K., Yuan, Z., Zuo, Z., Xu, T., Shen, X., Gao, C., 2019. Changes in Global Cloud Cover Based on Remote Sensing Data from 2003 to 2012. *Chin. Geogr. Sci.* 29, 306–315.  
<https://doi.org/10.1007/s11769-019-1030-6>
- Martilli, A., Roth, M., Chow, W.T.L., Demuzere, M., Lipson, M., Krayenhoff, E.S., Sailor, D., Nazarian, N., Voogt, J., Wouters, H., Middel, A., Stewart, I.D., Bechtel, B., Christen, A., Hart, M.A., 2020. Summer average urban-rural surface temperature differences do not indicate the need for urban heat reduction (preprint). Open Science Framework.  
<https://doi.org/10.31219/osf.io/8gnbf>
- Martins, P.B., 2000. Urbanizing World [WWW Document]. URL <http://www.prb.org/Publications/Reports/2000/AnUrbanizingWorldPDF619KB.aspx> (accessed 11.26.17).
- Massion, K., 2017. What Is an Urban Settlement? [WWW Document]. Bizfluent. URL

- <https://bizfluent.com/info-7890851-urban-settlement.html> (accessed 7.4.18).
- McCarthy, M.P., Best, M.J., Betts, R.A., 2010. Climate change in cities due to global warming and urban effects. *Geophys. Res. Lett.* 37. <https://doi.org/10.1029/2010GL042845>
- McCoy, D.T., Eastman, R., Hartmann, D.L., Wood, R., 2017. The Change in Low Cloud Cover in a Warmed Climate Inferred from AIRS, MODIS, and ERA-Interim. *J. Clim.* 30, 3609–3620. <https://doi.org/10.1175/JCLI-D-15-0734.1>
- McGranahan, G., Satterthwaite, D., 2003. Urban Centers: An Assessment of Sustainability. *Annu. Rev. Environ. Resour.* 28, 243–274. <https://doi.org/10.1146/annurev.energy.28.050302.105541>
- Memon, R.A., Leung, D.Y.C., Chunho, L., 2008. A review on the generation, determination and mitigation of urban heat island. *J. Environ. Sci. China* 20, 120–128. [https://doi.org/10.1016/s1001-0742\(08\)60019-4](https://doi.org/10.1016/s1001-0742(08)60019-4)
- Met Office, 2020. Weather and climate change [WWW Document]. Met Off. URL <https://www.metoffice.gov.uk/> (accessed 6.29.20).
- Middel, A., Krayenhoff, E.S., 2019. Micrometeorological determinants of pedestrian thermal exposure during record-breaking heat in Tempe, Arizona: Introducing the MaRTy observational platform. *Sci. Total Environ.* 687, 137–151. <https://doi.org/10.1016/j.scitotenv.2019.06.085>
- Miller, J.D., Hutchins, M., 2017. The impacts of urbanisation and climate change on urban flooding and urban water quality: A review of the evidence concerning the United Kingdom. *J. Hydrol. Reg. Stud.* 12, 345–362. <https://doi.org/10.1016/j.ejrh.2017.06.006>
- Mills, G., 2007. Cities as agents of global change. *Int. J. Climatol.* 27, 1849–1857. <https://doi.org/10.1002/joc.1604>
- Mishra, A.K., 2019. Investigating changes in cloud cover using the long-term record of precipitation extremes. *Meteorol. Appl.* 26, 108–116. <https://doi.org/10.1002/met.1745>
- Mohan, M., Kikegawa, Y., Gurjar, B.R., Bhati, S., Kolli, N.R., 2013. Assessment of urban heat island effect for different land use–land cover from micrometeorological measurements and remote sensing data for megacity Delhi | SpringerLink [WWW Document]. URL <https://link.springer.com/article/10.1007/s00704-012-0758-z> (accessed 7.26.19).
- Morissette, J.T., Privette, J.L., Justice, C.O., 2002. A framework for the validation of MODIS Land products. *Remote Sens. Environ., The Moderate Resolution Imaging Spectroradiometer (MODIS): a new generation of Land Surface Monitoring* 83, 77–96. [https://doi.org/10.1016/S0034-4257\(02\)00088-3](https://doi.org/10.1016/S0034-4257(02)00088-3)
- Morris, A.E.J., 1974. History of Urban Form by A E J Morris - AbeBooks [WWW Document]. URL <https://www.abebooks.co.uk/book-search/title/history-of-urban-form/author/a-e-j-morris/> (accessed 7.6.20).
- Mundia, C.N., Aniya, M., 2005. Analysis of land use/cover changes and urban expansion of Nairobi city using remote sensing and GIS. *Int. J. Remote Sens.* 26, 2831–2849. <https://doi.org/10.1080/01431160500117865>
- Murray, V., Ebi, K.L., 2012. IPCC Special Report on Managing the Risks of Extreme Events and Disasters to Advance Climate Change Adaptation (SREX). *J. Epidemiol Community Health* 66, 759–760.

- <https://doi.org/10.1136/jech-2012-201045>
- Mushore, T.D., Dube, T., Manjowe, M., Gumindoga, W., Chemura, A., Roustia, I., Odindi, J., Mutanga, O., 2019. Remotely sensed retrieval of Local Climate Zones and their linkages to land surface temperature in Harare metropolitan city, Zimbabwe. *Urban Clim.* 27, 259–271. <https://doi.org/10.1016/j.uclim.2018.12.006>
- MyGuide, 2017. Nigeria Travel Guide [WWW Document]. My Guide Niger. URL <https://www.myguidenigeria.com/> (accessed 7.24.20).
- Nairaland, 2018. Nairaland Forum [WWW Document]. URL <https://www.nairaland.com/> (accessed 7.24.20).
- Naroll, R.S., Bertalanffy, L. von, 1956. The principle of allometry in biology and the social sciences. *Gen. Syst. Yearb.*
- Nduka, I.C., Abdulhamed, A.I., 2011. Classifying Urban Climate Field Sites by “Thermal Climate Zones” the Case of Onitsha Metropolis [WWW Document]. ResearchGate. URL [https://www.researchgate.net/publication/267549851\\_Classifying\\_Urban\\_Climate\\_Field\\_Sites\\_by\\_Thermal\\_Climate\\_Zones\\_the\\_Case\\_of\\_Onitsha\\_Metropolis](https://www.researchgate.net/publication/267549851_Classifying_Urban_Climate_Field_Sites_by_Thermal_Climate_Zones_the_Case_of_Onitsha_Metropolis) (accessed 8.8.19).
- Neteler, M., 2010. Estimating Daily Land Surface Temperatures in Mountainous Environments by Reconstructed MODIS LST Data. *Remote Sens.* 2, 333–351. <https://doi.org/10.3390/rs1020333>
- Neuman, M., Smith, S., 2010. City Planning and Infrastructure: Once and Future Partners. *J. Plan. Hist.* 9, 21–42. <https://doi.org/10.1177/1538513209355373>
- Newman, P., Kenworthy, J., 1999. Sustainability and Cities: Overcoming Automobile Dependence. Island Press.
- Ng, E., Yuan, C., Chen, L., Ren, C., Fung, J.C.H., 2011. Improving the wind environment in high-density cities by understanding urban morphology and surface roughness: A study in Hong Kong. *Landsc. Urban Plan.* 101, 59–74. <https://doi.org/10.1016/j.landurbplan.2011.01.004>
- Nichol, J., Wong, M.S., 2005. Modeling urban environmental quality in a tropical city. *Landsc. Urban Plan.* 73, 49–58. <https://doi.org/10.1016/j.landurbplan.2004.08.004>
- Nordbeck, S., 1971. Urban Allometric Growth. *Geogr. Ann. Ser. B Hum. Geogr.* 53, 54–67. <https://doi.org/10.2307/490887>
- NPCN, 2018. National Population Commission of Nigeria | GHDx [WWW Document]. URL <http://ghdx.healthdata.org/organizations/national-population-commission-nigeria> (accessed 7.11.19).
- Nunez, M., Oke, T.R., 1977. The Energy Balance of an Urban Canyon. *J. Appl. Meteorol.* 16, 11–19. [https://doi.org/10.1175/1520-0450\(1977\)016<0011:TEBOAU>2.0.CO;2](https://doi.org/10.1175/1520-0450(1977)016<0011:TEBOAU>2.0.CO;2)
- OECD, 2014. OECD and Bloomberg Philanthropies: Cities and Climate... - Google Scholar [WWW Document]. URL [https://scholar.google.com/scholar\\_lookup?title=Cities%20and%20Climate%20Change%3A%20National%20Governments%20Enabling%20Local%20Action&publication\\_year=2014&author=OECD](https://scholar.google.com/scholar_lookup?title=Cities%20and%20Climate%20Change%3A%20National%20Governments%20Enabling%20Local%20Action&publication_year=2014&author=OECD) (accessed 4.27.19).
- Ofem, B., 2012. A Review of the Criteria for Defining Urban Areas in Nigeria. <https://doi.org/10.1080/09709274.2012.11906461>
- Office for National Statistics, 2017. Population estimates - Office for National Statistics [WWW Document]. URL <https://www.ons.gov.uk/peoplepopulationandcommunity/populationandmigration/populationestimates> (accessed 12.9.17).
- Ogunjobi, K.O., Oluleye, A., Ajayi, V.O., 2012. A long-term record of aerosol index from TOMS observations and horizontal visibility in sub-Saharan

- West Africa. *Int. J. Remote Sens.* 33, 6076–6093.  
<https://doi.org/10.1080/01431161.2012.676689>
- Ojeh, V.N., Balogun, A.A., Okhimamhe, A.A., 2016. Urban-Rural Temperature Differences in Lagos. *Climate* 4, 29.  
<https://doi.org/10.3390/cli4020029>
- Oke, T.R., 2006. Instrument and Observing Methods Report No. 81 51.
- Oke, T.R., 2002. *Boundary Layer Climates*. Routledge.
- Oke, T. R., 1995. The Heat Island of the Urban Boundary Layer: Characteristics, Causes and Effects, in: *Wind Climate in Cities*, NATO ASI Series. Springer, Dordrecht, pp. 81–107.  
[https://doi.org/10.1007/978-94-017-3686-2\\_5](https://doi.org/10.1007/978-94-017-3686-2_5)
- Oke, T.R., 1995. Classics in physical geography revisited: Sundborg, Å. 1951: Climatological studies in Uppsala with special regard to the temperature conditions in the urban area. *Geographica 22. Prog. Phys. Geogr. Earth Environ.* 19, 107–113.  
<https://doi.org/10.1177/030913339501900105>
- Oke, T.R., 1982. The energetic basis of the urban heat island. *Q. J. R. Meteorol. Soc.* 108, 1–24.  
<https://doi.org/10.1002/qj.49710845502>
- Oke, T.R., 1981. Canyon geometry and the nocturnal urban heat island: Comparison of scale model and field observations. *J. Climatol.* 1, 237–254.  
<https://doi.org/10.1002/joc.3370010304>
- Oke, T.R., 1973. City size and the urban heat island. *Atmospheric Environ.* 1967 7, 769–779.  
[https://doi.org/10.1016/0004-6981\(73\)90140-6](https://doi.org/10.1016/0004-6981(73)90140-6)
- Oke, T.R., 1970. The temperature profile near the ground on calm clear nights. *Q. J. R. Meteorol. Soc.* 96, 14–23.  
<https://doi.org/10.1002/qj.49709640703>
- Oke, T.R., Maxwell, G.B., 1975. Urban heat island dynamics in Montreal and Vancouver. *Atmospheric Environ.* 1967 9, 191–200.  
[https://doi.org/10.1016/0004-6981\(75\)90067-0](https://doi.org/10.1016/0004-6981(75)90067-0)
- Oliveira, V., 2016. *Urban Morphology: An Introduction to the Study of the Physical Form of Cities*. Springer.
- Oloyede, M.A., Akinbode, A., 2010. Towards Effective Physical Planning in Local Governments in Nigeria | Michael Oloyede Al [WWW Document]. ResearchGate. URL  
[https://www.researchgate.net/publication/250303778\\_Towards\\_Effective\\_Physical\\_Planning\\_in\\_Local\\_Governments\\_in\\_Nigeria](https://www.researchgate.net/publication/250303778_Towards_Effective_Physical_Planning_in_Local_Governments_in_Nigeria) (accessed 7.19.19).
- Omofonmwan, S.I., Osa-Edoh, G.I., 2008. The Challenges of Environmental Problems in Nigeria. *J. Hum. Ecol.* 23, 53–57.  
<https://doi.org/10.1080/09709274.2008.11906054>
- Omole, F.K., Akinbamijo, O.B., 2012. Land Development and Planning Laws in Nigeria: The Historical Account. *J. Law Policy Glob.* 8, 25–31–31.
- Os, B., Aa, A., 2016. Change Detection in Land Surface Temperature and Land Use Land Cover over Lagos Metropolis, Nigeria. *J. Remote Sens. GIS* 5, 1–7.  
<https://doi.org/10.4172/2469-4134.1000171>
- Qşqba, S.O., 1969. THE PHENOMENON OF LABOUR MIGRATION IN THE ERA OF BRITISH COLONIAL RULE: A NEGLECTED ASPECT OF NIGERIA'S SOCIAL HISTORY. *J. Hist. Soc. Niger.* 4, 515–538.
- Ouahabi, M.H., Benabdelouahab, F., Khamlichi, A., 2017. Analyzing wind speed data and wind power density of Tetouan city in Morocco by adjustment to Weibull and Rayleigh distribution functions. *Wind Eng.* 41, 174–184.  
<https://doi.org/10.1177/0309524X17709908>
- Pal, S., Ziaul, Sk., 2017. Detection of land use and land cover change and land surface temperature in English Bazar urban centre. *Egypt. J. Remote Sens.*

- Space Sci. 20, 125–145.  
<https://doi.org/10.1016/j.ejrs.2016.11.003>
- Palumbo, A., Mazzarella, A., 1980. Rainfall Statistical Properties in Naples. *Mon. Weather Rev.* 108, 1041–1045.  
[https://doi.org/10.1175/1520-0493\(1980\)108<1041:RSPIN>2.0.CO;2](https://doi.org/10.1175/1520-0493(1980)108<1041:RSPIN>2.0.CO;2)
- Pasquini, L., 2019. The urban governance of climate change adaptation in least-developed African countries and in small cities: the engagement of local decision-makers in Dar es Salaam, Tanzania, and Karonga, Malawi. *Clim. Dev.* 0, 1–12.  
<https://doi.org/10.1080/17565529.2019.1632166>
- Patz, J.A., Campbell-Lendrum, D., Holloway, T., Foley, J.A., 2005. Impact of regional climate change on human health. *Nature* 438, 310–317.  
<https://doi.org/10.1038/nature04188>
- Payton, N.I., 1995. The machine in the garden city: Patrick Geddes' plan for Tel Aviv. *Plan. Perspect.* 10, 359–381.  
<https://doi.org/10.1080/02665439508725829>
- Peng, S., Piao, S., Ciais, P., Friedlingstein, P., Ottle, C., Bréon, F.-M., Nan, H., Zhou, L., Myneni, R.B., 2012. Surface Urban Heat Island Across 419 Global Big Cities. *Environ. Sci. Technol.* 46, 696–703.  
<https://doi.org/10.1021/es2030438>
- Peterson, T.C., 2003. Assessment of Urban Versus Rural In Situ Surface Temperatures in the Contiguous United States: No Difference Found. *J. Clim.* 16, 2941–2959.  
[https://doi.org/10.1175/1520-0442\(2003\)016<2941:AOUVRI>2.0.CO;2](https://doi.org/10.1175/1520-0442(2003)016<2941:AOUVRI>2.0.CO;2)
- Piault, M.-H., 1963. Family and Social Change in an African City. *Homme* 3, 121–124.
- Pielke, R.A., 2013. Mesoscale Meteorological Modeling: Chapter 13. Examples of Mesoscale Models. Elsevier Inc. Chapters.
- Puseerit, J., Beringer, A.L., Inmuong, Y., Kaomuangoi, K., 2019. Understanding Urban Vulnerabilities to Climate Change Impacts in Khon Kaen and Mukdahan in Thailand. *Community Univ. Engagem. J.* 1, 1–13.
- Qihao, W., 2012. An Introduction to Contemporary Remote Sensing [WWW Document]. eBooks.com. URL <https://www.ebooks.com/en-gb/book/883325/an-introduction-to-contemporary-remote-sensing/qihao-weng/> (accessed 3.4.21).
- Qu, J.J., Gao, W., Kafatos, M., Murphy, R.E., Salomonson, V.V., 2007. *Earth Science Satellite Remote Sensing: Vol.1: Science and Instruments*. Springer Science & Business Media.
- Quattrochi, D.A., Goodchild, M.F., 1997. Scale in remote sensing and GIS.  
<https://doi.org/10.5860/choice.35-1541>
- Rabin, R.M., Martin, D.W., 1996. Satellite observations of shallow cumulus coverage over the central United States: An exploration of land use impact on cloud cover. *J. Geophys. Res. Atmospheres* 101, 7149–7155.  
<https://doi.org/10.1029/95JD02891>
- Ragatoa, D.S., Ogunjobi, K.O., Klutse, N.A.B., Okhimamhe, A.A., Eichie, J.O., 2019. A change comparison of heat wave aspects in climatic zones of Nigeria. *Environ. Earth Sci.* 78, 111.  
<https://doi.org/10.1007/s12665-019-8112-8>
- Rigo, G., Parlow, E., Oesch, D., 2006. Validation of satellite observed thermal emission with in-situ measurements over an urban surface. *Remote Sens. Environ., Thermal Remote Sensing of Urban Areas* 104, 201–210.  
<https://doi.org/10.1016/j.rse.2006.04.018>
- Rizwan, A.M., Dennis, L.Y.C., Liu, C., 2008. A review on the generation, determination and mitigation of Urban Heat Island. *J. Environ. Sci.* 20, 120–128.  
[https://doi.org/10.1016/S1001-0742\(08\)60019-4](https://doi.org/10.1016/S1001-0742(08)60019-4)
- Robine, J.-M., Cheung, S.L.K., Le Roy, S., Van Oyen, H., Griffiths, C., Michel, J.-P.,

- Herrmann, F.R., 2008. Death toll exceeded 70,000 in Europe during the summer of 2003. *C. R. Biol., Dossier : Nouveautés en cancérogenèse / New developments in carcinogenesis* 331, 171–178.  
<https://doi.org/10.1016/j.crvi.2007.12.001>
- Rohat, G., Flacke, J., Dosio, A., Dao, H., Maarseveen, M.V., 2019. Projections of Human Exposure to Dangerous Heat in African Cities Under Multiple Socioeconomic and Climate Scenarios - Rohat - 2019 - *Earth's Future* - Wiley Online Library [WWW Document]. URL <https://agupubs.onlinelibrary.wiley.com/doi/full/10.1029/2018EF001020> (accessed 1.3.20).
- Rose, M.H., 2001. Review of The Sanitary City: Urban Infrastructure in America from Colonial Times to the Present. *Environ. Hist.* 6, 478–480.  
<https://doi.org/10.2307/3985668>
- Rosenzweig, C., Solecki, W.D., Hammer, S.A., Mehrotra, S., 2011. Climate Change and Cities: First Assessment Report of the Urban Climate Change Research Network. Cambridge University Press.
- Rubin, N.H., 2009. The changing appreciation of Patrick Geddes: a case study in planning history. *Plan. Perspect.* 24, 349–366.  
<https://doi.org/10.1080/02665430902933986>
- Rybski, D., Reusser, D.E., Winz, A.-L., Fichtner, C., Sterzel, T., Kropp, J.P., 2017. Cities as nuclei of sustainability? *Environ. Plan. B Urban Anal. City Sci.* 44, 425–440.  
<https://doi.org/10.1177/0265813516638340>
- Sachindra, D.A., Ng, A.W.M., Muthukumaran, S., Perera, B.J.C., 2016. Impact of climate change on urban heat island effect and extreme temperatures: a case-study. *Q. J. R. Meteorol. Soc.* 142, 172–186.  
<https://doi.org/10.1002/qj.2642>
- Salomonson, V.V., Barnes, W.L., Maymon, P.W., Montgomery, H.E., Ostrow, H., 1989. MODIS: advanced facility instrument for studies of the Earth as a system. *IEEE Trans. Geosci. Remote Sens.* 27, 145–153.  
<https://doi.org/10.1109/36.20292>
- Santamouris, M., 2013. *Energy and Climate in the Urban Built Environment*. Routledge.  
<https://doi.org/10.4324/9781315073774>
- Sarkar, S., Phibbs, P., Simpson, R., Wasnik, S., 2018. The scaling of income distribution in Australia: Possible relationships between urban allometry, city size, and economic inequality. *Environ. Plan. B Urban Anal. City Sci.* 45, 603–622.  
<https://doi.org/10.1177/0265813516676488>
- Satterthwaite, D., 2007. Adapting to Climate Change in Urban Areas: The Possibilities and Constraints in Low- and Middle-income Nations. IIED.
- Schmidt-Nielsen, K., 1984. *Scaling: Why is Animal Size So Important?* Cambridge University Press.
- Schneider, A., Friedl, M.A., Potere, D., 2009. A new map of global urban extent from MODIS satellite data. *Environ. Res. Lett.* 4, 044003.  
<https://doi.org/10.1088/1748-9326/4/4/044003>
- Schwarz, N., Lautenbach, S., Seppelt, R., 2011. Exploring indicators for quantifying surface urban heat islands of European cities with MODIS land surface temperatures. *Remote Sens. Environ.* 115, 3175–3186.  
<https://doi.org/10.1016/j.rse.2011.07.003>
- Schwarz, N., Manceur, A.M., 2015. Analyzing the Influence of Urban Forms on Surface Urban Heat Islands in Europe. *J. Urban Plan. Dev. Div. ASCE* 141, A4014003.  
[https://doi.org/10.1061/\(ASCE\)UP.1943-5444.0000263](https://doi.org/10.1061/(ASCE)UP.1943-5444.0000263)
- SEDAC, 2017. *EarthData | SEDAC* [WWW Document]. URL <https://sedac.ciesin.columbia.edu/sea>



- rch/data?contains=population+data (accessed 1.25.20).
- Seto, K.C., Güneralp, B., Hutyra, L.R., 2012. Global forecasts of urban expansion to 2030 and direct impacts on biodiversity and carbon pools. *Proc. Natl. Acad. Sci.* 109, 16083–16088. <https://doi.org/10.1073/pnas.1211658109>
- Seto, K.C., Sánchez-Rodríguez, R., Fragkias, M., 2010. The New Geography of Contemporary Urbanization and the Environment. *Annu. Rev. Environ. Resour.* 35, 167–194. <https://doi.org/10.1146/annurev-environ-100809-125336>
- Shalaby, A., Tateishi, R., 2007. Remote sensing and GIS for mapping and monitoring land cover and land-use changes in the Northwestern coastal zone of Egypt. *Appl. Geogr.* 27, 28–41. <https://doi.org/10.1016/j.apgeog.2006.09.004>
- Sheng, L., Tang, X., You, H., Gu, Q., Hu, H., 2017. Comparison of the urban heat island intensity quantified by using air temperature and Landsat land surface temperature in Hangzhou, China. *Ecol. Indic.* 72, 738–746. <https://doi.org/10.1016/j.ecolind.2016.09.009>
- Short, J.R., 1982. *Housing in Britain: The Post-war Experience*. Routledge, London ; New York.
- Small, C.G., 2012. *The Statistical Theory of Shape*. Springer Science & Business Media.
- Smith, C.L., Webb, A., Levermore, G.J., Lindley, S.J., Beswick, K., 2011. Fine-scale spatial temperature patterns across a UK conurbation. *Clim. Change* 109, 269–286. <https://doi.org/10.1007/s10584-011-0021-0>
- SolarGIS, 2019. *Global Solar Atlas* [WWW Document]. URL <https://globalsolaratlas.info/support/release-notes> (accessed 1.25.20).
- Solomon, S., Intergovernmental Panel on Climate Change, Intergovernmental Panel on Climate Change (Eds.), 2007. *Climate change 2007: the physical science basis: contribution of Working Group I to the Fourth Assessment Report of the Intergovernmental Panel on Climate Change*. Cambridge University Press, Cambridge ; New York.
- Stefanovic, J.O., Yang, H., Zhou, Y., Kamali, B., Ogalleh, S.A., 2019. Adaption to climate change: a case study of two agricultural systems from Kenya. *Clim. Dev.* 11, 319–337. <https://doi.org/10.1080/17565529.2017.1411241>
- Stewart, I., Oke, T.R., 2010. Thermal differentiation of local climate zones using temperature observations from urban and rural field sites [WWW Document]. ResearchGate. URL [https://www.researchgate.net/publication/228420685\\_Thermal\\_differentiation\\_of\\_local\\_climate\\_zones\\_using\\_temperature\\_observations\\_from\\_urban\\_and\\_rural\\_field\\_sites](https://www.researchgate.net/publication/228420685_Thermal_differentiation_of_local_climate_zones_using_temperature_observations_from_urban_and_rural_field_sites) (accessed 11.8.19).
- Stewart, I.D., Oke, T., 2009a. A New Classification System for Urban Climate Sites. *Bull. Am. Meteorol. Soc.* Boston 90, 922–923.
- Stewart, I.D., Oke, T.R., 2012. Local Climate Zones for Urban Temperature Studies. *Bull. Am. Meteorol. Soc.* 93, 1879–1900. <https://doi.org/10.1175/BAMS-D-11-00019.1>
- Stewart, I.D., Oke, T.R., 2009b. Newly Developed “Thermal Climate Zones” for Defining and Measuring Urban Heat Island “Magnitude” in the Canopy Layer [WWW Document]. ResearchGate. URL [https://www.researchgate.net/publication/254774486\\_Newly\\_Developed\\_Thermal\\_Climate\\_Zones\\_for\\_Defining\\_and\\_Measuring\\_Urban\\_Heat\\_Island\\_Magnitude\\_in\\_the\\_Canopy\\_Layer](https://www.researchgate.net/publication/254774486_Newly_Developed_Thermal_Climate_Zones_for_Defining_and_Measuring_Urban_Heat_Island_Magnitude_in_the_Canopy_Layer) (accessed 8.12.19).
- Stewart, I.D., Oke, T.R., Krayenhoff, E.S., 2014. Evaluation of the ‘local climate zone’ scheme using temperature observations and model simulations.

- Int. J. Climatol. 34, 1062–1080.  
<https://doi.org/10.1002/joc.3746>
- Swanson, D.A., Tayman, J., Bryan, T.M., 2011. MAPE-R: a rescaled measure of accuracy for cross-sectional subnational population forecasts. J. Popul. Res. 28, 225–243.  
<https://doi.org/10.1007/s12546-011-9054-5>
- Terjung, W.H., Louie, S.S.-F., 1974. A Climatic Model of Urban Energy Budgets. Geogr. Anal. 6, 341–367.  
<https://doi.org/10.1111/j.1538-4632.1974.tb00519.x>
- Tizot, J.-Y., 2018. Ebenezer Howard’s Garden City Idea and the Ideology of Industrialism. Cah. Victoriens Edouardiens 87.  
<https://doi.org/10.4000/cve.3605>
- Tomlinson, C.J., Chapman, L., Thornes, J.E., Baker, C.J., 2012. Derivation of Birmingham’s summer surface urban heat island from MODIS satellite images. Int. J. Climatol. 32, 214–224.  
<https://doi.org/10.1002/joc.2261>
- Toomey, D., 2017. Investigating the Enigma of Clouds and Climate Change [WWW Document]. Yale E360. URL <https://e360.yale.edu/features/investigating-the-enigma-of-clouds-and-climate-change> (accessed 3.1.21).
- Torok, S.J., Morris, C.J.G., Skinner, C., Plummer, N., 2001. Urban heat island features of southeast Australian towns. Aust. Meteorol. Mag. 14.
- Tran, H., Uchiyama, D., Ochi, S., Yasuoka, Y., 2006. Assessment with satellite data of the urban heat island effects in Asian mega cities. Int. J. Appl. Earth Obs. Geoinformation 8, 34–48.
- Tsai, Y.-H., 2005. Quantifying Urban Form: Compactness versus “Sprawl.” Urban Stud. 42, 141–161.  
<https://doi.org/10.1080/0042098042000309748>
- Tsubaki, T., 2000. Planners and the public: British popular opinion on housing during the second world war. Contemp. Br. Hist. 14, 81–98.  
<https://doi.org/10.1080/13619460008581573>
- Turner, B., Moss, R.H., Skole, D.L., 1993. Relating land use and global land-cover change. No Source Inf. Available.
- Turner, J.C., 1968. Housing Priorities, Settlement Patterns, and Urban Development in Modernizing Countries. J. Am. Inst. Plann. 34, 354–363.  
<https://doi.org/10.1080/01944366808977562>
- UN 2010, 2010. World Urbanization Prospects 2009 Revision (United Nations 2010) | Urban Area | Urbanization [WWW Document]. Scribd. URL <https://www.scribd.com/document/78681125/World-Urbanization-Prospects-2009-Revision-United-Nations-2010> (accessed 11.14.17).
- UNDP, 2010. Human Development Report 2010 | Human Development Reports [WWW Document]. URL <http://hdr.undp.org/en/content/human-development-report-2010> (accessed 6.28.19).
- Unger, J., 2009. Connection between urban heat island and sky view factor approximated by a software tool on a 3D urban database. Int. J. Environ. Pollut. 36, 59.  
<https://doi.org/10.1504/IJEP.2009.021817>
- Unger, J., 2006. Modelling of the annual mean maximum urban heat island using 2D and 3D surface parameters. Clim. Res. 30, 215–226.  
<https://doi.org/10.3354/cr030215>
- Unger, J., Savic, S., Gal, T., 2011. Modelling of the Annual Mean Urban Heat Island Pattern for Planning of Representative Urban Climate Station Network [WWW Document]. URL [https://www.researchgate.net/publication/215620072\\_Modelling\\_of\\_the\\_Annual\\_Mean\\_Urban\\_Heat\\_Island\\_Pattern\\_for\\_Planning\\_of\\_Representative\\_Urban\\_Climate\\_Station\\_Network](https://www.researchgate.net/publication/215620072_Modelling_of_the_Annual_Mean_Urban_Heat_Island_Pattern_for_Planning_of_Representative_Urban_Climate_Station_Network) (accessed 6.1.20).
- United Nations, Department of Economic and Social Affairs, Population Division,

2019. World urbanization prospects: the 2018 revision.
- Urban, J., Holušová, K., Menšík, L., Čermák, J., Kantor, P., 2013. Tree allometry of Douglas fir and Norway spruce on a nutrient-poor and a nutrient-rich site. *Trees* 27, 97–110. <https://doi.org/10.1007/s00468-012-0771-y>
- Usman, S.U., Abdulhamed, I.A., Ibrahim, M., Iguisi, E.O., Azare, I.M., Ati, O.F., 2016. Classifying Urban Climate Field Sites by Local Climate Zones of Kaduna Metropolis Nigeria 6.
- Vancutsem, C., Ceccato, P., Dinku, T., Connor, S.J., 2010. Evaluation of MODIS land surface temperature data to estimate air temperature in different ecosystems over Africa. *Remote Sens. Environ.* 114, 449–465. <https://doi.org/10.1016/j.rse.2009.10.002>
- Verburg, P.H., Erb, K.-H., Mertz, O., Espindola, G., 2013. Land System Science: between global challenges and local realities. *Curr. Opin. Environ. Sustain.* 5, 433–437. <https://doi.org/10.1016/j.cosust.2013.08.001>
- Vining, D.R.J., Kontuly, T., 1978. Population Dispersal from Major Metropolitan Regions: An International Comparison. *Int. Reg. Sci. Rev.* 3, 49–73. <https://doi.org/10.1177/016001767800300102>
- Voogt, J.A., Oke, T.R., 2003. Thermal remote sensing of urban climates. *Remote Sens. Environ., Urban Remote Sensing* 86, 370–384. [https://doi.org/10.1016/S0034-4257\(03\)00079-8](https://doi.org/10.1016/S0034-4257(03)00079-8)
- Voogt, J.A., Oke, T.R., 1997. Complete Urban Surface Temperatures. *J. Appl. Meteorol.* 36, 1117–1132. [https://doi.org/10.1175/1520-0450\(1997\)036<1117:CUST>2.0.CO;2](https://doi.org/10.1175/1520-0450(1997)036<1117:CUST>2.0.CO;2)
- Wamsler, C., Brink, E., Rivera, C., 2013. Planning for climate change in urban areas: from theory to practice. *J. Clean. Prod.* 50, 68–81.
- Wan, Z., 2008. New refinements and validation of the MODIS Land-Surface Temperature/Emissivity products. *Remote Sens. Environ.* 112, 59–74. <https://doi.org/10.1016/j.rse.2006.06.026>
- Wan, Z., Dozier, J., 1996. A generalized split-window algorithm for retrieving land-surface temperature from space. *IEEE Trans. Geosci. Remote Sens.* 34, 892–905. <https://doi.org/10.1109/36.508406>
- Wan, Z., Zhang, Y., Zhang, Q., Li, Z., 2002. Validation of the land-surface temperature products retrieved from Terra Moderate Resolution Imaging Spectroradiometer data. *Remote Sens. Environ., The Moderate Resolution Imaging Spectroradiometer (MODIS): a new generation of Land Surface Monitoring* 83, 163–180. [https://doi.org/10.1016/S0034-4257\(02\)00093-7](https://doi.org/10.1016/S0034-4257(02)00093-7)
- Wan, Z., Zhang, Y., Zhang, Q., Li, Z.-L., 2004. Quality assessment and validation of the MODIS global land surface temperature. *Int. J. Remote Sens.* 25, 261–274. <https://doi.org/10.1080/0143116031000116417>
- Wan, Z.S.H., 2015. MOD11A1 MODIS/Terra Land Surface Temperature/Emissivity Daily L3 Global 1km SIN Grid V006. <https://doi.org/10.5067/MODIS/MOD11A1.006>
- Wang, ran, Ren, C., Xu, Y., Shi, Y., 2017. Mapping the local climate zones of urban areas by GIS-based and WUDAPT methods: A case study of Hong Kong [WWW Document]. ResearchGate. URL [https://www.researchgate.net/publication/320368260\\_Mapping\\_the\\_local\\_climate\\_zones\\_of\\_urban\\_areas\\_by\\_GIS-based\\_and\\_WUDAPT\\_methods\\_A\\_case\\_study\\_of\\_Hong\\_Kong](https://www.researchgate.net/publication/320368260_Mapping_the_local_climate_zones_of_urban_areas_by_GIS-based_and_WUDAPT_methods_A_case_study_of_Hong_Kong) (accessed 8.8.19).
- Wang, C., Middel, A., Myint, S.W., Kaplan, S., Brazel, A.J., Lukasczyk, J., 2018.

- Assessing local climate zones in arid cities: The case of Phoenix, Arizona and Las Vegas, Nevada. *ISPRS J. Photogramm. Remote Sens.* 141, 59–71.  
<https://doi.org/10.1016/j.isprsjprs.2018.04.009>
- Wang, R., Cai, M., Ren, C., Bechtel, B., Xu, Y., Ng, E., 2019. Detecting multi-temporal land cover change and land surface temperature in Pearl River Delta by adopting local climate zone. *Urban Clim.* 28, 100455.  
<https://doi.org/10.1016/j.uclim.2019.100455>
- Wang, Y., Berardi, U., Akbari, H., 2016. Comparing the effects of urban heat island mitigation strategies for Toronto, Canada.  
<https://doi.org/10.1016/J.ENBUILD.2015.06.046>
- Wang, Y., Li, Y., Sabatino, S.D., Martilli, A., Chan, P.W., 2018. Effects of anthropogenic heat due to air-conditioning systems on an extreme high temperature event in Hong Kong. *Environ. Res. Lett.* 13, 034015.  
<https://doi.org/10.1088/1748-9326/aaa848>
- Watkins, R., Palmer, J., Kolokotroni, M., Littlefair, P., 2002. The London Heat Island: results from summertime monitoring. *Build. Serv. Eng. Res. Technol.* 23, 97–106.  
<https://doi.org/10.1191/0143624402bt0310a>
- Webb, M.S., 2018. Local responses to the protection of medieval buildings and archaeology in British post-war town reconstruction: Southampton and Coventry. *Urban Hist.* 45, 635–659.  
<https://doi.org/10.1017/S0963926818000019>
- Weng, Q., 2011. *Advances in Environmental Remote Sensing: Sensors, Algorithms, and Applications*. CRC Press.
- Weng, Q., 2010. *Remote sensing and GIS integration theories, methods, and applications*. McGraw-Hill, New York.
- Weng, Q., 2009. Thermal infrared remote sensing for urban climate and environmental studies: Methods, applications, and trends. *ISPRS J. Photogramm. Remote Sens.* 64, 335–344.  
<https://doi.org/10.1016/j.isprsjprs.2009.03.007>
- Weng, Q., Lu, D., 2008. A sub-pixel analysis of urbanization effect on land surface temperature and its interplay with impervious surface and vegetation coverage in Indianapolis, United States. *Int. J. Appl. Earth Obs. Geoinformation* 10, 68–83.  
<https://doi.org/10.1016/j.jag.2007.05.002>
- West, G.B., Brown, J.H., 2005. The origin of allometric scaling laws in biology from genomes to ecosystems: towards a quantitative unifying theory of biological structure and organization. *J. Exp. Biol.* 208, 1575–1592.  
<https://doi.org/10.1242/jeb.01589>
- White, R., Engelen, G., 1993. Cellular Automata and Fractal Urban Form: A Cellular Modelling Approach to the Evolution of Urban Land-Use Patterns. *Environ. Plan. A* 25, 1175–1199.  
<https://doi.org/10.1068/a251175>
- Whitehand, J.W.R., 2001. The Physical Form of Cities: A Historico-Geographical Approach, in: *Handbook of Urban Studies*. SAGE Publications Ltd, London, pp. 69–87.  
<https://doi.org/10.4135/9781848608375>
- Whitehand, J.W.R., Whitehand, S.M., 1983. The Study of Physical Change in Town Centres: Research Procedures and Types of Change. *Trans. Inst. Br. Geogr.* 8, 483–507.  
<https://doi.org/10.2307/621964>
- Whitehand, J.W.R., Whitehand, S.M.R., 1984. The Physical Fabric of Town Centres: The Agents of Change. *Trans. Inst. Br. Geogr.* 9, 231.  
<https://doi.org/10.2307/622170>
- Wiedenhofer, D., Lenzen, M., Steinberger, J.K., 2013. Energy requirements of consumption: Urban form, climatic and socio-economic factors, rebounds and their policy implications. *Energy*

- Policy 63, 696–707.  
<https://doi.org/10.1016/j.enpol.2013.07.035>
- Wikipedia, 2020. Geography of Sheffield. Wikipedia.
- Wilks, D.S., 1995. Statistical Methods in the Atmospheric Sciences, Volume 59 - 1st Edition [WWW Document]. URL <https://www.elsevier.com/books/statistical-methods-in-the-atmospheric-sciences/wilks/978-0-12-751965-4> (accessed 4.28.21).
- Winsborough, H.H., 1962. City Growth and City Structure†. *J. Reg. Sci.* 4, 35–49. <https://doi.org/10.1111/j.1467-9787.1962.tb00903.x>
- Wouters, H., De Ridder, K., Poelmans, L., Willems, P., Brouwers, J., Hosseinzadehtalaei, P., Tabari, H., Vanden Broucke, S., van Lipzig, N.P.M., Demuzere, M., 2017. Heat stress increase under climate change twice as large in cities as in rural areas: A study for a densely populated midlatitude maritime region. *Geophys. Res. Lett.* 44, 8997–9007. <https://doi.org/10.1002/2017GL074889>
- Wright, A.J., Young, A.N., Natarajan, S., 2016. Dwelling temperatures and comfort during the August 2003 heat wave: Build. Serv. Eng. Res. Technol. <https://doi.org/10.1191/0143624405bt1360a>
- Wu, J., Jones, K., Li, H., Loucks, O., 2006. Scaling and Uncertainty Analysis in Ecology: Methods and Applications.
- Wu, X., Zhang, L., Zang, S., 2019. Examining seasonal effect of urban heat island in a coastal city. *PLOS ONE* 14, e0217850. <https://doi.org/10.1371/journal.pone.0217850>
- Xu, Y., Pu, L., Zhang, L., 2014. Spatial Pattern and the Process of Settlement Expansion in Jiangsu Province from 1980 to 2010, Eastern China. *Sustainability* 6, 8180–8194. <https://doi.org/10.3390/su6118180>
- Yamamoto, Y., 2006. Measures to Mitigate Urban Heat Islands 19.
- Yang, J., Wong, M.S., Menenti, M., Nichol, J., 2015. Modeling the effective emissivity of the urban canopy using sky view factor. *ISPRS J. Photogramm. Remote Sens.* 105, 211–219. <https://doi.org/10.1016/j.isprsjprs.2015.04.006>
- Yuan, F., Bauer, M.E., 2007. Comparison of impervious surface area and normalized difference vegetation index as indicators of surface urban heat island effects in Landsat imagery. *Remote Sens. Environ.* 106, 375–386. <https://doi.org/10.1016/j.rse.2006.09.003>
- Zhang, H., Qi, Z., Ye, X., Cai, Y., Ma, W., Chen, M., 2013. Analysis of land use/land cover change, population shift, and their effects on spatiotemporal patterns of urban heat islands in metropolitan Shanghai, China. *Appl. Geogr.* 44, 121–133. <https://doi.org/10.1016/j.apgeog.2013.07.021>
- Zhang, Q., Seto, K.C., 2011. Mapping urbanization dynamics at regional and global scales using multi-temporal DMSP/OLS nighttime light data. *Remote Sens. Environ.* 115, 2320–2329. <https://doi.org/10.1016/j.rse.2011.04.032>
- Zhang, Z., Xiao, R., Shortridge, A., Wu, J., 2014. Spatial Point Pattern Analysis of Human Settlements and Geographical Associations in Eastern Coastal China — A Case Study. *Int. J. Environ. Res. Public Health* 11, 2818–2833. <https://doi.org/10.3390/ijerph110302818>
- Zhao, L., Lee, X., Smith, R.B., Oleson, K., 2014. Strong contributions of local background climate to urban heat islands. *Nature* 511, 216–219. <https://doi.org/10.1038/nature13462>
- Zhou, B., Rybski, D., Kropp, J.P., 2017. The role of city size and urban form in the surface urban heat island. *Sci. Rep.* 7, 1–9. <https://doi.org/10.1038/s41598-017-04242-2>

- Zhou, B., Rybski, D., Kropp, J.P., 2013. On the statistics of urban heat island intensity. *Geophys. Res. Lett.* 40, 5486–5491. <https://doi.org/10.1002/2013GL057320>
- Zhou, D., Zhao, S., Liu, S., Zhang, L., Zhu, C., 2014. Surface urban heat island in China's 32 major cities: Spatial patterns and drivers. *Remote Sens. Environ.* 152, 51–61. <https://doi.org/10.1016/j.rse.2014.05.017>
- Zhou, B., Lauwaet, D., Hooyberghs, H., De Ridder, K., Kropp, J., Rybski, D., 2016. Assessing Seasonality in the Surface Urban Heat Island of London. *J. Appl. Meteorol. Climatol.* 55, 493–505. <https://doi.org/10.1175/JAMC-D-15-0041.1>
- Zhou, B., Rybski, D., Kropp, J.P., 2013. On the statistics of urban heat island intensity. *Geophys. Res. Lett.* 40, 5486–5491. <https://doi.org/10.1002/2013GL057320>
- Zhou, B., Rybski, D., Kropp, J.P., 2017. The role of city size and urban form in the surface urban heat island. *Sci. Rep.* 7, 1–9. <https://doi.org/10.1038/s41598-017-04242-2>
- Zhou, D., Zhao, S., Liu, S., Zhang, L., Zhu, C., 2014. Surface urban heat island in China's 32 major cities: Spatial patterns and drivers. *Remote Sens. Environ.* 152, 51–61. <https://doi.org/10.1016/j.rse.2014.05.017>
- Zhao, L., Lee, X., Smith, R.B., Oleson, K., 2014. Strong contributions of local background climate to urban heat islands. *Nature* 511, 216–219. <https://doi.org/10.1038/nature13462>

MODIS/Terra Land Surface Temperature and Emissivity Daily L3 Global 1km Grid SIN V006

<https://search.earthdata.nasa.gov/search>,

Data downloaded on 23<sup>rd</sup> August

2017(Earthdata, 2017). For a description of the dataset, see

<https://lpdaac.usgs.gov/products/mod11a1v006/>

<https://www.planninghelp.cpre.org.uk/planning-explained/history-of-the-planning-system>,

last accessed 26<sup>th</sup> September 2019.

## Data Sources

Meridian\_data, 2017

[https://digimap.edina.ac.uk/webhelp/os/data\\_information/os\\_products/meridian\\_2.htm](https://digimap.edina.ac.uk/webhelp/os/data_information/os_products/meridian_2.htm),

data downloaded on 31<sup>st</sup> January 2017